# 博士論文

# Stress and quality engineering of GaN growth on Si with in-situ wafer curvature analysis

（In situウエハ曲率解析によるシリコン上窒化ガリウム成長における応力・結晶品位の制御）

劉　才

# Stress and quality engineering of GaN growth on Si with in-situ wafer curvature analysis

In situウエハ曲率解析によるシリコン上窒化ガリウム成長における応力・結晶品位の制御

A dissertation submitted to the Graduate School of Engineering
The University of Tokyo
In partial fulfillment of the requirements for the degree of
Doctor of Philosophy

劉　才
Cai Liu

Under the supervision of
Professor Dr. Yoshiaki Nakano

September 2014

# Acknowledgements

There is an old Chinese saying that “Thirty years of age when a man should stand on his own feet.” Steve Jobs said “… the only way to do great work is to love what you do. If you haven't found it yet, keep looking.” Everyone was born with an innate mission to experience or complete this life. Pursing a Ph. D. degree is not only a good training to be an independent and qualified scientist or engineer with some new contribution to the knowledge of human beings, but more importantly, at least for me, it is also a journey to find the innate mission of mine. Even with deep paining and struggling, it was really a good journey to travel. I am so grateful to all the people I have met on this nice journey.

Firstly I have to convey my great appreciation and respect to Japanese people and government to support my study in Japan. I never imaged studying abroad if there is no such precious support. All people I met here are very warm and friendly, they are always happy to render help to others.

I would like to show my sincere gratitude to my advisor, Professor Yoshiaki Nakano, who gave me the chance to study in The University of Tokyo and supported my study here, and my co-advisor, Associate Professor Masakazu Sugiyama, who offered me the interesting research topic and much helpful advice from research to presentation with great patience. I have learned very much from their teachings and I could not have completed my dissertation without their teachings and support.

I also appreciate the help and critical comments from Professor Katsushi Fujii, Professor Yoshitaka Okada and Associate Professor Takuo Tanemura to point out some basic but critical problems in my research.

Special thanks to the cooperating company to support my work.

Besides, I could not have finished my work without great friendly help from many people, including Assistant Professor Hassanet Sodabanlu, Assistant Professor Yunpeng Wang, Assistant Professor Kentarou Watanabe, Assistant Professor Masanori Kubota and Assistant Professor Akio Higo. The help from some other people also enabled me to work smoothly, including Mr. Hongbo Wang, Mr. Manish Matthew, Ms. Kayo Koike, Mr. Akihiro Nakamura and all members of Nakano-Sugiyama-Tanemura Laboratory.

I should also give my most sincere thanks to the doctors and nurses in The University of Tokyo Hospital who offered me the best medical treatment and help me to recover from the illness quickly. They always make people warm like the sunshine in winter. Another group of people who I have to show my great appreciation to are my friends who were also chasing their dreams here for that they looked after me very carefully when I could not move on the bed in the hospital.

Last but not least, I would like to say “thank you” to convey my deepest love and gratitude to my parents and my wife and other families. They are always my endless source of power to go through any happiness and difficulty in the life. In the end, there are some

special words to my beloved wife, thank you for coming to my life, lighting it and enlightening me.

Cai Liu

Tokyo, September 2014

# Abstract of Dissertation

Stress and quality engineering of GaN growth on Si with in-situ wafer curvature analysis

（In situ ウエハ曲率解析によるシリコン上窒化ガリウム成長における応力・結晶品位の制御）

劉　才

This work has been devoted to the clarification of basic growth mechanism of GaN on Si employing AlN buffer layer and AlN interlayers, including the stress behavior of both GaN and AlN layers as well as the influence of AlN buffer and interlayers on the quality of GaN, based on the in-situ curvature monitoring and other characterizations. The unique points of this work are as follows.

(1) A model of ideal AlN interlayer to induce compressive stress in GaN layers has been proposed, based on systematic in-situ curvature monitoring and morphology observations. This model has pointed out the key features that ideal AlN interlayer should possess, which are small lattice constant close to neutral AlN and high-quality coherent upper interface of it. In most of the cases small lattice constant of the interlayer demands relaxed lower interface of it.

(2) A routine of arbitrary wafer bow design has been discovered and a program to realize it has been produced. Prior to applying this routine, the strain and stress states in every individual AlN and GaN layer under certain growth conditions should have been known. After setting the mechanical properties of AlN and GaN layers, arbitrary wafer bow design is available. This routine was put forward for the first time.

(3) Prototypes of innovative AlN interlayers have been invented and tested, following the model of ideal AlN interlayer. They are one-step pulse-injection method AlN IL, two-step low-temperature/pulse-injection AlN IL and two-step low-temperature/high-temperature AlN IL. All the interlayers employed in previous studies were one-step conventional AlN. These new AlN ILs grown by special methods or with special structure have proved the reliability of the ideal AlN IL model and are induced larger compressive strain in GaN than normal conventional AlN ILs.

The work flow started with demonstration of successful GaN growth on Si (111) substrate by clearing all obstacles. Following the sample structure, conventional AlN buffer layer and AlN interlayer were investigated successively, including their growth conditions, stress introduction in overlying GaN and influence on GaN quality. Then based on the in-situ curvature monitoring data, strain states in every layer were analyzed and model of ideal AlN interlayer and a routine of arbitrary bow design were proposed. In the end, three prototypes of innovative AlN interlayer were designed and tested.

The most important benefit of GaN-on-Si is cost reduction by using Si substrate and the advantages of combining nitrides and silicon. The basic difficulties of the growth of GaN on Si lie in the large lattice constant mismatch (~ 17%) and thermal expansion coefficient

mismatch (~ 54%) between them. This work aimed at understanding and clarifying the stress control mechanism and the roles of AlN buffer layer and AlN interlayers in the growth of GaN on Si.

The most serious difficulties included Si melt-back, Si surface nitridation and the stability of growth environment inside the reactor. There were many factors to facilitate Si melt-back, such as the adsorption of H atoms and cleanliness of Si surface, Ga contamination on Si surface from the parts in the reactor prior to the growth of AlN buffer layer, and most importantly the quality of AlN buffer layer. Ga contamination can be eliminated by using clean liner tube and susceptor parts, or AlN coating of the inner of reactor. Nothing was working to stop Si melt-back if the AlN buffer quality was poor. Finally, after changing for new gas purifiers, AlN buffer quality was improved significantly and Si melt-back was eliminated. Nitridation of Si surface was avoided by pre-flowing TMAl source, 10 s under flow rate of 22 sccm. Proper TMAl pre-flow also improved the GaN quality substantially. The chemical environment inside the reactor should be kept to be constant to yield controllable growth. The most important point was deposited GaN or Ga should be covered since they may cause Ga contamination on Si surface. Therefore, AlN coating or AlN dummy growth should be performed prior to every growth of GaN on Si.

Curvature can be adjusted by tuning the quality of AlN buffer layer which determines the stress in the 1$^{st}$ GaN, changing the growth conditions and the number of AlN interlayers, and tuning the growth mode and thickness of the 1$^{st}$ GaN. AlN buffer layer is important for both of the strain and quality of the 1$^{st}$ GaN. The AlN buffer with higher quality caused more compressive strain in the 1$^{st}$ GaN. It was initially compressively strained. The strain transited from being compressive to tensile as the thickness increased. However, the relaxation speed was depending on the growth conditions and quality of AlN buffer layer. The relaxation was very rapid and the critical thickness from being compressive strain to tensile was only several hundreds of nanometers, if the AlN buffer quality was low, such as grown at 1000 ℃. This was because of high-density defects in AlN buffer propagated into or caused more dislocations in overlying GaN and led to more rapid relaxation in GaN. The best AlN buffer layer which induced most compressive strain was grown at 1250 ℃, under V/III ratio of 3005 and with thickness of 110 nm. Growth conditions of conventional one-step AlN interlayers were studied intensively, including thickness from 4.5 nm to 45 nm, growth temperature from 600 ℃ to 1200 ℃ and V/III ratio from 115 to 9015. Optimized AlN interlayer which induced the most compressive strain in GaN was grown at 900 ℃, under V/III ratio of 1503 and with thickness of 9 nm. If it was too thin, it consisted of neighboring separated grain domains. In too thick AlN IL, cracking occurred. Both lost the capability of inducing compressive strain in GaN. If the growth temperature was too low like 600 ℃, although with smaller lattice constant, since it was amorphous and not coalesced, the GaN on it relaxed rapidly. In high-temperature (> 1000 ℃) ones, Ga diffusion into the interlayer happened, formed AlGaN with lattice constant more close to GaN and then small compressive strain in GaN. V/III has minimal influence on the performance of AlN IL if it was in the range from 500 to 1500. A model of ideal AlN IL was proposed based on the observations, with relaxed incoherent lower interface and high-quality coherent upper interface.

Based on the review of stress generation mechanisms in heterostructure, methodology of analysis was built. The tensile strain of AlN buffer layer ranged from 0.25% to 0.5% while the ideal misfit strain of AlN on Si is about 23.2%, which indicates that AlN buffer on Si is almost completely relaxed. The tensile strain decreases as the growth temperature is elevated. Such relaxation is favorable to stressing overlying GaN more compressively. Depending on the growth conditions of AlN buffer layer, the relaxation speed from compressive (~ -0.45%) to tensile strain (~ 0.05%) differs in the 1$^{st}$ GaN. The thickness of neutral point is only about 600 nm if the quality of AlN buffer is poor such as grown at 1100 ℃. On the best AlN buffer, compressive strain through the large thickness of 1.75 um can be maintained. In spite of smaller lattice constant between AlN and GaN, tensile strain in AlN interlayers is much higher than that in AlN buffer, which ranges from 1.45% to 1.9%. The relaxation was in the range from 22% to 42%, which is about only one third of that in AlN buffer. These results show that the crystal quality of AlN interlayers is better than that of AlN buffer layer. The largest compressive strain in GaN layers is about 0.45% on AlN interlayer grown at 900 ℃ and with thickness of 9 nm, which is the same of the initial value of the 1$^{st}$ GaN. This leads to compressive stress of about 2 GPa in GaN and is 2~3 times of that in previous publications. Curvature due to thermal stress was also calculated. Based on the strain and stress states in every individual stage, the curvature curve can be recovered and the final curvature and wafer bow can be predicted, using the arbitrary bow design program. The size of Si wafer which the curvature and wafer bow is easiest to be controlled is 6 inch, 150 mm.

Quality elevation of AlN buffer layer and 3D growth mode are the most effective methods to improve the quality of GaN. The same with compressive stress introduction in the 1$^{st}$ GaN, it also demands high-quality AlN buffer layer to produce high-quality GaN, since the defects in the buffer can propagate into overlying GaN and they can also act as defect sources to generate new dislocations in GaN. Using conventional AlN, higher quality is achieved at higher temperature, 1250 ℃ in this work, under mediate V/III ratio of 3005. By alternating growth mode from 2D to 3D, the FWHM of XRD rocking curves of the plane (10-10) reduced from 820 arcsec to 570 arcsec while that of (0002) plane keeps almost constant. Thick AlN interlayer (≥ 22 nm) is favorable to the reduction of dislocations in GaN, but not for stress inducing. Since it doesn’t coalesce completely, thin AlN IL (< 13 nm) increase the dislocation density in GaN by introducing new defects at the grain domain boundaries. Blue LEDs has been demonstrated.

Concepts of innovative prototypes of AlN interlayers were designed and tested, including one-step pulse-injection method AlN IL and two-step IL consists of lower low-temperature AlN and upper pulse-injection AlN or high-temperature AlN. In the structure of LT/HT-AlN, the growth temperature of HT-AlN higher is better such as 1200 ℃, with optimal thickness around 6 nm. They confirmed the solidity of ideal AlN model and showed the same performance of the best conventional AlN. For that the growth conditions of them were not optimized, more compressive strain in overlying GaN on them can be expected.

# Content

# 1 Introduction

Motive force, basic growth problems and status for the research of GaN-on-Si will be given in this chapter. Based on it, the motivation and target of this work would be proposed. By enumerating the demand of modern society and material advantages of nitrides and silicon, the motive force for the field of GaN-on-Si was introduced in section 1.1. Basic growth difficulties were given in 1.2. Research status from both the industry and academic communities was reviewed in 1.3. In the end of this chapter, motivation and content of this work was outlined.

## 1.1 Why GaN-on-Si?

Information and energy are almost the hottest topics in our modern society. This is a time that human beings are producing data in one hour more than in centuries hundreds years ago. Be confronted with explosive data, traditional electronic devices based on silicon cannot satisfy the present huge demand for massive high speed data storage, transmission and processing, with high energy consumption. In order to elevate the processing speed and lower the unit energy consumption per bite, people are working hard to transmit and process information using photons as carrier rather than electrons. Compared with electrons, movement of photons can be much more speed and energy efficient. III-V materials are the best practical option for optical and photonic devices due to their fantastic optical and electric properties, but of limited material resource and high cost. However, due to the advantages of resource abundance, well-developed growth and processing technologies, large size silicon wafer is very cheap and large scale fabrication on it can be done readily. This might be the driving force for both academic and industry communities to make a great investment in the field of incorporating devices based on V-III materials with silicon, to make photonic devices and circuits more powerful, cheaper, energy efficient and more environment-friendly. Nitrides-on-silicon is one of the most important branches of it.

On the other hand, in 2013, fossil energy source still supported more than 90% of the annual total energy consumption of the world [1]. Oil, natural gas and coal, which are the fossil energy family, can only serve the human society for about 53 years, 55 years and 230 years respectively [2]. No much time left for people to explore new energy which can play the role of present fossil energy in the future. People are showing great expectation of producing electricity from sunlight. Photovoltaic technology is a very promising method to realize it. Both silicon and nitride are fantastic materials for the fabrication of solar cells and harvesting sunlight.

Specifically, both silicon and nitrides are of fantastic material properties.

Silicon is the cornerstone of modern society. With mediate band gap value of 1.11 eV at room temperature and easy growth and doping process, it has been applied for producing electronic chips and solar cells from 1960s. For the information industry, almost all electric chips and processors were made from it. For the field of solar electric power generation, solar cells based on silicon hold the largest market share. To satisfy the enormous material consumption, harsh crystal quality requirement for making electronic devices, and to lower the cost by large-scale production, low price and high quality single crystal silicon wafer with large size up to 18 inches is available now [3]. Price is the most important competitiveness of it. In addition to the most developed crystal growth technology, the process technology for silicon is also the most mature. This is why people are working hard to incorporate V-III devices on the basis of existing advantages of silicon. Also, for its high crystal quality, well-developed processing technologies and low cost, silicon-based solar cells held the photovoltaic market share of about 90% in 2013 [1].

III-nitride is a fantastic material family, represented by gallium nitride (GaN). They are of direct energy band-gap ($E_g$) which ranges from 6.2 eV (aluminum nitride, AlN) to 0.7 eV eV (indium nitride, InN). Such a direct and wide $E_g$ range covers photon energy from deep ultra-violet, solar spectrum and far ultra-red spectrum [4]. With mediate $E_g$ of 3.4 eV and lattice constant of 3.189 Å between AlN and InN, as well as relatively easier growth, GaN comes to be the template material for the growth of other nitrides and devices made from them. AlN, InN and GaN of course, as well as their ternary compounds compose the active region of nitride devices. The direct band-gap makes it suitable for high electron mobility transistors (HEMT) [5], with electron mobility ($\mu_e$) of 900 $cm^2/V{\cdot}s$ for GaN. The very large band-gap makes nitrides can meet the market demand of two big field, which other material cannot do. First is the market of blue and ultra-violet light emission diodes (LED) and laser [6], using the ternary compound like AlGaN and InGaN as active layers. The other one is the market of devices working under high power or high temperature, such as high power switches. Take GaN as an example, thanks to its $E_g$ of 3.4 eV, the breakdown field of the devices makes from it could be as high as $3.3\times10^6$ V/cm which is about 10 times of that of Si and gallium arsenide (GaAs). The working temperature of them could be as high as 400 ~ 500 ℃. The direct and large band gap, the large band-gap off between nitrides and some other outstanding properties lead them to be the most appropriate candidate for fabricating the very high frequency [7] all-optical switches and photon detectors by applying multi-quantum well (MQW) or super-lattice (SL) structures [8]. InGaN with band-gap from 3.4 eV to 0.7 eV is an ideal material for high efficiency solar cells because it can cover the entire solar spectrum, although currently it is still hard to tune the indium content and band-gap freely [9]. Benefited from such great band-gap tunability, amazingly, monolithic white LED has been achieved without applying phosphor powder [10]. At present, the most dominant product of nitride device market is semiconductor LED, which is called as the fourth generation of lighting technology and much more energy efficient.

However, even with such broad application prospects, the basic difficulty hinders the development of nitride devices is that it is not easy to grow high quality nitride films, especially AlN and InN, as well as their alloys with GaN. This often causes the performance of fabricated devices is much lower than theoretical prediction. Besides this, the cost is also

another critical factor to limit its development and application in the market. The lack of cheap and large size lattice matching substrate for the epitaxy of nitrides is one of the main causes for both of the growth difficulty as well as the high cost. GaN is the only substrate available for nitride homo-epitaxy with very high price and small size less than 4 inches of diameter. Among substrates for hetero-epitaxy, SiC and ZnO are of the smallest lattice constant mismatch of 3.3% and 2.1% respectively. Like GaN free-standing wafer, their price is also very high and the size of them cannot be large. Currently, sapphire ($Al_2O_3$) is mostly being used for GaN epitaxial growth. The cost of wafer can be reduced by 90% by increasing procedure scale which is limited by the size of sapphire wafer.

**Table 1.1** Basic properties of GaN, Si, and GaAs [11].

| Material | $E_g$ | $\varepsilon$ | $\mu_e$ | $E_c$ | vs | $\kappa$ | JFM | KFM | BFM | BHFM |
|---|---|---|---|---|---|---|---|---|---|---|
| | eV | | $cm^2/V\cdot s$ | $10^6$ V/cm | $10^7$ cm/s | W/cm·K | $Ecvs/\pi^2$ | $\kappa(vs/\varepsilon)^{1/2}$ | $\varepsilon\mu Ec^3$ | $\mu Ec^2$ |
| **Si** | 1.1 | 11.8 | 1350 | 0.3 | 1.0 | 1.5 | 1 | 1 | 1 | 1 |
| **GaAs** | 1.4 | 12.8 | 8500 | 0.4 | 2.0 | 0.5 | 7.1 | 0.45 | 15.6 | 10.8 |
| **GaN** | 3.4 | 9.0 | 900 | 3.3 | 2.5 | 1.3 | 760 | 1.6 | **650** | 77.8 |
| **6H-SiC** | 3.0 | 9.7 | 370 | 2.4 | 2.0 | 4.5 | 260 | 4.68 | 110 | 16.9 |

The initial motivation to grow nitrides on silicon was to reduce the cost of nitride devices. In order to reduce the cost of LEDs further substantially, GaN-on-Si composite substrate for the growth of LEDs and other devices has been proposed since a decade ago [12]. As shown in Table 1.2, as a substrate for the growth of nitrides, there are some distinctive advantages with silicon. As mentioned above, the most attractive superiority of silicon is low cost, large size and the best crystal quality, benefited from the relatively easy and most developed growth technology. The cost of silicon is only one fourth of that of sapphire (2 inches). From the industry it shows that the cost reduction for wafer can be as high as 75% from 2’’ sapphire to 200 mm silicon [13]. The large size of silicon wafer up to 12 ~ 18 inches could be helpful to reduce the cost of products by expanding the product scale. Wafers with such large size for GaN, SiC or ZnO are nearly impossible. Another unique character for silicon is that it is conductive. This merit may simplify the structure of devices like LEDs by adopting vertical current flow structure, other than lateral structure for the devices on sapphire which suffers much larger resistance and more complicated fabrication processes. Additionally, hardness of silicon is much lower than other wafers, which also facilitates the dicing process and fabrication. These are the main but not all the attractive points of silicon as the substrate

**Table 1.2** Comparison of substrates for epitaxy of GaN [14]

| Substrate | $\Delta a$ | $\Delta\alpha$ | Cost | Size | Transparency | Hardness | Scalability | Overall |
|---|---|---|---|---|---|---|---|---|
| | % | % | | inch | | | | |
| **Si/GaN** | 18 | 54 | ◎ | 2-18 | × | O | ◎ | ◎ |
| **$Al_2O_3$/GaN** | 17 | 17 | O | 2-6 | O | ◎ | O | O |
| **SiC/GaN** | 4 | 36 | Δ | 2-3 | O | ◎ | × | Δ |
| **GaN/GaN** | 0 | 0 | Δ | 2 | O | ◎ | × | Δ |

for the epitaxy of nitrides. After growth, nitride devices could be incorporated into integrated circuits based on silicon.

The role of silicon in the combination with nitrides cannot be only the substrate, but also the active region, with combining the merits of both of them, for example, high efficiency multi-junction solar cells. Because indium content in InGaN cannot easily be high enough to achieve $E_g$ around 1 ~ 1.2 eV [15, 16], for the application of InGaN in multi-junction solar cells, other material should be introduced to absorb lower energy photons, and InGaN/Si could be one of good combinations. The theoretical efficiency of InGaN/Si two junction solar cells could be as high as 31% [17]. However, again, growth is the problem. Direct growth of GaN or InGaN on silicon is impractical [18] and could be only realized under some extreme conditions with very poor quality [19].

Based on the above discussion, the direct and primal motivation of GaN-on-Si is to lower the cost of nitride devices, with the big background that fabricating V-III optical devices on Si. Heterostructures combining and utilizing the material merits of both nitrides and Si is another attractive emerging field of research.

GaN template growth on silicon substrate is the first step and base for the following device structure growth and fabrication on it. The current research and development from the industry of GaN-on-Si technology is specially designed and mainly targeting the market of LEDs, due to that LED is the only popular practical product made from nitrides in the market at present. In the academic community, the research of GaN-on-Si is not limited to the application of LEDs only, but for basic scientific understanding and universal usage, such as HEMT, field effect transistors (FET) and so on. As will be shown in the following chapters, GaN template growth on silicon should be specially designed depending on the device structure on it.

## 1.2 Basic difficulties

**Table 1.3** Lattice constant at room temperature and the average thermal expansion coefficient for Si, GaN and AlN respectively.

| **Properties** | **Si (111)** | **GaN (0002)** | **AlN (0002)** |
|---|---|---|---|
| **Lateral LC a** (Å) | 3.840[a] | 3.189 | 3.112 |
| **LC mismatch ($\Delta a/a_{Si}$)**[b] | - | 16.9% | 19.0% |
| **TEC α** ($\times 10^{-6}$/K) | 2.59 | 5.59 | 6.43 |
| **TEC mismatch ($\Delta\alpha/\alpha_{GaN}$)** | -53.7% | - | 15% |

a: Lattice constant of Si is $a_{(100)}$ = 5.431 Å, $a_{(111)}$ = 5.431/$\sqrt{2}$ = 3.840 Å.

b: lattice constant mismatch calculation method is $\epsilon = \frac{a_s - a_f}{a_s} \times 100\%$.

GaN-on-Si growth by metal-organic vapor phase epitaxy (MOVPE) has been studied for a decade [12]. For the GaN growth on silicon, the most important two basic difficulties are stress control and quality enhancement. People have invested most of their time into how to

control the stress during and after growth to avoid cracking. Due to large lattice constant (LC) mismatch (~ 17%) and thermal expansion coefficient (TEC) mismatch (~ 54%) between GaN and Si, after cooling down, GaN suffers huge tensile stress and cracks easily. Achieving high quality of GaN on Si is also not straightforward. The stress in the epitaxial films would cause bowing of the substrate. Curvature measurement is for monitoring wafer bowing, the smaller absolute curvature value means less bowing. Wafer bowing close to zero is the ideal case for crack-free GaN. The large lattice constant difference causes very high dislocation density in epitaxial GaN about $10^{10}$ $cm^{-2}$ [20]. In this section, basic difficulties of growing GaN on Si caused by the huge lattice constant mismatch and thermal expansion coefficient mismatch would be reviewed.

### 1.2.1 Lattice constant mismatch

Lattice constant mismatch $\Delta a$ affects hetero-epitaxial growth through two aspects, growth stress $\sigma_g$ and defect introduction $\rho_d$. $\sigma_g$ and $\rho_d$ are directly proportional to $\Delta a$.

The stress caused by lattice constant mismatch strain $\varepsilon_{LC}$ is the main part of intrinsic stress, and could be expressed quantitatively. If the epitaxial film is completely strained by the substrate, the lattice constant mismatch strain $\varepsilon_m$ is defined as follows

$$\epsilon_m = \frac{a_s - a_{f0}}{a_{f0}} \tag{1-1}$$

$a_s$ is the lateral LC of the substrate, $a_{f0}$ is the natural lateral LC of the epitaxial film. If the film is not completely strained, the strain $\varepsilon$ and stress are defined as

$$\epsilon = \frac{a_f - a_{f0}}{a_{f0}} \tag{1-2}$$

$$\sigma = M \cdot \epsilon \tag{1-3}$$

respectively. $a_f$ is the strained lateral LC of the film. Eq. (1-3) is Hooke's law and $M$ is the elastic modulus of the film. In fact, generally, films are not completely strained by the substrate due to that it is usually not completely epitaxial. In addition, lattice constant is not constant, but dependent on temperature, as shown in Fig. 1.1. Both GaN and Si expand as the

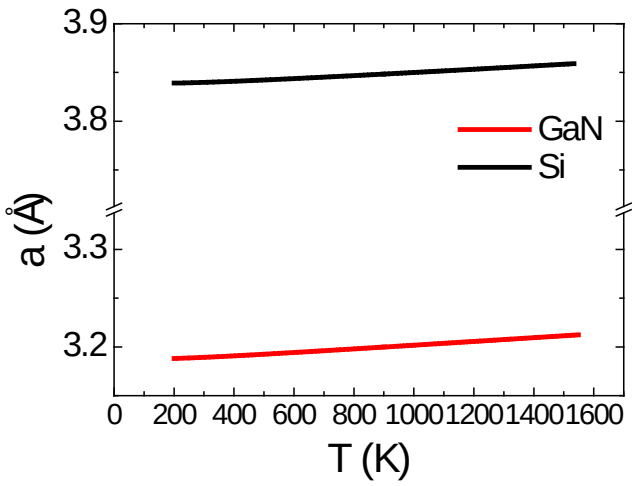


**Fig. 1.1** Temperature dependent lattice constant of GaN and Si.

temperature rises, but with different expanding rate, namely expansion coefficient. Expanding rate of GaN is larger than that of silicon, so the mismatch strain decreases as temperature increases, as shown in Fig. 1.2. For that the lateral lattice constant of GaN $a_{GaN}$ is always smaller than that of silicon $a_{Si}$, if GaN is grown directly on Si, it would suffer tensile stress $\sigma_{tensile}$ which could be as high as 92 GPa as calculated in Fig.1.2. This pressure is incredibly high. The pressure at the bottom of Mariana Trench in the Pacific, deepest location in the seas on the earth, is about 110 Map. The theoretical pressure in ideal GaN film on Si can be 900 times of that at the bottom of Mariana Trench. According to mechanics in thin film [21], the membrane force $f$ would be accumulated higher and higher as it grows thicker, and after some critical value, cracks in GaN will occur. In order to overcome or compensate the tensile stress, a solution is to introduce some other layers, such as AlN, with lateral LC smaller than that of GaN and induce compressive stress in it.

Another drawback of large lattice mismatch is high defect density introduction. During heteroepitaxial growth, the strain and stress caused by lattice mismatch could be partially relaxed by the generation of dislocations if the thickness of epitaxial layer exceeds some critical value [22, 23]. Dislocation density $\rho_d$ is proportional to the lattice mismatch $\epsilon_m$. For example, threading dislocation density stemmed from the glide of half-loops can be estimated by

$$\rho_d = \frac{\epsilon_m}{L_{ave} b \cos\alpha \cos\phi} \tag{1-4}$$

where $L_{ave}$ is the average length of misfit segments, $b$ is the length of the Burgers vector, $\alpha$ is the angle between the Burgers vector and line vector, and $\phi$ is the angle between the interface and normal to the slip plane [23]. In the case of GaN growth on Si, without proper quality control, the dislocation density usually can be as high as the order of magnitudes of $10^{10}$ cm$^{-2}$ [24]. Consequently, large lattice mismatch between nitrides and Si requests people to make special great endeavor to achieve high quality of GaN.

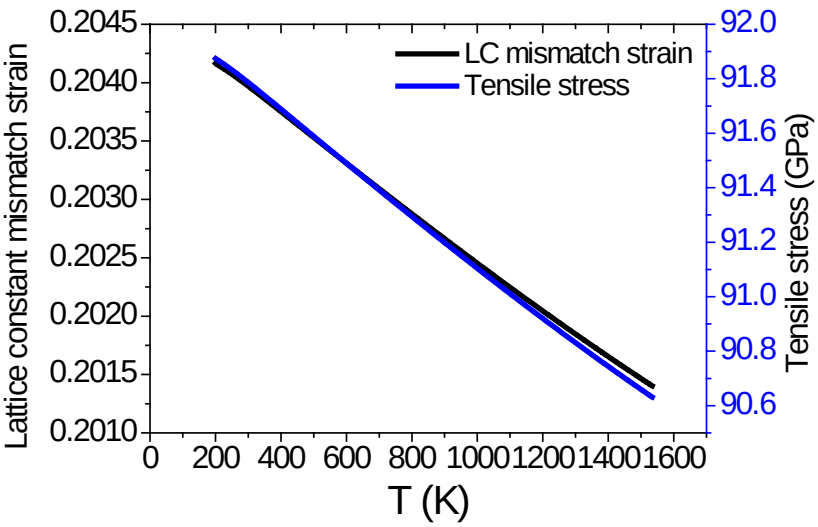


**Fig. 1.2** Temperature dependent lattice constant mismatch strain $\epsilon_m$ between GaN and Si and the tensile stress in GaN on Si.

### 1.2.2 Thermal expansion coefficient mismatch

Thermal expansion coefficient (TEC) mismatch causes thermal mismatch stress in heterostructure. Stress arises in hetero-multilayer when temperature ramps, for example temperature ramps during growth and cooling down after growth. Due to TEC difference, layers would expand or shrink with different rates and cause the change of LC mismatch. The case of GaN on Si is shown in Fig. 1.2. TEC is also not constant but dependent on temperature. As plotted in Fig. 1.3, the temperature dependent TEC of GaN is always higher than that of Si. Consequently, the LC difference between them decreases as temperature rises.

$$\epsilon_{Th} = \int [\alpha_s(T) - \alpha_f(T)] dT \tag{1-5}$$

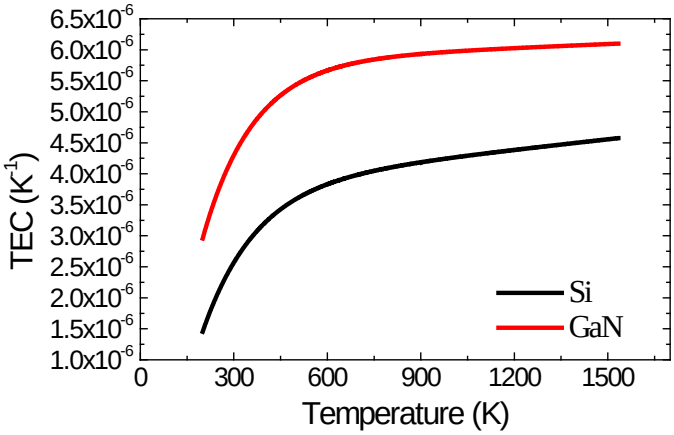


**Fig. 1.3** Temperature dependent thermal expansion coefficients of GaN and Si.

Thermal stress problem for GaN growth on Si occurs after growth during cooling down. Due to larger TEC than Si, lattice of GaN shrinks faster and more than that of Si, then tensile thermal mismatch stress emerges at GaN. Using Eq. (1-5), the tensile strain occurs in GaN on Si when the temperature decreases from the growth temperature of GaN at 1300 K to room temperature of 300 K is 0.001755 and the tensile stress could be about 0.79 GPa. But in the real case, bowing caused by thermal mismatch stress is much more significant than that of

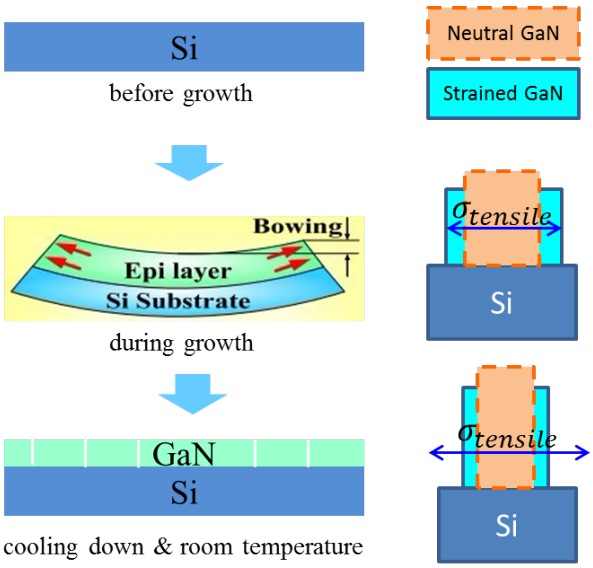


**Fig. 1.4** Schematic diagram of wafer bowing during growth and GaN cracking during cooling.

intrinsic stress caused by LC mismatch stress. Usually, cracking doesn't happen during growth but during cooling, as illustrated in Fig. 1.4. Viewed from the point of thermal expansion coefficient, if we want to compensate the tensile stress between GaN and Si during cooling down, some material with TEC smaller than that of Si is needed to be inserted in between GaN layers. Unfortunately, such material is hardly available using MOVPE.

In conclusion, the core of the difficulty for GaN growth on Si is tensile stress arises from both of the lattice constant mismatch and thermal expansion coefficient mismatch. The tensile stress is too large that causes cracks in GaN. The work have to do is how to introduce compressive stress to compensate it. As summarized in Fig. 1.5, people can apply some material with LC smaller than GaN to induce compressive stress at GaN layers, or with TEC smaller than Si to produce compressive stress during cooling down. From the discussion above, the only practical route is the former one. AlN is a good candidate. From the calculation in chapter 4, the ideal thermal tensile stress in GaN caused by cooling is around 0.8 GPa. In the structure consists of AlN buffer layer and interlayers, compressive stress is dominantly induced in GaN layers overlying on AlN interlayers and the sum of their thickness is roughly half of the total GaN thickness. As a result, the compressive stress in GaN on AlN interlayers should be larger than 1.6 GPa. On the other hand, quality improvement of GaN is also not straightforward. High quality buffer layer, 3D growth mode and masking and so on can be useful strategies to improve the quality of GaN.

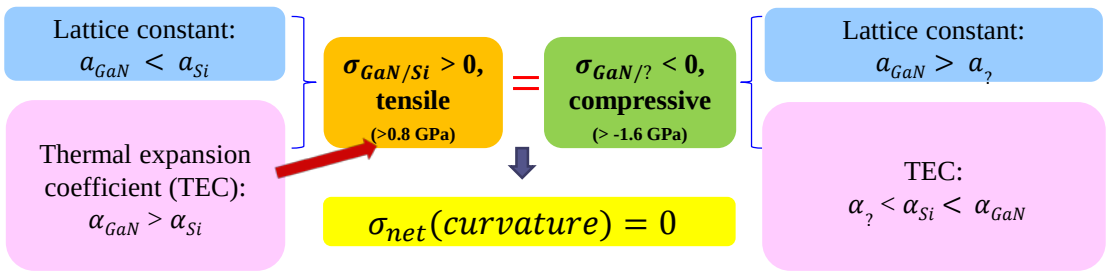


**Fig. 1.5** Summary of the core of GaN-on-Si and possible corresponding strategies.

## 1.3 Status

The research of GaN-on-Si started from the beginning of 2000s [25]. Because GaN cannot grow directly on silicon due to the alloy react between gallium and silicon. AlN is the first step and buffer layer for the growth of following layers. Inserting AlN interlayer (IL) into GaN is the first and simplest solution applied to tune the stress state in GaN [26]. Later some institute applied thick AlN/GaN super-lattice [27] or grading $Al_xGa_{1-x}N$ [28] following AlN buffer layer to control the tensile stress in GaN, without inserting AlN ILs.

GaN-on-Si is called as the future wafer. It has attracted intensive research from the industry and now the investment is still increasing, including Aixtron, Azzurro, TOSHIBA, Samsung, TOWA, imec, OSRAM and some of them are capable of supplying 8-inch GaN-on-Si wafer. They are aiming at the market of MOVPE systems and LED. GaN with thickness more than 10 um is mandatory to obtain device level quality with full width at half

maximum (FWHM) of X-ray diffraction (XRD) rocking curve around 280 arc sec for (0002) plane. This leads to very long growth time for one wafer (> 4 hours), which is not preferable for the industry and there is still plenty of room for improvement. However, the detailed growth and stress control mechanism is still not yet clarified properly or being hidden, especially the stress evolution during growth.

From the academic community, there are still lots of problems yet remains to be researched. Pioneering work is reviewed here briefly and will be introduced in detail in next chapters. The optimal growth condition for AlN layers is confidential and still in dispute.

(1) AlN buffer layer is the base for following layers and plays a critical role. People have studied the properties of GaN on AlN buffer layers grown under various conditions on Si [25, 29-37]. Most of them just related the growth conditions of AlN buffer layer to the performance of overlying GaN and try to figure out the optimum condition for AlN buffer, especially for the buffer layer consists of AlN and AlGaN multilayers. The adopted condition is not wide enough to cover the range which can yield better result. For example, the growth temperature for AlN buffer mostly was up to 1100 ℃, which actually could be higher. Very few work mentioned the stress evolution in AlN buffer layer and the overlying GaN which is very important and essential to understand the behavior of epi-layers. Raghavan et al investigated the stress in AlN but the growth condition is not optimal and cannot cover all the ranges [32]. Generally there are three types of structures for stress control in GaN-on-Si, as represented in Fig. 1.6. Type 1 is the mostly applied since it is the simplest and represents the basic principle of stress control as well as the role of AlN layers.

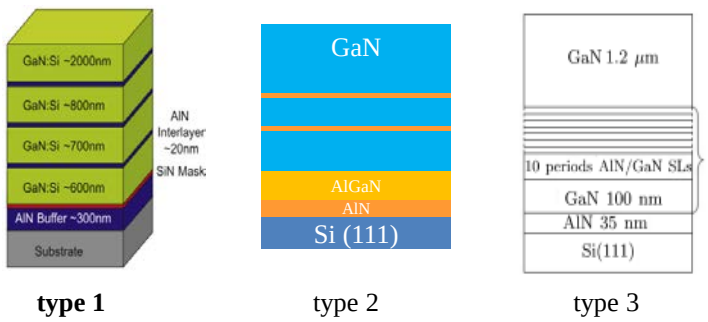


**Fig. 1.6** Types of previously studied structure of GaN-on-Si, type 1 (mostly applied): AlN buffer and AlN interlayers [38]; type 2: AlGaN/AlN composite buffer layer with or without interlayers [39]; type 3: AlN buffer layer and AlN/GaN superlattices intermediate layer [27].

(2) AlN IL is the main force to introduce compressive stress to GaN layers. The role and growth condition of AlN ILs is much more complicated than that of AlN buffer layer, since it is very thin (~ 10 nm) and much more vulnerable to growth conditions, so that people invested much effort working on it [20, 26, 40-49]. People investigated its effects on following GaN on it. They prefer to use low-temperature AlN IL and found that it has a separating effect in between neighboring GaN layers. But in fact the optimal growth temperature for AlN ILs is not necessarily low. Their adopted conditions including growth temperature, thickness and V/III ratio were not proper to understand the role of AlN IL fully in depth. Especially the direct TEM observation of AlN ILs and the interfaces at them was very less to understand the relaxation mechanism at themselves and GaN layers on them. It is mandatory to observe the

generation and propagation of dislocation at AlN ILs and through the whole structure. The morphology and misfit dislocation generation at AlN/GaN interfaces is critical to clarify the relaxation processes. The behavior of AlN ILs is far from being well understood and there is still large space to improve the performance of AlN ILs. People have no idea about what is ideal AlN IL.

(3) In the past publications, there was little data of in-situ curvature observation, which is the most accurate, direct and efficient way to access the stress and relaxation behavior of each individual layer. Without in-situ observation, it is hardly possible to know about stress transition directly in every individual layer, the relationship between stress introduction and quality and growth conditions. The ability of AlN ILs grown under various conditions to introduce compressive stress in overlying GaN cannot be accessed neither without in-situ observation. Otherwise people have to evaluate it by ex-situ methods like XRD or curvature measurement after growth, which may easily introduce considerable error if the sample is not delivered carefully.

(4) Quantitative theoretical analysis on stress evolution during growth and cooling also has not yet been done. Physics behind stress evolution and defect propagation is not completely clear. However, such knowledge is critical to allow us to design GaN-on-Si with any desired bowing for any device application freely as well as to simplify sample structure and shorten growth time as much as possible. A model for arbitrary wafer bow prediction and curvature simulation is not available. There are very few data about the compressive stress in GaN $\sigma_{cGaN}$. The limited previous results were summarized in Fig. 1.7a. The desired ideal $\sigma_{cGaN}$ is > 1.6 GPa and most of them were much lower than that then could not maintain the stress balance in the system. GaN quality was also much lower than that on sapphire.

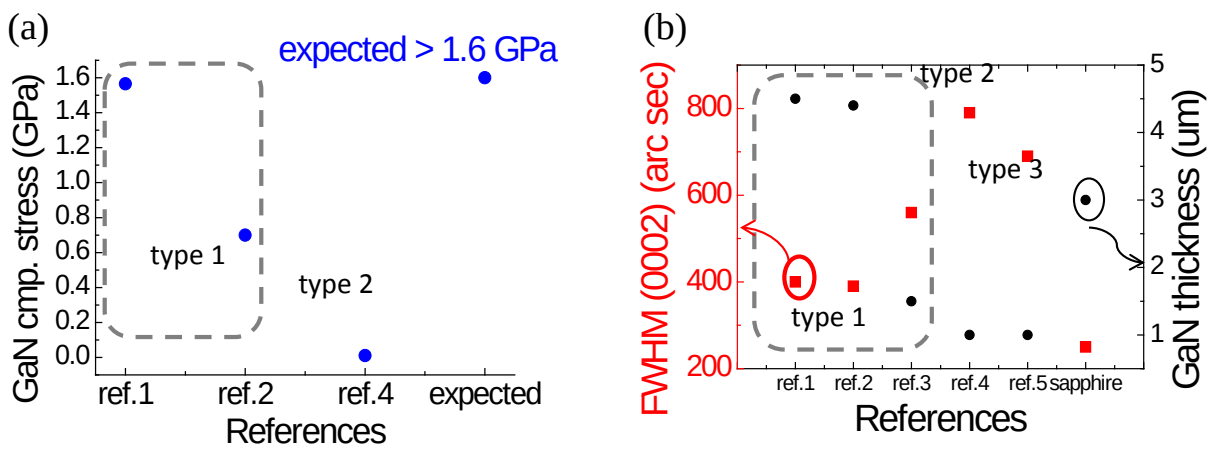


**Fig. 1.7** (a) compressive stress in GaN layers and (b) FWHM of XRD rocking curves of GaN-on-Si from the references*.

*ref.1: [49], ref.2: [38], ref.3: [46], ref.4: [50], ref.5: [51].

## 1.4 Motivation and targets

As reviewed in the previous section, for the MOVPE of GaN-on-Si, there are still some remaining problems to be researched. The content and targets of this dissertation are listed as follows.

(1) This work is devoted to understanding the growth mechanism of GaN on silicon, including stress control mechanism and quality effects. In detail, it involves the role of AlN buffer layer and AlN ILs, the strain and relaxation process in AlN layers and GaN layers on them, and their stress and quality effects on overlying GaN. One of the targets is to produce AlN interlayers which can induce compressive stress > 1.6 GPa in GaN.

(2) The second target is to build a model to design any desired wafer bow and simulate the in-situ curvature curves based on theoretical strain and stress analysis of each layer, through every stage of a growth.

(3) The third is developing new novel AlN ILs, which can introduce compressive stress in GaN more efficiently than conventional single-layer low-temperature AlN IL.

To achieve the targets above, in this research, the simplest structure is adopted to understand the growth behavior and build a model. As shown in Fig. 1.8, this structure starts with AlN buffer layer, and is followed by 1st-GaN, then several AlN ILs are inserted into GaN, and finally it ends with a thick top GaN layer. The strategies or originalities to achieve the targets above are as follows.

(1) High resolution 3-wavelength and 3-beam in-situ curvature monitoring is applied to record the curvature transition and stress evolution during growth and cooling down.

(2) Stress and strain relaxation and evolution through AlN and GaN layers is analyzed by combining the data from in-situ curvature monitoring, transmission electron microscopy (TEM), scanning electron microscopy (SEM), and atomic force microscopy (AFM), XRD rocking curve and reciprocal space mapping (RSM). The stress state and the quality of GaN are related to understand the role of AlN layers.

(3) Theoretical analysis of curvature curves are performed to reveal the stress and strain evolution in GaN layers. Thermal stress during growth and cooling is calculated to fit the curvature curves. Mechanical properties of AlN and GaN layers grown under

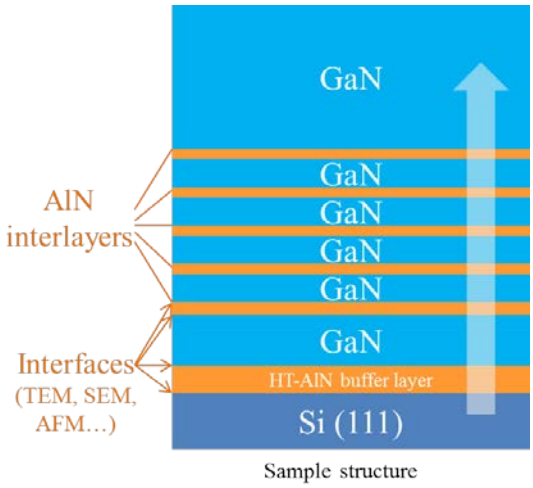


**Fig. 1.8** Sample structure in this work.

various conditions are summarized to build a model to design GaN-on-Si wafer with any bowing.

(4) Based on the idea of ideal AlN IL, original concepts of two-step IL which consists of lower low-temperature AlN and upper high-temperature AlN and pulse-injection AlN IL have been proposed and produced. Two-step AlN IL showed considerable improvement compared with the conventional single-step IL and proved that the assumption of ideal AlN IL was correct.

## 1.5 Synopsis of this dissertation

Experiments start from chapter 2 in this dissertation, with establishing the growth of GaN growth on Si. GaN growth on Si is not straightforward. There are some obstacles to be cleared before successful GaN growth on Si, including the alloying between gallium and silicon, namely Si melt-back, TMAl pre-flowing and AlN dummy growth. In the ambience of hydrogen, GaN cannot grow on Si directly and it reacts with Si, which is called Si melt-back. The causes of Si melt-back were searched including gallium deposition on Si, the quality enhancement of AlN buffer layer. In chapter 3, the effects of AlN buffer layer and AlN ILs on stress and strain evolution and relaxation mechanism at AlN layers and the overlying GaN were observed, by in-situ curvature monitoring, TEM, AFM and so on. The role of AlN buffer layer and ILs in controlling stress grown under various conditions was analyzed and optimal conditions were searched roughly. Based on the experimental results, a model of ideal AlN IL was proposed. Since then people know that what kind of AlN IL is desired to induce compressive stress in GaN layers most effectively. In chapter 4, based on in-situ curvature observation data, the stress and strain transition in every layer during growth and cooling were analyzed theoretically using Stoney equation, including lattice constant mismatch stress and thermal mismatch stress. After summarizing the mechanical properties of AlN and GaN layer grown under various conditions, a model was built to design the final curvature (bowing) of GaN-on-Si wafer. The problem of plastic deformation of Si substrate was discussed as well. 4-um-thick crack-free GaN on Si was achieved and blue LED was demonstrated on it. In chapter 5, the effects of AlN buffer layer and ILs on the quality of GaN were observed. The quality of GaN also has been improved by 3D growth. In chapter 6, based on the model of ideal AlN IL built in chapter 3, new original AlN IL structures and growth methods were proposed and tested, including pulse-injection-method AlN IL, low-temperature/pulse-injection-method combined two-step AlN IL and low-temperature/high-temperature combined two-step AlN IL. They showed promising result and can compressively stress the overlying GaN more efficiently than conventional single-layer low-temperature AlN ILs. In chapter 7, the content of this thesis was concluded. In the end in appendix, void formation by hydrogen etching in GaN and its effects on stress control and quality and optical properties of GaN were investigated.

## References

[1] H.H.G. Limited, *Global New Energy Report 2014*. 2014.

[2] sxcoal.com. *Time limit of available fossil energy*. 2014; Available from: http://www.sxcoal.com/ecology/3786029/showarticle.html.
[3] Wikipedia. *Wafer (electronics)*. 2014; Available from: http://en.wikipedia.org/wiki/Wafer_(electronics).
[4] M. Hadis, *Handbook of Nitride Semiconductors and Devices*. Vol. 1. 2008, Germany: WILEY-VCH.
[5] S. Arulkumaran, G.I. Ng, S. Vicknesh, H. Wang, K.S. Ang, J.P.Y. Tan, V.K. Lin, S. Todd, G.Q. Lo, and S. Tripathy,Direct Current and Microwave Characteristics of Sub-micron AlGaN/GaN High-Electron-Mobility Transistors on 8-Inch Si(111) Substrate, Jpn. J. Appl. Phys. ***51***, (2012).
[6] N. Shuji and C. Shigefusa F, *Introduction to Nitride Semiconductor Blue Lasers and Light Emitting Diodes*. 2000, Boca, Raton, London, New York, Washington, D.C.: CRC Press. 386.
[7] high frequency optical switch THz, (2013).
[8] H. Sodabanlu,Metalorganic Vapor Phase Epitaxy and Fabrication of 1.5 µm GaN/AlN MQWs Intersubband All-Optical Switches, (2010).
[9] A. Yamamoto, M.R. Islam, T.-T. Kang, and A. Hashimoto,Recent advances in InN-based solar cells: status and challenges in InGaN and InAlN solar cells, physica status solidi (c) ***7***, 1309(2010).
[10] M. Mathew, H. Sodabanalu, M. Sugiyama, and Y. Nakano,Orange/yellow InGaN/AlN nanodisk light emitting diodes, physica status solidi (c) ***10***, 1525(2013).
[11] 江川孝志, *LED のための GaN-on-Si 技術*. 2012.
[12] A. Dadgar, M. Poschenrieder, A. Reiher, J. Bläsing, J. Christen, A. Krtschil, T. Finger, T. Hempel, A. Diez, and A. Krost,Reduction of stress at the initial stages of GaN growth on Si(111), Applied Physics Letters ***82***, 28(2003).
[13] 2013; Available from: http://www.azzurro-semiconductors.com/.
[14] W.D. Nix and B.M. Clemens,Crystallite coalescence: A mechanism for intrinsic tensile stresses in thin films, Journal of Materials Research ***14***, 3467(1999).
[15] K.P. O'Donnell, I. Fernandez-Torrente, P.R. Edwards, and R.W. Martin,The composition dependence of the InxGa1−xN bandgap, J. Cryst. Growth ***269***, 100(2004).
[16] F.K. Yam and Z. Hassan,InGaN: An overview of the growth kinetics, physical properties and emission mechanisms, Superlattices and Microstructures ***43***, 1(2008).
[17] L. Hsu and W. Walukiewicz,Modeling of InGaN/Si tandem solar cells, J. Appl. Phys. ***104***, 024507(2008).
[18] A.G. Bhuiyan, A. Mihara, T. Esaki, K. Sugita, A. Hashimoto, A. Yamamoto, N. Watanabe, H. Yokoyama, and N. Shigekawa,MOVPE growth of InGaN on Si(111) substrates with an intermediate range of In content, physica status solidi (c) ***9***, 670(2012).
[19] K. Takemoto, H. Murakami, T. Iwamoto, Y. Matsuo, Y. Kangawa, Y. Kumagai, and A. Koukitu,Growth of GaN Directly on Si(111) Substrate by Controlling Atomic Configuration of Si Surface by Metalorganic Vapor Phase Epitaxy, Jpn. J. Appl. Phys. ***45***, L478(2006).
[20] A. Dadgar, M. Poschenrieder, J. Bläsing, O. Contreras, F. Bertram, T. Riemann, A. Reiher, M. Kunze, I. Daumiller, A. Krtschil, A. Diez, A. Kaluza, A. Modlich, M. Kamp, J. Christen, F.A. Ponce, E. Kohn, and A. Krost,MOVPE growth of GaN on Si(1 1 1) substrates, J. Cryst. Growth ***248***, 556(2003).
[21] L.B. Freund and S. Suresh, *Thin film materials*. 2003: Cambridge University Press.
[22] J.W. Matthews and A.E. Blakeslee,Defects in epitaxial multilayers. I. Misfit dislocations, Journal of Crystal Growth ***27***, 118(1974).
[23] J.E. Ayers, *Heteroepitaxy of Semiconductors*. 2007: CRC Press.
[24] A. Dadgar, M. Poschenrieder, J. Bläsing, O. Contreras, F. Bertram, T. Riemann, A. Reiher, M. Kunze, I. Daumiller, A. Krtschil, A. Diez, A. Kaluza, A. Modlich, M. Kamp, J. Christen, F.A. Ponce, E. Kohn, and A. Krost,MOVPE growth of GaN on Si(111) substrates, Journal of Crystal Growth ***248***, 556(2003).
[25] S. Zamir, B. Meyler, E. Zolotoyabko, and J. Salzman,The effect of AlN buffer layer on GaN grown on (111)-oriented Si substrates by MOCVD, J. Cryst. Growth ***218***, 181(2000).

[26] J. Bläsing, A. Reiher, A. Dadgar, A. Diez, and A. Krost,The origin of stress reduction by low-temperature AlN interlayers, Appl. Phys. Lett. ***81***, 2722(2002).
[27] Z. Liu, X. Wang, J. Wang, G. Hu, L. Guo, and J. Li,The influence of AlN_GaN superlattice intermediate layer on the properties of GaN grown on Si(111) substrates, Chinese Physics ***16***, 1467(2007).
[28] A. Able, W. Wegscheider, K. Engl, and J. Zweck,Growth of crack-free GaN on Si(111) with graded AlGaN buffer layers, J. Cryst. Growth ***276***, 415(2005).
[29] H. Lahrèche, P. Vennéguès, O. Tottereau, M. Laugt, P. Lorenzini, M. Leroux, B. Beaumont, and P. Gibart,Optimisation of AlN and GaN growth by MOVPE on Si(111), J. Cryst. Growth ***217***, 13(2000).
[30] Y. Dikme, G. Gerstenbrandt, A. Alam, H. Kalisch, A. Szymakowski, M. Fieger, R.H. Jansen, and M. Hueken,Investigation of buffer growth temperatures for MOVPE of GaN on Si(111), J. Cryst. Growth ***248***, 578(2003).
[31] Y. Lu, X. Liu, X. Wang, D.-C. Lu, D. Li, X. Han, G. Cong, and Z. Wang,Influence of the growth temperature of the high-temperature AlN buffer on the properties of GaN grown on Si(111) substrate, Journal of Crystal Growth ***263***, 4(2004).
[32] S. Raghavan and J.M. Redwing,In situ stress measurements during the MOCVD growth of AlN buffer layers on (111) Si substrates, Journal of Crystal Growth ***261***, 294(2004).
[33] M. Wu, B.S. Zhang, J. Chen, J.P. Liu, X.M. Shen, D.G. Zhao, J.C. Zhang, J.F. Wang, N. Li, R.Q. Jin, J.J. Zhu, and H. Yang,Effect of the N/Al ratio of AlN buffer on the crystal properties and stress state of GaN film grown on Si(111) substrate, Journal of Crystal Growth ***260***, 331(2004).
[34] S. Raghavan and J.M. Redwing,Growth stresses and cracking in GaN films on (111) Si grown by metal-organic chemical-vapor deposition. I. AlN buffer layers, J. Appl. Phys. ***98***, 023514(2005).
[35] E. Arslan, M.K. Ozturk, A. Teke, S. Ozcelik, and E. Ozbay,Buffer optimization for crack-free GaN epitaxial layers grown on Si(1 1 1) substrate by MOCVD, Journal of Physics D: Applied Physics ***41***, 155317(2008).
[36] W. Luo, X. Wang, L. Guo, H. Xiao, C. Wang, J. Ran, J. Li, and J. Li,Influence of AlN buffer layer thickness on the properties of GaN epilayer on Si(111) by MOCVD, Microelectronics Journal ***39***, 1710(2008).
[37] M. Wei, X. Wang, X. Pan, H. Xiao, C. Wang, Q. Hou, and Z. Wang,Effect of AlN buffer thickness on GaN epilayer grown on Si(111), Materials Science in Semiconductor Processing ***14***, 97(2011).
[38] P. Drechsel and H. Riechert,Strain controlled growth of crack-free GaN with low defect density on silicon (111) substrate Journal of Crystal Growth ***315***, 211(2011).
[39] K. Lin, E.Y. Chang, Y. Hsiao, W. Huang, and L. Tingkai,Growth of GaN film on 150mm Si(111) using multilayer AlNAlGaN buffer by MOCVD, applied Physics Letters ***91***, 222111(2007).
[40] A. Reiher, J. Bläsing, A. Dadgar, A. Diez, and A. Krost,Efficient stress relief in GaN heteroepitaxy on Si (111) using low-temperature interlayers, J. Cryst. Growth ***248***, 563(2003).
[41] B.S. Zhang, M. Wu, J.P. Liu, J. Chen, J.J. Zhu, X.M. Shen, G. Feng, D.G. Zhao, Y.T. Wang, H. Yang, and A.R. Boyd,Reduction of tensile stress in GaN grown on Si(111) by inserting a low-temperature AlN interlayer, Journal of Crystal Growth ***270***, 316(2004).
[42] G. Cong, Y. Lu, W. Peng, X. Liu, X. Wang, and Z. Wang,Design of the low-temperature AlN interlayer for GaN grown on Si (111) substrate, Journal of Crystal Growth ***276***, 381(2005).
[43] S. Raghavan, X. Weng, E. Dickey, and J.M. Redwing,Effect of AlN interlayers on growth stress in GaN layers deposited on (111) Si, Applied Physics Letters ***87***, 142101(2005).
[44] J.F. Wang, D.Z. Yao, J. Chen, J.J. Zhu, D.G. Zhao, D.S. Jiang, H. Yang, and J.W. Liang,Strain evolution in GaN layers grown on high-temperature AlN interlayers, Appl. Phys. Lett. ***89***, 152105(2006).
[45] W. Luo, X. Wang, L. Guo, H. Xiao, C. Wang, J. Ran, J. Li, and J. Li,The effect of low temperature AlN interlayers on the growth of GaN epilayer on Si (111) by MOCVD, Superlattices and Microstructures ***44***, 153(2008).

[46] D.K. Kim,Influence of the thickness of the 1st GaN layer under a low-temperature AlN interlayer on the properties of GaN layer grown on Si (111), Journal of Crystal Growth ***312***, 478(2010).
[47] R. Luo, P. Xiang, M. Liu, T. Chen, Z. He, B. Fan, Y. Zhao, Y. Xian, S. Huang, Z. Zheng, Z. Wu, H. Jiang, G. Wang, Y. Liu, and B. Zhang,Influence of V/III Ratio of Low Temperature Grown AlN Interlayer on the Growth of GaN on Si(111) Substrate, Jpn. J. Appl. Phys. ***50***, 105501(2011).
[48] H. Tang, J.M. Baribeau, G.C. Aers, J. Fraser, S. Rolfe, and J.A. Bardwell,Role of buried cracks in mitigating strain in crack free GaN grown on Si (111) employing AlN interlayer schemes, J. Cryst. Growth ***323***, 413(2011).
[49] S. Fritze, P. Drechsel, P. Stauss, P. Rode, T. Markurt, T. Schulz, M. Albrecht, J. Bläsing, A. Dadgar, and A. Krost,Role of low-temperature AlGaN interlayers in thick GaN on silicon by metalorganic vapor phase epitaxy, J. Appl. Phys. ***111***, 124505(2012).
[50] K. Cheng, M. Leys, S. Degroote, B.V. Daele, S. Boeykens, J. Derluyn, M. Germain, G.V. Tendeloo, J. Engelen, and G. Borghs,Flat GaN epitaxial layers grown on Si(111) by MOVPE using step-graded AlGaN intermediate layers, Journal of Electronic Materials ***35***, 592(2006).
[51] S.-H. Jang and C.-R. Lee,High-quality GaNSi(111) epitaxial layers grown with various Al0.3Ga0.7N/GaN superlattices as intermediate layer by MOCVD, Journal of Crystal Growth ***253***, 64(2003).

# 2 Procedure of successful GaN MOVPE on Si

This chapter is about the obstacles to successful GaN growth on Si and the strategies to eliminate them. Basic processes of Si surface cleaning, typical GaN MOVEP on Si procedure and basic characterization methods were introduced firstly in section 2.1. Section 2.2 explored the causes of Si melt-back, including gallium deposition on Si surface, holes in bad quality AlN buffer layer and hydrogen atoms absorption on Si surface. In section 2.3, the effect of TMAl pre-flowing was investigated. In section 2.4, the role and importance of AlN dummy growth to growing high quality GaN on Si was studied. Finally, the necessary measures and standard procedures to yield successful and repeatable GaN growth on Si were summarized in section 2.5.

## 2.1 Basic procedure of GaN MOVPE on Si

The basic procedure of GaN MOVPE on Si can be described briefly firstly. Samples were grown on 2-inch and 270-um-thick Si (111) wafers by AIX200/4HT-S MOVPE system. Prior to growth, Si wafer was boiled in hydrogen peroxide / sulfuric acid ($H_2SO_4$:$H_2O_2$=1:1) at 160 ℃ for 10 min to remove organic contamination on wafer surface. After 5 min of rinsing in running ultra-pure deionized water, wet cleaning in hydrofluoric acid (HF 5%) at room temperature for 1 min was performed to remove oxide film which would hinder the growth of nitrides on Si. 10 s of TMAl was pre-flowed prior to the AlN buffer layer to avoid nitridation of Si surface. Laser beams at three wavelengths were incident on the wafer to observe surface reflectance during growth. Reflectance at 405.9 nm is mainly applied to detecting the surface roughness. Reflectance at 632.5 and 951.3 nm both could be used to monitor the growth rate and growth mode using optical interference effect. The latter was also used to sense true temperature. Three laser beam spots were used to detect the wafer curvature and asphericity.

In the following part of this section, growth technology, in-situ monitoring and some characterization technologies will be introduced briefly.

### 2.1.1 Metal-organic vapor phase epitaxy

Metal-organic vapor phase epitaxy (MOVPE) is an epitaxy technology which utilizing metal-organics to carry metal precursors. It was started from the work of Manasevit in 1968 [1] and in the beginning it was also called as metalorganic chemical vapor deposition (MOCVD) to emphasize the vapor chemical reaction. Initially, the film quality by MOVPE was much worse than that of the film grown by other methods like liquid phase epitaxy (LPE). In 1975, thanks to the enhancement of source purity and improvement of growth process, homo-epitaxial GaAs with electron mobility of 120000 $cm^2/(V \cdot s)$ under 77 K was grown successfully by MOVPE [2]. After that, lots of people started to work on GaAs field effect transistor [3, 4], GaAs/GaAlAs injection laser in 1978 [5] and high efficiency solar

cells in 1980 [6] based on the growth technology of MOVPE. Since then, MOVPE attracted great interest from the academic community; it succeeded in growing AlInP and AlGaInP which could not be grown by other methods such as LPE and chloride or hydride vapor phase epitaxy. It was widely applied to producing red or yellow light emitting diodes (LED), red laser and high-efficiency solar cells. The most exciting breakthrough made by MOVPE was the success of growing the first p-n junction GaN blue LED in 1989 [7]. Until now, it has been proved that MOVPE is the best method to grow AlGaInN.

As mentioned above and illustrated in Fig. 2.1, in MOVPE, carrier gas $H_2$ or $N_2$ carries the metal-organic and/or hydrides continuously to the area of heated substrate in the reactor, and the epitaxial layer is formed on the surface of the substrate. Group-III and group-V precursors convect prior to arriving the area of substrate. There are two steps of reaction, including diffusion and reaction in vapor phase and on the substrate surface. The mechanism of vapor phase reaction is very complicated due to there are many types of intermediates of precursors. Adsorption and desorption of product atoms happens simultaneously. In order to achieve film growth, the adsorption rate should be higher than desorption rate.

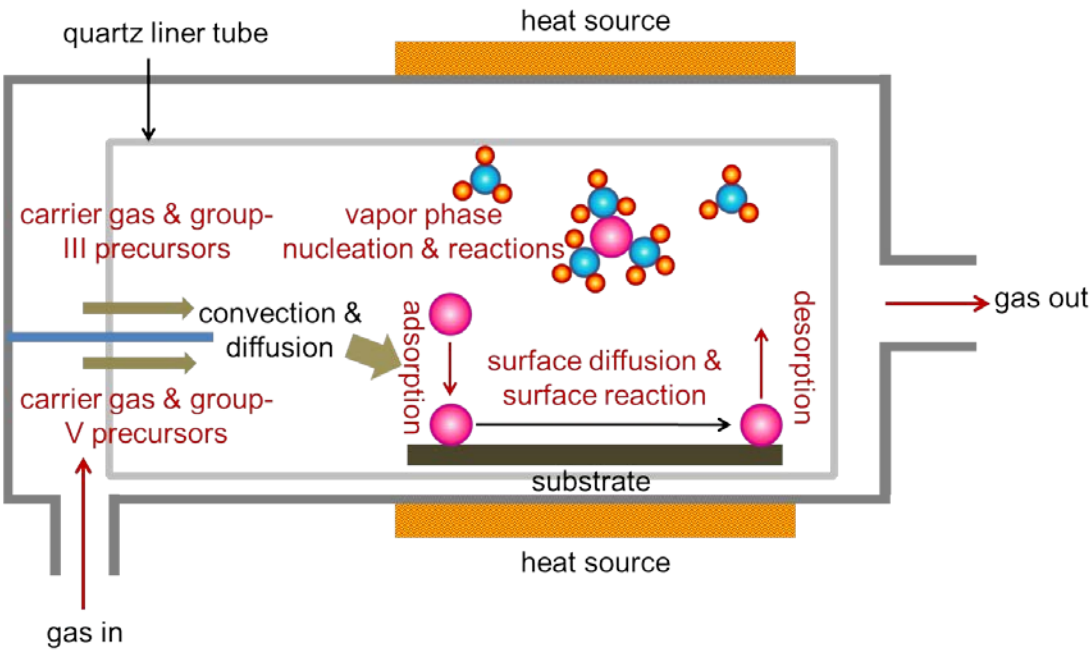


**Fig. 2.1** Schematic diagram of MOVPE reactor and reaction processes.

As represented in Fig. 2.2, MOVPE is a big and complicated system. It consists of five subsystems, which are control system, gas supplying system, reactor system, in-situ monitor system and tail gas treatment system. Control system controls and monitors every action of the whole system. It consists of a computer, operating software and I/O operators. The reactor system is the core of a MOVPE system. Every other subsystem serves it to yield high quality product. The design of the reactor determines the quality of epitaxial films and production efficiency. Depending on the design of the reactor, MOVPE systems can be classified into several types. The basic method based on the volume of the reactor classifies the MOVPE systems into research type and industrial production type. Depending on the operating pressure of the reactor, they can be classified into atmosphere-pressure MOVPE and low-

pressure MOVPE. The gas supplying system operates to feed the reactor with purified and flow rate controlled carrier gas, hydride source and metal-organic source. In-situ monitoring system is indispensable to monitor the growth when it is being performed and to collect the most important information of the growth such as growth mode, growth rate, surface roughness, growth temperature, curvature transition, wafer asphericity and so on. Finally, the tail gas after reaction which may contains toxics needs to be treated ahead of it is discharged into the atmosphere.

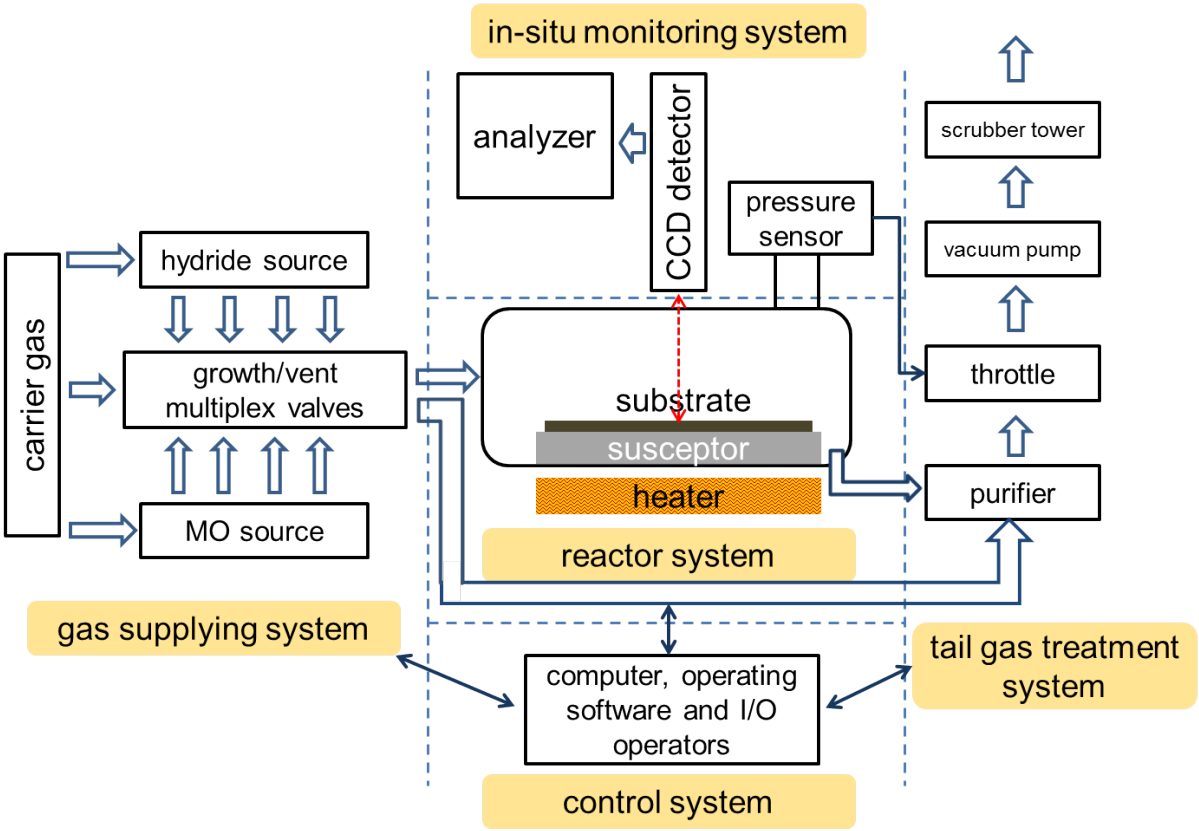


**Fig. 2.2** Illustration of the construction of MOVPE system.

### 2.1.2 In-situ curvature monitor

In the previous part, it has mentioned that in-situ monitor subsystem is a critical part of a MOVPE system to collect the most important growth information. In this work, the up to date type of in-situ monitor has been applied and would be introduced here. There are light beams of three wavelengths at 405.9 nm, 632.5 nm and 951.3 nm respectively to monitor the growth. The light beam of wavelength of 405.9 nm monitors the growth rate of AlN and the surface roughness of GaN. For the large bandgap of AlN, its growth oscillation pattern is more sensitive to the light of short wavelength. On the other hand, if the reflectance value is higher when the oscillation pattern at wavelength of 405.9 nm goes to constant stage, it means the film surface is smoother. The light beam at wavelength of 951.3 nm watches the growth mode and growth rate of GaN layer. More importantly, it detects the true growth temperature at the wafer surface. The information from the light beam at wavelength of 632.5 nm is similar to that obtained by 951.3-nm light. It is more useful to access the information of AlGaN growth.

The other very important information during MOVPE, especially for the growth of GaN on Si, is the film curvature or wafer bowing. Strain and stress at every individual layer can be calculated by measuring curvature. Curvature monitoring is critical for the performance of some devices such as solar cells and LEDs which contain quantum well structures. Residual stress in nano-structures such as quantum wells may lead to variation of bandgap profile in them and then the performance of the devices. In epitaxial thin film growth, substrate wafers often suffer convex or concave bending due to intrinsic growth stress or thermal mismatch stress. Such wafer bowing should be limited less than safe value, otherwise, it may cause cracking in the film or even with the substrate itself, or the performance of epitaxial film or the device structure might be deteriorated due to too large residual stress. Therefore, it is necessary to monitor wafer bowing during growth and cooling down, namely, the curvature.

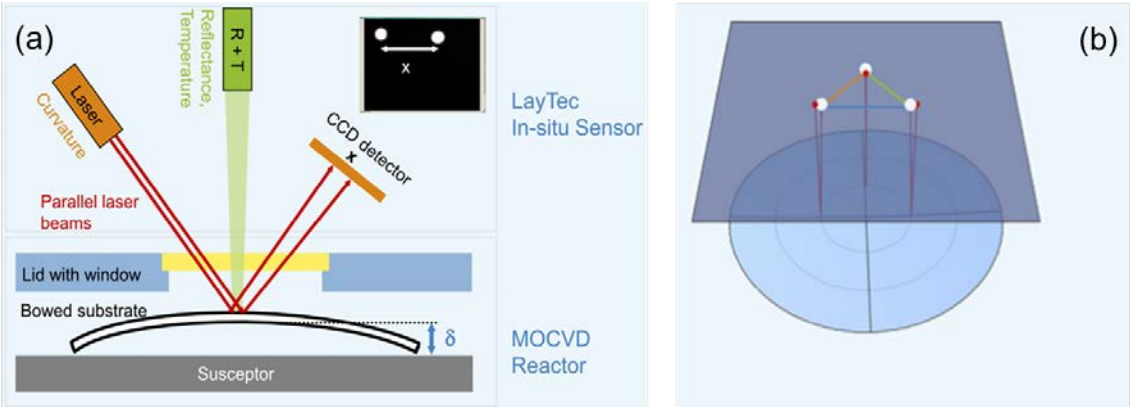


**Fig. 2.3** Schematic diagram of 3-beam in-situ curvature monitor [8].

The mechanism of curvature monitor was represented in Fig. 2.3a. The distance between parallel incident light beams would vary after being reflected by the bowing substrate. As illustrated in Fig. 2.3b, the new type curvature monitor applied in this work has three laser beams and can promote the accuracy of curvature measurement because it samples the wafer bowing information from more areas than conventional type with only two operating light beams. The three-beam monitor can capture other important information, wafer asphericity, which the two-beam type cannot access. In some cases, for example, GaN growth on Si, if the epilayer is too thick and the Si wafer suffers too much stress, plastic deformation may happen and it deforms asymmetrically which may introduce negative effects to the wafer and device performance. Therefore, asphericity should be monitored and plastic deformation should be avoided. If there is a sudden increasing jump of asphericity, it indicates plastic deformation has started. Some special treatment about the wafer or growth process has to be introduced to eliminate plastic deformation.

After growth, the sample should be characterized ex-situ to check its surface morphology, crystal quality and so on. As examples, two characterization technologies, scanning electron microscope (SEM) and X-ray diffraction (XRD) would be introduced briefly as follows.

### 2.1.3 Scanning electron microscope

A scanning electron microscope is a type of electron microscopes. It is based on the interaction between electron beams and the observed objects. When a high-energy incident electron beam bombards the surface of the material, secondary electrons, Auger electrons,

characteristic X-ray, a continuous X-ray spectrum of backscattered electrons, transmitted electrons as well as electromagnetic radiation in the visible, ultraviolet and infrared spectrum will be generated in the excited regions. Depending on the type of detectors and collected particles, different information of the specimen can be acquired. For example, information of micro-surface-morphology can be seen by collecting the secondary electrons and backscattered electrons, chemical composition information can be captured by collecting the excited X-ray from the specimen.

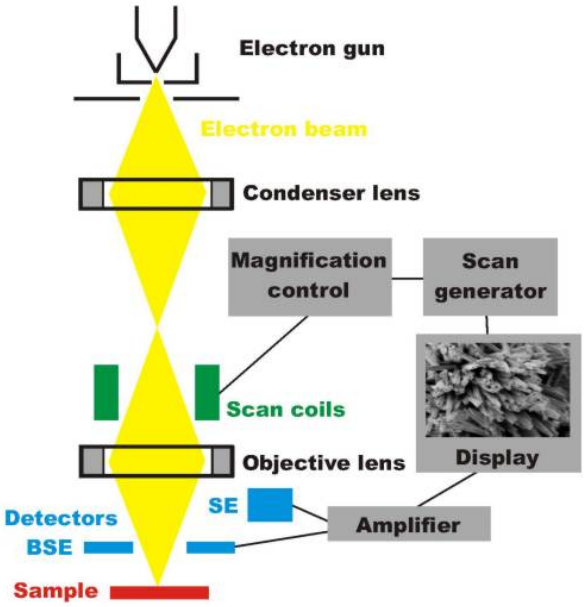


**Fig. 2.4** Schematic structure of a scanning electron microscope [9].

As represented by Fig. 2.4, a SEM consists of three subsystems, vacuum system, electron beam system and imaging system. There are two parts of the electron beam system, including electron gun and electromagnetic lenses. It works under very high vacuum (< $10^{-7}$ torr). The detector in imaging system should be chosen depending on the information people want to know. In this work, SEM was applied for capturing the surface morphology of GaN and AlN films, to check the crack density, Si melt-back, surface defect density as well as domain size and so on.

### 2.1.4 X-ray diffraction

Initially, X-ray diffraction is a technology to detect crystal quality content of the specimen based on the diffraction of X-ray through crystal planes. The Bragg Eq. (2-1) is the foundation stone of the whole XRD theory.

$$2d \sin\theta = n\lambda \tag{2-1}$$

with $d$ being the crystal plane distance, $\theta$ being the incident angle of X-ray, $\lambda$ being the wavelength of X-ray, as illustrated in Fig. 2.5. A great amount of information of the characterized material can be acquired using XRD. For known material, from the measured value of $d$, the crystal plane index can be derived; from the full width at half maximum of rocking curve measurement, crystal quality can be evaluated. For unknown specimen, from the XRD peak position and relative intensity, the chemical composition and concentration of

the individual component can be estimated. Using reciprocal space mapping (RSM) of XRD, the lattice constant of known crystal material can be measured and then the strain/stress at the film or bulk material can be calculated. In this work, for crystal growth, the most frequently being used characterization methods are XRD rocking curve and XRD RSM, to monitor the crystal quality and strain/stress in the material respectively.

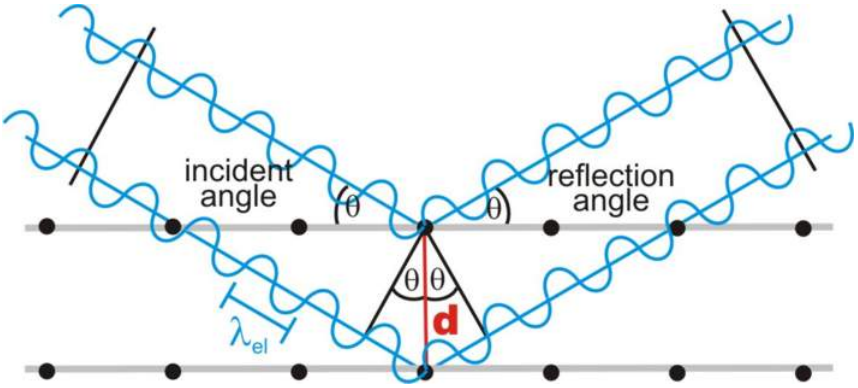


**Fig. 2.5** Illustration of XRD and derivation of Bragg equation [10].

## 2.2 Si melt-back

### 2.2.1 What Si melt-back is

GaN cannot grow on Si directly because metal gallium alloys with silicon in hydrogen ambience [11-14]. H atoms act as catalyst to initiate the alloying reaction between gallium and silicon. This mechanism can be expressed simply by reaction Eq. (2-2). As this melt-back etching reaction is initiated, it is not self-limiting and causes rough surface and deep hollows in Si substrate [15], as shown in Fig. 2.6. GaN can grow on Si but only under very particular conditions, using $N_2$ as carrier gas, at low temperature around 600 ℃ and with partial pressure of TMGa must be smaller than the vapor pressure of gallium around $1.62\times10^{-7}$ atm at 600 ℃ [11]. Melt-back etching effect of Si with gallium is not only harmful to the growth, but also might be helpful to reduce the threading dislocation density in GaN [14]. But for the case of GaN growth on Si, Si melt-back should be eliminated.

$$Si + Ga \xrightarrow{H} SiGa_x \tag{2-2}$$

The methods to eliminate Si melt-back lie in how to stop the possibility of reaction between Si and gallium. Firstly, gallium should be kept from depositing on silicon surface. Isolation between gallium and silicon can be realized by coating the reactor wall and parts and depositing AlN buffer layer on Si prior to the growth of GaN. Secondly, because gallium cannot react with silicon without catalyzing of hydrogen, so it is necessary to remove the adsorbed H atoms from the Si surface. Three possible problems which may cause Si melt-back are introduced and solved in the following part of this section.

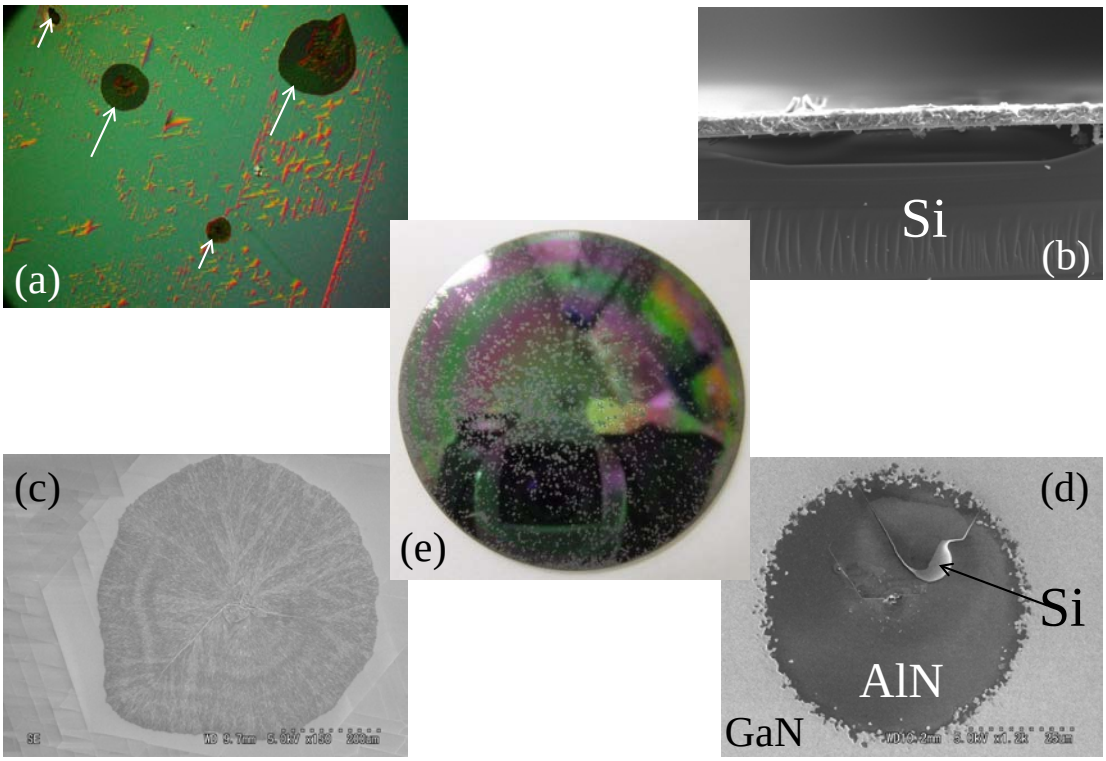


**Fig. 2.6** Si melt-back. (a) GaN surface photograph by Nomarski microscope; (b) Cross section SEM image of a hollow formed by melt-back etching; (c) Alloyed GaN with Si; (d) Melted Si emerged from the underneath of AlN buffer layer; (e) The entire surface of GaN with distributed Si melt-back spots photographed by a camera.

### 2.2.2 Gallium deposition on Si wafer surface

In MOVPE system, as illustrated in Fig. 2.1, there is a quartz liner tube as the space where the reaction occurs and the film deposits on the substrate. Substrate wafer is supported by the susceptor. Around the rotating wafer substrate and susceptor, there are some covering and fixing O-rings. Taking the deposition of GaN as an example, usually there is some deposition of GaN or metal gallium on the reactor wall and the parts around the susceptor. The reaction is expressed by reaction Eq. (2-3).

During the early stage of a growth, for example temperature ramping up and the thermal cleaning of wafer surface, in the atmosphere of $H_2$ and at high temperature more than 1000 ℃, the deposited GaN is decomposed into metal gallium and ammonia, and the deposition of metal gallium is melted or sublimated. At high temperature and large hydrogen flow rate, thermal decomposition is the dominant mechanism for GaN decomposition, as shown by Eqs. (2-4) ~ (2-6) [16]. In $H_2$ ambience, the onset temperature for GaN decomposition is much lower compared to that in inert environment (i.e. $N_2$, Ar or vacuum) [16]. In $H_2$, decomposition mechanism also differs from that at high temperature, as expressed by Eq. (2-7) [17-19].

$$Ga(CH_3)_3(l) + NH_3(g) + H_2(g) \rightarrow GaN(s) + 3CH_4(g) + H_2(g) \quad (2\text{-}3)$$

$$2GaN(s) \rightarrow 2Ga(g) + N_2(g) \quad (2\text{-}4)$$

$$2GaN(s) \rightarrow 2Ga(l) + N_2(g) \rightarrow 2Ga(g) \quad (2\text{-}5)$$

$$GaN(s) \rightarrow GaN(g) \; or \; (GaN)_x \; (g) \quad (2\text{-}6)$$

$$GaN(s) + 3/2\, H_2 \rightarrow GaN(l) + NH_3(g) \quad (2\text{-}7)$$

**Table 2.1** Trials to eliminate Si melt-back caused by possible gallium contamination on Si surface.

| **Trials** | **Si melt-back** |
|---|---|
| 275 nm AlN dummy coating | Occurs |
| 550 nm AlN dummy coating | Occurs |
| Completely clean reactor (liner-tube and susceptor parts) | Occurs |

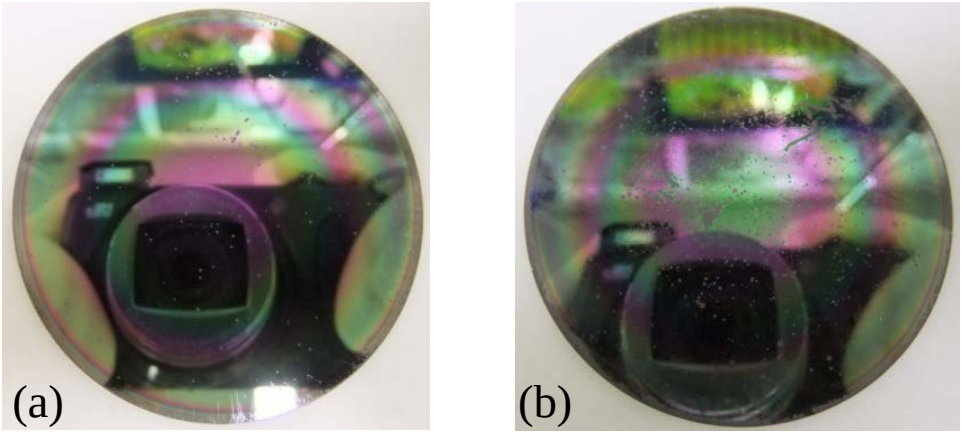


**Fig. 2.7** GaN surface with grey Si melt-back spots . AlN coating with thickness of 275 nm (a) and 550 nm (b) prior to the growth of GaN on Si.

**Fig. 2.8** GaN surface with Si melt-back spots, grown in a clean reactor, with all new parts.

At high temperature during temperature ramping up and thermal cleaning, decomposed or deposited metal gallium may transfer from the reactor wall and inner parts to the surface of Si wafer and initiate the reaction between gallium and silicon. Once the reaction starts, it would worsen the quality of AlN buffer layer and lead to holes in it which acts as reaction path for gallium and silicon. In order to stop the pollution of gallium from the liner tube and susceptor

parts to the Si surface, AlN coating of the inside part of the liner tube was performed to cover the GaN or metal gallium deposition and stop the sublimation of gallium, with thickness of 275 nm and 550 nm. As shown in Fig. 2.7, even with AlN coating thickness of 550 nm, Si melt-back still occurred. In order to check whether gallium contamination on Si surface is the only source of melt-back etching or not, a cleaned liner tube without any deposition and brand-new covering O-ring parts were used, then all possible gallium sources have been eliminated. Despite of all these efforts, as in Fig. 2.8, considerable numbers of Si melt-back spots still dispersed on the surface. These trials are summarized in Table 2.1. This shows that at least, gallium contamination is not the only cause of Si melt-back and some other possible ones should be figured out and cleared.

### 2.2.3 Si Surface cleaning and hydrogen atom adsorption

Surface state of Si wafer is an important factor affecting the alloying of Si with gallium. First of all is the cleanliness. Cleaning of Si surface includes chemical and physical methods. Both wet cleaning in advance of loading it to the reactor and thermal desorption at high temperature right before the growth of buffer layer are mandatory. Otherwise, Si melt-back might occur, though Si surface state is not the only reason which could lead to melt-back.

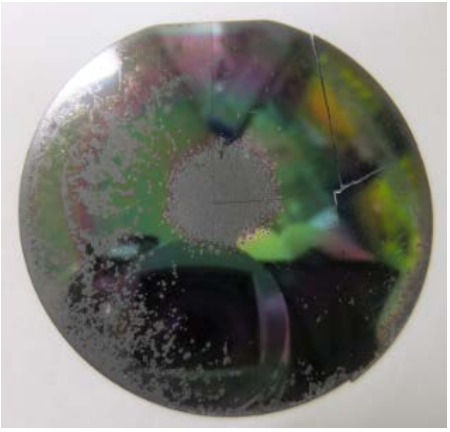

**Fig. 2.9** Surface of GaN grown on Si without cleaning.

Si wafers for the production of semiconductor devices must be subject to stringent cleaning. A trace contamination would lead to low-quality film and device failure. Since the real surface of Si wafers is exposed to the air and oxidation absorption occurs on it, usually there is a very thin (several Å to tens of nm) layer of oxide on the surface. The surface energy levels can absorb some other contaminating substance. The purpose of cleaning is to remove surface contaminants, including organic and inorganic such as $SiO_2$. Some of these impurities exist as ions or atomic state, and some as form of a film or particulates on the silicon surface. Organic pollutants include photoresist, residue organic solvents, synthetic waxes, and grease or fibers brought by human contact devices, tools or utensils. Inorganic contaminants include heavy metals gold, copper, iron, chromium and so on, seriously affecting the minority carrier lifetime and the surface conduction; alkali metal such as sodium, causing serious leakage; slag particles include silicon contamination, dust, bacteria, microorganisms, fibers and other

organic colloid, will cause various defects. There are two kinds of decontamination methods involving physical cleaning and chemical cleaning.

Chemical cleaning is to remove invisible contamination like atoms, ions. There are many methods, such as solvent extraction, acid washing (sulfuric acid, nitric acid, aqua regia, a variety of mixed acid and so on) and plasma method. Among them, hydrogen peroxide solution system is the best with little environmental pollution. The general approach is to clean the Si surface with acidic cleaning solution with the composition ratio of $H_2SO_4$: $H_2O_2$ = 1:1 or 4:1. Strong oxidizing cleaning solution removes organics by decomposing them. Due to the strong oxidation effect of $H_2O_2$ and complexation effect of acids, many metal ions forms water-soluble complexes and be flew away with water. Even though using $H_2SO_4$ and $H_2O_2$, sulfur atoms with density of $2\times10^{10}$ $cm^{-2}$ would be left on the surface of Si, they as well as $SiO_2$ and some other metallic pollutants will be removed completely with DHF solution (HF:($H_2O_2$):$H_2O$). Without wet chemical cleaning of Si surface, GaN on it will be of poor quality and dirty surface, as photographed in Fig. 2.9.

**Table 2.2** Trials of Si substrate surface cleaning.

| **Surface cleaning** | **Si melt-back** |
|---|---|
| No cleaning | Occurs |
| Wet cleaning: $H_2SO_4$:$H_2O_2$(1:1) at 170 ℃ 10min, 5% HF, 1 min | Occurs |
| Wet cleaning + Desorption in $H_2$ at 1100 ℃, 10/15/20 min | Occurs |

After loading the cleaned Si wafer and prior to the start of the growth of AlN buffer layer, there is a stage of thermal desorption at 1100 ℃ under the ambience of $H_2$. At such high temperature, hydrogen is of very strong reducibility. Almost any residual organic pollutant or $SiO_2$ can be removed, if there is still something remaining. Nevertheless, as summarized in Table 2.2, Si melt-back occurred in all the cases with or without wet chemical cleaning, and in the cases of physical thermal cleaning at higher than 1000 ℃ for 10 to 20 min. This showed that Si substrate surface cleanliness is only one of the possible causes of Si melt-back.

As mentioned in part 2.2.1, H atoms adsorbed on Si surface can act as catalyst of alloying between silicon and gallium. H atoms are adsorbed by bonding with hanging bonds on Si surface [12]. As the coverage of H atoms on Si surface increases, the absolute adsorption energy of gallium or aluminum atoms decreases and the number of their adsorbed atoms also increases [12]. Therefore, if the growth process is not proper, the stage of thermal desorption under ambience of $H_2$ might be a reason that facilitate Si melt-back if there are some hydrogen atoms absorbed. In order to figure out the influence of thermal desorption cleaning in $H_2$, thermal desorption with and without $N_2$ was tested, as shown in Table 2.3.

First of all, GaN direct growth under atmosphere of $N_2$ on Si was achieved without any Si melt-back but it is almost amorphous (not shown here). As Fig. 2.10d shows, if there was only 10 min of thermal desorption in $H_2$, Si melt-back occurred. If the 10-min of thermal desorption was followed by 5-min thermal desorption in $N_2$, the GaN surface became clean without Si melt-back, as shown in Fig. 2.10a. In other words, in order to remove the adsorbed

H atoms or avoid H atoms adsorption during the stage of temperature ramping up and thermal cleaning, the carrier gas was changed from $H_2$ to $N_2$, or the thermal cleaning in $H_2$ was followed by pure $N_2$ flowing to remove the adsorbed H atoms, as shown in Table 2.3 and Fig. 2.10. It was shown that Si melt-back didn't occur in the samples which the substrate was thermal cleaning ended with pure $N_2$ flowing with or without $H_2$ prior to it. But for the samples thermally cleaned only by flowing $N_2$, the edge area is rough, and crystal quality of GaN is also poorer, although no Si melt-back exists. The cause yet remains to be clarified, and Si surface nitridation in nitrogen atmosphere may account for the quality degradation of GaN on Si thermal cleaned in nitrogen [20]. From these experiments we can conclude that thermal cleaning in $H_2$ ambience is mandatory to acquire high quality GaN on Si. $N_2$ is inert, and $H_2$ is more active to remove the oxides or organics on Si surface and yields better GaN quality.

**Table 2.3** Atmosphere during thermal cleaning to avoid H atom adsorption.

| Sample No. | $H_2$ (min) | $N_2$ (min) | Si melt-back | Wafer edge area |
|---|---|---|---|---|
| **a** | 10 | 5 | No | OK |
| **b** | - | 5 | No | Rough |
| **c** | - | 10 | No | Rough |
| **d** | 10 | - | occurs | Rough |

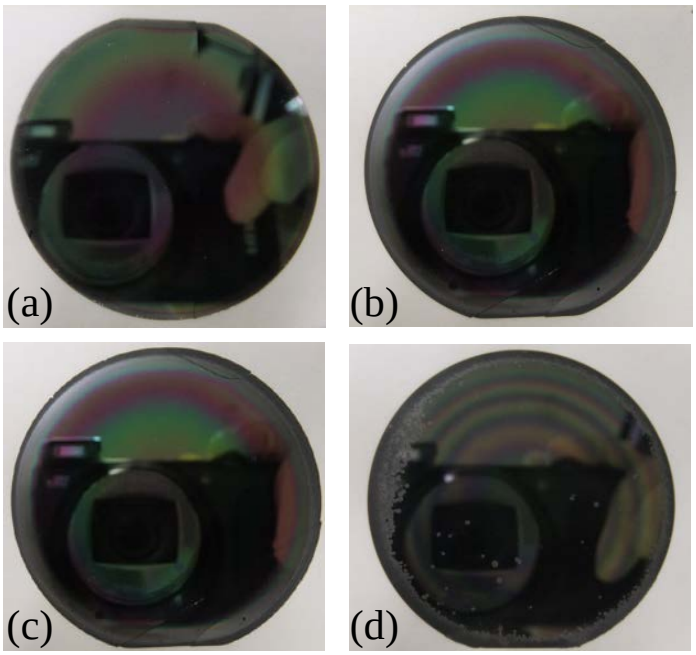


**Fig. 2.10** Adsorbed H atoms removal by thermal cleaning in $N_2$ atmosphere.

### 2.2.4 Quality of AlN buffer layer

High-quality AlN buffer layer is the key to stop gallium reaction with silicon, by isolating them physically. The mechanism of silicon melt-back etching by gallium through AlN buffer

layer is illustrated in Fig. 2.11a. If the quality of AlN is not good enough, there will be some pin holes inside it. During the growth of GaN, gallium precursors can go to the surface of Si through these pin holes and reacts with silicon. As long as the alloying reaction is launched, it would not stop and the hollow beneath GaN film become larger and larger. Si would be melted, break AlN and GaN then go to the surface. The alloy spot of Ga and Si become larger and larger, and cover the surface of GaN, as the photos shown in Fig. 2.6. If the quality of AlN buffer layer is good enough, there is no path for Ga to reach the Si wafer and can keep them from alloying, as represented by Fig. 2.11b.

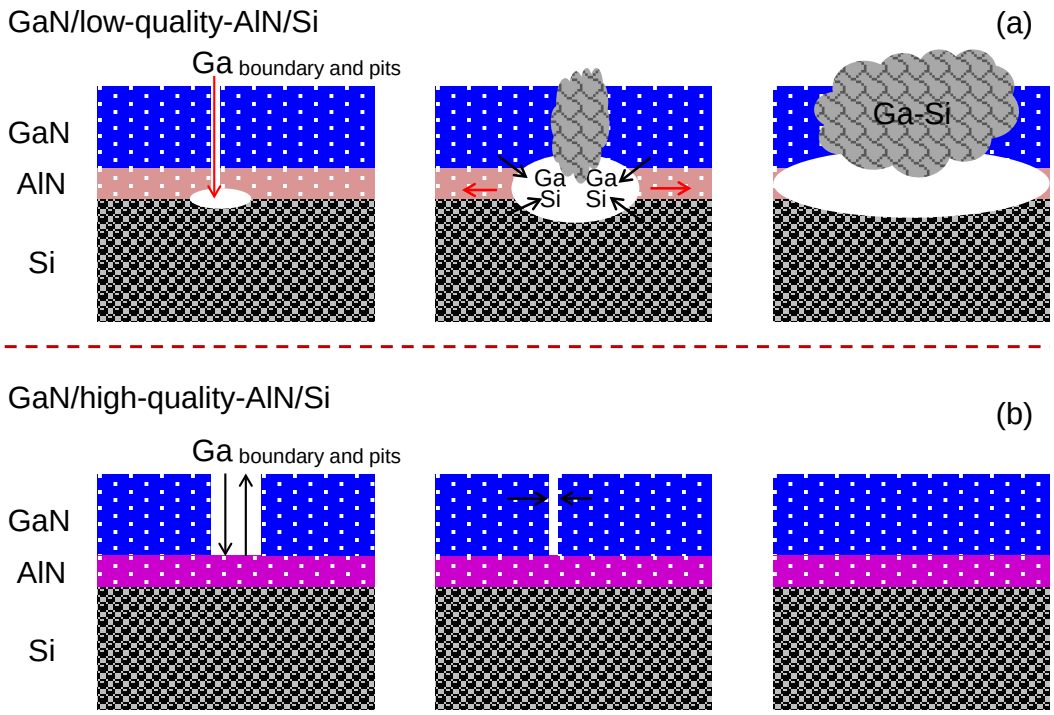


**Fig. 2.11** Reaction between Ga and Si through pin holes in low-quality AlN buffer layer.

Considerable efforts have been done to improve the quality of AlN buffer layer, as summarized in Table 2.4. In order to eliminate the influence from GaN or gallium deposition in the reactor, AlN dummy coating was performed prior to every growth batch. Almost all factors that might influence the quality of AlN have been tested, such as growth temperature, V/III ratio, thickness, although all these didn't work. Bi-layer buffer consists of 80-nm-thick AlN and 80-nm-thick AlGaN has also been tried, and neither worked. Normally, these conditions are proper to yield better quality AlN. Failure of these trials shows that there was some unknown reason which was keeping this MOVPE system from yielding high-quality AlN buffer layer, although almost all possible conditions had been tested. To conforming this, 150-nm-thick sputtered AlN buffer layer was prepared ex-situ. After sputtering, Si wafer with sputtered AlN buffer layer was loaded into the MOVPE reactor to grow GaN on it. For this sample, there was no Si melt-back at all, although the quality and surface of GaN is a complete mess, as shown in Fig. 2.12a. This verified that MOVPE-grown AlN buffer layer cannot cover Si surface completely.

After testing all possible factors leading to Si melt-back, there must be some unknown problem which is not relating to the growth conditions and can cause Si melt-back. Finally, we changed the gas purifiers of $H_2$ and $N_2$. With new gas purifiers and AlN dummy coating, Si melt-back disappeared completely. So it can be deduced that there must be some impurities in carrier gas, especially $H_2$. The impurities remain yet to be detected further. A guess is that one of the most influent impurities might be water, because the dew point was very high (> -50℃) inside the $H_2$ and $N_2$ gas lines. Therefore, if growth conditions and processes are proper, the gas purity might be the key factor of the quality of AlN.

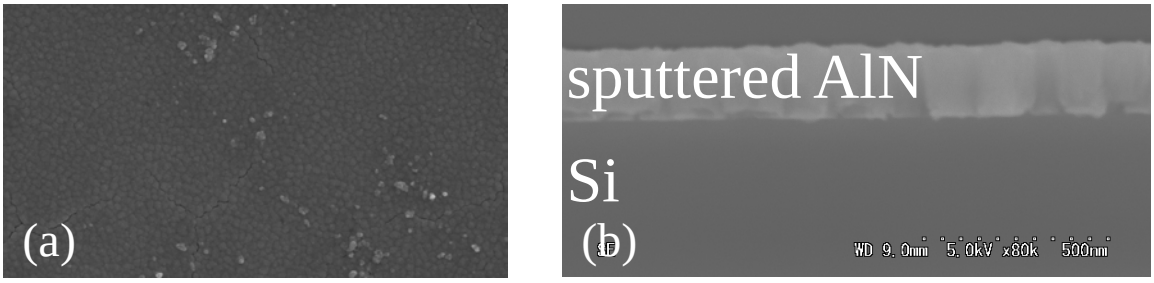


**Fig. 2.12** (a) Surface of GaN grown on sputtered AlN buffer layer with no Si melt-back; (b) Cross section image of sputtered AlN buffer layer on Si.

**Table 2.4** Effort to improve the quality of AlN buffer layer to eliminate Si alloying with gallium.

| Condition | Values | Si melt-back |
|---|---|---|
| **Temperature** | 950/1100/1200 ℃ | Occurs |
| **V/III ratio** | 470/1003 | Occurs |
| **Thickness** | 80/115/230 nm | Occurs |
| **Bi-layer** | AlGaN (80 nm)/AlN (80 nm) | Occurs |
| **Sputtering** | 150-nm sputtered AlN | **No** |
| **Gas purity ($H_2$, $N_2$)** | New gas purifiers | **No** |

## 2.3 TMAl pre-flowing

TMAl pre-flow is another critical step for successful GaN growth on Si. It is executed after thermal cleaning and right before the growth of AlN buffer layer. Prior to flowing $NH_3$, TMAl is pre-flowed for several or tens of seconds to form several monolayers of Al atoms to isolate Si surface and $NH_3$ to keep Si surface from nitridation, as expressed by Eqs. (2-8) ~ (2-9) [20, 21]. Using molecular beam epitaxy (MBE) GaN can grow on 1-nm-thick silicon nitride buffer layer but with poor quality [22]. Pre-flowing of 60 s of $NH_3$ prior to the growth of AlN was performed to test the effect of Si wafer surface nitridation on the growth of GaN. The result in Fig. 2.13 shows that not only the growth of GaN was not successful but also Si melt-back occurred a lot. The timing scheme of TMAl pre-flowing is like the chart in Fig. 2.14a, with flow rate of 22 sccm, pre-flow time of TMAl varied from 0 s to 8 s. The surface of the sample without TMAl pre-flowing (0 s) is very rough except the central area. Due to insufficient Al coating of Si surface, the rough area suffered from nitridation. As the TMAl

pre-flowing time increased to 2 s, the rough area decreased to the very narrow part at the edge. When the pre-flowing time was longer than 4 s, rough area has been eliminated. From the ring shape of rough area in the outer part of the wafer, it can be derived that due to the rotation of the substrate, TMAl precursor arrives at the center of the wafer first. This is why although the designed TMAl pre-flowing time was 0 s for the sample in Fig. 2.15a, the central part was still clean and smooth. For the samples with designed TMAl pre-flowing time, there is a distribution of the thickness of Al coating and it is thicker in the central part than that in the edge area. There is a compromised Al coating thickness which is optimal for all the area of the wafer.

$$Si + 2NH_3\ (g) \rightarrow Si(NH_2)_2(g) + H_2(g) \tag{2-8}$$

$$3Si(NH_2)_2 \rightarrow Si_3N_4 + N_2(g) + 3H_2(g) \tag{2-9}$$

**Fig. 2.13** Surface of GaN on $NH_3$ pre-flowed Si surface.

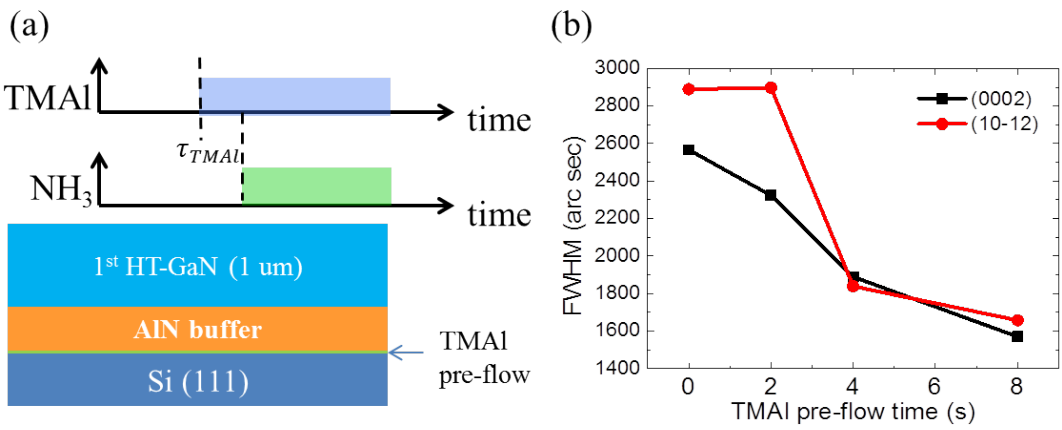


**Fig. 2.14** (a) Representation of TMAl pre-flowing. (b) FWHM of XRD rocking curve of GaN grown with varied TMAl pre-flow time.

Nitridation of Si surface is not the only criterion to choose the time of TMAl pre-flowing, because it also affects the crystal quality of overlying GaN. If the target was only eliminating Si nitridation, 4 s of TMAl pre-flowing was sufficient. However, it can be longer to achieve GaN of higher quality. Fig. 2.14b is the FWHM of XRD rocking curve of GaN grown with different TMAl pre-flow time. As the pre-flow time of TMAl increases from 0 to 8 s, not only the surface of GaN becomes more and more mirror-like, but also the quality of GaN

improves a lot. Under optical microscope, the number of Si melt-back spots also decreased significantly and it was eliminated in the sample with 8 s of TMAl pre-flowing. Following the tendency of the FWHM plots, it is reasonable to conclude that GaN quality can be higher if the TMAl pre-flowing time is longer. But too thick Al coating also deteriorate the quality of GaN. Consequently, there is a proper TMAl pre-flowing time. Base on the result of TMAl pre-flowing time of 8 s, it is deduced that more 2 s is safe. In all later growth, although theoretically, it should be optimized further experimentally, the pre-flow time was fixed to be 10 s and showed good results.

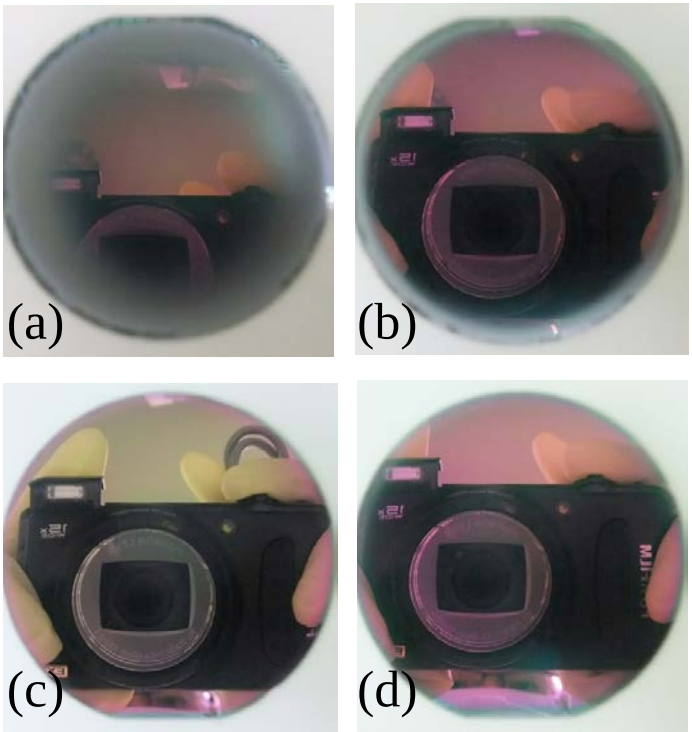


**Fig. 2.15** Surface of GaN grown with TMAl pre-flow time of (a) 0 s; (b) 2 s; (c) 4 s; (d) 8 s.

In the end of this section, it should be noticed that the optimal TMAl pre-flowing time depends on the design of the reactor and the flow rate of TMAl source. For every individual type of reactor, it has its own optimal TMAl pre-flowing time and it should be searched by series of experiments.

## 2.4 AlN dummy coating

Dummy growth is being performed frequently when people are using MOVPE system, for both of research and manufacture, although the content and process of dummy growth varies depending on the desired sample structure. Dummy growth is a part of the daily routine maintenance of MOVPE systems to maintain the stable growth conditions of the reactor. As a process of a dummy growth, baking at high temperature (> 1100 ℃) under atmosphere of ammonia and hydrogen can clean the reactor and gas lines. Dummy growth can keep the inner environment of the reactor to be stable, this is critical for some growth which is sensitive to it, such as GaN growth on Si. The content of a dummy growth depends on the

film which would be grown after it. Generally, it is GaN dummy growth for the growth of GaN on sapphire. But for the growth of GaN on Si, the content of dummy growth should be AlN. There are two examples of growth series without an AlN dummy. In section 2.2.2, AlN dummy was applied to eliminate the problem of Si melt-back. However, it has been proved that AlN dummy could not stop Si melt-back.

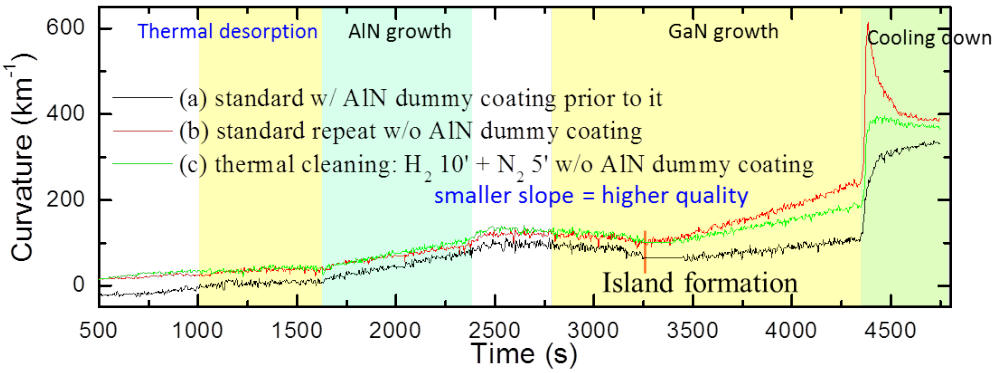


**Fig. 2.16** Effect of AlN dummy growth, example I.

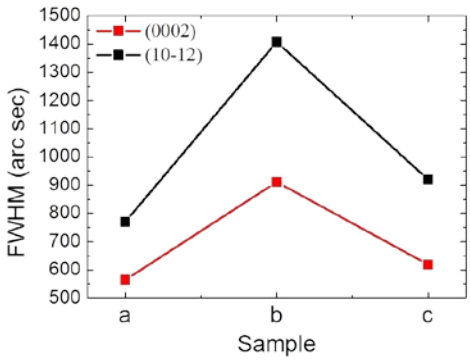


**Fig. 2.17** FWHM of XRD rocking curve of continuously grown samples.

**Example I**: Continuously repeating growth in Fig. 2.16. Three samples were grown continuously without AlN coating dummy growth in between; the growth mode of GaN for all three samples was 3D growth. But there was an AlN dummy growth prior to the first sample (a). The conditions for sample (a) and (b) are exactly the same; the only difference is that there was no AlN coating dummy prior to sample (b). From curvature observation in Fig. 2.16, no difference could be distinguished before the growth stage of GaN, i.e. thermal desorption, AlN growth and temperature ramping up. In curvature transition curves, they differ from the stage of island formation, as marked in Fig. 2.16. The 3D growth of sample (a) lasted much longer than that of sample (b), as shown by the straight line duration with no variation. In sample (b) the 3D growth was very short and coalesced rapidly. After coalescence, growth mode of GaN turned from 3D growth to 2D growth, so that the stress in GaN evolved from slightly compressive to tensile. From Stoney equation we know that the slope of curvature curve indicates the stress magnitudes and higher slope means larger stress. Tensile stress in GaN of sample (b) is much higher than that of sample (a). Consequently, as curvature curves shown, sample (b) cracked during cooling while crack in sample (a) was much less. The same as sample (b), before the growth of sample (c) there was no AlN coating dummy growth also, but the difference was that during thermal desorption, there was 5 min

extra thermal cleaning in nitrogen atmosphere. 3D growth period in sample (c) was shorter than that in sample (a) but longer than in sample (b). The stress in GaN of sample (c) lies also between (a) and (b). The final residual stress during and after cooling down of sample (c) was also in between sample (a) and (b), as well as the amount of cracks. As indicated in Fig. 2. 17, the crystal quality of GaN also shows the same tendency as that of the slope of curvature evolution, namely the stress strength.

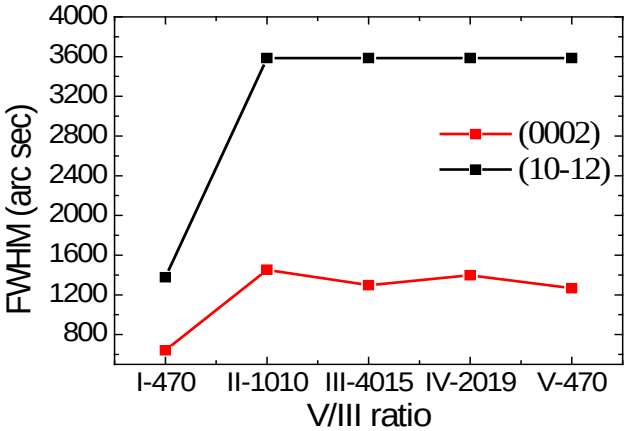


**Fig. 2.19** FWHM of XRD rocking curve of GaN on AlN buffer layer grown under various V/III ratio. FWHM of (10-12) plane exceeded the upper limit, so it was shown the same for sample 2 to 4.

**Example II**: V/III ratio tests of AlN buffer layer. This was designed to investigate the effect of V/III ratio of AlN buffer layer on the properties of GaN without AlN dummy growth in between them. From sample 1 to sample 4, V/III ratio of AlN buffer layer varied from 470 to 4019 while all other conditions were kept the same. Growth mode of GaN was 2D layer-by-layer growth to avoid the influence from coalescence during 3D growth. Sample 5 was designed to repeat the growth of sample 1. AlN coating dummy growth was performed only prior to sample 1 and no AlN dummy before the following samples. As shown by the curvature curves in Fig. 2.18, except sample 1, the stress behavior of all other four samples are exactly the same. From sample 2 to sample 5, during the growth of GaN, it showed no dependence of GaN performance on the V/III ratio of AlN buffer layer. The quality of GaN shown in Fig. 2.19 also acts the same as it of curvature transition. Actually, as would be shown later, GaN performance should be dependent on it.

The detailed and exact mechanism behind the phenomena of uncontrollable growth is not well understood and yet to be investigated further. However, the possible process can be discussed. In the two examples above, the difference between the first sample and the following sample is that prior to the first sample there was an AlN coating dummy growth. As discussed in the part of 2.2.2, the effect of AlN coating is to cover the GaN and metal gallium deposition inside the reactor. Influence of gallium origins from the reaction between it and silicon and may lead to Si melt-back. From the problem of uncontrollability here, although after using new gas purifiers for $H_2$ and $N_2$, the problem of Si melt-back had been solved due to the quality improvement of AlN buffer layer even without AlN coating dummy growth, GaN and metal gallium deposition still affects the growth. We suspect that the influence started from the stage of thermal cleaning. If there is no AlN coating dummy prior

to a growth, Si wafer will be exposed to the surroundings of the deposition of GaN or metal gallium. Then during thermal cleaning or desorption at high temperature above 1000 ℃, some gallium atoms may be adsorbed on the surface of Si but the amount is not enough to initiate Si melt-back. Since the quality of AlN is good enough to isolate the TMGa source and Si surface during GaN growth and stop the reaction between them, no Si melt etching occurs. But the adsorbed gallium atoms might change the surface state of Si substrate and affects the growth quality of AlN buffer layer and then the growth of following GaN layer. In next chapters we can know that gallium adsorption should have worsened the quality of AlN buffer layer but not worse enough to cause Si melt-back. Although how gallium atoms adsorption influence the growth of AlN buffer layer is not clear. For the samples with AlN coating prior to it, deposition of GaN or gallium was covered by AlN coating and the influence from it had been eliminated. On the contrary, such problem doesn't exist for the growth of GaN on sapphire. Ga or GaN deposition inside the reactor doesn't affect the quality of GaN growth on sapphire. The comparison between GaN growth on Si and sapphire shows that the difference between them lies in the substrate surface state which may be contaminated by a trace of metallic GaN.

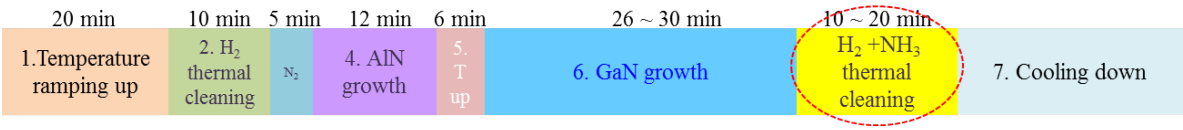


**Fig. 2.20** Thermal cleaning was performed in the end of a growth in $H_2$ and $NH_3$ atmosphere to improve controllability.

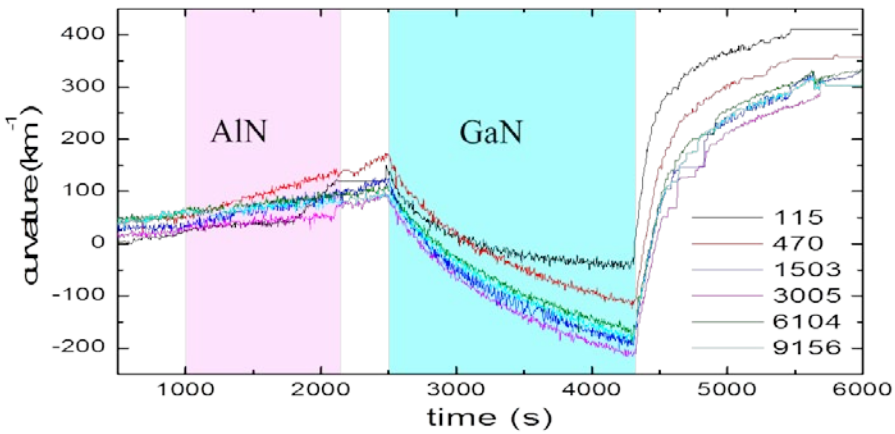


**Fig. 2.21** Curvature of GaN growth on Si, V/III ratio for AlN buffer layer varied from 115 to 9156.

So the difference between growth with and without AlN coating prior to them might be the gallium adsorption state on Si wafer surface. AlN dummy coating is an effective way to realize controllable growth. Similar to GaN and gallium deposition, there might be also some AlN and aluminum deposition inside the reactor, but the Al adsorption on Si surface is not harmful to AlN growth. On the contrary, proper amount of it is good for the growth of AlN, like the effect of TMAl pre-flowing to stop silicon nitride formation. Besides AlN coating, there is also some other method to eliminate the influence of GaN and gallium, such as thermal cleaning in HCl atmosphere which is more convenient than AlN coating but not available in our system.

In example I, from sample (c) it can be known that thermal cleaning in $N_2$ ambience is also working to improve controllability somehow but not good enough. Thermal desorption in nitrogen might be helpful to remove adsorbed H atoms from the surface of Si and then the adsorption of gallium atoms. However, on the other hand, annealing in nitrogen may cause Si nitridation and deteriorate the growth on III-nitrides on silicon. This argument is reasonable because the edge area of the surface of sample (c) in example I was rough. It is hopeful that the combination of AlN coating and thermal cleaning in nitrogen might be more effective to improve growth controllability by reducing more adsorbed H atoms, yet to be tested.

Some other efforts also have been tried to improve reproducibility and avoid AlN coating. Although AlN is working to enhance reproducibility, it is time consuming and costly. Adding thermal cleaning in mixture atmosphere of hydrogen and ammonia at high temperature in the end of a growth prior to cooling was tested, as shown in Fig. 2.20. Effect of this measure is not stable and more or less works. Like thermal desorption of Si wafer in nitrogen, it also might be harmful to the growth. Annealing in hydrogen at high temperature may lead to GaN decomposition and destroy the surface of a sample, as discussed in part 2.2.2. So this method was not applied anymore.

Applying AlN coating, experiments of V/III ratio test for AlN buffer layer like that in example II of uncontrollability test were repeated. The result of curvature was shown in Fig. 2.21. It is clear that the performance of GaN is strongly dependent on the growth conditions of AlN buffer layer, such as V/III ratio which shown here. Based on all the experiments above, AlN dummy coating is a practical and effective method to achieve high controllability for the growth of GaN on Si, although it consumes much time and is not recommendable to industrial production.

## 2.5 Conclusion - standard procedure

By summarizing the problems and solutions above, based on the conditions of our

1. High purity gases ($H_2$, $N_2$ & $NH_3$)
2. 500-nm-thick AlN coating dummy growth
3. Si wafer wet cleaning: $H_2SO_4$:$H_2O_2$ (1:1), 170 ℃ 10min, 5% HF, 1 min
4. Thermal cleaning in $H_2$ for 10 min at 1100 ℃
5. TMAl pre-flow: 22 sccm, 10s
6. Growth of AlN buffer layer
7. Growth of GaN
8. ……

**Fig. 2.22** Standard procedure for growing GaN on Si.

laboratory, a standard procedure to ensure successful growth of GaN on Si is proposed and established for the first time here. This procedure is shown in Fig. 2.22.

First of all, the purity of gases (ammonia and carrier gases of $H_2$ and $N_2$) and metal-organic sources must be high enough. Gas purity is critical for MOVPE, especially for growing AlN, because it is more sensitive to the gas purity than other composition like GaN. In this work, almost all possible factors which might lead to Si melt-back had been checked and the problem couldn't be solved until the gas purifiers for $H_2$ and $N_2$ was exchanged with new ones, although the species of impurity were not clear. After applying new purifiers, the dew point of both $H_2$ and $N_2$ decreased to around -90 ℃ and then water in the carrier gas could be removed.

Secondly, in order to achieve controllable growth, AlN dummy growth is compulsory prior to every real designed growth of GaN on Si. GaN and Ga deposition inside the reactor can contaminate the Si surface during thermal desorption and deteriorate the quality of GaN on Si. AlN dummy coating can cover the GaN and Ga deposition with AlN and keep Si surface from being contaminated by Ga. Without AlN dummy coating, GaN growth on Si would be uncontrollable and insensitive to the variation of growth conditions.

The next critical step is Si cleaning by wet chemical method. The particles, organic pollutants and Si oxide should be removed completely; otherwise GaN quality on it cannot be good. The detail of cleaning was shown in the third step in Fig. 2.22. It is followed by thermal cleaning in the reactor to desorb the possible residual pollutants on Si wafer surface. Following it, TMAl pre-flowing must be performed to keep Si surface being nitridized. However, the optimal TMAl pre-flowing time is depending on the type of reactor and TMAl flow rate. Then the following steps are the growth of AlN buffer layer, GaN layer, AlN interlayers, and top GaN layer and so on.

## References


[1] H.M. Manasevit,Single-crystal GaAs on insulating substrates, Applied Physics Letters ***12***, 156(1968).

[2] Y. Seki, K. Tanno, K. Lida, and E. Ichiki,Properties of epitaxial GaAs layers from a Triethylgallium and Arsine system, Journal of Electrochem Society ***122***, 1108(1975).

[3] J.P. Duchemin, J.P. Hirtz, M. Razeghi, M. Bonnet, and S.D. Hersee,GaInAs and GaInAsP materials grown by LP MOCVD for microwave and optoelectronic applicatioins, Journal of Crystal Growth ***55***, 64(1981).

[4] J.P. Hirtz, J.P. Duchemin, and J.P. Hirtg,GaInAsP/InP DH laser emitting at 1.15 um grown by LP MOCVD, Electronics Letter ***16***, 275(1980).

[5] R.D. Dupuis and P.D. Dapkus,Continuous room temperature operation of GaAlAs-GaAs DH laser grown by MOCVD, Applied Physics Letters ***32***, 406(1978).

[6] R.R. Saxena, V. Aebi, and C.B. Cooper,High-efficiency GaAlAs concentrator solar cells by MOCVD, Journal of Applied Physics ***51***, 4501(1980).

[7] H. Amano, M. Kito, K. Hiramatsu, and I. Akasaki,P-type conduction in Mg-doped GaN treated with low-energy electron beam irradiation (LEEBI), Japanese Journal of Applied Physics ***28***, L2112(1989).

[8] L. Inc., *Introduction of Laytech in-situ monitor for MOVPE*. 2012.

[9] E. Zurich. *Scanning Electron Microscopy (SEM)*. 2014; Available from: http://www.microscopy.ethz.ch/sem.htm.
[10] Z. ETH. *Bragg's Law of Diffraction*. 2014; Available from: http://www.microscopy.ethz.ch/bragg.htm.
[11] K. Takemoto, H. Murakami, T. Iwamoto, Y. Matsuo, Y. Kangawa, Y. Kumagai, and A. Koukitu,Growth of GaN Directly on Si(111) Substrate by Controlling Atomic Configuration of Si Surface by Metalorganic Vapor Phase Epitaxy, Jpn. J. Appl. Phys. ***45***, L478(2006).
[12] Y. Matsuo, Y. Kangawa, R. Togashi, K. Kakimoto, and A. Koukitu,Influence of hydrogen coverage on Si(111) substrate on the growth of GaN buffer layer, J. Cryst. Growth ***300***, 66(2007).
[13] W. Li, J.-f. Chen, and T. Wang,Study of GaN adsorption on the Si surface, Appl. Surf. Sci. ***256***, 191(2009).
[14] H. Ishikawa and K. Shimanaka,Reduction of threading dislocations in GaN on in-situ meltback-etched Si substrates, J. Cryst. Growth ***315***, 196(2011).
[15] A. Dadgar, M. Poschenrieder, J. Bläsing, O. Contreras, F. Bertram, T. Riemann, A. Reiher, M. Kunze, I. Daumiller, A. Krtschil, A. Diez, A. Kaluza, A. Modlich, M. Kamp, J. Christen, F.A. Ponce, E. Kohn, and A. Krost,MOVPE growth of GaN on Si(1 1 1) substrates, J. Cryst. Growth ***248***, 556(2003).
[16] D.D. Koleske, A.E. Wickenden, R.L. Henry, J.C. Culbertson, and M.E. Twigg,GaN decomposition in H2 and N2 at MOVPE temperatures and pressures J. Cryst. Growth ***223***, 466(2001).
[17] E.E. Zavarin, D.S. Sizov, W.V. Lundin, A.F. Tsatsulnikov, R.A. Talalaev, A.V. Kondratyev, and O.V. Bord,In-situ investigatioins of GaN chemical unstability during MOCVD, Proceedings of the Fifteenth International European Conference on Chemical Vapor Deposition (EUROCVD-15) ***2005-09***, 299(2005).
[18] E.V. Yakovlev, R.A. Talalaev, A.S. Segal, A.V. Lobanova, W.V. Lundin, E.E. Zavarin, M.A. Sinitsyn, A.F. Tsatsulnikov, and A.E. Nikolaev,Hydrogen effects in III-nitride MOVPE, J. Cryst. Growth ***310***, 4862(2008).
[19] Y.-H. Yeh, K.-M. Chen, Y.-H. Wu, Y.-C. Hsu, and W.-I. Lee,Hydrogen etching on the surface of GaN for producing patterned structures, J. Cryst. Growth ***314***, 9(2011).
[20] H.L. Zhu, D.R. Yang, L. Wang, and D.L. Due,Thermal nitridation kinetics of silicon wafers in nitrogen atmosphere during annealing, Thin Solid Films ***474***, 326(2005).
[21] F.L. Riley,Silicon Nitride and Related Materials, Journal of the American Ceramic Society ***83***, (2004).
[22] Y. Nakada, I. Aksenov, and H. Okumura,GaN heteroepitaxial growth on silicon nitride buffer layers formed on Si (111) surfaces by plasma-assisted molecular beam epitaxy, Appl. Phys. Lett. ***73***, 827(1998).

# 3 Experimental observation of stress control by conventional AlN

As discussed in chapter 1, the critical problem for the growth of GaN on Si is stress control during and after growth to eliminate cracking. This chapter is about the experimental observation of stress behavior during the growth. The simplest structure of applying AlN buffer layer and AlN interlayers (ILs) to induce compressive stress in GaN layers is adopted in this work to understand the basic effects of AlN layers and elementary mechanisms of stress control. This chapter starts with section 3.1, an introduction, including interpretation of a curvature transition, possible strategies to realize zero curvature (bowing) at room temperature and a basic model to explicate how compressive stress was induced and relaxed in GaN layers. The effects of AlN buffer layer and conventional ILs grown under various conditions were discussed carefully in section 3.2 and 3.3 respectively. The adjustment of curvature by GaN layers was observed in section 3.4. The concept of conventional AlN mentions that AlN is grown under fixed conditions continuously in one step without any special techniques such as patterning, multi-step growth or pulse injection, which would be introduced in chapter 6.

## 3.1 Introduction

### 3.1.1 Curvature transition curve

As has been introduced in part 2.1.2, curvature value is the reflection of wafer bowing. Higher absolute curvature value means larger bowing and our goal is achieving bowing close to zero after growth at room temperature. In order to be convenient for describing and interpreting the data from curvature monitoring and the stress behavior of individual layers, meanings of the curves of curvature transition, temperature ramping and reflectance pattern of a typical growth were overviewed here briefly.

Fig. 3.1 shows the structure and in-situ monitoring curves of a demonstration growth of GaN on Si with stress control applying 100-nm-thick AlN buffer layer and 15-nm-thick AlN ILs which induced compressive stress in GaN layers. Data of temperature and growth reflectance was shown in Fig. 3.1a and curvature transition is shown in Fig. 3.1b respectively. From the beginning to the end, the growth was divided into 12 stages. During stage 1, after loading Si wafer, wafer temperature ramped up from room temperature to desorption temperature or thermal cleaning temperature (~ 1100 ℃), reactor pressure decreased from atmosphere to 100 mbar. In this stage, curvature curve went to apparent tensile side, which meant the wafer went to be concave, might due to temperature difference between edge and center. Usually, there was temperature difference between edge and center of 20 ~ 30 ℃. Then in stage 2, the temperature was stabilized and kept at about 1020 ℃ to clean the Si

wafer surface by removing adsorbed H atoms and organics. After thermal cleaning, the conditions ramped for the growth of AlN buffer layer in stage 3. In this particular growth, AlN buffer layer was grown at true temperature of 1000 ℃, pressure was 50 mbar.

During stage 3, tensile stress emerged because the lattice constant of AlN is smaller than that of Si. Therefore, curvature value rose at a constant slope which means a constant stress. Reflectance oscillation at wavelength of 950 nm which was accompanied with the growth of

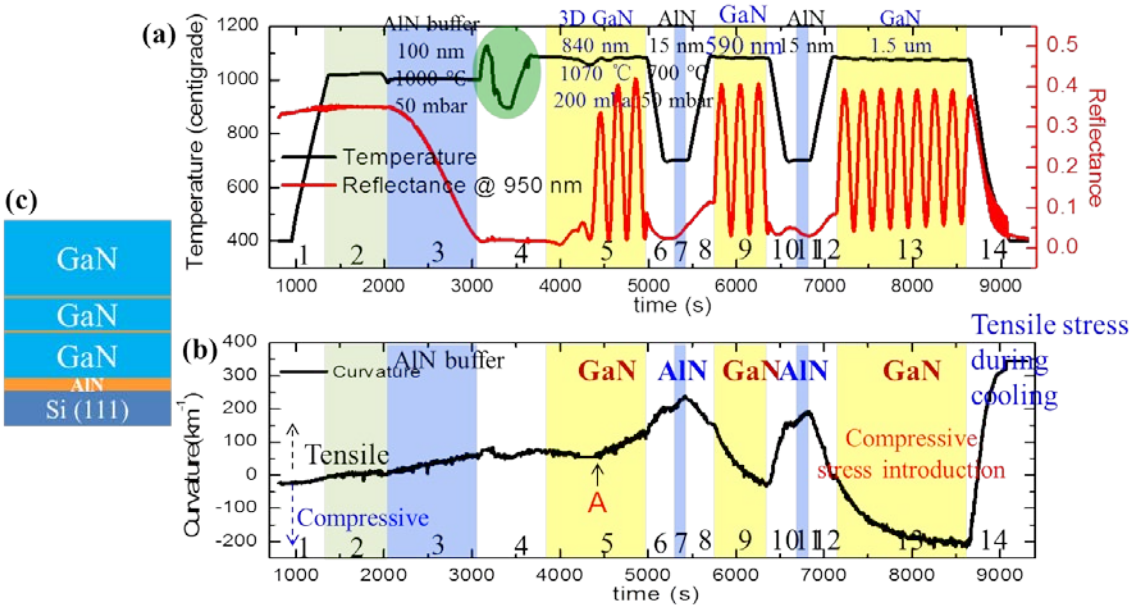


**Fig. 3.1** In-situ monitoring data of a typical growth, (a) temperature and reflectance at wavelength of 950 nm; (b) curvature transition curve and (c) sample structure.

AlN buffer layer also started due to interference effect. In stage 4, reactor environment was adjusted for the growth of the first GaN layer. The disorder in temperature was due to temperature tuning to recover susceptor rotation. During this period, there was no much change about reflectivity and curvature because there was no growth. Stage 5 is the growth of the 1$^{st}$ GaN by 3D mode at temperature of about 1070 ℃ and pressure of 200 mbar. Due to it was 3D mode, it even caused slight compressive stress in GaN before coalescence. The mechanism of compressive stress generation during 3D growth would be introduced later. Before 2D film was formed by coalescence around point A, as marked in Fig. 3.1b, there was a period of 3D island growth during which the reflectance was close to zero and the curvature signal could not be captured neither. Since the structure of 3D nuclei islands separated the connection between AlN buffer layer and GaN, the overlying GaN could not be strained by the underlying AlN buffer layer effectively and then no compressive stress was induced in GaN. On the other hand, because of smaller lattice constant of GaN than that of Si, after coalescence, GaN suffered tensile stress. About the temperature curve in Fig. 3a, what should be noticed is the temperature fluctuation in the period circled by the green area. It was not a designed process during the growth. In the MOVPE system, rotation of susceptor often failed during growth. Sometimes, it could be recovered by drastic temperature ramping. The temperature fluctuation was also such a trial to recover the rotation and it succeeded.

Stage 6 was condition ramping for the growth of the first AlN IL. As temperature and pressure decreased to 700 ℃ and 50 mbar respectively, tensile stress was induced in the

epitaxial layer due to larger thermal expansion coefficient of nitrides than that of Si. As temperature decreased, nitrides shrunk more than Si and then tensile stress was introduced in nitrides. Following it in stage 7 was the growth of AlN IL and curvature increased further due to smaller lattice constant of AlN than GaN. Oppositely, in stage 8, as temperature increased, compressive stress was induced and curvature value decreased. Stage 9 was the growth of the $2^{nd}$ GaN. As it was grown on AlN IL, it was compressively strained and the curvature curve went down to the compressive side more. Stage 10, 11 and 12 were the repeat of stage 6, 7 and 8. Stage 13 was the growth of the top GaN. Significant compressive stress was induced at the initial part when the thickness of GaN was less than 200 nm. As GaN grew, it relaxed gradually and in the end curvature saturated, compressive stress could not be induced anymore. Finally in stage 14, it cooled from growth temperature to room temperature in 15 min. This was a critical stage that due to very large temperature drop of more than 1000 ℃, huge tensile stress occurred in epitaxial films and this might cause cracking.

So the description above is an example of a growth, especially how to understand the curvature transition in every each stage. What has to be emphasized is that for understanding the transition of curvature curve, some of it was caused by the intrinsic stress due to epitaxial growth such as in stage 3, 5 while some other was caused by thermal stress due to thermal expansion coefficient different between nitrides and silicon, like in stage 6, 8, 10, 12 and 14. It should be noted that this growth procedure showed above might not be the ideal case for GaN growth on Si.

### 3.1.2 Strategies to achieve zero bow

As mentioned previously, our target is through proper stress control to realize curvature or bowing of the wafer around zero with no cracking caused by tensile stress after growth at room temperature. It has already been discussed in section 1.2 that the basic strategy is applying inserted ILs with lattice constant smaller than it of GaN to induce compressive stress to compensate tensile stress origins from thermal mismatch during cooling. Available material for ILs here to induce compressive stress in III-nitride is AlN or AlGaN. Specifically, by comparing the cracked and crack-free samples, as illustrated in Fig. 3.2, curvature or bowing could be tuned through the following several strategies. The cracked sample was shown by the black curve with final estimated curvature value of over 600 $km^{-1}$ to the tensile side. On the contrary for the crack-free sample shown by the red curve, the final curvature value was around 50 $km^{-1}$, which caused no cracking in the film.

The first strategy is tuning AlN buffer layer. In Fig. 3.2, growth conditions of AlN buffer layers of cracked and crack-free growth were different. This not only affects the strength of tensile stress in the buffer layer itself, but also determines the stress behavior of following GaN layer. For example, on AlN buffer layers grown under different conditions, GaN may suffer tensile or compressive stress, and the strain relaxation rate might also differ. Consequently, AlN buffer layer remains to be optimized to induce as much compressive stress in the following GaN layer as possible.

The second path to control the stress is applying AlN ILs, which would be most critical and most complicated. Like AlN buffer layer, AlN ILs also should be optimized to induce compressive stress in GaN layers as efficiently as possible. On AlN ILs grown under different growth conditions, difference of compressive stress or curvature increase to the compressive side could be very large. These growth conditions include temperature, V/III ratio and thickness and so on. Micro-structure and surface morphology may differs a lot and the strain relaxation mechanism at both AlN ILs and GaN layer on them based on those difference is very complicated and yet to be understood properly.

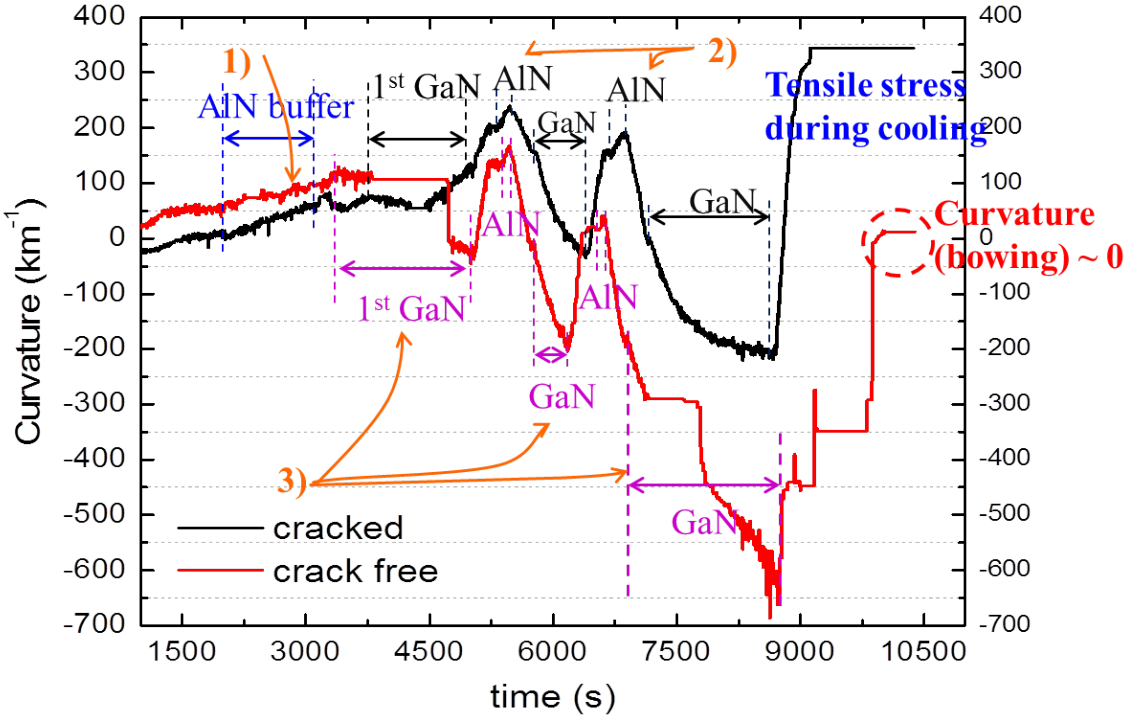


**Fig. 3.2** Strategies to achieve curvature value or bowing close to 0 in the end of a growth at room temperature by comparing crack-free and cracked growth.

The third complementary approach is adjusting the thickness and growth mode of GaN. For the GaN layers overlying AlN ILs, as the thickness increases, the curvature goes further to the compressive direction and the wafer gets more concave bowing. On the other hand, for samples with thicker total GaN layer, tensile stress caused by thermal mismatch during cooling would also be higher. Curvature value or bowing and film thickness can be related through Stoney formula. Growth mode also affects the stress behavior of GaN, especially the 1st GaN on AlN buffer layer. 3D growth has an effect that separates or relives the confinement from the lattice of AlN buffer layer to overlying GaN. GaN grown by layer-by-layer or 2D growth mode is confined or strained by underlying AlN buffer layer much more strongly.

### 3.1.3 Stress introduction and strain relaxation mechanisms

This part it devoted to an introduction of a theoretical model to interpret the factors of stress introduction in hetero-structures and some strain relaxation theory.

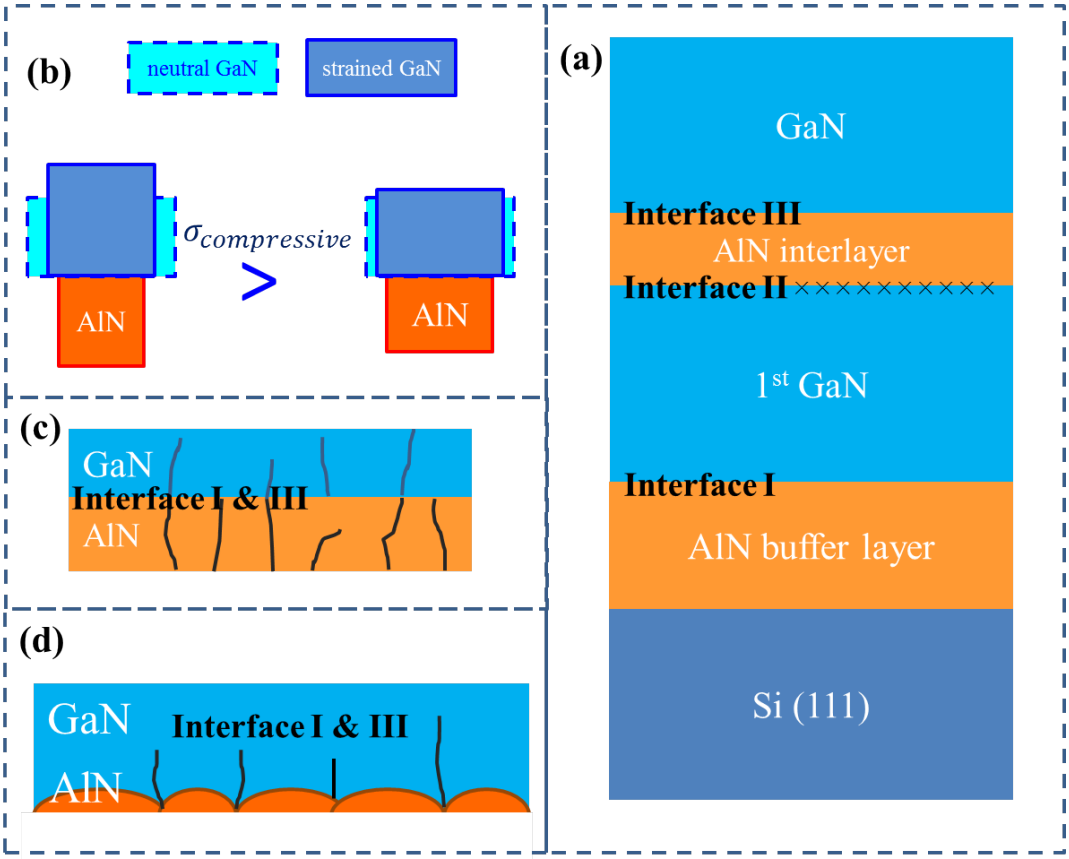


**Fig. 3.3** Schematic image of interfaces in AlN/GaN multilayers. (a) Interfaces in the growth structure; (b) compressive stress caused by lateral lattice constant difference; (c) coherent GaN growth on smooth AlN; (d) GaN on AlN 3D islands.

Theoretically, there are two factors that determine how effective an AlN IL can introduce compressive stress to the overlying GaN layer.

The first is the difference in lateral lattice spacing between AlN IL and GaN at interface I and III in Fig. 3.3b, which should be larger. This can be expressed by Eq. (3-1). Since the growth conditions of GaN were fixed, lattice constant of AlN layers can be tuned by adjusting growth conditions. The most influential condition is growth temperature and low temperature (LT) is preferable to acquire small lattice constant of AlN ILs. Another mechanism is relaxation. Highly relaxed AlN ILs hold smaller lattice constant close to its neutral value. This demands that at the lower interface of an AlN IL (interface II in Fig. 3.3a), AlN should be relaxed as much as possible.

$$\sigma_{GaN} = M_{GaN} \cdot \varepsilon_{GaN} = M_{GaN} \cdot \frac{a_{Al(Ga)N} - a_{GaN}}{a_{GaN}} \tag{3-1}$$

Another important factor to determine the lattice constant is the compound composition, in the case if AlGaN exists. For the interlayers to induce compressive stress in GaN layers, some researchers are using AlGaN [3]. Even though the intended interlayer is AlN, the actual grown compound can be AlGaN [4], due to the diffusion of gallium to AlN interlayers. Therefore, the percentage of gallium atoms is also a determinable factor of the lattice constant of interlayers. As predicted by Vegard's law, the lattice constant of $Al_xGa_{1-x}N$ as function of Al content is calculated as [5, 6]

$$a_{Al_xGa_{1-x}N} = 3.1986 - 0.0891x \text{ Å} \quad \text{and} \quad c_{Al_xGa_{1-x}N} = 5.2262 - 0.2323x \text{ Å} \qquad (3\text{-}2)$$

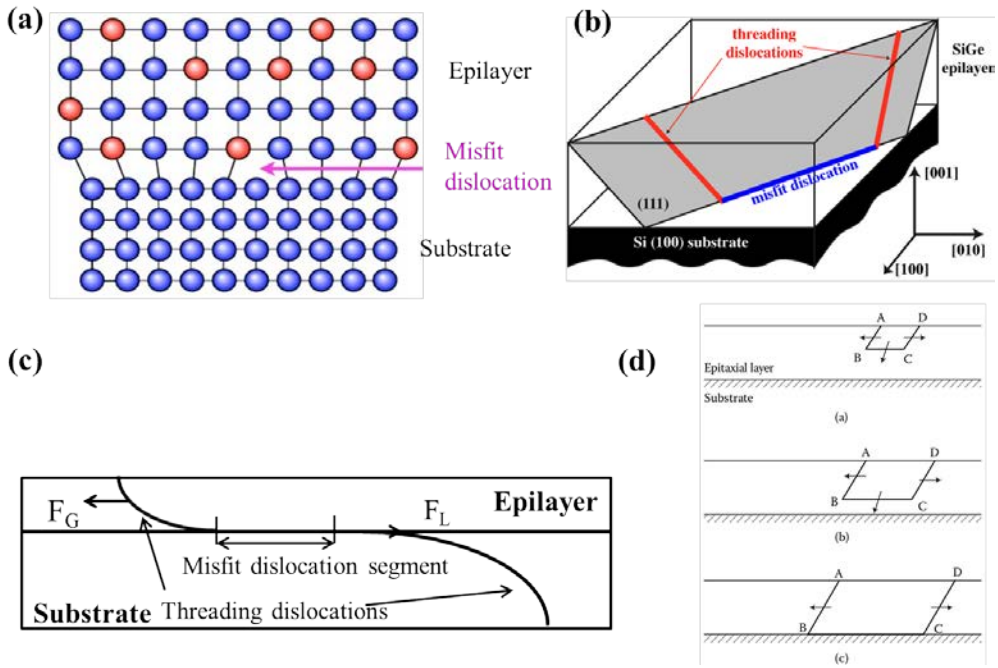


**Fig. 3.4** Schematic diagram of threading dislocation and misfit dislocation. (a) Misfit dislocation structure [1]; (b) formation of threading dislocation and misfit dislocation by the glide of half-loops from the surface of the epilayer [1]; (c) bending of threading dislocation and formation of misfit dislocation; (d) gliding process of a half-loop [2].

The second factor of how effectively the AlN layer can stress the overlying GaN compressively is the interface quality of AlN(underlying)/GaN(overlying), which should be as high-quality as possible. In the cases here (interface I and III in Fig. 3.3a), the interface quality is generally determined by the quality of underlying AlN, for that the growth conditions of overlying GaN are proper and yielding good quality. To strain overlying GaN effectively, GaN growth on it should be coherent and in layer-by-layer mode, which is dependent on the quality of underlying AlN. The quality information of AlN includes the defect density in it, morphology, grain boundary length, cracks and so on, i.e., all factors which may cause relaxation in AlN itself or following GaN.

Relaxation is favorable in underlying AlN but not in overlying GaN. Relaxation in AlN can reduce the average in-plane lattice constant of it and increase the lattice constant difference between GaN and AlN, which is advantageous and can be grouped under the first factor. On the contrary, relaxation should be avoided as much as possible in GaN. Consequently, it is necessary to introduce some relaxation mechanisms in hetero-epilayers.

There are some mechanisms to explain the lattice relaxation behavior in hetero-structures. The first basic one is the bending of substrate threading dislocations, which has been utilized to yield critical thickness for hetero-epitaxial growth films by Matthews and Bakleslee [7]. During heterogeneous epitaxial growth, intrinsic growth stress arises from the lattice constant difference between the epilayer and substrate can bend the existing threading dislocations in the substrate when they propagate to the epilayer, associated with producing a misfit

dislocation at the interface and a threading dislocation in the epilayer, as sketched in Fig. 3.4c. As shown is Fig. 3.4a, strain energy in epilayer could be relieved by elastic deformation of lattices or plastic deformation, i.e., the formation of misfit dislocations. Under stress and gliding force in the film, dislocation generated in the film can move to the edge of the wafer, during which the misfit dislocation length is increased and the strain energy could be relaxed. In very few cases, the threading dislocation can move out of the wafer. Relaxation, i.e., the amount of strain that could be relaxed, by misfit dislocations at the interface can be calculated as follows [2]

$$\delta = 2D_s L_{ave} b \cos\alpha \cos\phi \tag{3-3}$$

where $\delta$ is the relaxation, $D_s$ is the threading dislocation density in the substrate, $L_{ave}$ is the average length for a misfit dislocation segment, $\alpha$ is the angle between the Burgers vector and line vector of the misfit dislocation, and $\phi$ is the angle between the interface and the normal to the slip plane which the plane of threading dislocation in the epilayer slips in. As shown in Fig. 3.4c, if the threading dislocation density $D_s$ in underlying AlN is large, GaN would relax very fast.

As illustrated by Fig. 3.4d, glide of half-loops can be another mechanism to produce misfit dislocations at the interface to relieve the strain in the epilayer. The strain relaxation mechanism by it is the same as that by the glide of threading dislocations from the substrate or underlying layer in Fig. 3.4c. The essential difference is that half-loop origins from the surface of the epilayer rather than the bottom interface. A half-loop can cause two new dislocations in the epilayer if they cannot move out of the edge of the wafer. Threading dislocation density $D_e$ caused by this mechanism in epilayer can be calculated as [2]

$$D_e = \frac{\delta}{L_{ave} b \cos\alpha \cos\phi} \tag{3-4}$$

where $\delta$ is the relaxed strain, other symbols have the same meaning as those in Eq. (3-3). This mechanism does not relate to the surface of the underlying layer.

Injection of edge dislocations at island boundaries is a very important strain relaxation mechanism in highly mismatched hetero-epilayers grown in a Volmer-Weber (three-dimensional) mode. In the case of 3D growth, pure edge misfit dislocations occur spontaneously at the boundaries of the growing islands prior to coalescence, and then glide on the interface. Smaller grain size and higher grain density can introduce more dislocations in the overlying layer. If the strain has been relaxed completely prior to islands coalescence, the epilayer would exhibit low threading dislocation density. Otherwise, when the misfit strain is not fully relaxed during coalescence, further relaxation process may be needed, by the glide of dislocation half-loops from the surface accompanied by introducing more threading dislocations, as shown in Fig. 3.4d. Especially, as illustrated in Fig. 3.3d, for the case of GaN grown on LT-AlN interlayer with thickness of around 10 nm, LT-AlN interlayers often grow in Volmer-Weber mode. Since AlN islands don't coalesce completely, grain boundaries can easily act as the source of half-loops and they cause large number of threading dislocation by gliding in AlN interlayer. Furthermore, if the thickness is small, island boundaries can introduce geometrically necessary dislocations by matching the atomic bonds at the region of coalescence between neighboring islands [2]. Conclusively, Volmer-

Weber mode grown heteroepitaxial layers may contain large threading dislocation, such as in AlN interlayers and an AlN buffer layer and this is not favorable for the following growth of GaN, as explicated by Eq. (3-3).

In addition, there are some other strain relaxation mechanisms. Mechanism of nucleation of Shockley partial dislocations accounts for the misfit dislocation structure and critical thickness difference between epilayers which is suffering tensile and compressive stress. Cracking is also an important mechanism for lattice strain relaxation in tensile epilayers. Such cracking arises from the tensile stress during growth but not the thermal stress during cool-down. For example, AlN interlayers on GaN suffer tensile stress during growth. Cracking has been observed especially in HT-AlN ILs.

As mentioned previously, relaxation is favorable in AlN layers as it can reduce the lattice constant of AlN and make it more close to its neutral value. Therefore, in respect of this point, any mechanism which could cause strain relaxation in AlN is desired. Then many approaches can be adopted to relax AlN as much as possible, such as growing AlN interlayers under conditions yielding poor quality with high dislocation density, Volmer-Weber (3D) growth mode or even introducing cracking.

But on the contrary, for the same reasons, in respect of the growth and strain of overlying GaN, as base layer for the growth of overlying GaN, high quality AlN layers are also desirable. Our goal is to introduce compressive stress or strain in GaN as much as possible. In another word, any factor which may relax the strain in GaN layers should be eliminated. From Eq. (3-3), relaxation in GaN is proportional to the threading dislocation density in underlying AlN layers. From Eq. (3-4), larger threading dislocation density in GaN, more strain would be relaxed. By mechanisms of dislocation replication and multiplication, homogenous and heterogeneous dislocation nucleation and so on, heteroepitaxial layers may contain $10^5$ times the threading dislocation density of their substrate [2]. In other words, defects and dislocations in AlN layers would be the sources of overlying GaN and higher defect density in AlN causes larger dislocation density in GaN layer and yields more strain relaxation and then less compressive stress in it. Consequently, Volmer-Weber growth mode of AlN is beneficial to the relaxation of its lattice but detrimental to the strain in GaN. Similarly, cracking in AlN layers also weakens the ability of AlN layers to strain overlying GaN. In addition, although smooth AlN is not necessary for the introduction of compressive stress in GaN layer, but to grow GaN coherently and get it more compressively stressed, smooth AlN surface is also desired.

In conclusion, based on the discussion above, for a single AlN layer under GaN, there is a compromise or balance between the relaxation of AlN and the quality of overlying GaN. That is to say, the quality of AlN layer should not be too good or too bad, especially the interlayers. Or, for the ideal case, for the AlN interlayer, the lower interface II should be completely relaxed and its upper interface III is perfect. Therefore, the relaxation of AlN should take place at the lower interface II via misfit dislocations and desired case is that the dislocations do not propagate to the upper interface III (Fig. 3.3a). Thickness of AlN interlayers should also be limited before cracking occurs.

## 3.2 Stress introduction by AlN buffer layer

Although in some cases AlGaN might follow as a part of a buffer layer, AlN is nearly the only available option to start with for the growth of nitrides on Si. It is not only concerned with compressive stress introduction to the following GaN layer, more importantly, AlN should be applied firstly to eliminate the etching react of silicon and gallium, as what has been discussed in section 2.2. This section is about the experimental observation of compressive stress introduction in the first layer of GaN on AlN buffer layers grown under various conditions, by in-situ curvature monitor. It was found that GaN acts significantly differently on AlN buffer layer grown under different conditions. Some other characterization methods such XRD, atomic force microscope (AFM) and scanning electron microscope (SEM) were applied to account for such difference of the stress-strain behavior of GaN layer.

Prior to expounding the effects of AlN buffer layer on the stress behavior of GaN on it, some basic properties and growth mechanism of AlN will be reviewed briefly firstly. AlN has a very high melt point of 3350 K due to the high bond energy between Al and N atoms. The direct bandgap of 6.2 eV of AlN at room temperature is the highest among compound semiconductors [8-10]. Due to the large bandgap, AlN plays a pivotal role in the AlGaN ternary system and is necessary in most heterostructure devices fabricated in nitrides, especially the blue and ultra-violet LED and lasers. In part because of the large cohesive energy of Al and N bonds, at the original stage of the development of III-nitrides, it relied on AlN more than the other two binary compound cousins in AlGaInN system, i.e., GaN and InN [11]. For example, originally, the epitaxial growth of GaN has been utilizing two-step grown AlN buffer layer and achieved pretty GaN quality [12, 13]. If the conditions are optimal, the quality of GaN on sputtered AlN buffer layer can be even better than that on LT-GaN nucleation layer, for the growth on the substrates of both sapphire and silicon [14, 15]. Additionally, there are some more attractive features with AlN, such high hardness, high thermal conductivity and high resistance to chemicals [16, 17]. These beneficial properties partially come from the highest enthalpy of its growth reaction and the highest decomposition temperatures above 1300 ℃ [18, 19]. Due to its smallest lattice constant in AlGaInN system, in many cases, it is applied not only to construct the desired band structure in nitride devices, but also to adjust the stress state in the device, by inducing compressive stress in the overlying layer.

The activation energy for the diffusion of Al atoms on substrate surface is very high of 1.17 eV and leads to low mobility of Al atoms on growth surface [20, 21]. That is why the growth of AlN tends to be Volmer-Weber mode and forms grain domains or islands, on a variety of substrates including sapphire, silicon and SiC. Two-dimensional smooth surface formed by step-flow growth is difficult for the growth of AlN. Therefore, in order to improve the mobility of Al atoms on the growth surface, for its MOVPE, high temperature is more indispensable, and high V/III ratio is not necessary. The metal-organic source for the MOVPE of AlN is trimethylaluminum ($(CH_3)_3Al$, or short as TMA). The possible reactions could be [22, 23]

$$2(CH_3)_3Al + 2NH_3(g) + H_2(g) \rightarrow 2(CH_3)_2Al{:}NH_3(a) + 2CH_4(g) \qquad (3\text{-}5)$$

$$2(CH_3)_2Al{:}NH_3(a) \rightarrow CH_3Al(NH_2)_2AlCH_3(a) + 2CH_4(g) \quad (3\text{-}6)$$

$$CH_3Al(NH_2)_2AlCH_3(a) \rightarrow Al(NH)_2Al + 2CH_4(g) \quad (3\text{-}7)$$

and

$$Al(NH)_2Al \rightarrow 2AlN(a) + H_2(g). \quad (3\text{-}8)$$

The pre-reaction between TMA and $NH_3$ is very strong and they should be well separated before the growth starts on the substrate. Since the affinity binding between Al and C or O is very high, it is difficult to grow high purity AlN. Based on the reasons above, generally, good AlN is grown at high temperatures up to 1400 ℃ to enhance the mobility of Al atoms [24] and low pressure to reduce the incorporation of impurities of C, O and so on. Two-step growth is adopted by Ohba et al. firstly. A 20-nm thick AlN nucleation layer was formed at 1200 ℃, and the epilayer was grown in the temperature range of 1270 to 1450 ℃. The V/III ratio was varied from 1.2 to 4. Benefited from high temperature and then the improved Al surface mobility, the surface both for the nucleation layer and the final film surface was very smooth [25]. Kaeding et al. also took two-step method to grow AlN, but under low pressure (76 Torr) and at lower temperature [26]. They applied LT-nucleation layer at 690 ℃ and with V/III ratio of 2.9. Followed that, the epitaxial AlN was grown at 1130 ℃, with V/III of 36.4. Even with the thickness exceeded 1 um, there were still grooves and hexagonal islands on the surface which did not coalesced fully. These studies showed that high temperature above 1200 ℃ is indispensable to achieve high quality and smooth AlN thin film.

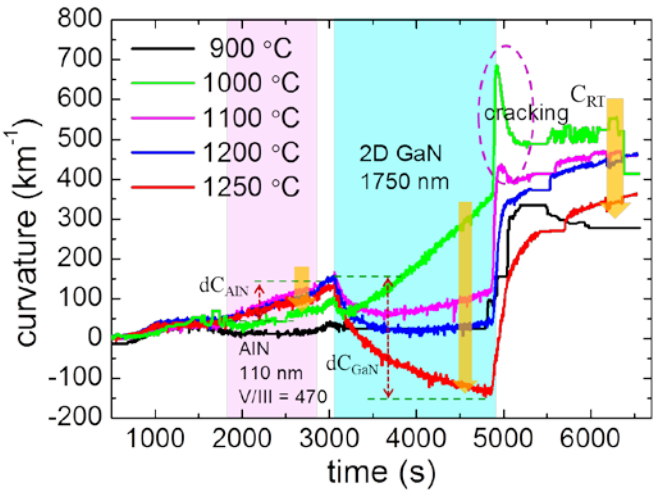


**Fig. 3.5** Curvature transition during the growth of GaN on AlN buffer layers grown at 900 ℃, 1000 ℃, 1100 ℃, 1200 ℃ and 1250 ℃, with V/III of 470.

### 3.2.1 Temperature effect

As introduced above, temperature is a decisive factor for the growth of nitride, especially AlN. In most previous studies, the growth temperature for AlN buffer layer was limited to be lower than 1100 ℃. In this range, best GaN quality was obtained at the AlN buffer layer grown at temperature close to 1100 ℃ [27]. Generally, in order to get high quality AlN epilayer, the growth temperature is higher than 1300 ℃ [28]. Similarly, since high quality

AlN buffer layer is desirable to improve the performance of GaN on it, growth temperature for AlN buffer layer higher than 1100 ℃ was applied in this study. As shown in Fig. 3.5, it was increased from 900 ℃ to 1250 ℃. Actually, GaN growth on AlN buffer layer grown at 800 was also tried and not shown here because GaN cannot grow on it epitaxially but with not coalesced grains with various crystallographic orientations. It is obvious that the growth temperature of AlN buffer is very effective on the stress behavior of GaN layer, during the growth and after.

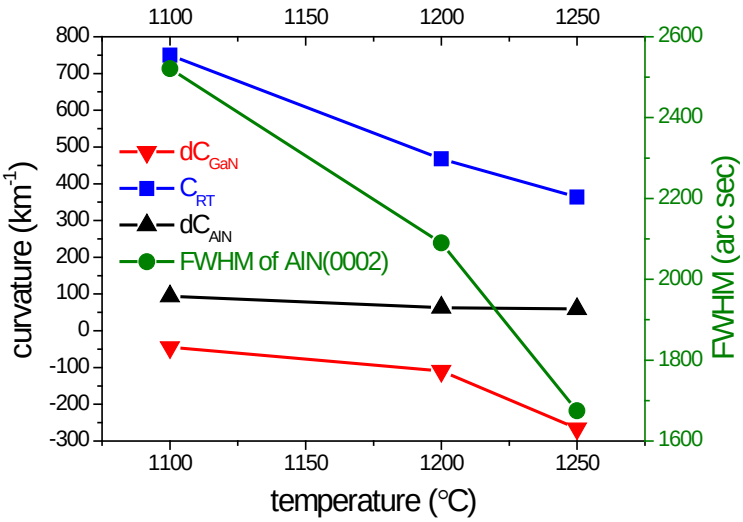


**Fig. 3.6** Summary of the curvature increment (absolute value) in AlN ($dC_{AlN}$, tensile) and GaN ($dC_{GaN}$, compressive), final curvature at room temperature ($C_{RT}$) and XRD FWHM of AlN buffer.

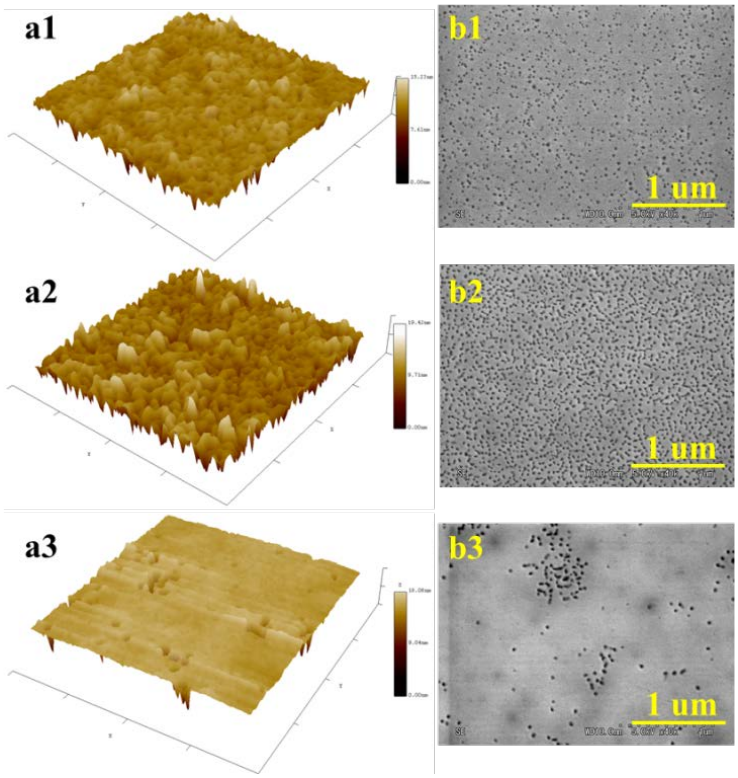


**Fig. 3.7** AFM (line a, left column) and SEM (line b, right column) images of AlN buffer layers grown at 1100 ℃ (a1 and b1), 1200 ℃ (a2 and b2), 1250 ℃ (a3 and b3). Scanning area for AFM is $2 \times 2$ um$^2$.

Because what we care is curvature or bowing, our target is to achieve final curvature or bowing value of the wafer around zero after growth at room temperature, in this chapter, discussion would be based on the analysis of curvature transition and variation. This is a more direct and intuitive method to read and understand the curvature behavior of growths under various conditions. The quantitative analysis of the stress and strain of individual layers will be carried out in the next chapter. Based on Stoney formula, higher curvature slope indicates larger stress in the film. Since the thickness of AlN buffer layer and GaN layer were fixed to be 110 nm and 1.75 um respectively here, absolute variation of curvature value reflects the amount of stress.

The in-situ curvature transition during growth and cool-down was recorded as Fig. 3.5. From Fig. 3.5, the absolute curvature increments in individual growth stage were extracted in Fig. 3.6, including the curvature increase of AlN buffer and GaN, to the tensile and compressive side respectively. The final curvature at room temperature, which we care most and the FWHM of XRD rocking curve of AlN buffer were also incorporated in Fig. 3.6. As the curvature curve showed, there were three stages to be analyzed one by one, i.e., curvature transition in AlN buffer, GaN and during cool-down.

Firstly, about the curvature transition in AlN buffer, the stress is constant from the beginning of the growth to the end. In small thickness up to 110 nm, the stress in AlN on Si was tensile and constant, from nucleation and 3D islands coalescence [29]. The constant stress indicates that there is no dramatic phase transition or coalescence process during the growth up to 110 nm. As growth temperature of it increases from 900 ℃ to 1100 ℃, the curvature slope, namely the tensile stress in AlN buffer, increased. Such increase indicates an improvement of crystal quality. At low temperature below 800 ℃, AlN tended to be amorphous or polycrystalline and didn't induce stress inside it. As the growth temperature increases, AlN becomes more crystalline and epitaxial, and could be strained by the substrate of Si effectively. On the contrary, from 1100 ℃ to 1250 ℃, the tensile stress in AlN buffer layer decreased with rising temperature. This is consistent with previous result about AlN growth on Si that from growth temperature of 1100 ℃ the stress in AlN drops slightly, although the mechanism has not been well clarified yet [30]. Such decrease is preferable for controlling the overall stress for GaN on Si, although the difference was minimal. Both the XRD rocking curve FWHM in Fig. 3.6 and the surface images by AFM and SEM in Fig. 3.7 showed considerable quality and surface roughness improvement of AlN buffer as the growth temperature increased. It became more and more epitaxial as the growth temperature rose. At 1250 ℃, the pit density and roughness decreased significantly. However, based on the relaxation mechanisms introduced in part 3.1.3, higher crystal quality usually means smaller strain relaxation and higher stress in the film, which was conflicting with the experiment observation here. But from the view of temperature dependent lattice constant difference ($d_a$), since smaller $d_a$ yields less strain and then less stress, as plotted in Fig. 3.8, the decreasing $d_a$ between Si and AlN as increasing temperature may account for the dropping stress in HT-AlN buffer. Nonetheless, further characterization and analysis is needed to interpret the curvature and stress behavior of AlN buffer here.

Secondly, in the stage of GaN growth, due to larger lattice constant than AlN, all overlying GaN went through compressive strain except the failed one grown on 900-℃-AlN buffer, at least at the initial growth stage. To our greatest interest, compressive stress introduced in GaN layer was increased significantly as the growth temperature for AlN buffer layer increased. In order to compensate the tensile stress which was applied to GaN layer during cooling down, compressive stress in GaN should be introduced as much as possible during growth. The growth of GaN on 900-℃-AlN buffer was not successful with a great number of V-pits. Then the light beams for the curvature monitor were scattered and no signal went to the sensor, so the curvature curve couldn't be collected for it. From the growth temperature for AlN buffer layer ($T_{AlN}$) of 1000 ℃, GaN can be grown epitaxially. As $T_{AlN}$ increases, GaN on it can be strained more and more compressively, and the strain relaxation rate from compressive to tensile got slower and slower. At $T_{AlN}$ of 1000 ℃, GaN was strained compressively only at the first 40 nm. Around thickness of 40 nm, the strain shifted from compressive to tensile immediately. Such relaxation process became slower and slower when GaN was on AlN grown at 1100 ℃ and 1200 ℃. As $T_{AlN}$ was raised to 1250 ℃, GaN was always compressively strained through the thickness of 1.75 um, which was expected.

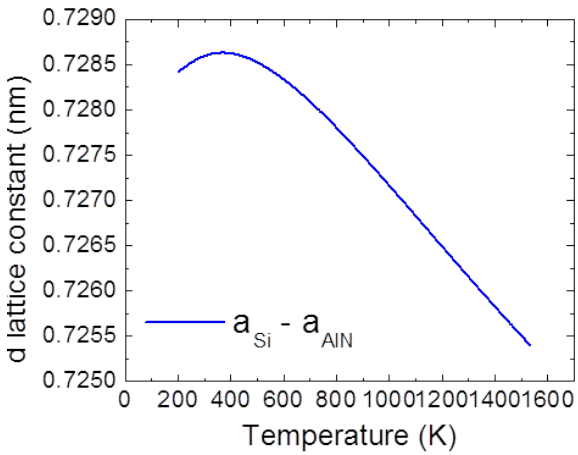


**Fig. 3.8** In-plane lattice constant difference between Si and AlN as a function of temperature.

In order to investigate why the growth temperature of AlN buffer layer could affect the performance of the overlying GaN layer so significantly, we put forward some hypothesis based on the interface between AlN buffer layer and GaN on it, as proposed in part 3.1.3. The surface of AlN buffer layers were characterized by AFM and SEM, as shown in Fig. 3.7. Tow indicators, namely, the roughness and dislocation density of AlN buffer layer surface, are important to describe the quality of AlN itself as well as interface ideality between AlN and GaN. Due to extremely high dislocation density of a 110-nm-thick AlN buffer layer on Si, pit density observed from SEM images was adopted here instead of dislocation density.

Roughness of root mean square (RMS) from AFM and pit density from SEM images for the surface of AlN buffer layers were listed in Table 3.1. As growth temperature increased from 1100 ℃ to 1200 ℃, both of the RMS and pit density doubled. From the AFM images, however, the surface grown at 1200 ℃ looked more crystalline and with larger crystal grains and higher quality than the surface grown at 1100 ℃, as verified directly by FWHM of XRD rocking curve for AlN buffer layers in Fig. 3.7. Due to very small thickness of 110 nm, only

(0002) plane is measurable. Probably this is why the ability for AlN buffer layer grown at 1200 ℃ to introduce compressive stress in succeeding GaN layer has been improved only a little while the quality of GaN on it has been enhanced a lot.

**Table 3.1** RSM and pit density of the surface of AlN buffer layers.

| Temperature (℃) | RMS (nm) | Pit density ($cm^{-2}$) |
|---|---|---|
| 1100 | 1.095 | 1.70E+10 |
| 1200 | 2.064 | 2.90E+10 |
| 1250 | 1.094 | 2.40E+09 |

With only 50 ℃ increase in temperature from 1200 ℃, the morphology of AlN buffer layer surface was completely different. The surface was much smoother, due to higher atomic mobility for aluminum atoms at higher temperature [31]; pit density also decreased sharply to one tenth of that on AlN grown at lower temperature. FWHM of XRD rocking curve in Fig. 3.7 also showed considerable quality improvement. This indicated directly that AlN grown at higher temperature has higher quality, which is consistent with AFM and SEM observation results. Consequently, the curvature value at the end of GaN growth converted from tensile side to compressive side by variation of approximately 100 $km^{-1}$. On the other hand, after cooling down, the curvature value caused by tensile stress decreased from more than 500 $km^{-1}$ to 364 $km^{-1}$. All these behaviors indicated that the elastic mechanical properties of AlN and GaN layers have been improved a lot, which were brought by their quality improvement due to growth temperature elevation for AlN buffer layer, as shown in Fig. 3.6, while the quality information of GaN would be given in chapter 5.

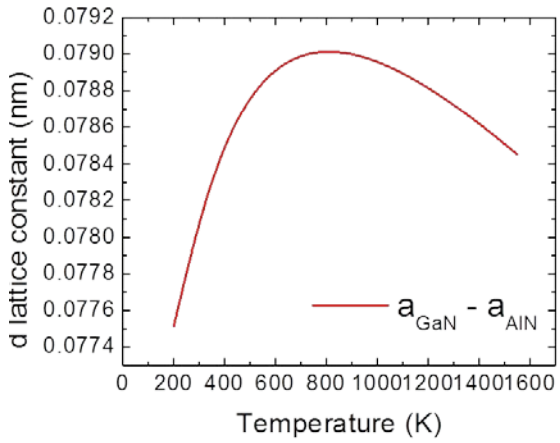


**Fig. 3.9** In-plane lattice constant difference between GaN and AlN as a function of temperature.

Based on the consistent results from AFM, SEM and XRD rocking curve, it's safe to assume that AlN grown at higher temperature has higher quality and lower threading dislocation density. Using the knowledge of strain relaxation in part 3.1.3, higher dislocation density leads to higher misfit dislocation density in the interface of GaN/AlN, then larger amount of relaxed strain in overlying GaN [2, 32, 33]. Higher density threading dislocation propagates or be multiplied from AlN buffer to GaN. This is why GaN on 1100 ℃ AlN relaxed and went to tensile strain much faster than that on higher temperature AlN buffer

layers. The strain evolution during the growth of GaN will be analyzed quantitatively in chapter 4. The common feature for all three samples is that during the initial stage of GaN growth it relaxes rapidly and become stable or saturated after large thickness.

As discussed in part 3.1.3, another important cause to account for the strength of compressive stress in GaN is the lattice constant difference between it and underlying AlN buffer which was grown at different temperatures. The primary factor to determine the lattice constant is growth temperature. The in-plane lattice constant difference between GaN and AlN as a function of temperature is plotted in Fig. 3.9. It shows that $d_a$ between GaN and AlN decreases when the temperature is higher than 530 ℃, which would weaken the ability of AlN to strain overlying GaN. However, because AlN buffer is highly relaxed, so this effect of reduced $d_a$ on the strain in GaN may be very weak. On the other hand, since the quality of GaN/AlN interface was improved significantly, enhancing influence on the strain in GaN from the improvement of interface should have overtaken the weakening effect from decreasing $d_a$.

Thirdly, also most importantly as our final target, the tensile curvature value after cooling down was reduced from more than 500 $km^{-1}$ to 364 $km^{-1}$ as growth temperature for AlN buffer was increased from 1100 ℃ to 1250 ℃. For the sample with the AlN buffer layer grown at 1100 ℃, during cooling down, the curvature curve transient showed sudden drop, which indicates that cracking of GaN occurred at that time due to extraordinary high tensile stress that GaN film suffers. If no cracking occurred, positive curvature to the tensile side exceeding 750 $km^{-1}$ would be predicted. As observed by naked eyes under light, crack was much less for the sample with AlN buffer layer grown at higher temperature.

In conclusion for this part of growth temperature effect of AlN buffer layer, based on interface analysis, in order to induce compressive stress in GaN as much as possible, and to acquire smaller tensile stress after growth at room temperature, the quality of AlN buffer should be as high as possible and elevating growth temperature of AlN buffer is a very effective way. Higher temperature more than 1200 ℃ can enhance the AlN quality, reduce the defect density and enhance the smoothness of AlN surface considerably. Then the high compressive stress can be introduced in the 1$^{st}$ GaN layer efficiently, while in most other researches, they got only tensile stress in the 1$^{st}$ GaN layer [34].

### 3.2.2 V/III ratio effect

Although for the growth of AlN, V/III is not as influential as temperature, but without proper V/III, high quality AlN can hardly be grown. Temperature determines the quality of AlN predominately, for example it is amorphous, polycrystalline, or single crystalline. There are some general problems for the MOVPE of AlN. The growth rate of AlN is usually very low, under mostly being used conditions it is 0.3 – 1.5 um/hour, as plotted in Fig. 3.10, about 1/10 ~ 1/4 of that of GaN. Another problem is the pre-reaction and parasitic reactions between group-III and group-V precursors. Generally, to achieve a good quality, ammonia should be supplied with large excess, i.e., very high V/III ratio. On the other hand, to achieve high growth rate, TMAl should be flowed sufficiently. If the flow rate of precursors is too

high, parasitic gas phase pre-reactions occurs easily [35-39]. Pre-reactions occur in gas phase and nanoparticles of AlN are carried away by the flow from the upstream to the downstream. Some particles deposit on sample surface and roughen it. Consequently, V/III ratio also affects the morphology and surface roughness of AlN considerably [40] there should be a proper range of it. All these can affect the stress and strain behavior of overlying GaN.

In general, V/III ratio for the growth of AlN can be varied from 1 to above 10000 [39]. The tested V/III here varies from 115 to 9156. Curvature transition during growth and cool-down was shown in Fig. 3.11. In Fig. 3.12, the absolute curvature increase in AlN buffer and GaN

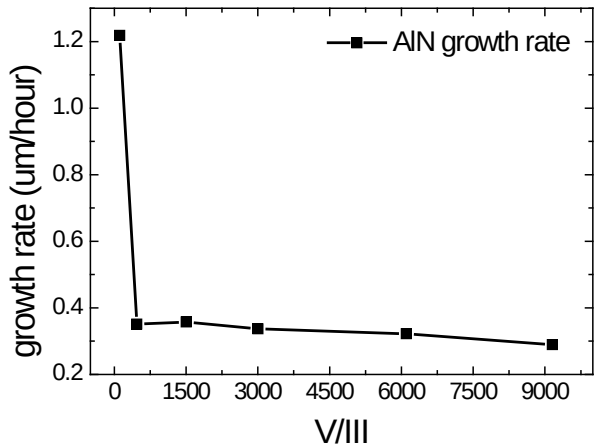


**Fig. 3.10** AlN growth rate as a function of V/III.

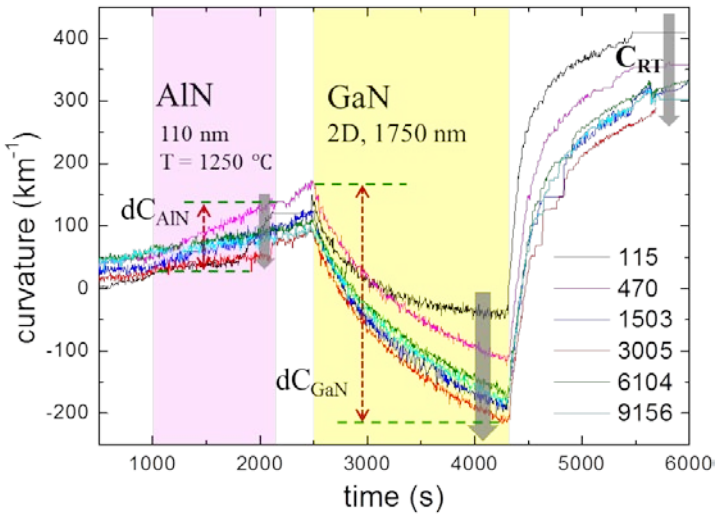


**Fig. 3.11** Curvature transition during the growth of GaN on AlN buffer layers grown under varying V/III ratio from 115 to 9156, at temperature of 1250 ℃ and with thickness of 110 nm.

and the final curvature at room temperature were extracted from the curvature transition curves in Fig. 3.11. Although the effect on GaN curvature transition from V/III ratio of AlN buffer growth is not as large as that of temperature, it does influence the strain and stress in AlN itself and GaN substantially. The overall tendency is that there exists a proper V/III ratio which can introduce the highest compressive stress in GaN and yield the lowest curvature at room temperature, and the proper V/III ratio here is shown to be around 3005. For this V/III ratio, the tensile stress in the AlN buffer is also the smallest.

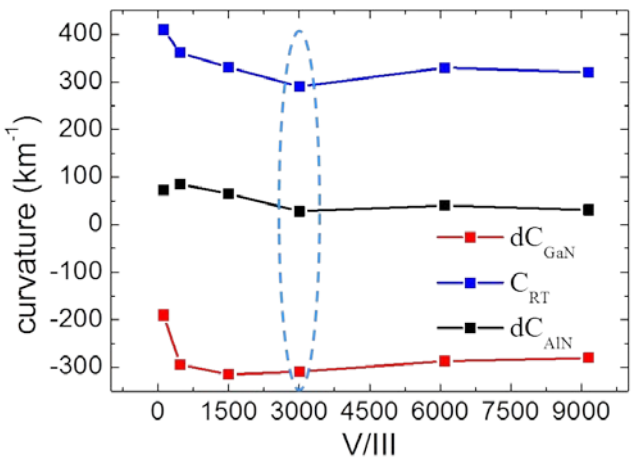


**Fig. 3.12** Summary of the curvature increment (absolute value) in AlN ($dC_{AlN}$, tensile) and GaN ($dC_{GaN}$, compressive), final curvature at room temperature ($C_{RT}$).

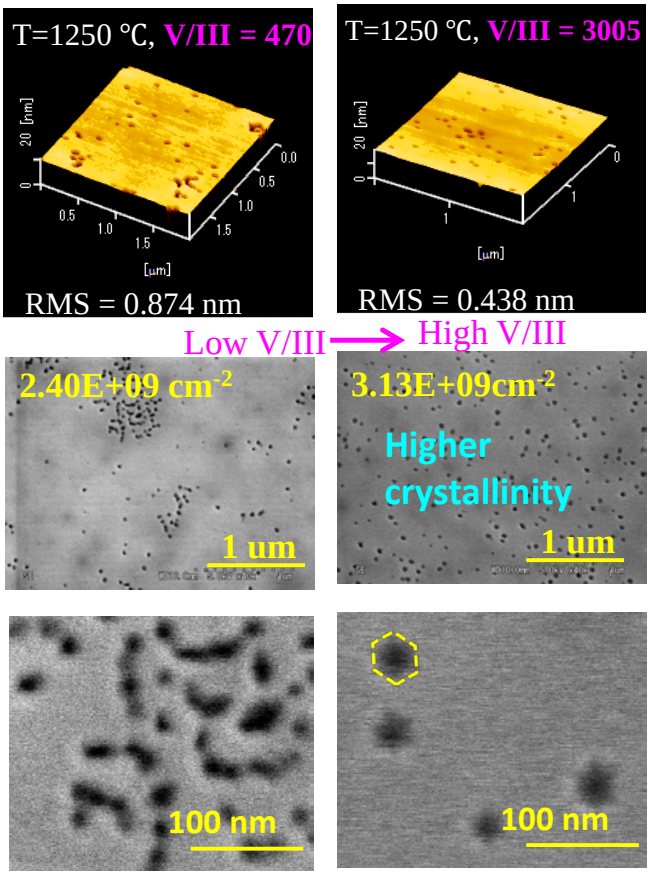


**Fig. 3.13** AFM and SEM of the surface of AlN buffer layers grown under V/III ratio of 470 and 3005.

In the first stage of AlN buffer growth, the curvature increase to the tensile direction in the same thickness can be a reflection of AlN quality. The same as temperature test, AlN buffer grows at constant curvature slope, i.e., constant stress, under various V/III ratio, while the slope differs depending on the V/III. With the fixed thickness of 110 nm, the tensile stress in AlN buffer grown under low V/III ratio less than 1500 is 2 ~ 3 times of that grown under high V/III ratio more than 1500. In the temperature test, such difference was attributed to the

variation of lattice difference between AlN and Si at different growth temperature. But this mechanism cannot be applied here due to the fixed temperature of 1250 ℃. The cause here might be related to the crystal grain size, length of grain boundaries and the binding force between the atoms on the boundaries of neighboring grains. Smaller grains cause less intrinsic stress in the film. From the SEM images in Fig. 3.13, we can see that V/III ratio can also affect the crystallinity. Under low V/III ratio at 470, the pit shape is not regular and doesn't show any crystalline facet. While in the left column, under the V/III ratio of 3005, like the pits in GaN, the pits show a shape of regular hexagons with six tilted facets, which are an indication of the hexagonal crystal system for nitrides [41]. The appearance of hexagonal pits verifies the substantial quality improvement brought by the optimal V/III ratio. Then there is a question that, why the intrinsic stress in AlN with better quality is smaller? This needs to be investigated further.

In GaN layer, all samples went through compressive stress within the thickness of 1750 nm. The curvature increase $dC_{GaN}$ in GaN was small around 170 $km^{-1}$ on the AlN buffer grown at low V/III ratio at 115. After that, variation of $dC_{GaN}$ was not large, from 280 $km^{-1}$ to 315 $km^{-1}$, and the highest value appeared around the V/III ratio of AlN from 1500 to 3000. The final curvature after cool-down at room temperature ($C_{RT}$) is what we care most, should be as close to zero as possible. Opposite to the tendency of $dC_{GaN}$, $C_{RT}$ is higher at low V/III of AlN buffer. It decreased from 410 $km^{-1}$ to 331 $km^{-1}$ as the V/III ratio rose from 115 to 1500. After that, the variation was small, and the lowest $C_{RT}$ appeared around V/III ratio of AlN growth of 3005. As shown in Fig. 3.13 and discussed above, this improvement was brought by the optimization of AlN buffer surface, which includes the enhancement of crystallinity and reduction of surface roughness, for example RSM decreased from 0.874 nm to 0.438 nm as the V/III ratio increased from 470 to 1500. It can be expected that after V/III ratio of 1500, the quality and surface morphology of AlN doesn't change very much. This would be verified by the XRD rocking curve measurement of GaN layers on them in chapter 5, in which shows the variation of the quality of GaN was very small on AlN grown under V/III ratio from 1500 to 9156.

### 3.2.3 Thickness effect

As well known, for hetero-epitaxial growth, the dislocation density is inversely proportional to the film thickness [42-45]. In other words, for the same hetero-epitaxial material system, thicker film has higher quality. In the analysis of the influence of growth temperature of AlN buffer layer on the stress behavior of GaN, we know that AlN with higher quality induced larger compressive stress in the first GaN. Since the quality of AlN buffer layer can be improved by its thickness, then the thickness of AlN should also affects the stress behavior of GaN on it. As well known, not like GaN, it is not easy to grow high quality AlN on sapphire. Usually, for thick AlN (~ 2 um) the edge type dislocation density is around the level of $10^9$ $cm^{-2}$ in comparison to GaN with it of $10^8$ $cm^{-2}$ [46, 47]. In the study by Kaeding et al. [26], on sapphire, original AlN nucleation grains coalesce completely until it grew to 2.1 um. The threading dislocation density for the thickness of 1.05 um and 2.1 um was $1.1\times10^{10}$ $cm^{-2}$ and $5\times10^9$ $cm^{-2}$ respectively, which decreased by one fold. By relating the

FWHM of XRD rocking curve of the planes of (0002) and (20-21) and thickness from 0.35 ~ 2.8 um, edge dislocation density decreased with increasing thickness while screw dislocation density didn't change a lot.

In order to investigate the effect of AlN buffer thickness on compressive introduction to GaN layer, GaN growth on AlN buffer with thickness of 55 nm, 110 nm and 220 nm was tested. The in-situ curvature observation curves are plotted in Fig. 3.14. In the stage of AlN

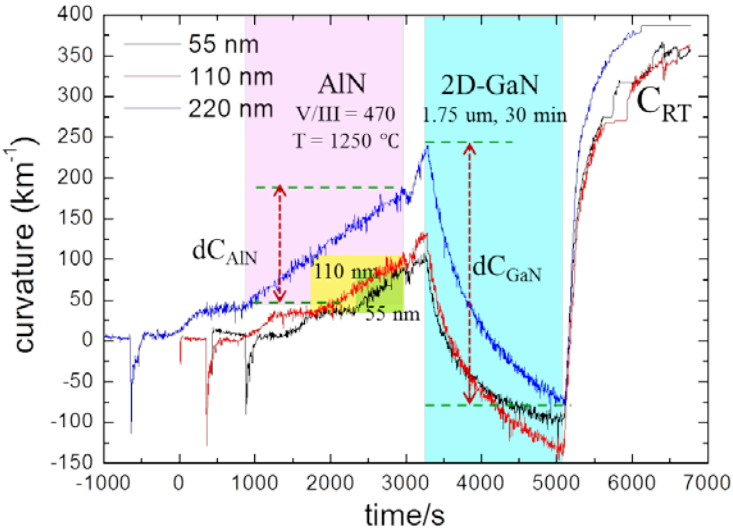


**Fig. 3.14** Curvature transition during the growth and cool-down of GaN on AlN buffer with thickness of 55 nm, 110 nm and 220 nm.

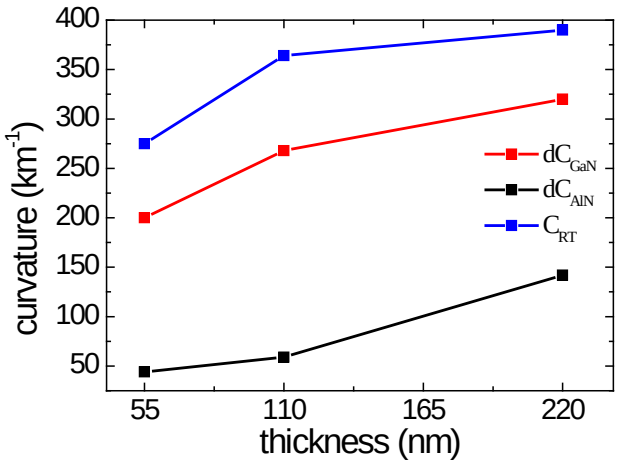


**Fig. 3.15** Summary of the curvature increment (absolute value) in AlN ($dC_{AlN}$, tensile) and GaN ($dC_{GaN}$, compressive), final curvature at room temperature ($C_{RT}$).

growth, because the growth conditions were fixed to be identical, so the curvature curves for the three samples in this stage were parallel with the similar stress. As illustrated in Fig. 3.15, both of $dC_{GaN}$ and $C_{RT}$ rose as the buffer thickness increased. But the slope of the curve of $dC_{GaN}$ from 110 nm to 220 nm is about 1/4 of that in the thickness range from 55 nm to 110 nm. It can be imaged that, as a function of AlN buffer thickness, curvature increase to compressive direction in GaN rose rapidly in the range of AlN buffer thickness from very small value (10 nm for example) to 110 nm, and in the following range from 110 nm to larger

value more than 220 nm, $dC_{GaN}$ increasing rate slowed down and get saturated gradually. Based on the behavior in temperature test that better AlN buffer induce higher compressive stress in overlying GaN, the phenomenon here indicates the quality improvement of AlN buffer is a function of its thickness. It can be speculated that the quality of AlN buffer improves dramatically in the original stage of growth, as the thickness becomes large, quality improvement gets less and less efficient. This is consistent with the researches which have been mentioned above in the beginning of this part.

However, although $dC_{GaN}$ enhanced by thickening AlN buffer thickness, the final curvature at room temperature $C_{RT}$ also rose considerably. This acts contrarily to the previous studies on temperature and V/III ratio, in which $C_{RT}$ decreases as $dC_{GaN}$ increases. This can be attributed to the curvature increase to the tensile side in AlN buffer, by both lattice mismatch stress and thermal mismatch stress during cool-down. As thickness increases, the curvature increment to tensile side in AlN buffer also increased a lot. Another source of tensile curvature increment comes from thermal mismatch during cool-down. According to Stoney formula, thicker film brings higher curvature increment. Consequently, compressive curvature increment in GaN could not compensate the tensile opponent arose in AlN buffer layer, and caused the increase of final curvature $C_{RT}$ at room temperature.

## 3.3 Effects of AlN interlayers

### 3.3.1 Introduction

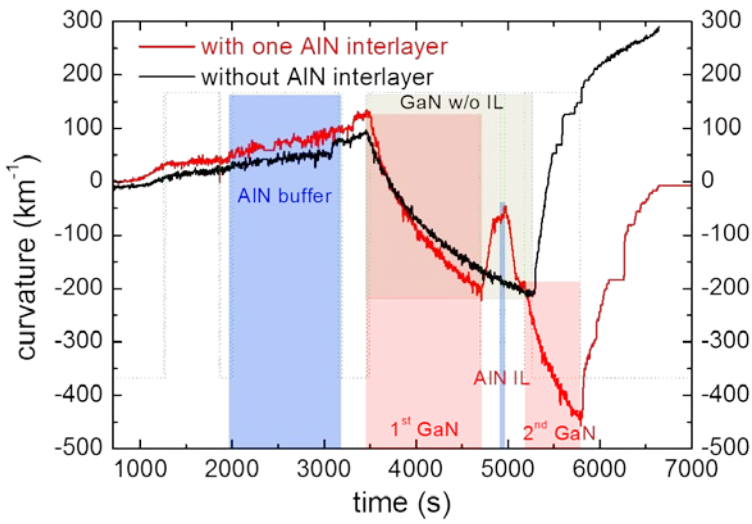


**Fig. 3.16** Curvature comparison between samples with and without an AlN interlayer.

For this particular material system, precise stress control is one of the most important targets, not only for getting crack-free GaN, but also for engineering the stress effect on devices on it. To achieve this, since the lonely AlN buffer layer cannot induce enough compressive stress, as a key, AlN interlayers (ILs) has been applied to enhance it. As compared in Fig. 3.16, with the same total GaN thickness of 1.75um, further curvature to the compressive side of 250 $km^{-1}$ could be introduced by the insertion of a single AlN interlayer. With an AlN interlayer, the final curvature at room temperature also went to around 0 and it

was totally crack free. Therefore, the application of AlN ILs is compulsory for producing crack-free GaN on Si. To optimize the structure and growth conditions, it is critical to understand the stress behaviour of AlN IL itself and its effect on the overlying GaN layer, as a function of the growth conditions of AlN ILs. High sensitivity in-situ curvature monitoring allows us to directly access to the stress and strain in the layer under growth, and it is quite suitable and helpful for such a comprehensive study.

AlN interlayer was first applied to reducing the dislocation density in GaN and the control of stress to yield crack free AlGaN on sapphire [48, 49]. The role of AlN or AlGaN interlayers in the growth of GaN on Si has been studied by Dadgar, Bläsing, Reiher, Fritze et. [3, 4, 50, 51]. They studied the effect of growth temperature and showed that low-temperature AlN interlayer acted as a separating layer between neighbouring GaN layers and was more effective in controlling stress. Dimitrakopulos investigated the strain accommodation and relaxation mechanisms at AlN interlayers with thickness from 3 to 100 nm in GaN grown by MBE on Si using Transmission Electron Microscopy (TEM) [52]. No line defect was observed when the thickness was less than 6 nm, while above it, a-type misfit and threading dislocations occurred and cause relaxation principally. Growth conditions of AlN ILs have been studied by some other authors also [34, 53-57], while there are some problems with their experiments and that might degrade the reliability of their results. Firstly and most importantly, none of them applied in-situ direct curvature monitor to observe the effect of AlN ILs on the stress introduction to the subsequent GaN layer. Only indirect methods, e.g. scanning electron microscope (SEM), atomic force microscope (AFM), X-ray diffraction (XRD), to obtain the information of surface roughness, crack density, lattice constants and so on to access the effect from AlN ILs. These indirect methods could not obtain the exact stress transition process quantitatively. Secondly, their adopted conditions might be not optimal. For instance, most adopted thickness ranged from 10 to 28 nm, which has already exceeded the theoretical critical thickness of AlN on GaN of less than 8 nm [58]. Thirdly, indispensable comparison between the effect of AlN ILs before and after relaxation was missed. The tested V/III ratio range was too narrow from 640 to 1707 that sometimes

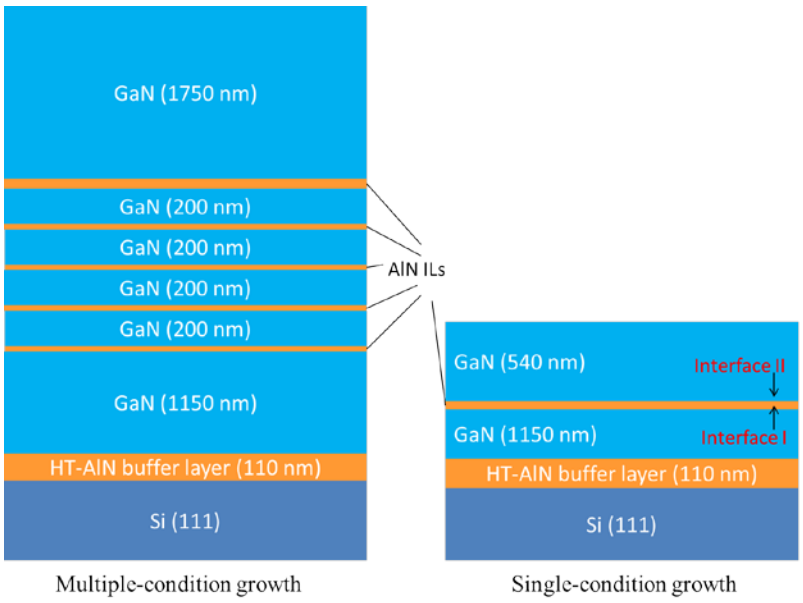


**Fig. 3.17** Schemes of multi- and single-condition structures.

cannot cover the influence from the fluctuation of reactor conditions. In addition, there was very little direct observation of AlN ILs by TEM, to access the information of their morphology, defects, thickness, composition and interfaces, which is critical to understand the relaxation of themselves and stress introduction in overlying GaN. Finally, no qualitative theoretical model was proposed to understand the behaviour of AlN ILs on introducing compressive stress to GaN layers.

**Table 3.2** Conditions of AlN ILs in multi-condition structure.

| Condition | set values (bottom to top) | fixed conditions |
|---|---|---|
| thickness | 4.5/9/12.5/22.5/45 nm | 900 ℃, V/III = 1503 |
| temperature | 1200/1050/900/750/600 ℃ | 6 nm, V/III = 1503 |
| V/III ratio | 470/1503/3005/6010/9015 | 6 nm, 900 ℃ |

In this study, we compared the ability of introducing compressive stress by AlN ILs grown under different conditions by direct in-situ curvature monitoring. Three groups of samples were designed to investigate the influence of growth conditions of AlN ILs with very large ranges, including temperature from 600 ℃ to 1200 ℃, thickness from 4.5 nm to 45 nm, and V/III ratio from 470 to 9015, respectively. This work didn't target optimizing the growth conditions of AlN interlayers precisely but to show a methodology to survey them quickly through only 3 samples and relatively proper range can be obtained. Based on the behaviour of AlN ILs, a model of ideal AlN IL which may introduce compress stress most effectively was proposed.

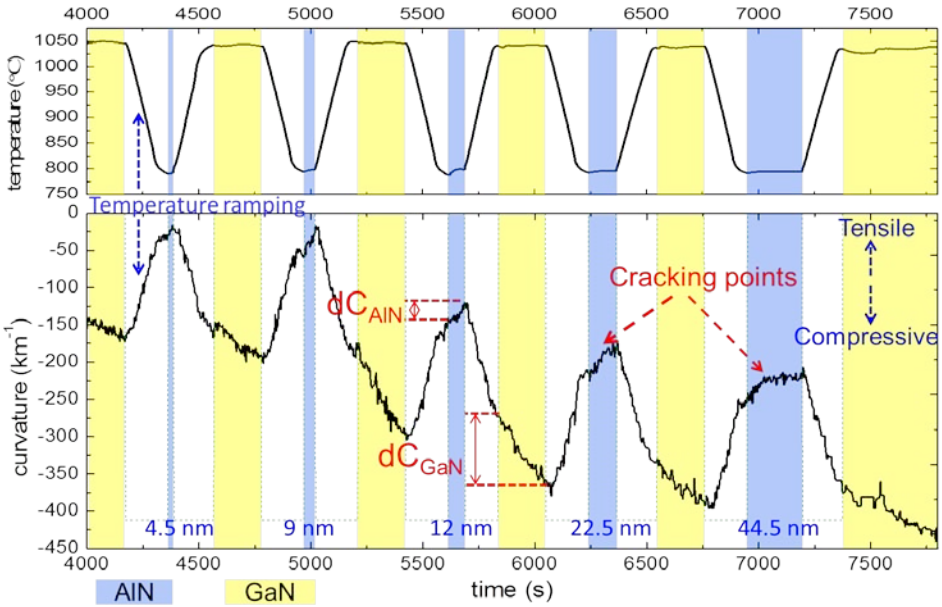


**Fig. 3.18** Thickness test, an example of curvature and temperature transition during the growth of AlN ILs and GaN layers on them. Transition in white periods is due to thermal expansion.

The sample structures will be illustrated in detail firstly. As shown in Fig. 3.17, two structures were designed to make comparison as reliable as possible. One was called a multi-condition structure. For example, for temperature comparison, from the bottom to top, the growth temperature of AlN ILs increased from 600 ℃ to 1200 ℃ with a step of 150 ℃, while all the other conditions were kept the same. The other single-condition structure incorporated

just a single AlN IL, to eliminate the influence of preceding GaN/AlN structures on the following ones under investigation in multi-condition structure. For the single-condition structure, the AlN IL condition was varied in different growth batch. Single-condition samples have been grown for temperature and thickness investigation, but not for V/III ratio yet since its effect was not very significant.

First of all, the growth rate of AlN under various conditions was calibrated by growing bulk layers with thickness more than 500 nm to obtain accurate AlN IL thickness. Prior to strict control growth, preliminary growth batches were proceeded to find out the proper conditions roughly, e.g. temperature around 900 ℃, V/III ratio around 1500 and thickness of about 9 nm before relaxation. These were adopted as the base condition in strict control tests.

Fig. 3.18 is an example of curvature transition during the growth of AlN ILs and GaN layers on them, for AlN IL thickness study. As marked by $dC_{GaN}$, the ability of AlN to introduce compressive stress to the overlying GaN layer was evaluated in terms of the increase in curvature to the compressive direction in a 200-nm thick GaN. Tensile curvature increase in an AlN IL was also observed to clarify the tensile stress accumulation and the relaxation of AlN ILs, as marked by $dC_{AlN}$. Fig. 3.19 is an example for single-condition structure sample. $dC_{AlN}$ and $dC_{GaN}$ have also been extracted to evaluate the effects of AlN ILs. But for $dC_{GaN}$, the value is only from the first 200 nm of the top GaN, in order to compare them with the layers in multi-condition samples because GaN thickness in them in between AlN ILs was 200 nm. A model to describe the role of AlN ILs of introducing compressive stress to GaN layers would be proposed based on the lower and upper interfaces at AlN ILs, as marked in Fig. 3.17.

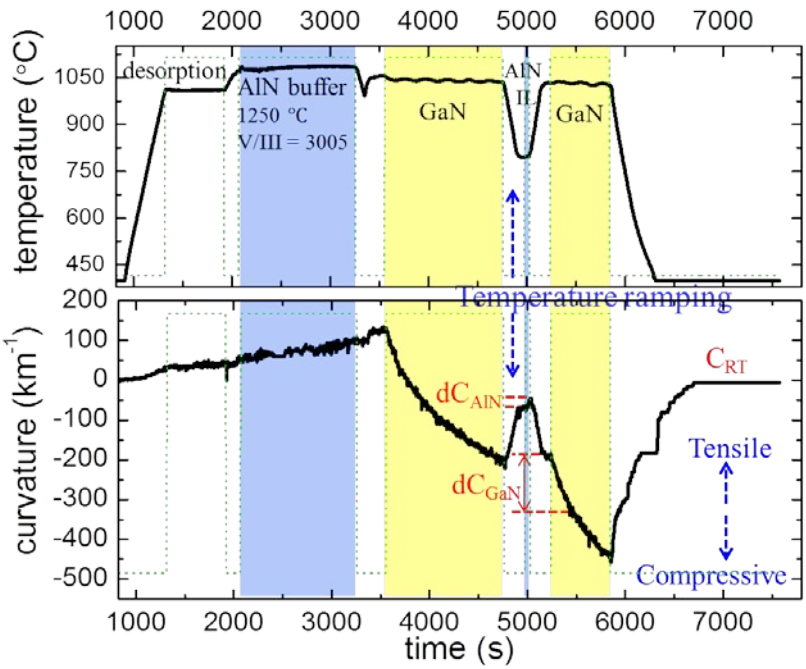


**Fig. 3.19** An example of curvature transition corresponding to temperature for a single-condition growth for AlN interlayer investigation.

In order to compensate the tensile stress in GaN on Si due to large thermal expansion coefficient difference between them during wafer cooling, it is desired that a single AlN IL

could introduce compressive stress to GaN layer as much as possible. Prior to the discussion about the effects of AlN ILs, some theory about stress and strain introduction is reviewed here again briefly. As discussed in part 3.1.3, theoretically, there are two factors that determine how effective an AlN IL can introduce compressive stress to the overlying GaN layer.

The first is the difference in lateral lattice spacing between AlN IL and GaN $d_{a(GaN-AlN)}$, which should be larger. Since the growth condition for GaN has been fixed, so the lattice constant of it $a_{GaN}$ has also been fixed. Then $d_{a(GaN-AlN)}$ will be determined only by the lattice constant of AlN ILs $a_{AlN}$. Factors determining $a_{AlN}$ include growth temperature, composition fluctuation (by Ga diffusion) and its relaxation. To yield smallest $a_{AlN}$, it was being expected that the growth temperature of it is low and it is pure AlN without any gallium contamination. It is also desired that the relaxation in AlN ILs is very large. This demands that at the lower interface of AlN IL (interface I in Fig. 3.20), AlN should be relaxed as much as possible, although the relaxation mechanism is complicated.

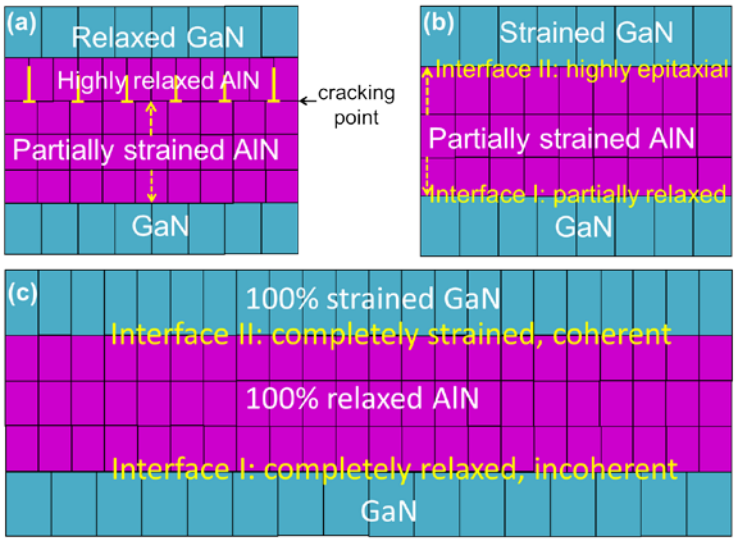


**Fig. 3.20** Models based on interfaces for interpreting the behavior of AlN ILs (a) with cracking, (b) without cracking and (c) ideal case.

The second factor is the quality of interface II, which should be as high as possible. For this request, an AlN IL should be accompanied by very low defect density. GaN growth on it should be coherent and in layer-by-layer mode, which is dependent on the quality of AlN. When this is satisfied, the lateral lattice spacing of GaN can be confined to be closer to that of AlN and GaN lattice would be more compressively strained. Lattice relaxation during the growth of an AlN IL can minimize the lateral lattice spacing of AlN, but it generally induces high density dislocation and deteriorates the upper interface of the AlN ILs, as illustrated in Fig. 3.20a. Therefore, for the ideal case, the relaxation of AlN should take place at the lower interface I via misfit dislocations and the desired case is that the dislocations do not propagate to the upper interface II. Besides the formation of dislocations, cracking is another way to release the strain energy in epitaxial films. After cracking, strain energy is relieved. On the other hand, the ability of this film to strain the overlying film is reduced also. So, for a single

AlN IL, there is a compromise between the benefits and disadvantages brought by the relaxation of it.

### 3.3.2 Thickness effect

Thickness comparison was designed to observe the tensile stress development and the ability of introducing compressive stress of AlN ILs as a function of thickness. Tested thickness range was chosen from 4.5 nm to 45 nm to cover the critical thickness of AlN on GaN. Samples with multiple and single AlN interlayers were both grown and were marked as "-*m*" and "-*s*" respectively in Fig. 3.22.

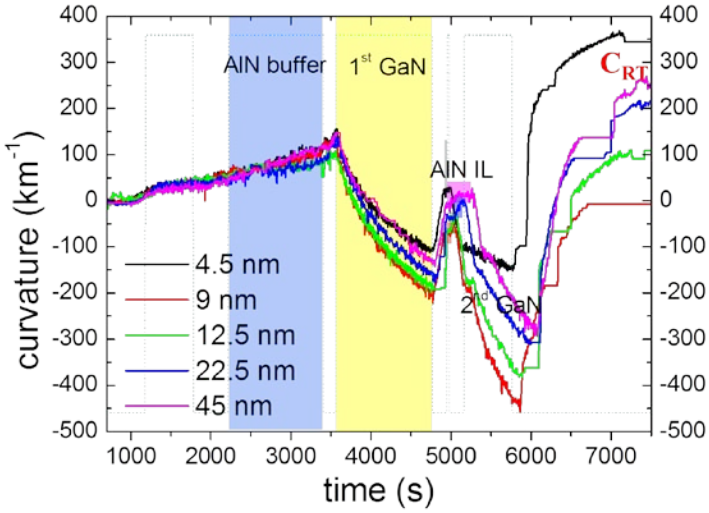


**Fig. 3.21** Curvature transition of single-condition samples for thickness study of AlN interlayers.

Results of in-situ curvature monitor for multi-condition and single-condition thickness study samples were plotted in Fig. 3.18 and Fig. 3.21 respectively. Curvature increment in AlN ILs and overlying GaN layers and final curvature at room temperature in single-condition samples were extracted and marked in Fig. 3.22 as "$dC_{AlN}$", "$dC_{GaN}$" and "$C_{RT}$" respectively. From Fig. 3.22, about the amount of compressive curvature introduction in GaN layers, both in multi-condition samples and single-condition samples, the most effective AlN interlayer was of thickness of 9 nm. The optimal thickness for AlN interlayer which can introduce the most compressive stress may be around 9 nm. About the tensile curvature increment in AlN interlayers $dC_{AlN}$, both multi-AlN-interlayer test and single-AlN-interlayer test showed that it increased as the thickness was doubled from 4.5 nm to 9 nm and after that it almost saturated. But after that, it got saturated or even went through a slight reduction.

Strictly speaking, in multi-condition sample it is unavoidable that the preceding layers influence the following ones. According to the strain relaxation mechanisms, besides lattice constant mismatch, dislocation density of the underlying layer affects the strain and stress behavior of overlying layer. Generally, if growth conditions are proper, the quality of preceding layer determines that of the following layer. The preceding GaN layer and growth mode influence the dislocation density in the following AlN interlayer and that of the overlying GaN, then the strain relaxation behavior of it. Therefore, in order to compare the

effects of AlN ILs grown under various conditions on the properties of overlying GaN layer, the quality of GaN under all AlN ILs should be exactly identical, which is very hard to achieve. The higher GaN quality leads to less negative influence on multi-condition AlN IL study. To check such influence, the multi-condition sample for AlN IL thickness investigation was grown with AlN IL thickness sequence from bottom to up of 4.5, 9, 12.5, 22.5 and 45 nm, and the reversed sequence, which marked as "-*m*" and "-*m'*" respectively. To eliminate the unfavorable influence of multi-condition structure, the average of $dC_{GaN\text{-}m}$ and $dC_{GaN\text{-}m'}$ is more reliable and close to the result of single-condition series except the thickness of 9 nm. From Fig. 3.22, about the amount of compressive curvature introduction in GaN layers, in "-*m*" sample and single-condition series, the most effective AlN interlayer was of thickness of 9 nm. While in "-*m'*" sample, this was shown to be 12.5 nm. In spite of such difference, this doesn't change the overall tendency that the optimal thickness for AlN interlayer which can introduce the most compressive stress may be in the range from 9 to 12.5 nm; growth sequence of AlN ILs doesn't change the result significantly. About the tensile curvature increase in AlN interlayers, both multi-AlN-interlayer test and single-AlN-interlayer test showed that it increased as the thickness was doubled from 4.5 nm to 9 nm and after that it almost saturated.

When the thickness is too small, around 4.5 nm for example, AlN IL is strained mostly compared with other layers so its lattice constant gets closer to that of GaN. Smaller lattice

constant difference induces minimal compressive curvature increase in overlying GaN. When the thickness rises to the range of 9 to 12.5 nm, it relaxes more that it strains the overlying GaN layer more compressively. Compressive curvature increase in GaN dropped drastically from the thickness of 12.5 nm. In Fig. 3.18 and Fig. 3.21, the tensile curvature increase at AlN interlayers saturated. Especially at interlayers with thickness of 22.5 and 45 nm, there are saturation points around thickness of 11 nm.

It is supposed that cracking occurred around the saturation point. This has been verified by AFM scanning of the surface morphology of AlN ILs (Fig. 3.23c). Roughness of root mean square (RMS) was also marked in the pictures. For 4.5-nm-thick AlN IL, because it was too thin, only about 10 monolayers, the crystal grains were very small and the surface was relatively smooth. The growth of AlN ILs on GaN was not pure epitaxial layer-by-layer mode, but started with very small grain domains with size of about 10 nm. Because the amount of grains was very large and boundaries between them could act as defect sources, GaN grown on it would get relaxed quickly. When the thickness rose to 9 nm, coalescence of original fine grains started, it exhibited continuous but larger crystal domains with clear grain boundaries. No cracks could be observed in these two samples. In Fig. 3.18, it can be figured out that in 22.5-nm- and 45-nm-thick AlN ILs, cracking occurred around the thickness of 11 nm. So, for the 12.5-nm-thick AlN IL, cracking has already started. This may be why $dC_{GaN}$ starts to decrease from AlN IL thickness of 12.5 nm. When the thickness was increased to 22.5 nm, coalescence of the small and fine grains has completed and the surface was quiet smooth. However, it showed considerable cracks. In Fig. 3.23c, there are two kinds of cracks. Some crack originated during cool-down due to the huge tensile stress caused by thermal mismatch between nitrides and Si substrate, like the wide and straight crack lines marked as type-I by yellow dash circle. Such crack was caused by the cracking of underlying GaN, but not the top AlN IL itself. The other type of crack was very fine and with irregular shape, as marked as type-II by red dash line circles. Type-II crack arose during the growth of AlN IL itself but not after growth. As marked in Fig. 3.18, for AlN ILs with thickness of 22.5 nm and 45 nm, there was a sudden drop of the slope of curvature curve, namely the drop of tensile stress in AlN ILs. This can be observed also in single-condition growth in Fig. 3.21. Sudden stress drop can be a proof of the occurrence of cracking to release the strain energy in AlN ILs, because only relaxation by cracking is not continuous. This was consistent with the results from other researches that cracking of AlN epitaxial films on GaN occurs during growth but not post-growth cooling in samples grown by MOCVD [59]. During the initial growth stage, due to relatively low temperature and reduced Al ad-atom mobility, there are some dynamical platelets and the thin AlN IL is formed by the coalescence of them. The regions of such coalescence have been proposed as sites introducing misfit dislocation. It also has been postulated that deep grooves between grains can evolve into cracks with increasing AlN IL thickness [52]. After cracking, AlN ILs could not sustain enough shear stress to strain the overlying GaN layers on them highly compressively. Cracking in AlN ILs also indicated the difference between the growth of AlN on GaN and Si. Because lattice constant of AlN $a_{AlN}$ is much closer to $a_{GaN}$ than $a_{Si}$, growth of AlN on GaN at mediate and high temperature is more epitaxial by 2D layer-by-layer growth or the mixture mode of 2D and 3D, but it is completely 3D growth on Si. Then the strain energy releasing mechanism between them also

differs significantly. As shown in curvature curves, the stress of AlN buffer layer grown on Si held a constant stress without any sudden change up to 110 nm. Cracking in thick AlN ILs make them more relaxed, but also reduced their ability to strain the overlying GaN. Due to crack net, it became not as continuous as thin AlN ILs and made the overlying GaN get relaxed more rapidly.

On the other hand, the theoretical critical thickness for AlN on GaN is 7.56 nm [58]. Experimentally, in MBE grown samples, no line defects could be observed at AlN ILs on GaN with thickness below 6 nm [52], although the detailed growth process may differs slightly between MOCVD and MBE grown materials. Due to the lower misfit dislocation density at AlN ILs, threading dislocation propagated into following GaN might be less thus the relaxation of it might be also slower. The small tensile curvature close to 0, namely the convex bowing, is our final target.

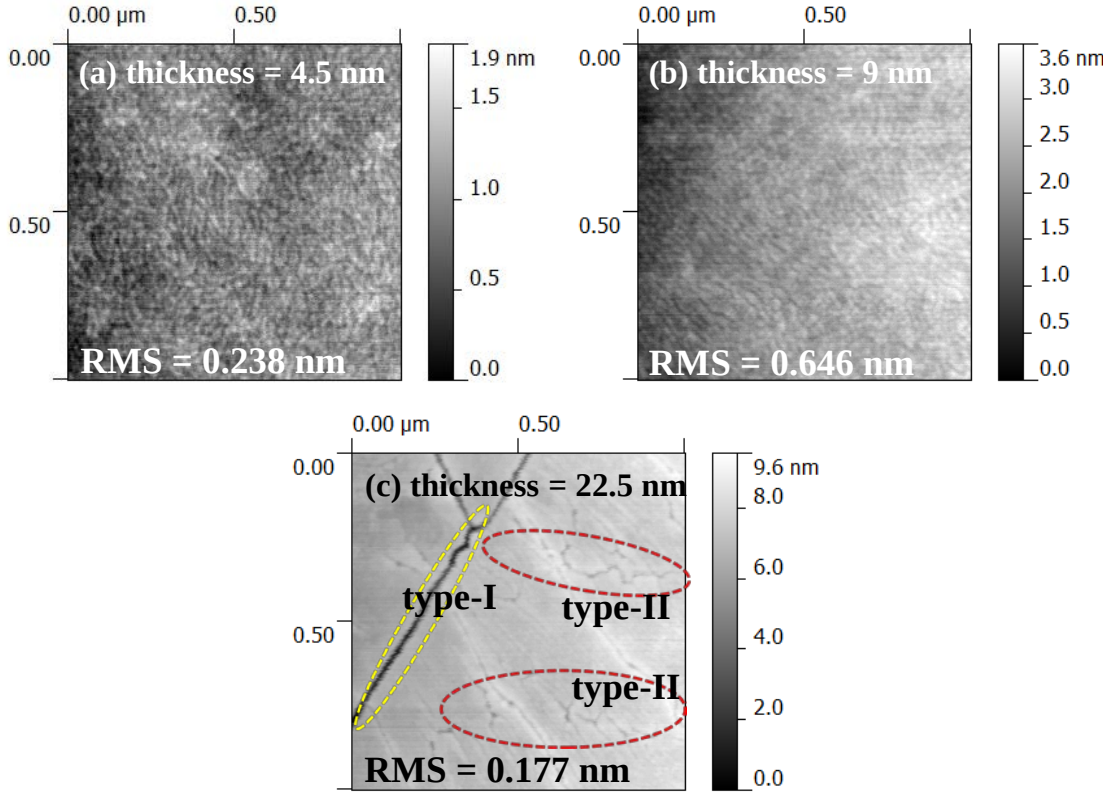


**Fig. 3.23** AFM images of the surface of AlN IL with thickness of (a) 4.5 nm, (b) 9 nm and (c) 22.5 nm, grown under V/III of 1505 and at temperature of 900 ℃.

For the single-AlN-IL series, the final tensile curvature at room temperature $C_{RT\text{-}s}$ was also extracted in Fig. 3.22. The one with 9-nm-thick AlN IL achieved smallest tensile curvature increase and yielded crack-free GaN. The tendency was that the samples with higher $dC_{GaN}$ hold lower $C_{RT}$. $C_{RT}$ was not determined only by AlN ILs, but also by the AlN buffer. Although the growth conditions for AlN buffer layer and the 1st GaN was designed to be the same, but due to some unfixable reasons from Si wafer and the MOVPE system, it differed slightly from growth to growth. Such systematic condition fluctuation led to slight variation of the stress in AlN buffers and the 1st GaN. Such fluctuation and variation doesn't affect the

tendency of the results. The sum of compressive curvature increment of the 1st and the 2nd GaN layer determines the final curvature $C_{RT}$. The stress fluctuation in AlN buffer and 1st GaN doesn't change the effect tendency of AlN ILs. The tensile stress during cool-down $\sigma_t$ arose from the all two GaN layers and so did the compressive stress $\sigma_c$. If the AlN IL is not proper, $\sigma_c$ cannot compensate tensile thermal mismatch stress $\sigma_t$ and $C_{RT\text{-}s}$ will be much larger than net compressive curvature increase in the 2nd GaN. If AlN IL is optimal and $\sigma_c$ is large enough to compensate $\sigma_t$, then $C_{RT\text{-}s}$ would be around zero.

By comparing the results of multi-condition and single-condition samples, although strictly speaking, in multi-condition sample it is unavoidable that the preceding layers influence the following ones, it still leads to the same tendency as that of single-condition samples. It means that in multi-condition sample, the influence from the bottom layers could not change the properties of top AlN ILs substantially and this method is reliable.

### 3.3.3 Temperature effect

As well known, temperature and V/III ratio are the two most important factors that determine the quality of AlN. In series of temperature and V/III ratio comparison, thickness of an AlN IL was fixed to be 9 nm, which was limited to avoid the influence of cracking.

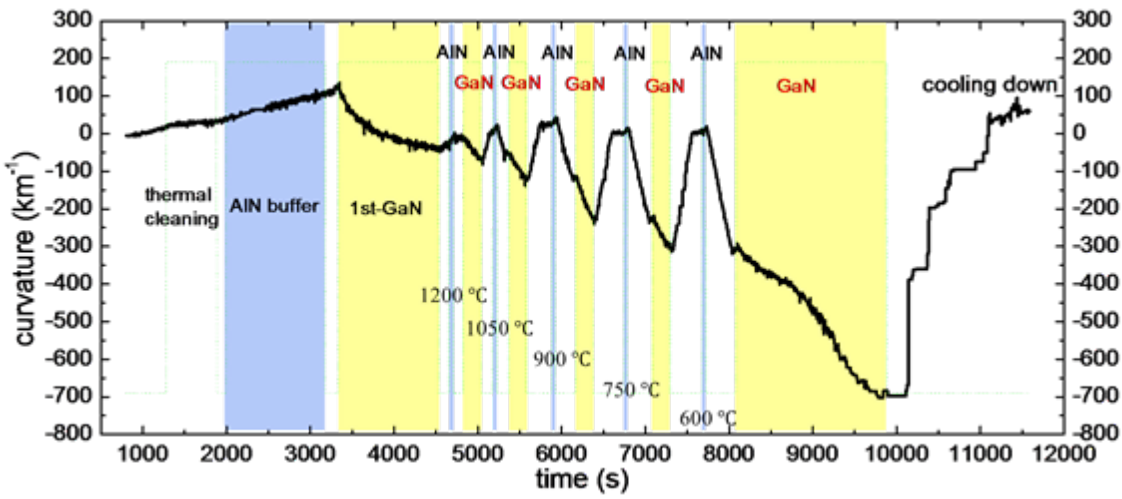


**Fig. 3.24** Curvature curve of multi-condition growth for temperature study of AlN IL.

Fig. 3.24 is the curvature transition curve of the multi-condition growth for temperature study of AlN ILs. From the bottom to the up, growth temperature for AlN ILs were test in a very large range from 1200 ℃ to 600 ℃. The curvatures increment to tensile side in AlN ILs $dC_{AlN}$ and that to compressive side in overlying GaN $dC_{GaN}$ in multi-condition and single-condition samples as well as final curvature at room temperature in single-condition samples $C_{RT\text{-}s}$ were extracted in Fig. 3.25. $dC_{AlN}$ increased slightly as growth temperature was elevated. The peak $dC_{GaN}$ appeared around 900 ℃ both for multi-condition and single-condition samples. The final curvature after growth $C_{RT\text{-}s}$, what we care mostly, the best and lowest value also turned up around 900 ℃. So it could be concluded that the optimal growth temperature for AlN ILs should be around 900 ℃. This was quite different from the study by

Reiher and Bläsing et al. [4, 50], which showed that the tensile stress at room temperature increases proportionally to the rising temperature and AlN IL grown around 600 ℃ was optimal and led to the smallest value.

It is not straight forward to discuss why the relatively optimal growth temperature for AlN ILs was around 900 ℃. The discussion would be expanded in three aspects including effects of growth temperature, composition of ILs and relaxation. These three aspects are not completely independent, and they influence each other.

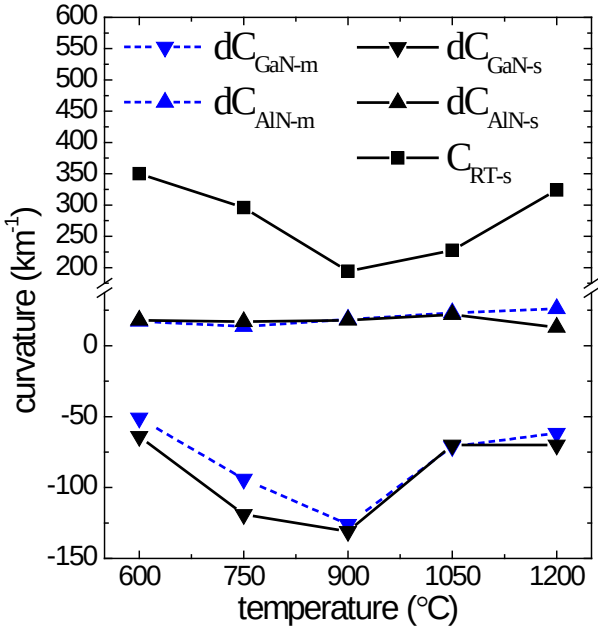


**Fig. 3.25** Compressive curvature increase in GaN and tensile curvature increase in AlN ILs during temperature comparison of multi- (-*m*) and single-condition (-*s*) growth; $C_{RT\text{-}s}$ is the final curvature after growth at room temperature for single-AlN-interlayer samples.

Temperature is a decisive condition for AlN growth [60, 61]. The most direct effect of temperature on $dC_{GaN}$ originates from the temperature dependence of the lattice constant difference between GaN and AlN, $a_{GaN} - a_{AlN}$. As plotted in Fig. 3.9, the highest $a_{GaN} - a_{AlN}$ emerges around 530 ℃. In the study here, actually, due to some reason from the MOVPE heating system, the temperature here is the setting value but not the true temperature. Usually, true temperature is about 100 ℃ lower than the setting point. So, at setting point of 900 ℃, the true value is around 800 ℃ while the $a_{GaN} - a_{AlN}$ is not the largest. If growth temperature $T_{AlN}$ was the only factor that determines the lattice constant of AlN ILs, $T_{AlN}$ should be kept as low as possible. This indicated that there might be some other factor which could also determine the lattice constant of the interlayers and surpass the influence of $T_{AlN}$. However, this is a plausible argument since $a_{GaN}$ is fixed because it is always grown at the identical temperature of 1130 ℃. Therefore, the growth temperature of AlN ILs should be as low as possible to yield the smallest $a_{AlN}$. For AlN ILs grown at 1050 ℃ and 1200 ℃, thermal expansion of lattice constant accounted for the reduction of $dC_{GaN}$ partially, but not for it of the LT-AlN ILs. Then, for LT-AlN ILs, some other mechanism must have overtaken the influence of $a_{GaN} - a_{AlN}$ dependence on temperature.

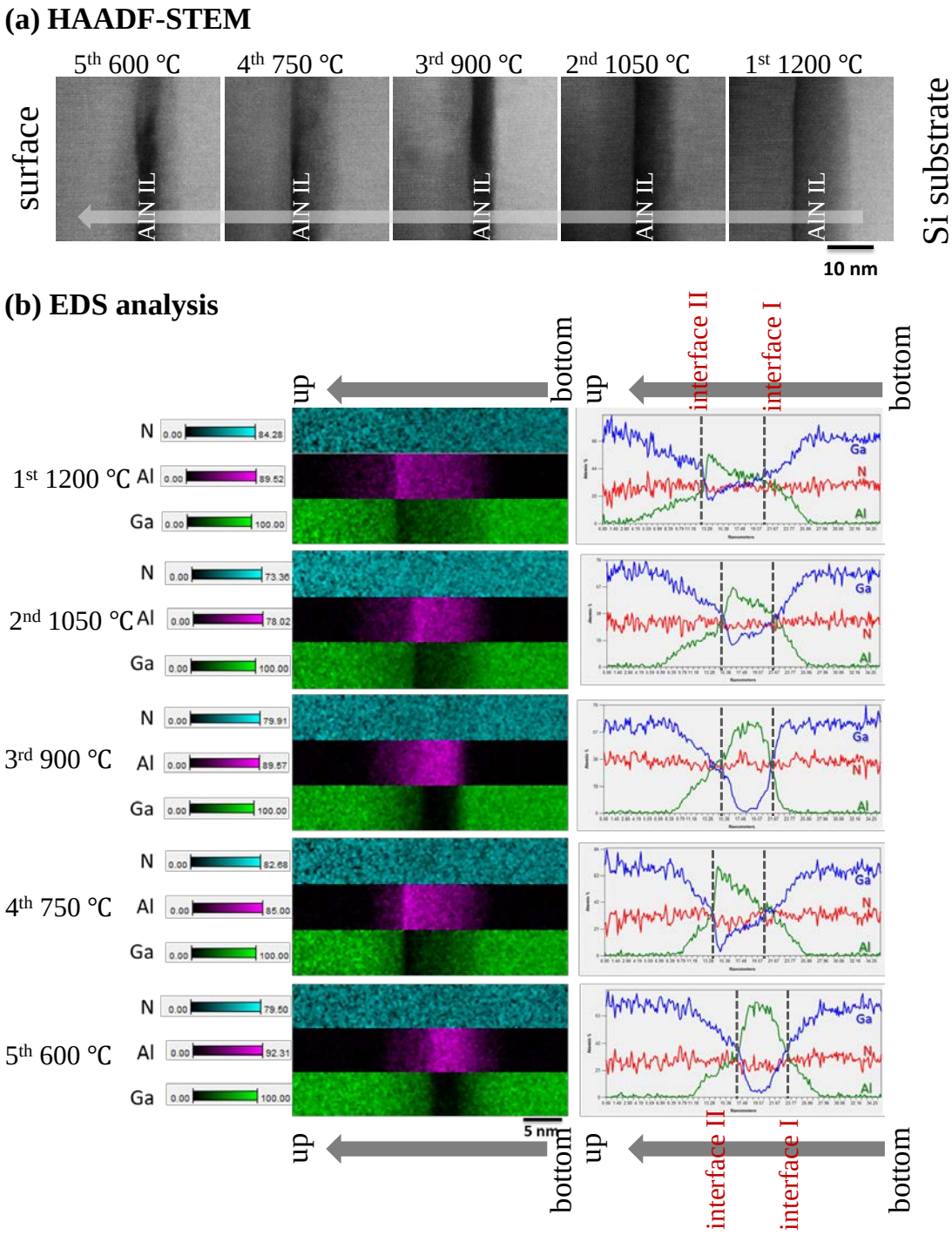


**Fig. 3.26** (a) Cross section image of ILs by TEM and (b) Al, GaN and N content around ILs by EDS.

Another decisive factor of the in-plane lattice constant of interlayers is their composition, if they are not pure AlN but AlGaN. Even though in the growth recipe the interlayers were designed to be AlN, but it was possible that the true product of interlayers tended to be AlGaN. This has been noticed by Reiher et al [4]. By XRD reciprocal space mapping (RSM), they estimated the lateral lattice constant of the ILs. Because it was larger than the value of AlN, then they assumed that there was an intermixing of LT-AlN and subsequently grown

HT-AlGaN. It strongly depends on the AlN-IL growth temperature and the gallium content increases with increasing deposition temperature. This method might be not accurate and precise for that $a_{AlN}$ might has been enlarged by straining, at least partially. Here for the first time the composition around the interlayers has been analyzed by energy dispersive spectroscopy (EDS), and cross section morphology of ILs has been observed by TEM, as shown in Fig. 3.26.

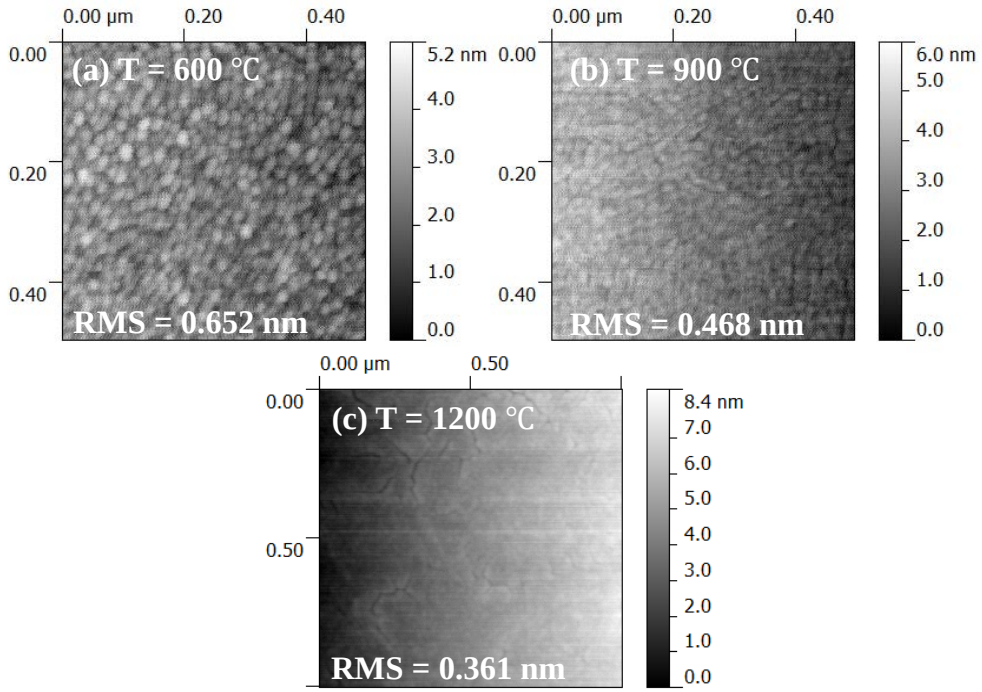


**Fig. 3.27** AFM images of the surface of AlN ILs grown at temperatures of (a) 600 ℃, (b) 900 ℃ and (c) 1200 ℃, under V/III ratio of 1505 and with thickness of 6 nm.

In Fig. 3.26a, most interfaces were very vague; the contrast was very weak around interfaces and it was very difficult to assign the location of them. Weak color contrast means weak composition contrast. Sharp contrast corresponds to sharp composition transition, and weak contrast represents gradual composition change. This is consistent with the EDS analysis in Fig. 3.26b. Interfaces marked in EDS images were not the precise location of interfaces but just approximation of them. Let's focus on the area in between the two approximated interfaces first. The most impressive information was that gallium existed in AlN ILs, the content of it depended on growth temperature of AlN ILs. Ga content increased with increasing AlN growth temperature.

For what people most concerned, only elements of Al, Ga and N have been analyzed. In this case, in order to eliminate the influence of gallium addition, high $NH_3$ flow rate was kept high (> 1000 sccm) intentionally until right before the growth of AlN ILs to avoid GaN decomposition. However, some of the ILs still have been found to be not pure AlN but with gallium content. The result here showed much higher Ga percentage at high temperature (HT) AlN than that at low temperature (LT). For ILs grown at 1200 ℃ and 1050 ℃, Ga content was about 30% and 20% respectively. The reason may be that at temperature higher than 1000 ℃, even $NH_3$ flow rate higher than 1000 sccm, it could not keep GaN from

decomposing completely. Or, GaN decomposition occurred very quickly right prior to the growth of AlN ILs during ramping down of $NH_3$ flow rate for the growth of AlN. Brunner et al found gallium in AlN grown at 1400 ℃ near the interface of AlN and sapphire substrate [18]. They attributed it to the GaN deposition and decomposition in the reactor. Dadgar et al also got similar findings [62]. Metal Ga from decomposed GaN diffused into AlN IL during its growth. This could be verified by the composition at the interfaces. The upper interface of HT ILs (interface II) was sharp but the lower one was not clear with gradual composition transition. For much lower $dC_{GaN}$ at temperature higher than 1000 ℃, this reason might be more important than growth temperature that smaller $\Delta a_{GaN-AlN}$ at high temperature.

Among LT-ILs, the one grown at 900 ℃ has the lowest Ga content close to zero percent and the ratio of the content of Al and Ga is the highest. This accounted for the largest $dC_{GaN}$ around 900 ℃ dominantly. It is natural that Ga content was very low in LT-ILs due to lower decomposition rate at low temperature. Most lower and upper interfaces of LT-ILs were not as sharp as the upper interface of the HT-ILs. The mechanism of the gradual composition transition around the interfaces of ILs may differ from that of lower interface of HT-ILs. Origin of gallium in LT-ILs might be due to large roughness caused by Volmer-Weber growth mode, but not GaN decomposition at HT. From AFM images in Fig. 3.27, at 600 ℃, AlN IL tended to be 3D grain domains of feature size of 20 nm with the largest roughness of 0.652 nm. As the growth temperature rose to 900 ℃, the grain domains grew larger to the size of 25 nm and it became smoother with smaller RMS of 0.468 nm. When the growth temperature was elevated further to 1200 ℃, with smallest RMS of 0.361 nm, it looked more epitaxial in layer-by-layer step flow mode and does not show any grain domains but lots of fine crackles emerged. So, about the EDS results for LT-ILs, for the lower interfaces, gallium may come from decomposed GaN or rich gallium during the growth of GaN; for the upper interfaces, due to the large roughness, the GaN/AlN interfaces looke like zigzag lines and the detecting electron beam could not only include AlN IL but also overlying GaN. The higher Ga content in 750-℃-IL than that in 900-℃-IL may due to the GaN growth in the grain boundary between AlN grains, although it needs further investigation. For the upper interfaces of HT-ILs, because it grew in the mode close to layer-by-layer growth with much smoother surface, the GaN/AlN interfaces tend to be very sharp. On the other hand, the lattice constant of AlN ILs should be smaller than HT ones and $\Delta a_{GaN-AlN}$ should be larger at LT. This also should have led to higher $dC_{GaN}$ at LT but not in fact. Therefore, the view of IL composition and lattice constant difference $\Delta a_{GaN-AlN}$ cannot account for the low $dC_{GaN}$ for LT-AlN ILs and there must be some other mechanism for it.

As reviewed previously, AlN grown at LT-s around 600 ~ 700 ℃ tended to be amorphous of low quality. Higher growth temperature leads to better AlN, namely, it becomes more and more crystalline as growth temperature increases. AFM images of the surface of AlN ILs grown under temperature of 600 ℃, 900 ℃ and 1200 ℃ in Fig. 3.27 revealed the morphology of them and verified the relationship between growth temperature and quality of AlN. This is also consistent with the increasing tensile curvature at AlN ILs as the growth temperature was raised. In Fig. 3.25, $dC_{AlN}$ and the stress in AlN ILs showed a slight increase from low to high temperature. 3D grain structure is more efficient to relax the stress at AlN ILs, compared with the 2D epitaxial film grown at 1200 ℃. The relaxation mechanism between AlN ILs grown at

low and high temperatures differs significantly. For the low-temperature ones, 3D grains morphology with very small connection between grains is the most efficient relaxation mechanism. While in high-temperature AlN ILs, this relies on misfit dislocation generation and cracking, which is not as efficient as 3D structures.

Because the growth was processed in the ambience of $H_2$, GaN may be decomposed [63]. Reiher et al. considered gallium diffusion into AlN ILs. Gallium content rose from less than 0.2 to more than 0.6 as the growth temperature of AlN ILs increased from 600 ℃ to 1145 ℃. Therefore in fact, the real lateral lattice constant of AlN ILs was closer to that of overlying GaN when it was grown at higher temperature and it compensated tensile stress during cooling less effectively. In this case, in order to eliminate the influence of gallium addition, high $NH_3$ flow rate was performed intentionally until growth of AlN ILs to avoid GaN decomposition. Their adopted AlN IL thickness ranged from 10 to 15 nm which may introduce cracks. They accessed the tensile stress at room temperature by XRD while the curvature by in-situ monitor was observed here, which is more accurate and reliable.

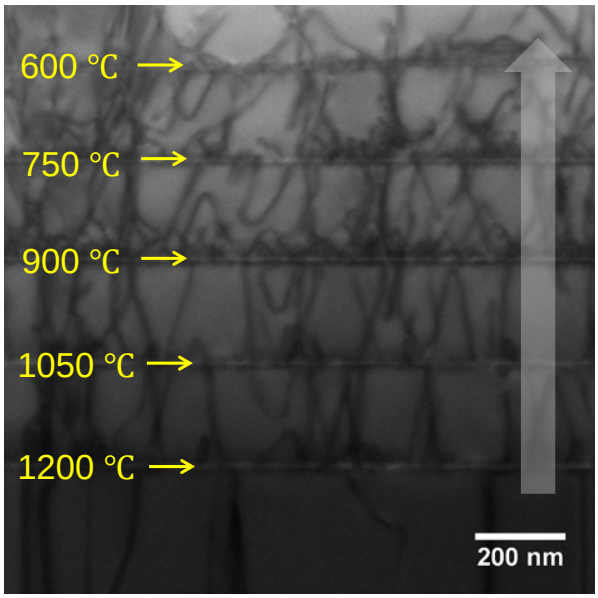


**Fig. 3.28** TEM image of multi-condition sample for temperature comparison, marked areas are the location of AlN interlayers, in between them are GaN layers.

When it was grown at 600 ℃, the quality of the AlN IL as well as the interface II was supposed to be very poor. The surface of AlN IL might be very rough with very high defect density. As growth temperature went up to 900 ℃, the quality of both the AlN IL and interface II was supposed to get better and better. However, as shown in TEM image of Fig. 3.28, AlN IL grown at 900 ℃ looks introducing most dislocations into overlying GaN layer. On the other hand, just due to high defect density in it, it relaxed most thus induced highest compressive stress in the following GaN. After 900 ℃, though the quality of both AlN ILs and the interface II become higher, another competing factor arises, that is the lattice constant difference between AlN and GaN. Lattice constant of AlN is larger when it is grown at higher temperature. Then it is much smaller when AlN ILs were grown at temperature above 900 ℃ than that grown at 1050 ℃. As a result, much less compressive stress can occur. About the

tensile curvature increase in AlN ILs, the basic tendency is that it gets larger and larger as growth temperature increases. This is also an indication of crystal quality improvement of AlN ILs. As for the interface I, in order to obtain smaller lateral lattice spacing in AlN ILs, it is desired that an AlN IL is less strained by the underlying GaN which demands a highly relaxed interface. Regarding this point, lower growth temperature is preferred.

Based on all the discussion above, an ideal case of AlN IL was proposed, as shown in Fig. 3.20c. The lower interface of it should be completely relaxed and incoherent, and its upper interface should be completely strained and coherent. Due to the low contrast in TEM and EDS images in Fig. 3.26, though the designed thickness is 6 nm, it is hard to tell the true thickness of ILs, and it seems to vary from 5 nm to 10 nm. The reasons include gallium incorporation in ILs and GaN filling into grain boundaries between neighboring AlN grains due to large roughness or 3D growth at low temperature.

For temperature comparison, single-condition samples were also done to check the influence of underlying GaN/AlN interfaces in a multi-condition sample on the behavior of AlN ILs. It showed that again, in Fig. 3.25, two methods resulted in the same tendency, which means topmost AlN/GaN stack in multi-condition sample was almost free from the influence of underlying layer structures. In other words, proper growth conditions for AlN ILs can be searched roughly through only three growths series of growth temperature, thickness and V/III ratio, which is incredibly efficient. Although here more precise experiments with finer conditioning are needed if to search the optimized growth conditions for AlN ILs, but it is not the target of this study.

### 3.3.4 V/III effect

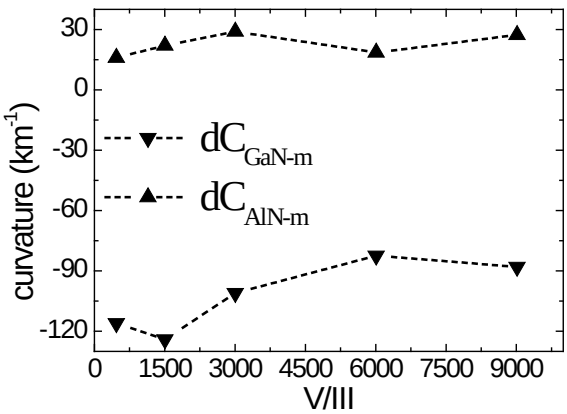


**Fig. 3.29** Compressive curvature increase in GaN and tensile curvature increase in AlN ILs during V/III ratio comparison multi-condition growth.

Although V/III ratio may affect the compressive stress introduction to GaN, it is not as significant as that of thickness and temperature, as shown in Fig. 3.29. The variation of $dC_{GaN}$ is only about 30% between the largest value under V/III ratio around 1503 and the smallest value under that around 6010. Compressive curvature change in GaN layers increased as the V/III ratio rising up to 1503. After that, it started to decrease and kept almost constant after V/III of 3005. As indicated by $dC_{AlN}$ in Fig. 3.29, tensile stress in AlN ILs increased as V/III

went up to 3005, which indicated crystal quality improvement. After V/III ratio of 1503, maybe surface roughness of AlN ILs degraded and caused reduction of $dC_{GaN}$.

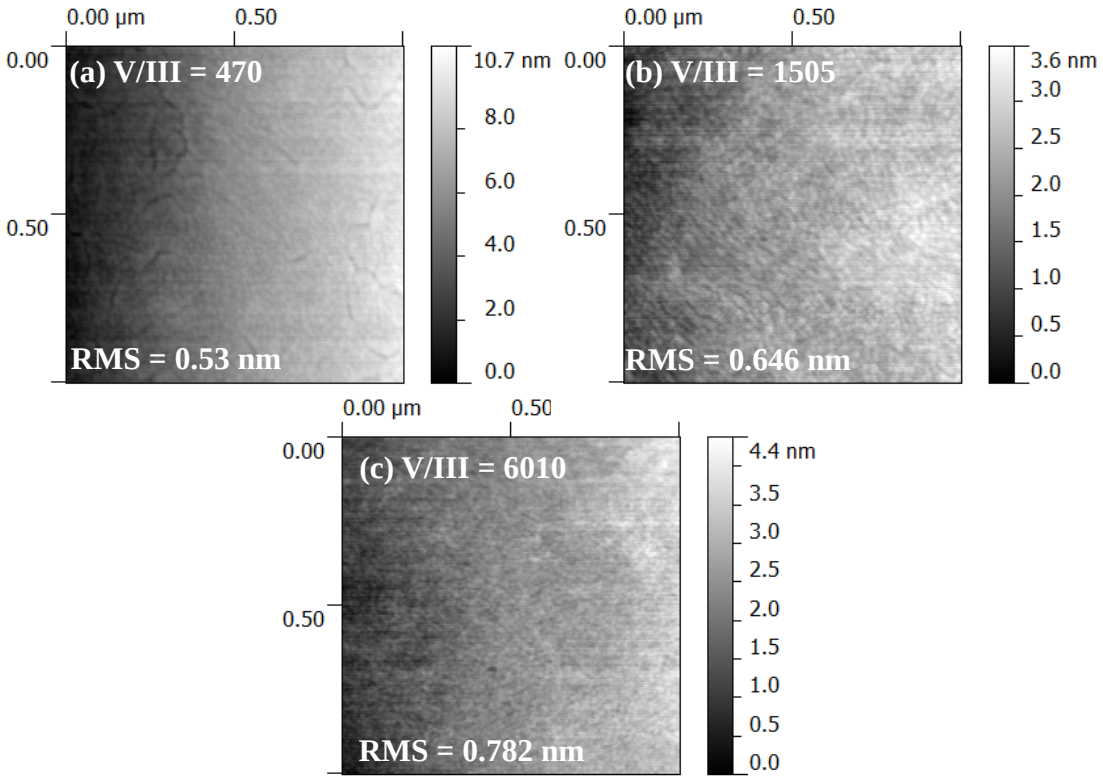


**Fig. 3.30** AFM images of the surface of AlN ILs grown under various V/III ratio.

From AFM images in Fig. 3.30, the roughness of AlN ILs surface (upper interface of AlN ILs) became larger with increasing V/III ratio. The V/III ratio was tuned by varying the flow rate of $NH_3$ while keeping the flow rate of TMAl constant. The increasing roughness with V/III ratio was attributed to the lowered surface diffusion length of Al ad-atoms due to large $NH_3$ amount under high V/III ratio by some mechanism which has not been clarified yet [64, 65]. Under low V/III ratio of 470, although the roughness was the smallest, $dC_{GaN}$ was reduced by the existence of crackles. Under high V/III ratio of 6010, compared with the surface of that grown under V/III ratio of 1505, the morphology didn't change considerably while the roughness increased and $dC_{GaN}$ decreased by about 30%. As discussed in section of 3.3.3, large roughness would cause GaN filling in the boundaries between AlN grains around the upper interface of AlN ILs. This may deteriorate the ability of AlN ILs to induce compressive stress in GaN layers. Based on such discussion, although absolute smooth AlN IL surface is not necessary to induce compressive stress in GaN, smoother surface is contributory to higher $dC_{GaN}$.

## 3.4 Curvature adjustment by GaN growth mode and thickness

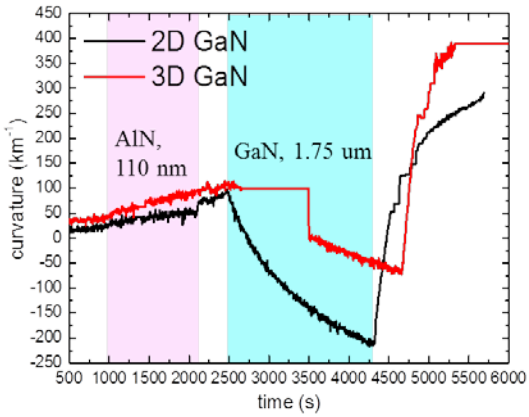


**Fig. 3.31** Effect of GaN growth mode on curvature evolution.

Since the stress formation mechanism is dependent on the growth mode, which basically can be classified into three modes of Volmer-Weber mode (island growth mode or 3-dimensional growth mode), Frank-van der Merwe mode (layer-by-layer growth mode or 2-dimensional growth mode) and Stranski-Krastanov mode (the mixture of the former two of 3D and 2D growth mode), so the growth mode can be utilized to tune the curvature (bow). For the direct proportional relationship between curvature (bow) and film thickness, $\Delta\kappa \propto \Delta h_f$, it can be known that bowing of the wafer can also be simply adjusted by tuning the thickness of GaN films. Here some examples will be shown.

Stress origins in thin films and the dependence of stress evolution and growth mode will be reviewed in the next chapter. Here just the result of growth effect of GaN growth mode on curvature evolution during and after growth was shown in Fig. 3.31. Because 3D-grown film starts with separating islands, it is less strained than 2D in-plane films, and the stress is smaller than in 2D grown films. With the same thickness of 1.75 um, the compressive curvature value increased from -70 km$^{-1}$ to -230 km$^{-1}$ while the growth mode was shifted from 3D growth mode to 2D growth mode. As the 2D-grown film was more compressively bowed, the final tensile curvature at room temperature after cooling was also much lower than that of 3D-grown one, which is desired. Therefore, with regard to more efficient bowing control, 2D growth mode is more favorable.

**Table 3.3** Thickness of GaN layers (in nm).

| No. | 1$^{st}$ | 2$^{nd}$ | 3$^{rd}$ | 4$^{th}$ | 5$^{th}$ | 6$^{th}$ | Total (nm) | $\kappa$ (km$^{-1}$) |
|---|---|---|---|---|---|---|---|---|
| **A** | **860** | 250 | 250 | 250 | 250 | 1750 | 3610 | -324 |
| **B** | **590** | 250 | 250 | 250 | 250 | 1750 | 3340 | -379 |
| **C** | 430 | 250 | **390** | **390** | **390** | 1750 | 3600 | -479 |

As compressive stress was induced at GaN layers, and thermal stress occurred during cooling is also a function of GaN thickness, so thickness of GaN layers could be tuned to adjust the final curvature. In Table 3.3 the structure of 3 samples was listed. The 1$^{st}$ layer of GaN in all samples in Table 3.3 was grown with 3D growth mode. Depending on the quality of AlN buffer layer, the stress in the 1$^{st}$ GaN can evolve to tensile or compressive side after

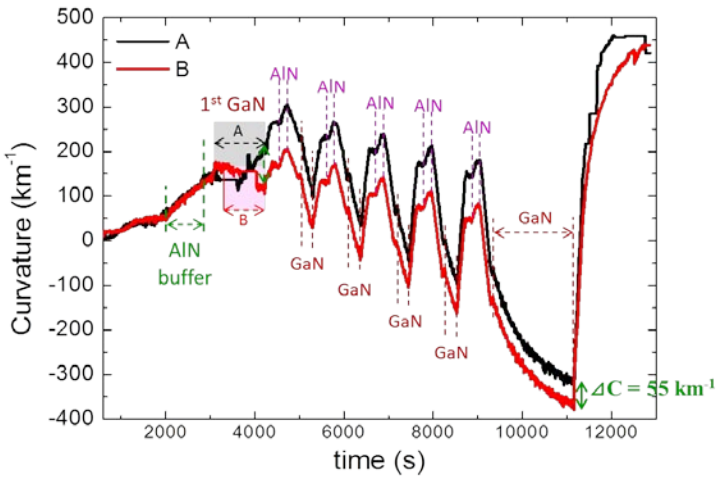


**Fig. 3.32** An example of increasing curvature to the compressive side by reducing the thickness of the 1st GaN.

coalescence. In order to reduce the curvature to the tensile side and increase it to the compressive side, the thickness of the 1st GaN can be reduced if its stress goes to the tensile side or be increased if the stress goes to compressive side. In Fig. 3.32, from sample A to B, as the thickness of the 1st GaN was reduced from 860 nm to 590 nm, the compressive curvature in the end of the growth was increased by 70 $km^{-1}$, and the final tensile curvature at room temperature was also reduced significantly. Besides the 1st GaN layer, the thickness of GaN layers in between AlN ILs can also adjust the amount of compressive curvature, as shown by the example in Fig. 3.33. From sample B to C, in the linear curvature increase range before GaN started rapid relaxation, as the thickness of three layers of GaN was increased from 250 nm to 390 nm, $\Delta\kappa$ to the compressive side in each layer was also increased proportionally. Similarly, to obtain enough compressive curvature, we can add the number of AlN ILs and GaN layers. To summarize, the growth mode, thickness and number of GaN layers provide us more freedom to design the expected curvature and bowing of the wafer after growth.

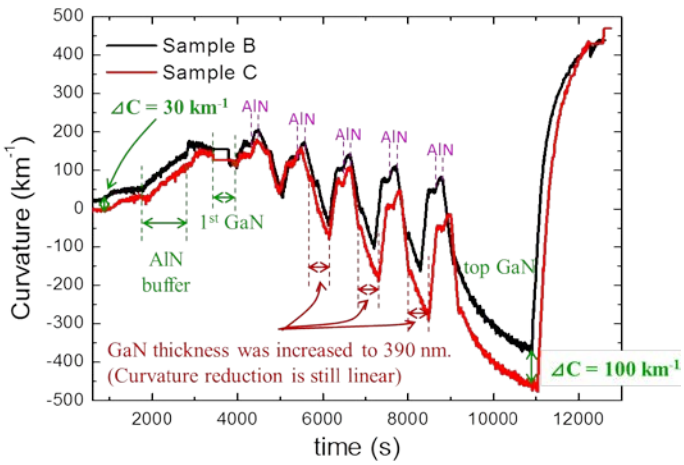


**Fig. 3.33** An example of increasing curvature to the compressive side by increasing the thickness of the GaN layers.

## 3.5 Conclusion

In this chapter, potential strategies of adjusting the wafer bowing/curvature of GaN-on-Si had been examined. First of all, compressive stress should be induced in GaN layers. The behaviors of compressive stress (curvature increase to the down side) introduction by both conventional AlN buffer layer and AlN interlayers had been observed experimentally and the behaviors had been discussed based on the growth conditions and strain relaxation theory. And then, growth mode and the thickness of individual GaN layers can also tune the wafer curvature. Based on experimental observation and theoretical discussion, the ideal cases of AlN buffer layer and interlayer which could induce most compressive stress in overlying GaN layers and proper conditions for growing them have been clarified.

For interpreting the curvature behavior, after showing examples of the curves of a growth, the theoretical models of stress generation and strain relaxation mechanisms in epitaxial layers were introduced in advance of the experimental results.

AlN buffer layer is a critical step and its quality should be as high as possible. Why?

It not only affects the growth mode and quality of the following GaN, but also determines the stress in GaN. Specifically, the morphology, surface roughness, grain size and defect density affects the properties of overlying GaN significantly. If the quality of AlN buffer layer is poor, for example as if it was grown at low temperature around 600 ℃, it could not grow epitaxially and tended to be amorphous or polycrystalline consisted of big grains with multi-orientated facets. Then GaN was hard to be grown on such AlN buffer layer and also of various ununiformed crystal facets. On low-temperature AlN buffer layer, although the lattice constant of it was smaller than that of high-temperature one, but the quality of it was too poor to strain the overlying GaN effectively due to the existence of a great amount of dislocations. Based on strain relaxation theory proposed by Matthew etc., high-density dislocation leads to much more rapid strain relaxation in epitaxial layers. For example, on AlN buffer layer grown at mediate temperature of 900 ~ 1000 ℃, the compressive stress in GaN relaxed rapidly in tens of nanometers and transited to tensile stress. The high-quality AlN buffer layer is epitaxial and crystalline, of smooth surface and low-density dislocation. GaN on it can also be grown epitaxially with controllable growth mode (2D or 3D) and high quality. The stress is much higher and can be kept compressive in a large thickness (> 2 um). So the quality of AlN buffer layer should as high as possible. High-quality can be obtained at higher temperature in the range of 1200 ~ 1400 ℃, since high temperature enhances the surface mobility of Al ad-atoms. Growth temperature is the most decisive factor. V/III ratio is also important to yield highly crystalline and smooth AlN surface and the proper value is in the range of 450 ~ 1500. Generally larger thickness leads to better quality. Quality improving rate drops as thickness increases, following a logarithmic function with a base number > 1. Thicker AlN buffer layer induce larger compressive stress in overlying GaN while introducing larger tensile curvature (concave bowing). If the thickness of AlN buffer is too large, the final curvature at room temperature can be larger to the tensile side in spite of higher compressive stress in GaN. Therefore, there is an optimal value of AlN buffer layer thickness and it is in the range of 100 ~ 150 nm. In this work, the thickness of 110 nm was adopted.

The case for AlN interlayers is more complicated, because the mechanism of the influence of growth temperature and thickness on the compressive stress in overlying GaN is not straight forward. To understand the role of AlN interlayers grown under various conditions and search for the ideal AlN interlayer, the method of multi-condition checking in one sample was applied. Double checking single-condition growths were also performed and it verified the reliability of multi-condition checking. Based on theoretical discussion, the ideal case of AlN interlayer which could induce compressive stress in GaN most effectively has been proposed. The lower interface of it should be completely relaxed with high crystal quality while the upper interface should be coherent to strain the overlying GaN as much as possible. Such ideal AlN interlayer is very hard to be realized in a single-layer of thickness only about 10 nm. However, the best AlN interlayer which could be achieved under practical conditions was grown at 900 ℃, under V/III ratio of 1500 and of thickness of about 9 nm. Growth temperature should be as low as possible if only take account of the lattice constant of AlN interlayer $a_{AlN}$. But it was not the case of the real experimental results. The best temperature appeared around a mediate value of 900 ℃. Similar to the case of AlN buffer layer, if the growth temperature was too low, AlN interlayer would be amorphous or of low quality. The growth mode was 3D and the film was formed by grains with large boundary. These small grains or islands were not well connected with each other and then could not induce shear stress in overlying GaN. On the other hand, high-density dislocation generated in following GaN at the source sites at grain boundaries. So the low-temperature AlN interlayer cannot introduce large compressive stress in GaN. For the high-temperature interlayer grown at temperature higher than 1050 ℃, the crystal quality of it improved a lot and less dislocation in GaN to relax the compressive strain rapidly. Nonetheless, high-temperature interlayer held larger lattice constant. More detrimental was, GaN was decomposed at such temperature range and gallium diffusion into the interlayers happened. So the interlayer was not pure AlN but AlGaN with even larger lattice constant which was closer to that of GaN. Then high-temperature AlN interlayer was not suitable for stress control in GaN-on-Si wafer. Consequently, there is a mediate compromise growth temperature around 900 ℃, at which the quality of AlN interlayer is enhanced, and no AlGaN generation. Like growth temperature, there is also an optimal thickness for AlN interlayer around 9 nm. If it was too thin, it was strained by the underlying GaN and the lattice constant was closer to that of GaN. The morphology of too-thin interlayer was worse than thick one and the film was imperfect with grain boundaries. As it became thicker, relaxation also increased. If it was too thick, for example thicker than 15 nm, some drastic strain relaxation mechanism would occur, such as cracking. Cracks in the interlayer can also deteriorate the ability of it of straining GaN compressively. Therefore there is a proper thickness around 9 nm with good morphology but no cracking. V/III ratio is not as influential as that of growth temperature and thickness.

## References


[1] J.P. Douglas. *Misfit Dislocation*. 2014; Available from: http://userweb.eng.gla.ac.uk/douglas.paul/SiGe/misfit.html.

[2] J.E. Ayers, *Heteroepitaxy of Semiconductors: Theory, Growth and Characterization*. 2007, New York: CRC Press, Taylor & Francis Group. 161-241.

[3] S. Fritze, P. Drechsel, P. Stauss, P. Rode, T. Markurt, T. Schulz, M. Albrecht, J. Bläsing, A. Dadgar, and A. Krost,Role of low-temperature AlGaN interlayers in thick GaN on silicon by metalorganic vapor phase epitaxy, J. Appl. Phys. ***111***, 124505(2012).
[4] A. Reiher, J. Bläsing, A. Dadgar, A. Diez, and A. Krost,Efficient stress relief in GaN heteroepitaxy on Si (111) using low-temperature interlayers, J. Cryst. Growth ***248***, 563(2003).
[5] O. Ambacher, J. Majewski, C. Miskys, A. Link, M. Hermann, M. Eickhoff, M. Stutzmann, F. Bernardini, V. Tilak, B. Schaff, and L.F. Eastman,Pyroelectric properties of Al(In)GaN/GaN hetero- and quantum well structures, Journal of Physics Condensed Matter ***14***, 3399(2002).
[6] A. Zoroddu, F. Bernardini, P. Ruggerone, and V. Fiorentini,First-principles prediction of structure, energetics, formation enthalpy, elastic constants, polarization, and piezoelectric constants of AlN, GaN, and InN: Comparison of local and gradient-corrected density-functional theory, Physical Review B ***64***, (2001).
[7] J.W. Matthews and A.E. Blakeslee,Defects in epitaxial multilayers. I. Misfit dislocations, Journal of Crystal Growth ***27***, 118(1974).
[8] S. Strite and H. Morkoç,GaN, AlN, and InN: A review, J. Vac. Sci. Technol. B ***10***, 1237(1992).
[9] I. Vurgaftman, J.R. Meyer, and L.R. Ram-Mohan,Band parameters for III–V compound semiconductors and their alloys, J. Appl. Phys. ***89***, 5815(2001).
[10] M.T. Hardy, D.F. Feezell, S.P. DenBaars, and S. Nakamura,Group III-nitride lasers: a materials perspective, Materials Today ***14***, 408(2011).
[11] H. Morkoç, *Handbook of Nitride Semiconductors and Devices*. Vol. 1. 2008: Wiley-VCH Verlag GmbH & Co. KGaA.
[12] S. Nakamura and G. Fasol, *The blue laser diode-GaN based light emitters and lasers*. 1997: Springer.
[13] H. Amano, N. Sawaki, I. Akasaki, and Y. Toyoda,Metalorganic vapor phase epitaxial growth of a high quality GaN film using an AlN buffer layer, Applied Physics Letters ***48***, 353(1986).
[14] T. Yamada, T. Tanikawa, Y. Honda, M. Yamaguchi, and H. Amano,Growth of GaN on Si(111) Substrates via a Reactive-Sputter-Deposited AlN Intermediate Layer, Jpn. J. Appl. Phys. ***52***, 08JB16(2013).
[15] C.H. Yen, W.C. Lai, Y.Y. Yang, C.K. Wang, T.K. Ko, S.J. Hon, and S.J. Chang,GaN-Based Light-Emitting Diode With Sputtered AlN Nucleation Layer, IEEE Photonics Technology Letters ***24***, 294(2012).
[16] O. Madelung, *Semiconductors - Basic Data*. 1996, New York: Springer. 69.
[17] M.E. Levinshtein, S.L. Ramyantsev, and M.S. Shur, *Properties of Advanced Semiconductor Materials*. 2001, New York: Jonh Wiley & Sons, Inc. 31.
[18] F. Brunner, H. Protzmann, M. Heuken, A. Knauer, M. Weyers, and M. Kneissl,High-temperature growth of AlN in a production scale 11 × 2'' MOVPE reactor, physica status solidi (c) ***5***, 1799(2008).
[19] Y. Kumagai, K. Akiyama, R. Togashi, H. Murakami, M. Takeuchi, T. Kinoshita, K. Takada, Y. Aoyagi, and A. Koukitu,Polarity dependence of AlN {0001} decomposition in flowing H2, J. Cryst. Growth ***305***, 366(2007).
[20] V. Jindal and F. Shahedipour-Sandvik,Density functional theoretical study of surface structure and adatom kinetics for wurtzite AlN, J. Appl. Phys. ***105***, 084902(2009).
[21] H. Kröncke, S. Figge, T. Aschenbrenner, and D. Hommel,Growth of AlN by pulsed and conventional MOVPE, J. Cryst. Growth ***381***, 100(2013).
[22] H. Liu, D.C. Bertolet, and J.W. Rogers,The surface chemistry of aluminum nitride MOCVD on alumina using trimethylaluminum and ammonia as precursors, Surface Science ***320***, 145(1994).
[23] A.C. Jones, C.R. Whitehouse, and J.S. Roberts,Chemical approaches to the Metalorganic CVD of Group-III Nitrides, Chemical Vapor Deposition ***1***, 65(2004).
[24] M. Imura, K. Nakano, N. Fujimoto, N. Okada, K. Balakrishnan, M. Iwaya, S. Kamiyama, H. Amano, I. Akasaki, T. Noro, T. Takagi, and A. Bandoh,Dislocations in AlN Epilayers Grown on Sapphire

Substrate by High-Temperature Metal-Organic Vapor Phase Epitaxy, Jpn. J. Appl. Phys. ***46***, 1458(2007).
[25] Y. Ohba and R. Sato,Growth of AlN on sapphire substrates by using a thin AlN buffer layer grown two-dimensionally at a very low V/III ratio, J. Cryst. Growth ***221***, 258(2000).
[26] J.F. Kaeding, Y. Wu, T. Fujii, R. Sharma, P.T. Fini, J.S. Speck, and S. Nakamura,Growth and laser-assisted liftoff of low dislocation density AlN thin films for deep-UV light-emitting diodes, J. Cryst. Growth ***272***, 257(2004).
[27] S. Zamir, B. Meyler, E. Zolotoyabko, and J. Salzman,The effect of AlN buffer layer on GaN grown on (111)-oriented Si substrates by MOCVD, J. Cryst. Growth ***218***, 181(2000).
[28] M.L. Nakarmi, B. Cai, J.Y. Lin, and H.X. Jiang,Three-step growth method for high quality AlN epilayers, Phys. Status Solidi (a) ***209***, 126(2012).
[29] S. Raghavan and J.M. Redwing,Intrinsic stresses in AlN layers grown by metal organic chemical vapor deposition on (0001) sapphire and (111) Si substrates, Journal of Applied Physics ***96***, 2995(2004).
[30] S. Raghavan and J.M. Redwing,In situ stress measurements during the MOCVD growth of AlN buffer layers on (111) Si substrates, Journal of Crystal Growth ***261***, 294(2004).
[31] T. Uchida, K. Kusakabe, and K. Ohkawa,Influence of polymer formation on metalorganic vapor-phase epitaxial growth of AlN, J. Cryst. Growth ***304***, 133(2007).
[32] S. Raghavan, I.C. Manning, X. Weng, and J.M. Redwing,Dislocation bending and tensile stress generation in GaN and AlGaN films, Journal of Crystal Growth ***359***, 35(2012).
[33] S. Raghavan and J.M. Redwing,Growth stresses and cracking in GaN films on (111) Si grown by metal-organic chemical-vapor deposition. I. AlN buffer layers, Journal of Applied Physics ***98***, 023514(2005).
[34] S. Raghavan, X. Weng, E. Dickey, and J.M. Redwing,Effect of AlN interlayers on growth stress in GaN layers deposited on (111) Si, Applied Physics Letters ***87***, 142101(2005).
[35] J. Han, J.J. Figiel, M.H. Crawford, M.A. Banas, M.E. Bartram, R.M. Biefeld, Y.K. Song, and A.V. Nurmikko,OMVPE growth and gas-phase reactions of AlGaN for UV emitters, J. Cryst. Growth ***195***, 291(1998).
[36] A.A. Allerman, M.H. Crawford, A.J. Fischer, K.H.A. Bogart, S.R. Lee, D.M. Follstaedt, P.P. Provencio, and D.D. Koleske,Growth and design of deep-UV (240–290nm) light emitting diodes using AlGaN alloys, J. Cryst. Growth ***272***, 227(2004).
[37] J.R. Creighton, G.T. Wang, W.G. Breiland, and M.E. Coltrin,Nature of the parasitic chemistry during AlGaInN OMVPE, J. Cryst. Growth ***261***, 204(2004).
[38] S. Keller, G. Parish, P.T. Fini, S. Heikman, C.H. Chen, N. Zhang, S.P. DenBaars, U.K. Mishra, and Y.F. Wu,Metalorganic chemical vapor deposition of high mobility AlGaN/GaN heterostructures, J. Appl. Phys. ***86***, 5850(1999).
[39] A.V. Lobanova, K.M. Mazaev, R.A. Talalaev, M. Leys, S. Boeykens, K. Cheng, and S. Degroote,Effect of V/III ratio in AlN and AlGaN MOVPE, J. Cryst. Growth ***287***, 601(2006).
[40] Y.M. Zhao, G.S. Sun, X.F. Liu, J.Y. Li, W.S. Zhao, L. Wang, M.C. Luo, and J.M. Li. *Effects of V/III Ratios on the Properties of AlN Grown on Si (111) Substrate by LP-MOCVD* in *8th International Conference on Solid-State and Integrated Circuit Technology*. 2006. Shanghai: IEEE.
[41] T. Kozawa, T. Kachi, T. Ohwaki, and Y. Taga,Dislocation Etch Pits in GaN Epitaxial Layers Grown on Sapphire Substrates, Journal of The Electrochemical Society ***143***, L17(1996).
[42] J.E. Ayers, L.J. Schowalter, and S.K. Ghandhi,Post-growth thermal annealing of GaAs on Si(001) grown by organometallic vapor phase epitaxy, J. Cryst. Growth ***125***, 329(1992).
[43] S. Akram, H. Ehsani, and I.B. Bhat,The effect of GaAs surface stabilization on the properites of ZnSe grown by organometallic vapor phase epitaxy, J. Cryst. Growth ***124***, 628(1992).
[44] S. Kalisetty, M. Gokhale, K. Bao, J.E. Ayers, and F.C. Jain,The influence of impurities on the dislocation behavior in heteroepitaxial ZnSe on GaAs, Appl. Phys. Lett. ***68***, 1693(1996).

[45] P. Sheldon, K.M. Jones, M.M. Al-Jassim, and B.G. Yacobi,Dislocation density reduction through annihilation in lattice-mismatched semiconductors grown by molecular-beam epitaxy, J. Appl. Phys. ***63***, 5609(1988).
[46] M.E. Vickers, M.J. Kappers, R. Datta, C. McAleese, T.M. Smeeton, F.D.G. Rayment, and C.J. Humphreys,In-plane imperfections in GaN studied by x-ray diffraction, Journal of Physics D: Applied Physics ***38***, A99(2005).
[47] S. Figge, H. Kröncke, D. Hommel, and B.M. Epelbaum,Temperature dependence of the thermal expansion of AlN, Appl. Phys. Lett. ***94***, 101915(2009).
[48] H. Amano, M. Iwaya, T. Kashima, M. Katsuragawa, I. Akasaki, J. Han, S. Hearne, J.A. Floro, E. Chason, and J. Figiel,Stress and Defect Control in GaN Using Low Temperature Interlayers, Jpn. J. Appl. Phys. ***37***, 1540(1998).
[49] M. Iwaya, S. Terao, N. Hayashi, T. Kashima, H. Amano, and I. Akasaki,Realization of crack-free and high-quality thick AlGaN for UV optoelectronics using low-temperature interlayer, Appl. Surf. Sci. ***159-160***, 405(2000).
[50] J. Bläsing, A. Reiher, A. Dadgar, A. Diez, and A. Krost,The origin of stress reduction by low-temperature AlN interlayers, Appl. Phys. Lett. ***81***, 2722(2002).
[51] A. Dadgar, M. Poschenrieder, J. Bläsing, O. Contreras, F. Bertram, T. Riemann, A. Reiher, M. Kunze, I. Daumiller, A. Krtschil, A. Diez, A. Kaluza, A. Modlich, M. Kamp, J. Christen, F.A. Ponce, E. Kohn, and A. Krost,MOVPE growth of GaN on Si(1 1 1) substrates, J. Cryst. Growth ***248***, 556(2003).
[52] G.P. Dimitrakopulos, E. Kalesaki, P. Komninou, T. Kehagias, J. Kioseoglou, and T. Karakostas,Strain accommodation and interfacial structure of AlN interlayers in GaN, Cryst. Res. Technol. ***44***, 1170(2009).
[53] G. Cong, Y. Lu, W. Peng, X. Liu, X. Wang, and Z. Wang,Design of the low-temperature AlN interlayer for GaN grown on Si (111) substrate, Journal of Crystal Growth ***276***, 381(2005).
[54] R. Luo, P. Xiang, M. Liu, T. Chen, Z. He, B. Fan, Y. Zhao, Y. Xian, S. Huang, Z. Zheng, Z. Wu, H. Jiang, G. Wang, Y. Liu, and B. Zhang,Influence of V/III Ratio of Low Temperature Grown AlN Interlayer on the Growth of GaN on Si(111) Substrate, Jpn. J. Appl. Phys. ***50***, 105501(2011).
[55] W. Luo, X. Wang, L. Guo, H. Xiao, C. Wang, J. Ran, J. Li, and J. Li,The effect of low temperature AlN interlayers on the growth of GaN epilayer on Si (111) by MOCVD, Superlattices and Microstructures ***44***, 153(2008).
[56] J.F. Wang, D.Z. Yao, J. Chen, J.J. Zhu, D.G. Zhao, D.S. Jiang, H. Yang, and J.W. Liang,Strain evolution in GaN layers grown on high-temperature AlN interlayers, Appl. Phys. Lett. ***89***, 152105(2006).
[57] B.S. Zhang, M. Wu, J.P. Liu, J. Chen, J.J. Zhu, X.M. Shen, G. Feng, D.G. Zhao, Y.T. Wang, H. Yang, and A.R. Boyd,Reduction of tensile stress in GaN grown on Si(111) by inserting a low-temperature AlN interlayer, Journal of Crystal Growth ***270***, 316(2004).
[58] A.M. Sanchez, F.J. Pacheco, S.I. Molina, J. Stemmer, J. Aderhold, and J. Graul,Critical Thickness of High-Temperature AlN interlayer in GaN on Sapphire, J. Electronic Mater. ***30***, 17(2001).
[59] S.J. Hearne, J. Han, S.R. Lee, J.A. Floro, D.M. Follstaedt, E. Chason, and I.S.T. Tsong,Brittle-ductile relaxation kinetics of strained AlGaN/GaN heterostructures, Appl. Phys. Lett. ***76***, 1534(2000).
[60] M.-J. Lai, L.-B. Chang, T.-T. Yuan, and R.-M. Lin,Improvement of crystal quality of AlN grown on sapphire substrate by MOCVD, Cryst. Res. Technol. ***45***, 703(2010).
[61] Y.A. Xi, K.X. Chen, F. Mont, J.K. Kim, E.F. Schubert, C. Wetzel, W. Liu, X. Li, and J.A. Smart,Optimization of High-Quality AlN Epitaxially Grown on (0001) Sapphire by Metal-Organic Vapor-Phase Epitaxy, J. Electronic Mater. ***36***, 533(2007).
[62] A. Dadgar, A. Krost, J. Christen, B. Bastek, F. Bertram, A. Krtschil, T. Hempel, J. Bläsing, U. Haboeck, and A. Hoffman,MOVPE growth of high-quality AlN, J. Cryst. Growth ***297***, 306(2006).
[63] D.D. Koleske, A.E. Wickenden, R.L. Henry, J.C. Culbertson, and M.E. Twigg,GaN decomposition in H2 and N2 at MOVPE temperatures and pressures J. Cryst. Growth ***223***, 466(2001).

[64] A.V. Lobanova, E.V. Yakovlev, R.A. Talalaev, S.B. Thapa, and F. Scholz,Growth conditions and surface morphology of AlN MOVPE, J. Cryst. Growth ***310***, 4935(2008).
[65] K. Uehara, Y. Aota, S. Kameda, H. Nakase, Y. Isota, and K. Tsubouchi,Growth of Atomically Flat-Surface Aluminum Nitride Epitaxial Film by Metalorganic Chemical Vapor Deposition, Jpn. J. Appl. Phys. ***44***, 2987(2005).

# 4 Theoretical analysis of stress and strain behavior

The previous chapter only focused on the experimental results about stress, curvature/bowing control and the effects of AlN layers grown under various conditions. This chapter is the quantitative fitting and theoretical analysis of the stress and strain evolution during and after growth. The first section was an introduction of Stoney equation to calculate wafer curvature. The second section was about the mechanisms of stress origination in heterostructure. The subjects that would be analyzed in this work were also fixed. Section 4.3 was the analysis of AlN buffer layer and GaN grown on it. Next in section 4.4 the stress and strain in AlN interlayers and overlying GaN layers was analyzed. Following that, the problem of plastic deformation of Si substrate was discussed. In the last section of 4.6, the strategy of designing arbitrary wafer bowing for GaN-on-Si was proposed, which is most attractive to producers.

## 4.1 Stoney formula

Curvature reflects bowing of a wafer. People need to know the relationship between the stress in the film and the curvature. Stoney equation was built for it. It can estimate the wafer curvature caused by the stress originated from the deposition of films on it. Using Stoney equation, stress in epitaxial film can be observed experimentally through accessing wafer curvature. In the beginning of 1900s, people found that when they try to protect the silver film deposited on glass in searchlight reflector by depositing another layer of nickel on it, when the thickness of nickel exceeded some considerable thickness, silver film would peel off together with nickel film. G. G. Stoney studied this phenomenon using a model of nickel deposition on a steel ruler. In order to predict the bending dependence on the thickness of nickel film thickness, he derived the original form of Stoney equation to calculate the bowing of the steel ruler from the stress at the deposited nickel film. He used mechanical method by taking moments balance between the steel ruler and the nickel film, which would not be introduced in detail here [1, 2, 7].

Energy method is another method which is much more universal and applicable to more complex cases without modifications. Here the derivation would be repeated simply. Let's consider a system consists of a circular substrate with radius $R$ and thickness$h_s$, and a film with thickness$h_f$. This film is bonded to the substrate, not with its natural size and but with distributed external stretching force $f$ acting on the edge with direction from the center to the edge so that its strain is exactly the lattice mismatch strain, and supposing that the film is suffering tensile stress, as shown in Fig. 4.1a and b. After realizing the external force $f$, the film lattice would contract to be close to its neutral lattice constant. Since it is supported by

the substrate, the contracting film causes compressive stress in the substrate (tensile in the film) and concave bowing, as shown in Fig. 4.1c.

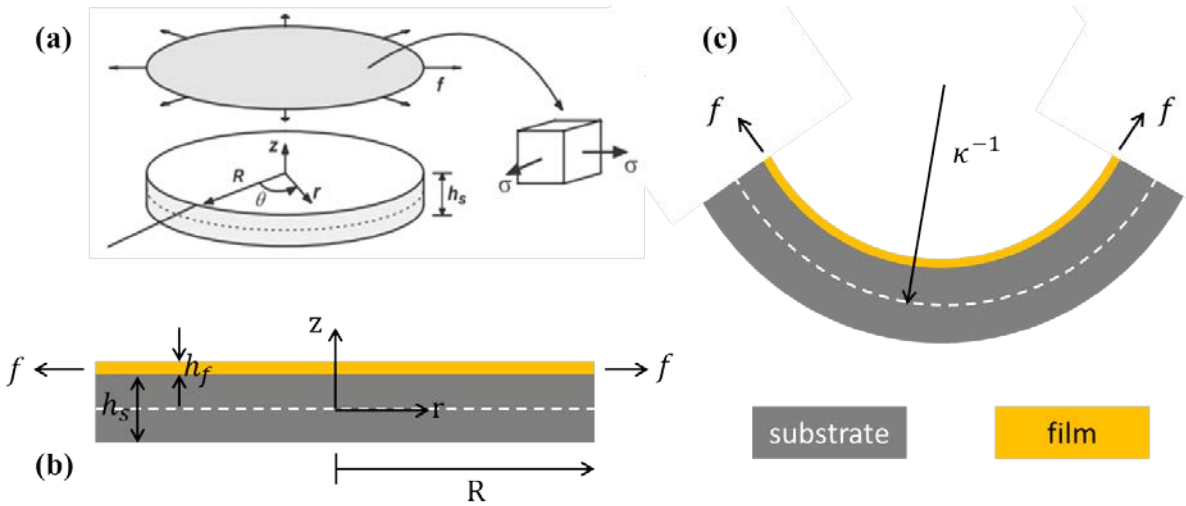


**Fig. 4.1** (a) and (b): The loading force $f$ causes an equi-biaxial state of stress everywhere in the film, illustrated by $\sigma$, $f$ is also called as membrane force [2]. (c): Concave bowing of the substrate caused by the membrane force $f$ in the film.

A cylindrical $r$, $\theta$, $z$ – coordinate system is introduced to describe the behavior of the system of the substrate and film. The following discussion is based on some assumptions. The most important points are listed here. First of all, the film contributes negligibly to the mechanical properties, elastic stiffness for example, of the system consisted of the film and substrate. This usually demands that the thickness of the film should be far smaller than that of the substrate, $h_f \ll h_s$. In the system, it is expected that the normal stress component $\sigma_{zz} = 0$ everywhere. The membrane force $f$ is caused by lattice mismatch alone and the contribution to $f$ from the substrate deformation is negligible. Substrate deformation as well as the curvature of the mid-plane of the substrate should be spatially symmetric, uniform and independent of angle $\theta$. More strict assumptions was stipulated elsewhere [2].

The routine of energy method is to evaluate the potential of the whole system and search for the conditions to keep the stable state of the system with the lowest energy. When the wafer bowing occurred and the substrate is strained due to the membrane force $f$, supposing the curvature is $\kappa$, the strain energy density throughout the substrate is

$$U(r,z) = M_s(\epsilon_0 - \kappa z)^2, \tag{4-1}$$

where $M_s = E_s/(1-\nu_s)$ is the biaxial modulus of the substrate, $\epsilon_0$ is the extensional strain of the substrate mid-plane and $\kappa z$ is extensional strain due to bending at any position $z$ with respect to the mid-plane of the substrate. The total potential energy of the substrate in the state in Fig. 4.1(c) is

$$\begin{aligned} V(\epsilon_0,\kappa) &= 2\pi \int_0^R \int_{-h_s/2}^{h_s/2} U(r,z) r dz dr + 2\pi f u_r(R, h_s/2) R \\ &= \pi R^2 M_s h_s \left(\epsilon_0^2 + \tfrac{1}{12}\kappa^2 h_s^2\right) + 2\pi R^2 f \left(\epsilon_0 - \tfrac{1}{2}\kappa h_s\right). \end{aligned} \tag{4-2}$$

where the second term is the external potential energy caused by the relaxation of the external force $f$, $u_r$ is the radial deformation of the substrate. The energy stable position can be obtained by differentiating the total potential energy $V$ with respect its variations $\epsilon_0$ and $\kappa$, which renders their differential being zero, $\partial V/\partial\epsilon_0 = 0$ and $\partial V/\partial\kappa = 0$. This leads to

$$\epsilon_0 = -\frac{f}{M_s h_s} \tag{4-3}$$

$$\kappa = \frac{6f}{M_s h_s^2}. \tag{4-4}$$

Since the loading agent $f$ is the same as the membrane force in the film originates from the lattice mismatch stress $\sigma_m$ but with opposite sign, then it is

$$f = -\sigma_m \cdot h_f \tag{4-5}$$

Following Hooke's law, film mismatch stress $\sigma_m$ is

$$\sigma_m = M_f \cdot \epsilon_m \tag{4-6}$$

The curvature expression in Eq. (4-4) is the famous Stoney formula, and it can be expressed more specifically as

$$\kappa = \frac{6f}{M_s h_s^2} = \frac{6\sigma_m h_f}{M_s h_s^2} = \frac{6M_f \cdot \epsilon_m h_f}{M_s h_s^2} \tag{4-7}$$

Until now, the relationship between wafer curvature κ and film stress $\sigma_f$ and strain $\epsilon_f$ has been built. However, generally, the factor strain $\epsilon$ in equation originates from not only the lattice mismatch $\epsilon_m$, but also some other factors such as thermal expansion coefficient (TEC) mismatch $\epsilon_{TEC}$ which can also cause and change the lattice constant mismatch. Then ϵ can be expressed as

$$\epsilon_f = \epsilon_m + \epsilon_{TEC} + \cdots \tag{4-8}$$

Consequently, the general expression of Stoney formula should be

$$\kappa = \frac{6\sigma_f h_f}{M_s h_s^2} = \frac{6M_f \cdot \epsilon_f h_f}{M_s h_s^2} = \frac{6M_f \cdot (\epsilon_m + \epsilon_{TEC} + \cdots) h_f}{M_s h_s^2} \tag{4-9}$$

For the system of GaN-on-Si, the total strain ϵ can be approximately the sum of lattice constant mismatch $\epsilon_m$ and thermal expansion coefficient $\epsilon_{TEC}$, which would be discussed later.

What should be noted that is in Eq. (4-4), $f$ is the force acting in the film. The sign of it is

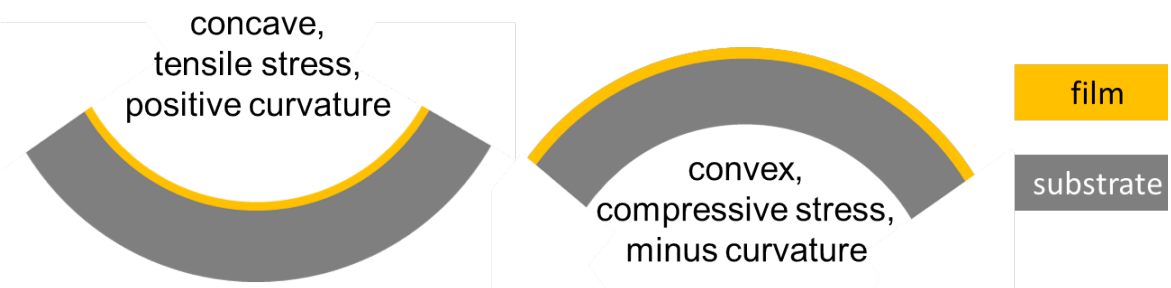


**Fig. 4.2** Substrate suffers convex bending under compressive stress, and concave bending under tensile stress.

determined by the direction of it, if it suffers tensile stress, which the direction is the same with that of the direction of the coordinate, then the sign is positive and the wafer bending is concave with positive curvature value. Conversely, when the film suffers compressive stress, the wafer bowing is convex with minus curvature value, as represented in Fig. 4.2.

## 4.2 Stress and its origins in heterostructure

Due to the difference of properties between materials, stress and strain exists almost in all heterostructures, the difference is that stress may be beneficial or detrimental or neutral to the performance of devices depending on the structure and material. The development of semiconductor devices is also a history of the development of heterostructure physics and its realization. Since currently most of the devices are based on heterostructure which works at their active regions, it is essential that stress and strain should be considered when to design the device, grow and fabricate it. Origins of stress in heterostructures are extraordinary complicated, depending on the material system, structure, growth method, growth mode, external environment and so on. In most of the cases, it is hard to cover all possible origins of stress and only the most dominant ones would be took account of during analysis. Generally, people divide stress into two classifications, intrinsic stress and extrinsic stress. Nevertheless, there is no strict, global and unified definition of them. In spite of it, their definition and possible origins would be reviewed briefly as follows. Based on it, take account of the material and growth process in this study, the analysis subject and method would be established afterward.

### 4.2.1 Intrinsic stress and its origins

In heterostructure, intrinsic stress generally refers to the stress raises during the growth of the film, for which it is also named as growth stress. There are many complicated mechanisms to interpret the origins of stress in the film, depending on the deposition method, growth mode, the microstructure of the film, the property difference between the film and substrate and so on. Since in most cases, the film is our study object, take it as the center, stress can occur at its lower interface (between it and the substrate or underlying layer), in itself and at its upper interface or surface. The description of stress origination mechanisms would follow this sequence; it is also the process of the growth of the film, from bottom to up. It is beyond the target here to cover all possible mechanisms in detail. Instead, regarding the material and growth method here, the most important ones would be introduced briefly [8].

#### 4.2.1.1 Stress origins at the lower interface

- Misfit stress

Misfit stress is one of the most dominant stress origins for the case of epitaxial growth. It origins from the lateral lattice constant difference between the epi-layer and the substrate or underlying layer. Usually, in heterostructure, the lateral lattice constants of epi-layer and underlying layer are not identical. The lattice of the deposited film ($a_f$) is constrained by that

of the underlying layer ($a_s$) and is forced to be the same as$a_s$. Then the first layers grow pseudomorphically. The misfit strain $\epsilon_m$ is defined as Eq. (1-1) and is repeated here

$$\epsilon_m = \frac{a_{s0} - a_{f0}}{a_{f0}} \tag{4-10}$$

with $a_{s0}$and $a_{f0}$ being the neutral value of the lattice of substrate and film which are stress-free. In most cases, substrate is assumed to be stiff and $a_s$ doesn't change. The misfit stress $\sigma_m$ caused by misfit strain can be calculated as

$$\sigma_m = M_f \cdot \epsilon_m = M_f \cdot \frac{a_{s0} - a_{f0}}{a_{f0}} \tag{4-11}$$

with $M$ being the biaxial elastic modulus of the film. The magnitude of $\sigma_m$ can be 1 ~ 10 GPa, which is very huge compared with the contributions of other mechanisms and is the most dominant and influential one [8, 9]. However, the misfit stress calculated by Eq. (4-10) is only the ideal case that the film is completely strained, which is almost impossible. In fact, as introduced in chapter 3, there are many strain relaxation mechanisms to relief the misfit strain. The true strain after relaxation is given by

$$\epsilon = \frac{a_f - a_{f0}}{a_{f0}} \tag{4-12}$$

with $a_f$ being the relaxed lattice constant. Even for the perfect pseudomorphical growth, it would relax by forming misfit dislocations if the thickness is beyond a critical value which is usually several or tens of nanometers [10, 11]. The relaxation amount $\varsigma$ is defined as

$$\varsigma = \frac{a_f - a_s}{a_{f0} - a_{s0}} \times 100\% \tag{4-13}$$

with $a_{f0}$ and $a_{s0}$ being the neutral lattice constant of the film and substrate respectively, and $a_f$ and $a_s$ being the strained lattice constant of the film and substrate under the growth conditions respectively. As it is assumed that the substrate is stiff and $a_{s0}$ doesn't change, so $a_s = a_{s0}$. Misfit stress is the most important intrinsic stress that to be considered in this study. The sign of stress follows the conventional regulation that if the film suffers tensile stress ($a_{s0} - a_{f0} > 0$) it is positive and if the stress is compressive ($a_{s0} - a_{f0} < 0$) it is negative. So does the curvature.

- Solid state reactions and/or diffusion

This mechanism refers to the cases that there is solid phase reaction or specie diffusion at the interface between a substrate and the film on it [8]. When there is solid phase reaction, new compound is formed at the interface. After the formation of new compound, the diffusion of reactant to the other side continues. Both processes can be accompanied by the raise of stress. Stress can also be induced if there is only diffusion from one side to the other. For example, the oxygen incorporation in Al substrate diffuses to the clean Al film on it. The diffused atom species can incorporate into the crystal lattice of the film and leads to lattice constant variation and then induce stress at the interface. For the particular case here, the react between gallium and silicon also leads to the stress relief during the growth by forming voids in silicon substrate and Ga-Si alloy spots in the film and destroying the epitaxial

structure of nitrides on silicon. These large size (1 ~ 100 um) structural defects keep the growth from forming an entire film.

#### 4.2.1.2 Intrinsic stress within the films

This is the most complicated part of the origins of stress since it relates to the microstructure of the film during the processes of growth.

- Small-angle grain boundaries

This mechanism exists in polycrystalline and amorphous films which consist of numerous randomly oriented grains with small angles and size from several nanometers to micrometers and contain a great concentration of grain boundaries. There are gaps between these grains and the interatomic forces tend to close them and then result in tensile stress in neighboring crystallites [8].

- Domain walls or coalescence of grain boundaries

This only emerges in epitaxial films grown in Volmer-Weber mode. The as contacted islands have larger surface energy $\gamma_s$ (Fig. 4.3a) than the interface energy $\gamma_i$ (Fig. 4.3b). The system total free energy can decrease by forming interface and annihilating free surface. At the beginning of coalescence, similar to the mechanism above of small-angle grain boundaries, the interatomic forces between neighboring islands tends to close their gap and this leads to a short period of tensile stress. Next, during coalescence and increase of thickness, atoms arrive at and fill the grain boundaries or domain walls, resulting in compressive stress. The later stage is similar to the process of insertion of excess atoms in grain boundaries.

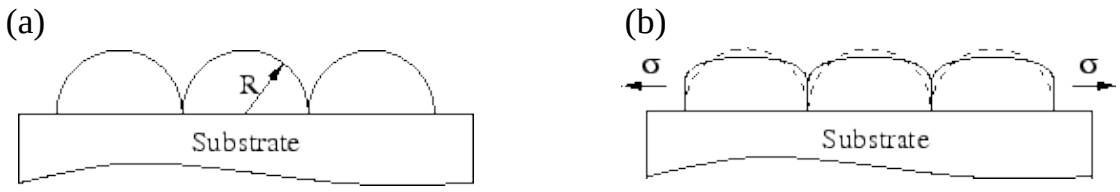


**Fig. 4.3** Compressive stress generation during coalescence of crystal islands [12].

- Recrystallization processes

Stress may emerges during the processes of recrystallization, during growth, annealing and after growth, especially in the films with inferior quality. Recrystallization brings better crystal quality. In some cases, recrystallization may increase the density of the film and cause shrinkage of it. Since the film is attached to the substrate tightly and the substrate tends to keep the film from shrinkage and then tensile stress in the film is generated [8, 12].

- Annihilation of excess vacancies

In most cases, there is a great deal of vacancies in crystals. They can annihilate in the grains, at the boundaries, at the free surfaces and the surfaces of internal cavities. No stress is caused if they are annihilated at the surfaces while a tensile stress is built up if they are

annihilated in the grains or at the boundaries for that their annihilation generates gaps and the grains tends to move to close the gap [12].

- Impurities

Impurities can cause stress even in homogenous epitaxial growth by doping the film. This mechanism has been mentioned in the introduction of the mechanism of solid state diffusion at the interface in the last subsection. Impurities or dopants can replace the lattice site of some original atom species. Due to the difference of the radius between the impurity atoms and the atoms of the epitaxial film, true lattice constant of the film can be changed [8].

There are some other mechanisms that can induce intrinsic stress within the film, such as the lattice expansion in capillarity effect, the capillarity stress and so on [8].

### 4.2.2 Stress contributions from the upper interface (or film/vacuum surface)

For the layers which are sandwiched between two other layers, its upper interface is the interface between it and the overlying layer. If there is some mechanism reviewed above works at the interface, stress can be induced there. For a top layer, the upper interface is film/vacuum interface, or surface. Stress arises at the surface.

- Surface stress

This concept comes from the description of surface tension of liquid surface. For the surface molecules of liquid, due to the lack of molecular in the vacuum and balancing forces from them, the surface molecules tend to be pulled inwards and cause some internal pressure. The case for solid is similar to that for liquid. Due to a great amount of hanging bonds on the surfaces, usually the interatomic distance of the surface layer is difference from that of the bulk. The surface can be elastically stretched to lower the surface density and surface energy [8].

### 4.2.3 Extrinsic stress and thermal stress in elastic multilayer system

Extrinsic stress refers to the stress caused by external factors, not arises from the growth material system. The mostly mentioned external factor is temperature variation. For heterostructures, not only the lattice constant might be mismatching, but also the thermal expansion coefficient $\alpha$ differs. Usually, during growth, cooling down or even operating (of devices), there is temperature change $\Delta T$, in some cases it can be very huge (e.g. $\Delta T$ > 1000 ℃ for the growth of nitrides). Due to the difference of $\alpha$, the amount of expansion or shrinkage for different material may differs significantly and then introduce thermal strain and stress in the multi-layer system. This is called as thermal stress.

In the simplest system consists of only one layer of film on a substrate, the thermal strain in the film is given as

$$\epsilon_{th} = -\int\left[\alpha_f(T) - \alpha_s(T)\right]dT \tag{4-14}$$

If the thermal expansion coefficients are assumed to be constant (in fact it is not true) then equation (4-14) can be simplified to be

$$\epsilon_{th} \approx -(\alpha_f - \alpha_s) \cdot \Delta T \tag{4-15}$$

And then thermal stress $\sigma_{th}$ is given by

$$\sigma_{th} = M_f \cdot \epsilon_{th} = -M_f \cdot \int [\alpha_f(T) - \alpha_s(T)] dT \approx -M_f \cdot (\alpha_f - \alpha_s) \cdot \Delta T \tag{4-16}$$

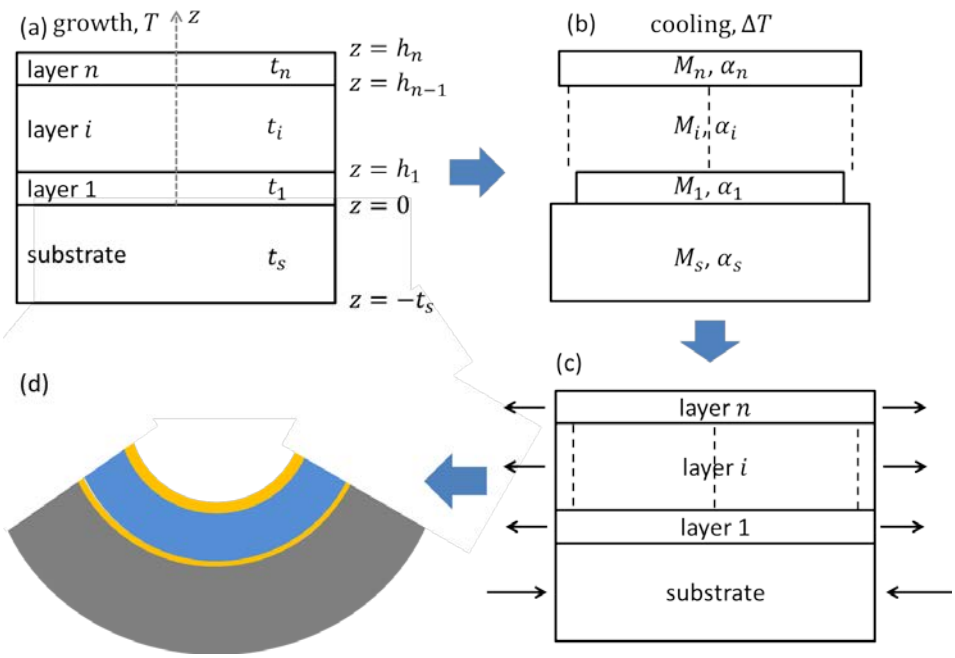


**Fig. 4.4** Thermal stress generation in elastic multi-layer system during cooling down.

The case in a multi-layer system is much more complicated than above. Such a system was shown in Fig. 4.4 schematically. Every layer is of individual biaxial modulus $M_i$, thermal expansion coefficient $\alpha_i$ and thickness $t_i$. Since growth stress is not included and the thermal stress is the only source of stress considered here, in Fig. 4.4a the sample is supposed to be stress free at growth temperature $T$, while they have to be superposed when to calculate the true stress of each layer. For simplicity, thermal expansion coefficient $\alpha$ of every layer is assumed to be constant (temperature independent). When the system cooled down to room temperature, every individual layer experiences an unconstrained differential shrinkage, such that thermal strains, $\alpha_i \Delta T$ and $\alpha_s \Delta T$ exist in every layer (Fig. 4.4b). Then uniform tensile or compressive stresses are imposed on the individual layers to maintain displacement compatibility (Fig. 4.4c). In the end, bending occurs due to asymmetric stresses in the system (Fig. 4.4d) [13].

Based on the model above, resultant system curvature, thermal stress in every film layer can be calculated as follows [13]. The final curvature of the entire system, $\kappa$, is the sum of the every individual contribution of the thermal mismatch curvature $\kappa_i$ between the substrate and each film layer, and can be expressed as

$$\kappa_i = \frac{6 M_i t_i (\alpha_i - \alpha_s) \Delta T}{M_s t_s^2} \tag{4-17}$$

$$\kappa = \sum_{i=1}^{n} \kappa_i = 6 \sum_{i=1}^{n} \frac{M_i t_i (\alpha_i - \alpha_s) \Delta T}{M_s t_s^2}. \tag{4-18}$$

People are concerned about the stresses in individual layers of a multilayer system for that they may be very influential to the performance of the devices which are fabricated from multilayer structure. The first-order and zero-order approximation of thermal stress in individual layers can be expressed in terms of the curvature as

$$\sigma_i = -\frac{M_s t_s^2}{6 t_i} \kappa_i + \frac{2 M_i t_s}{3} \kappa \qquad (i\text{=1 to } n) \tag{4-19}$$

and

$$\sigma_i = M_i (\alpha_s - \alpha_i) \Delta T = -\frac{M_s t_s^2}{6 t_i} \kappa_i \qquad (i\text{=1 to } n). \tag{4-20}$$

respectively. Compared with the solution of exact closed-form, the result of first-order approximation is more accurate than that of zero-order approximation. Such difference lies in the Eq. (4-20) which shows that the thermal stress in individual layer is independent on the presence of other layers. In Eq. (4-19), the first-order approximation, $\sigma_i$ is related to the multilayer system, which leads to more accurate results.

What else should be noted is that, this calculation model is for the system which consists of perfect elastic multilayer. It needs further modification when it is applied to the system with imperfect elastic layers, such as polycrystalline or amorphous layers.

### 4.2.4 Analysis method in this study

To analyze the stress and strain in GaN layers and AlN buffer layer and interlayers, both the intrinsic and extrinsic stress should be included. Only the thermal stress is considered as extrinsic stress. It is so huge for the growth of nitrides on silicon substrate and enormous crack can be caused by it. About the intrinsic stress, although it is epitaxial growth in this study, for which the stress origination mechanism is much simpler than the case for polycrystalline growth by other growth methods, it is still next to being impossible to examine the possible origins one by one. Since it is epitaxial growth, the misfit stress is supposed to be the most dominant source of stress except the 3D growth of GaN. This assumption has been verified to make sense because during most growth stages the curvature curve has constant slope. If there is some other competing mechanism to yield stress, in most cases, there would be some interaction between them and leads to stress variation during every individual stage. Even though if there are some other minimal stress sources, it is included here by considering the overall stress $\sigma_{all}$ and strain $\epsilon_{all}$. On the other hand, it is also almost impossible to calculate or simulate the stress and strain directly if the micro-structure and defect types and concentration are not available. Because AlN and GaN grown by MOVPE are far from perfect single crystal but with various high density defects and furthermore the defect information is dependent on growth conditions, so it is difficult to estimate the microstructure and defect information. In addition, not all stress mechanisms can be modeled quantitatively, such as recrystallization process and annihilation of excess vacancies. For the case of high quality AlN and GaN, which is the case that there is no microstructures like grains and gaps, it is possible to estimate the dislocation types and

density by XRD or TEM and calculate the strain relaxation caused by the dislocations [14]. The defect information cannot be accessed individually for each sub-layer by XRD, although the strain might be possible to be calculated using the strained lattice constant values measured by XRD. However, still it is impossible to simulate the stress and strain directly using the ideal mechanical properties of those materials, which is only reliable for the ideal case. Therefore, the strategy here is to extract the overall stress and strain for every individual layer from the in-situ curvature data, using Stoney equation. The Stoney equation is repeated here

$$\kappa = \frac{6\sigma_f h_f}{M_s h_s^2} = \frac{6M_f \cdot \epsilon_f h_f}{M_s h_s^2} \qquad (h_s \gg h_f) \tag{4-21}$$

with $\kappa$ being the curvature of the substrate, $\sigma_f$, $h_f$, $M_f$ and $\epsilon_f$ being the stress, thickness, biaxial elastic modulus and strain of the film respectively, $M_s$ and $h_s$ being the biaxial elastic modulus and thickness of the substrate. If the strain $\epsilon_f$ is not constant and evolves as a function of the film thickness, i.e. $\epsilon_f = \epsilon_f(h_f)$, then the integral and differential form of curvature are

$$\kappa = \int \frac{6M_f \cdot \epsilon(h_f)}{M_s h_s^2} dh_f \tag{4-22}$$

$$d\kappa \approx \frac{6M_f \cdot \epsilon(h_f)}{M_s h_s^2} dh_f \tag{4-23}$$

respectively. Consequently, then the overall strain and stress derived from curvature are

$$\epsilon_{all} = \frac{M_s h_s^2}{6M_f} \cdot \frac{d\kappa}{dh_f} \tag{4-24}$$

$$\sigma_{all} = M_f \cdot \epsilon_{all} = \frac{M_s h_s^2}{6} \cdot \frac{d\kappa}{dh_f} \tag{4-25}$$

respectively. The stress expressed as Eq. (4-25) is called incremental stress, which is derived from the slope of curvature curve [15]. The $\sigma \cdot h \sim h$ curve is usually being used to analyze the stress and strain behavior of thin films [15-18].

In multi-layer structure, if the latest layer doesn't influence the underlying layers, the total curvature of the wafer can be the sum of the curvature caused by every individual layer, as follows [19]

$$\kappa = \sum_{i=1}^{n} \kappa_i = \frac{6}{M_s h_s^2} \sum_{i=1}^{n} h_i M_i \cdot \epsilon_i(h_i) \tag{4-26}$$

with *n* being the number of multilayers.

In this study, the stress and strain in every individual layer would be extracted from the curvature curve by using Eqs. (4-24) ~ (4-25) respectively and then be analyzed. The thermal stress will be calculated using Eqs. (4-14) ~ (4-16). Then the total stress $\sigma_{all}$ in the film consists of two parts, as expressed as follows

$$\sigma_{all} = \sigma_{itr} + \sigma_{th} \tag{4-27}$$

with $\sigma_{itr}$ and $\sigma_{th}$ being the intrinsic stress and thermal stress respectively. For the stages of film growth of AlN and GaN, because temperature is almost constant, the increment of overall stress consists of only intrinsic stress, as noted by

$$\Delta\sigma_{all} = \Delta\sigma_{itr} \qquad \text{(During growth)} \tag{4-28}$$

For stages there is no growth but only temperature ramping, the increment of overall stress comes from only thermal stress, then

$$\Delta\sigma_{all} = \Delta\sigma_{th} \qquad \text{(During temperature ramping).} \tag{4-29}$$

The assumption of Eq. (4-28) is valid because for nitrides, the microstructure doesn't change and no intrinsic stress variation during annealing or thermal cycling by temperature ramping [14, 20], except recrystallization occurs when to anneal the compounds like GaN and AlN grown at low temperature. This has also been verified by a thermal cycling experiment shown in Fig. 4.5. This sample contains high-temperature AlN buffer layer and one AlN interlayer and GaN layers on them. After growth, three thermal cycles were performed and every cycle consists of 5 min of annealing at low temperature and high temperature respectively. During thermal cycling, in every cycle, the curvature curve can be repeated exactly, including the curvature value at low temperature and high temperature, as well as the slope during temperature ramping. All these behavior indicates that no intrinsic stress variation occurred during thermal cycling and the curvature transition was caused by only thermal stress. This also conveys that nitrides are of very high thermal stability. The quality, microstructure and defect density didn't change during annealing or thermal cycling, which makes them highly suitable for the application at high temperature. As introduced above, any evolution of the crystal quality, microstructure and defect information can lead to intrinsic stress variation.

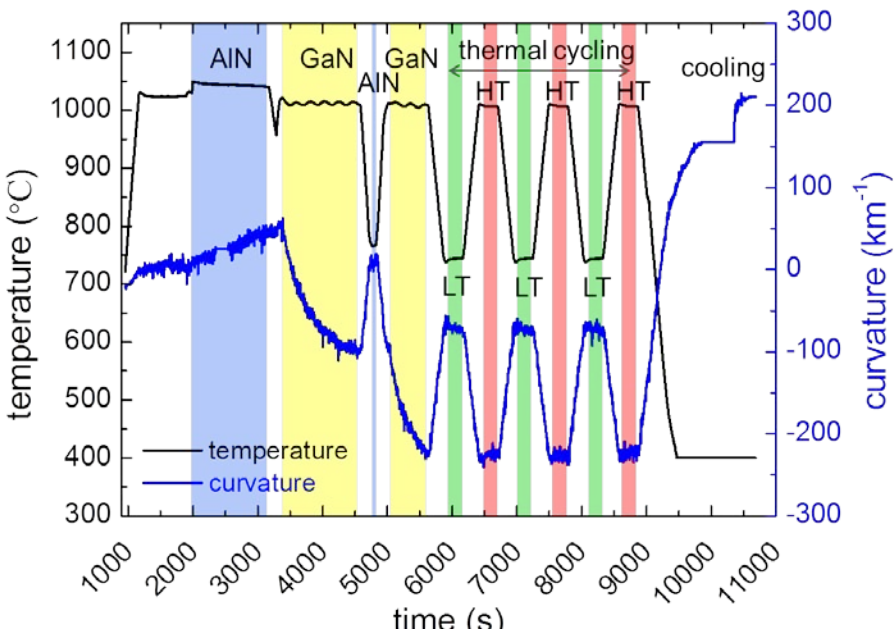


**Fig. 4.5** Thermal cycling test of GaN/AlN/GaN/AlN/Si sample by annealing at low temperature (LT) and high temperature (HT) for 5 min respectively.

The analysis would be divided into two parts, the part of AlN buffer layer and GaN on it and the part of AlN interlayer and the overlying GaN in section 4.3 and 4.4 respectively. In section 4.5, the stress in Si wafer and the problem of its plastic deformation is analyzed.

**Table 4.1** The correspondence of Si wafer size (diameter) and wafer thickness [1].

| **Size (inch)** | **2** | **3** | **4** | **5** | **5.9** | **7.9** | **11.8** | **17.7** |
|---|---|---|---|---|---|---|---|---|
| **Size (mm)** | 51 | 76 | 100 | 130 | 150 | 200 | 300 | 450 |
| **Thickness (um)** | 275 | 375 | 525 | 625 | 675 | 725 | 775 | 925 |

Besides curvature, wafer bow $\delta$ is another more practically important property to device fabrication, which is expected to be as small as possible. $\delta$ can be calculated from curvature $\kappa$, they are related as [21]

$$\delta = \frac{l^2}{8R} = \frac{l^2}{8}\kappa \tag{4-30}$$

with $R$ being the radius of curvature, $l$ being the diameter of the wafer.

Since the wafer size practically applied in industrial fabrication can be as large as 8 inch, the results in this work would be extended to the cases of Si wafer size from 2 inch to 17.7 inch, which render this work more useful for references. Because the wafer thickness $h_s$ and diameter $l$ are needed for calculating curvature $\kappa$ and wafer bow $\delta$ respectively, there are summarized in Table 4.1 for the later calculation.

### 4.2.5 Material parameters

This section is the analysis of stress and strain in AlN buffer layers grown under varied conditions and that in GaN grown above them. Material parameters are listed in Table 4.1. In order to get lattice constant at high temperature and the thermal strain and stress, thermal expansion coefficient (TEC) $\alpha$ is indispensable. TEC $\alpha$ of Si, AlN and GaN are not constants but functions of temperature. Lattice constant $a(T)$ at temperature $T$ is given by [4]

$$a(T) = a_0\left[\int_{273.2}^{T} a(T)dT + 1\right]. \tag{4-31}$$

The temperature dependent thermal coefficient $\alpha(T)$ is assumed to be an empirical formula [4]

$$\alpha(T) = \left\{C_1\left[1 - \exp\left(-C_2(T - C_3)\right)\right] + C_4T\right\} \times 10^{-6}K^{-1} \tag{4-32}$$

Usually, in publications, only the measured and calculated lattice constant has been given, but no direct expression of thermal expansion coefficient like Eq. (4-32). It has to be derived from the measured temperature dependent lattice constant data from the publications [4, 5, 22]. There are two models which are named Debye model and Einstein model respectively to calculate the lattice constant of crystals. The difference of the results of these two is minimal and ignorable, but the form of Einstein model is simpler [5]. Using Einstein model, $a(T)$ can be can be calculated by

$$a(T) = a_0 + a_0\alpha_\infty\theta_E \frac{1}{\exp(\theta_E/T)-1} \qquad \text{Einstein model} \tag{4-33}$$

with $a_0$ being the fitted lattice constant value at 0 $K$, $\alpha_\infty$ being the lattice expansion coefficient of the high temperature limit, $\theta_E$ being the Einstein temperature [22]. They are listed in Table 4.2.

**Table 4.2** Parameters in Einstein model of lattice constant of AlN and GaN.

| | $a_0$ (Å) | $\alpha_\infty$ ($10^{-6} \cdot K^{-1}$) | $\theta_E$ ($K$) |
|---|---|---|---|
| **AlN [3]** | 3.1105 | 6.9±0.3 | 1025±25 |
| **GaN [5]** | 3.1882 | 19.8±1.1 | 636±13 |

Then the temperature dependent lattice expansion coefficient can be theoretically defined as the product of the reciprocal of the lattice constant and the first derivative of Eq. (4-33) at that temperature [5], as follows

$$\alpha(T) = \frac{1}{a(T)} \cdot \frac{\mathrm{d}a(T)}{dT} \tag{4-34}$$

Then by fitting the result of Eq. (4-34), the parameters in Eq. (4-32) can be obtained and were listed in Table 4.3. Using the fitted parameters, lateral lattice constant and TEC of Si, AlN and GaN were plotted in Fig. 4.6.

**Table 4.3** Material parameters. Thickness is the value of the sample for AlN buffer layer study.

| Material | $M$(GPa) | $h$ (um) | $a_{RT}$ (Å) | $C_1$ | $C_2$ | $C_3$ | $C_4$ |
|---|---|---|---|---|---|---|---|
| **Si** | 228 | 275 | 5.43 [4] | 3.725 | 0.00588 | 124.0 | 0.0005548 |
| **AlN** | 470 [6] | 0.11 | 3.112 | 6.122 | 0.004437 | 165.3 | 0.0003302 |
| **GaN** | 450 [6] | 1.71 | 3.189 | 5.786 | 0.006174 | 86.43 | 0.0002051 |

## 4.3 Stress and strain in AlN buffer layer and overlying GaN

The analysis in this subsection consists the strain $\epsilon$ and stress $\sigma$ of AlN buffer grown under various conditions (three typical temperatures and two typical V/III ratio), strain evolution of GaN layer on them as well as the thermal strain of the whole sample. In Fig. 4.7, the growth was divided into 3 stages, stage I of AlN growth, stage II of GaN growth and stage III of cooling down.

- **AlN buffer layer growth**

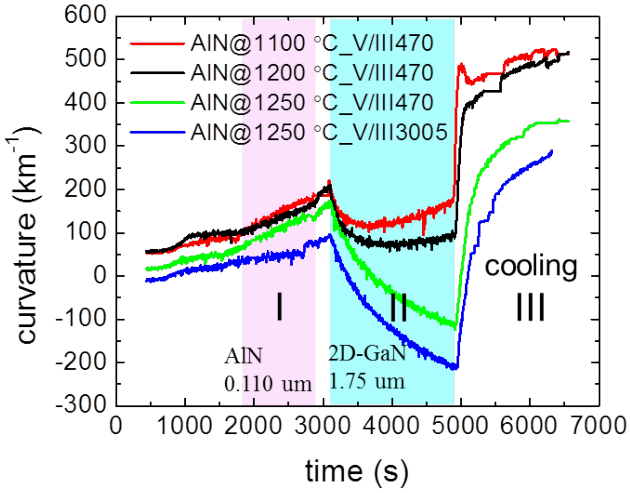


**Fig. 4.7** Curvature curves of growth of GaN on AlN buffer layer.

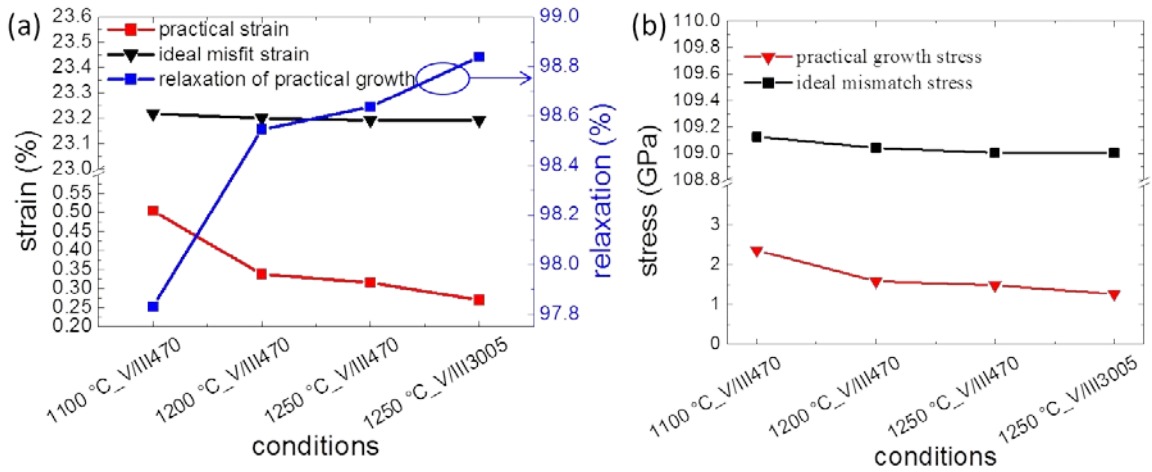


**Fig. 4.8** (a) Ideal misfit strain, practical growth strain and relaxation and (b) ideal misfit stress and practical growth stress of AlN buffer layer.

Within a limited thickness (e.g. < 500 nm), there was no variation of the strain and stress for AlN grown on Si since the slope of curvature curve was a constant, although it differed under varied growth conditions. Four samples grown under representative conditions were chosen here, with temperature varied from 1100 ℃ to 1250 ℃ and V/III ratio from 470 to 3005. The growth strain and stress were extracted from the experimental curvature curve. In Fig. 4.8, due to $\alpha_{AlN} > \alpha_{Si}$, both of the ideal misfit strain $\epsilon_m$ and growth strain $\epsilon$ decreased as temperature was raised; the latter is only 1~2% of the former. True lattice constant of AlN

buffer layer at growth temperature $a_{true-AlN}$ as well as relaxation $\varsigma_{AlN-bf}$ can be obtained using Eq. (4-12) and Eq. (4-13) respectively. $\varsigma_{AlN-bf}$ was very high and increased from 97.8% to 98.6% as the growth temperature was raised from 1100 ℃ to 1250 ℃, from the beginning of its growth. This is an indication that the growth of AlN on Si was far from pseudomorphic growth but started with neighboring islands or crystallites, which can relax most of the misfit strain. In chapter 3 it was shown that as growth temperature increases, the quality of AlN buffer improves. Then this leads to a difficulty that why the relaxation rate is larger in better AlN. The assumption that AlN buffer consists of connecting crystal columns may help to interpret it. As the growth temperature increases, the quality of AlN crystal columns increases while the connection or coalescence of the columns gets weaker. Then the pulling tension force at the column boundaries is less and the buffer get more relaxed. Although the ideally completely strained AlN lattice constant should be larger, as the relaxation becomes larger, the true AlN lattice constant (not shown) is even smaller under better growth conditions (higher temperature and mediate V/III). This is also a factor that GaN was more compressively stressed on better AlN buffer. Wafer size dependence of curvature and wafer bow for the AlN/Si samples of strain under real growth conditions and ideal misfit strain were plotted respectively in Fig. 4.9. It is impressive that with only 0.11-um thick AlN layer on Si, if it is completely strained, it would cause huge stress (Fig. 4.8b), curvature and wafer bow, which are dozens of folds of the real case. Relaxation is helpful to release tensile stress in AlN buffer. Under the same strain, as the wafer size and thickness become larger, curvature is dropping while bow is rising. With diameter $l$ smaller than 100 mm, curvature dropping rate is large and the reduction becomes small after that. Variation of wafer bow is small if $l$ is less than 150 mm. It starts to increase with a constant rate if $l$ is bigger than 150 mm. From the curves in Fig. 4.9, it is clear that to yield small bow, curvature should be as small as possible. On the other hand, under identical film strain, wafers with diameter around 150 mm are easier to achieve both small curvature and bow.

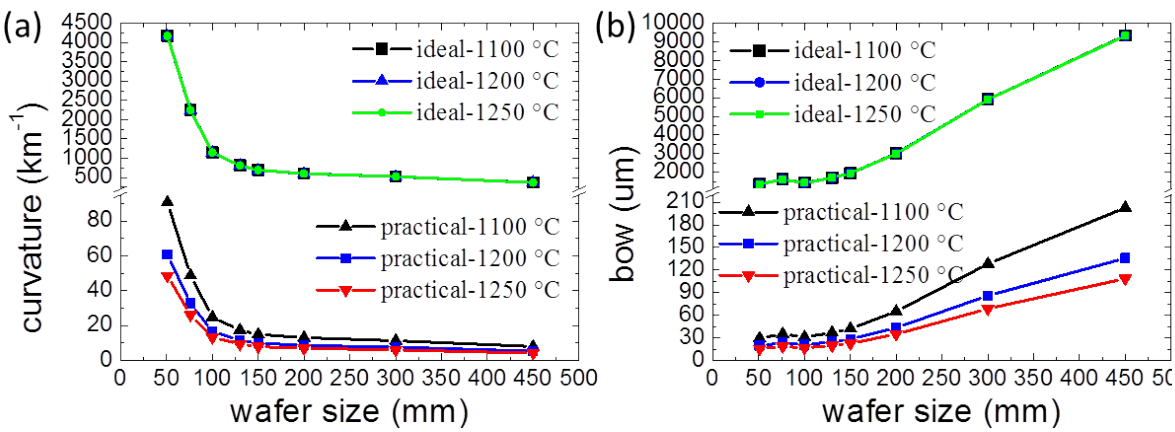


**Fig. 4.9** (a) Curvature and (b) wafer bow as functions of wafer size, with ideal misfit stress and practical growth stress of AlN buffer layer respectively.

- **The 1st GaN layer**

$$d\kappa \approx \frac{6M_f \cdot \varepsilon(h_f)}{M_s h_s^2} dh_f, \rightarrow \varepsilon(h_f), \rightarrow \kappa = \int \frac{6M_f \cdot \varepsilon(h_f)}{M_s h_s^2} dh_f \quad (4\text{-}35)$$

Next is the analysis of the strain and stress of GaN on AlN buffer layers, which are extracted from the curvature curves using Eqs. (4-24) and (4-25). The procedure of strain extraction and curvature fitting is shown as expression (4-35), in which the curvature curve is recovered using extracted strain to check the accuracy of the extracted strain. Since the raw

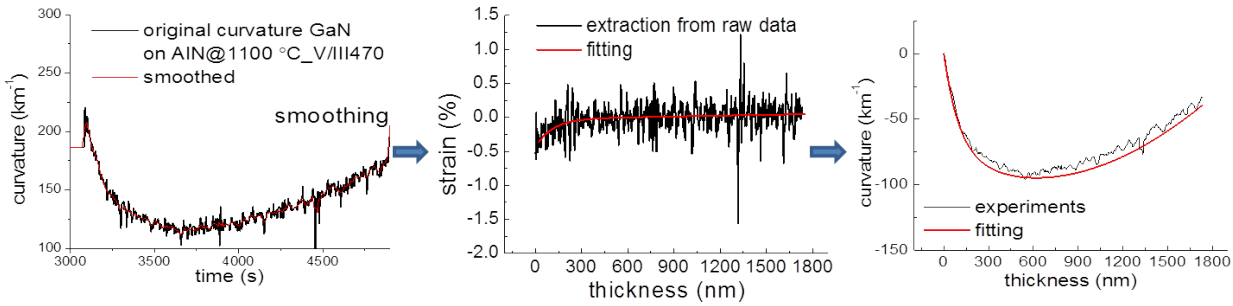


**Fig. 4.10** The procedure of strain extraction and curvature recovery.

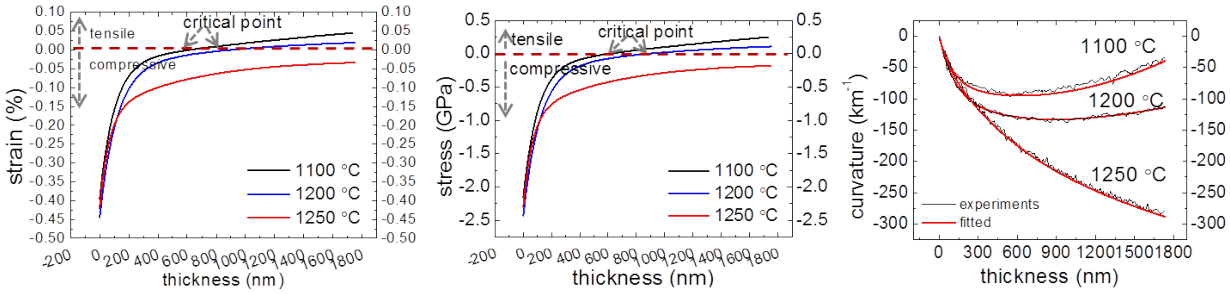


**Fig. 4.11** Fitted strain, stress and curvature of GaN layers on AlN grown at 1100 ℃, 1200 ℃ and 1250 ℃.

curvature data is very rough with large fluctuation, it was firstly smoothed prior to strain extraction. This procedure is also schematically graphed in Fig. 4.10. Following this procedure, the fitted strain and stress was obtained in Fig. 4.11. Using the fitted strain, the recovered curvature curves matched the raw data very well. In the beginning of the first tens of nanometers of GaN, initial strain and strain relaxation rate for all the three samples were more or less the same. In the first 200 nm, the strain relaxed rapidly from the initial value of -0.0045 to about -0.0005 for the samples with AlN buffer grown at 1100 ℃ and 1200 ℃ , to about -0.0012 for the sample with AlN buffer layer grown at 1250 ℃. After that, the relaxation rate slowed down. The difference is that, from the extracted strain, for samples with AlN buffer layer grown at 1100 ℃ and 1200 ℃, there was a transition from compressive strain to tensile. The point that the strain evolves from compressive to tensile is called critical point. The thickness corresponding to the critical point for GaN on 1100-℃ grown AlN (~ 600 nm) is smaller than that on 1200-℃ grown AlN (~ 950 nm). The strain in GaN on 1250-℃ AlN is always compressive within thickness of 1750 nm. In a word, GaN relaxes faster on lower-temperature AlN buffer than that on higher-temperature one. This can be attributed to the quality of GaN/AlN interface. In chapter 5 it will be shown that the quality of AlN buffer and GaN on it is both better if the growth temperature of AlN buffer is higher. Then the threading dislocation density at GaN/AlN is lower for higher-temperature AlN buffer layer. According to the strain relaxation mechanisms introduced in chapter 3, higher threading dislocation in the substrate or underlying layer leads to larger relaxation in the overlying layer.

There is another question has to be answered is that why the strain of GaN on AlN evolved to be tensile. As the lattice constant of GaN is larger than that of AlN, it should be compressively strained. This leads to an analysis of the source of GaN layer suffered. As shown in Fig. 4.12, GaN suffers compressive stress from the AlN buffer and tensile stress from the Si substrate. Within the neutral point, the lattice of GaN is constrained by smaller AlN lattice and is compressively strained. Since great amount of dislocations exist on the GaN/AlN interface and the compressive strain is relaxed as the thickness increases. In this stage, the compressive stress caused by AlN buffer is larger than the tensile stress. At the neutral point, GaN lattice relaxed to its neutral state and the compressive stress from AlN $\sigma_{cmp.GaN/AlN}$ and the tensile stress from Si substrate $\sigma_{tensile.GaN/Si}$ got balanced. Beyond neutral point, the influence from AlN buffer cannot constrain GaN lattice anymore and $\sigma_{tensile.GaN/Si}$ became dominant and GaN lattice suffered tensile strain. In a limiting case, supposing that GaN thickness is much larger than that of AlN buffer $h_{GaN} \gg h_{AlN}$ that the thickness of AlN buffer is ignorable, then the stress in GaN shows most influence from Si substrate. If the quality of AlN buffer is good enough, overlying can be compressively strained within a very large thickness. In another imaged case, if the substrate is not Si but free-standing AlN, then GaN grown on it can only be compressive strained and evolves to neutral state and will never go to tensile side.

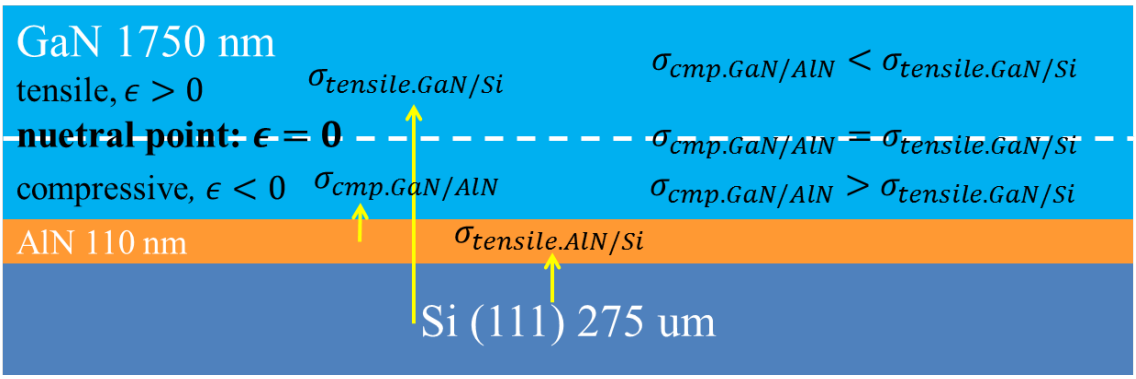


**Fig. 4.12** Stress sources in GaN layer.

- **Cooling down**

The third stage is cooling. Since there is no growth and no microstructure evolution after during cooling, so in this stage the stress is only induced by thermal effect, i.e. thermal stress. In Fig. 4.13a it shows that for all samples the curvature increment from the end of GaN growth to room temperature is about 490 km$^{-1}$, except cracking occurred in the sample with AlN buffer grown at 1100 ℃. If only consider the effect of GaN layer for that the thickness of AlN is very small compared with that of GaN, the curvature caused by thermal stress can be calculated as follows

$$\Delta\kappa_{th-cool} = \frac{6}{M_{Si}h_{Si}^2}\int_{1323}^{310}\{M_{GaN}h_{GaN}[\alpha_{Si}(T) - \alpha_{GaN}(T)]\}dT = 491 \text{ km}^{-1} . \quad (4\text{-}36)$$

The calculated curvature increment caused by GaN only is slightly larger than the true value. The calculated temperature was the true temperature but not setting point. Compared with the experimental result, it was shown that AlN buffer layer didn't contribute to the

tensile curvature increment during cooling. This may be due to the relaxation of AlN buffer layer. In Fig. 4.13b, it was the curvature curve of a single AlN buffer layer on Si. Because the TEC of AlN $\alpha_{AlN}$ is larger than that of Si $\alpha_{Si}$, the same as GaN, during cooling down, the tensile strain in AlN should be larger and larger and the curvature value should increase by 31.6 km$^{-1}$. However, in fact, contrarily, it decreased by 70 km$^{-1}$, which indicated that AlN has relaxed but not more strained during cooling. This is an indication that AlN is not perfect epitaxial continuous film on Si but crystalline grains instead. As it cools, the grains contract and their volume decreases, the grains are more disconnected and independent from each other, which results in weaker bonding and connection between neighboring grains and reduced stress in AlN buffer. Combining the effect of tensile strain generation during cooling and relaxation of AlN buffer, it is reasonable that the true tensile curvature increment during cooling down is smaller than the theoretical prediction.

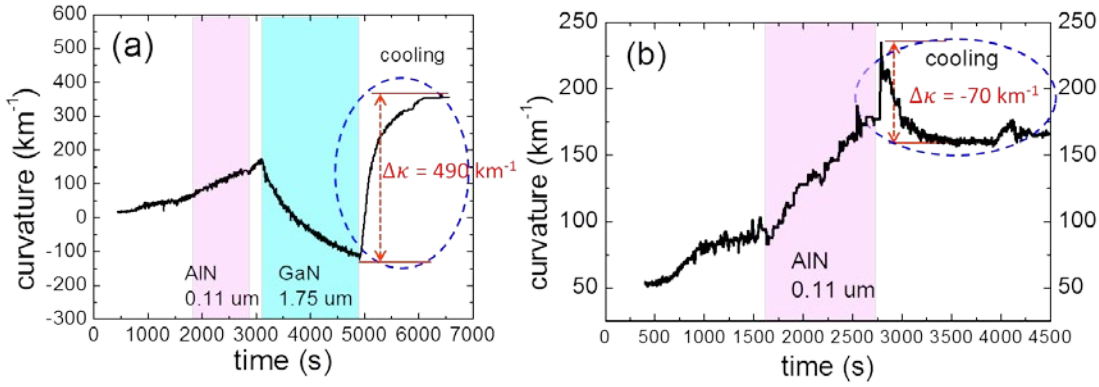


**Fig. 4.13** Curvature increment during cooling of (a) GaN/AlN/Si sample and (b) AlN/Si sample.

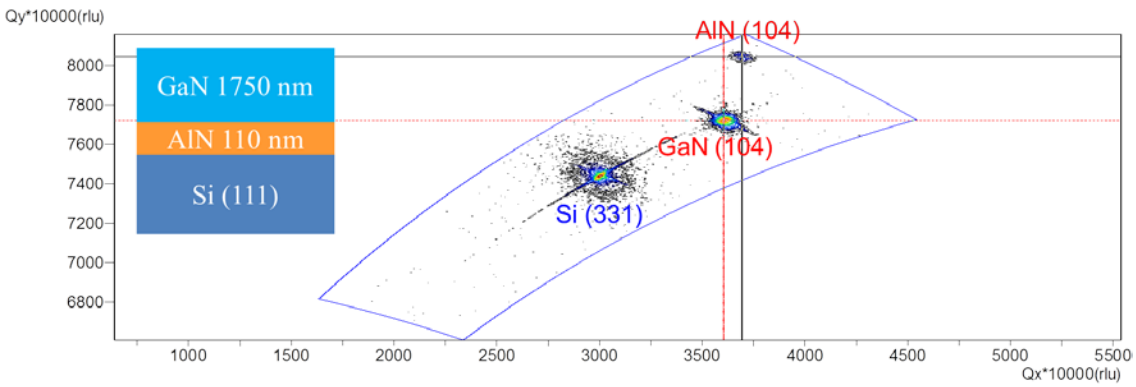


**Fig. 4.14** An example of XRD RSM measurement of sample GaN/AlN/Si.

In fact, the strain of AlN buffer and GaN layer can be measured by XRD reciprocal space mapping (RSM). In crystallography, in the reciprocal space, every plane index is represented by a point [23, 24]. The ideal coordinates value in the reciprocal space $Q_x$ and $Q_y$ can be calculated using plane index and the lattice constant of the corresponding crystal. For nitrides, $Q_x$ and $Q_y$ can be calculated as

$$Q_x = \frac{1}{a}\sqrt{\frac{4}{3}(h^2 + hk + k^2)},\ Q_y = \frac{l}{c} \tag{4.37}$$

with $a$ and $c$ being the lateral and vertical lattice constant respectively, $(hkl)$ being the plane index. $Q_x$ and $Q_y$ can be measured directly by XRD RSM. From the measured $Q_x$ and $Q_y$ values, the true lattice constant of $a$ and $c$ can be obtained. As shown in Fig. 4.14, plane (104) of AlN and GaN is parallel with the plane of Si (331). The true strain of AlN and GaN at room temperature $\epsilon_{RT}$ can be calculated from the measured lattice constant using Eq. (4-10). As $\epsilon_{RT}$ has been obtained, based on the thermal stress in the individual film layer of Eq. (4-19), the strain at growth temperature $\epsilon_{GT}$ can be calculated by

$$\epsilon_{GT} = \epsilon_{RT} - \epsilon_{th} = \epsilon_{RT} - \int_{T_G}^{T_R}[\alpha_s(T) - \alpha_f(T)]dT - \frac{2}{3}h_s\kappa \,. \tag{4.38}$$

**Table 4.4** Strain in AlN buffer layer at growth temperature ($\epsilon_{GT}$) and room temperature ($\epsilon_{RT}$), derived from XRD RSM, in-situ curvature measurement and thermal strain ($\epsilon_{th}$) calculation, respectively.

| **AlN buffer conditions** | $\epsilon_{RT-AlN}$ | $\epsilon_{GT-AlN-1}$ | $\epsilon_{GT-AlN-2}$ | $\epsilon_{th-GaN}$ |
|---|---|---|---|---|
| | by XRD | calculation | In-situ curvature | calculation |
| **1100 ℃ /470 (V/III)** | 0.53397% | 0.3655267% | 0.504% | 0.1684433% |
| **1250 ℃ /470 (V/III)** | 0.32168% | 0.1346176% | 0.338% | 0.1870624% |
| **1250 ℃ /3005 (V/III)** | 0.26380% | 0.0767376% | 0.270% | 0.1870624% |

**Table 4.5** Strain in GaN layer at growth temperature ($\epsilon_{GT}$) and room temperature ($\epsilon_{RT}$), derived from XRD RSM, in-situ curvature measurement and thermal strain ($\epsilon_{th}$) calculation, respectively.

| **AlN buffer conditions** | $\epsilon_{RT-GaN-1}$ | $\epsilon_{GT-GaN}$ | $\epsilon_{RT-GaN-2}$ | $\epsilon_{th-GaN}$ |
|---|---|---|---|---|
| | by XRD | calculation | curvature at RT | calculation |
| **1100 ℃ /470 (V/III)** | 0.3794% | -0.0110682% | 0.1861095% | 0.1971777% |
| **1250 ℃ /470 (V/III)** | 0.2643% | -0.0676309% | 0.1295468% | 0.1971777% |
| **1250 ℃ /3005 (V/III)** | 0.2518% | -0.0877015% | 0.1094762% | 0.1971777% |

The role of AlN buffer layer in curvature variation during cooling down should be examined carefully. If it is supposed to be perfect epitaxial film, in AlN/Si sample, it should add 31.6 $km^{-1}$ more tensile curvature to the total during cooling. Instead, in fact, curvature of the sample with only a layer of AlN on Si dropped by 70 $km^{-1}$ during cooling. In sample with GaN/AlN/Si structure, AlN buffer layer almost didn't contribute to the tensile stress increment during cooling, which is consistent with the data from XRD RSM and in-situ curvature measurement in Table 4.4. This means that the strain of AlN state kept almost constant during cooling, because it was sandwiched in GaN/AlN/Si sample and constrained by GaN layer and Si substrate. The results from XRD RSM measurement are consistent with that of in-situ curvature measurement that as the growth conditions became better, AlN was less strained.

As shown in Table 4.5, the strains in GaN layer at both growth and room temperature was measured and calculated. They are not constant as functions of thickness. Since there was no thermal strain in AlN buffer layer, the final curvature values were adopted to evaluate the

strain in GaN layer at room temperature by ignoring the presence of AlN buffer layer. The values of room-temperature strain $\epsilon_{RT-GaN-2}$ estimated from room-temperature curvature and calculated growth-temperature strain $\epsilon_{GT}$ in the table can be regarded as average strain through the whole layer. $\epsilon_{RT-GaN-1}$ was also measured by XRD RSM, but they were about two times of the values estimated from room-temperature curvature. The calculated average strains $\epsilon_{GT-GaN}$ are slightly compressive. They are very close to the average values of the strain curves in Fig. 4.11. Similarly, the values of $\epsilon_{RT-GaN-2}$ are close to the average of calculated strain distribution in GaN layer at room temperature, corresponding to the growth conditions of AlN buffer layer. This verifies that the simplification and assumption of the thermal strain only between GaN and Si regardless of the existence of AlN buffer layer is valid and $\epsilon_{RT-GaN-2}$ are reliable. The much higher $\epsilon_{RT-GaN-1}$ obtained by XRD RSM may be the strain state of the top part of GaN layer which is of the highest tensile strain. This is reasonable because the incident angle of (104) plane is very small and the sampled depth of X-ray might be only tens of nanometers and the large percentage of the collected diffracted X-ray signal was also from that part.

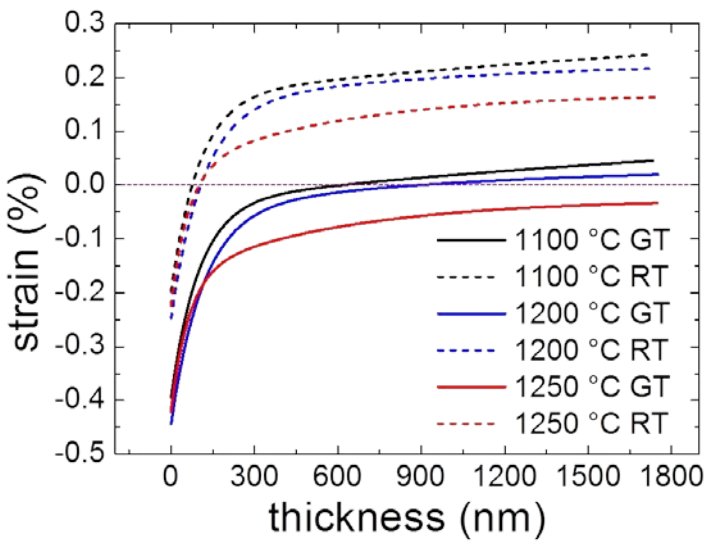


**Fig. 4.15** Strain distribution in GaN layer grown on condition varied AlN buffer layers, as a function of thickness at growth temperature (GT, solid lines) and room temperature (RT, dashed lines), respectively.

## 4.4 Stress and strain in AlN interlayers and overlying GaN

Using the same fitting procedure in the previous section, the analysis in this section consists of three parts including the growth strain and stress in AlN interlayers, GaN layers and thermal stress in every temperature transition period. Since AlN buffer layer and the 1st GaN layer have been analyzed in the last section, they will not be addressed in this section. The growth stages that would be analyzed in this section are shown in Fig. 4.16. Because of the occurrence of plastic deformation of Si during the growth of top GaN, the strain and stress evolution in the stage of the growth of the top GaN and cooling down would not be analyzed for that the apparent strain and stress extracted from the curvature curve could not reflect the true strain and stress state in these two stages but also contains the influence of

plastic deformation from the Si substrate. The problem of plastic deformation would be discussed in next section. The analysis in this section can let us know the strain and stress in AlN interlayer grown under various conditions as well as that of overlying GaN layer. Three samples for the tests of thickness, growth temperature and V/III ratio of AlN interlayers would be analyzed.

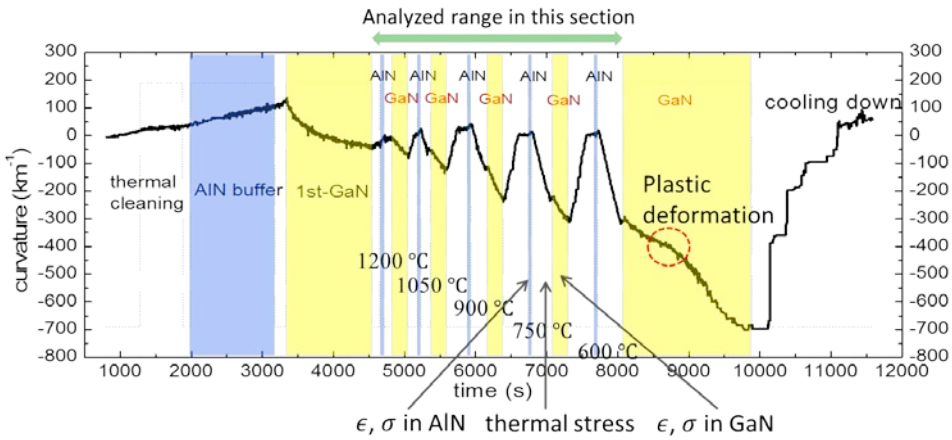


**Fig. 4.16** An example of curvature transition curve of growth temperature test of AlN interlayers, the range that would be analyzed in this section was marked.

- **Thickness test of AlN interlayers**

Firstly, the strain and stress of AlN interlayers is inspected. The curvature increment during the growth of AlN interlayers for thickness effect investigation was shown and

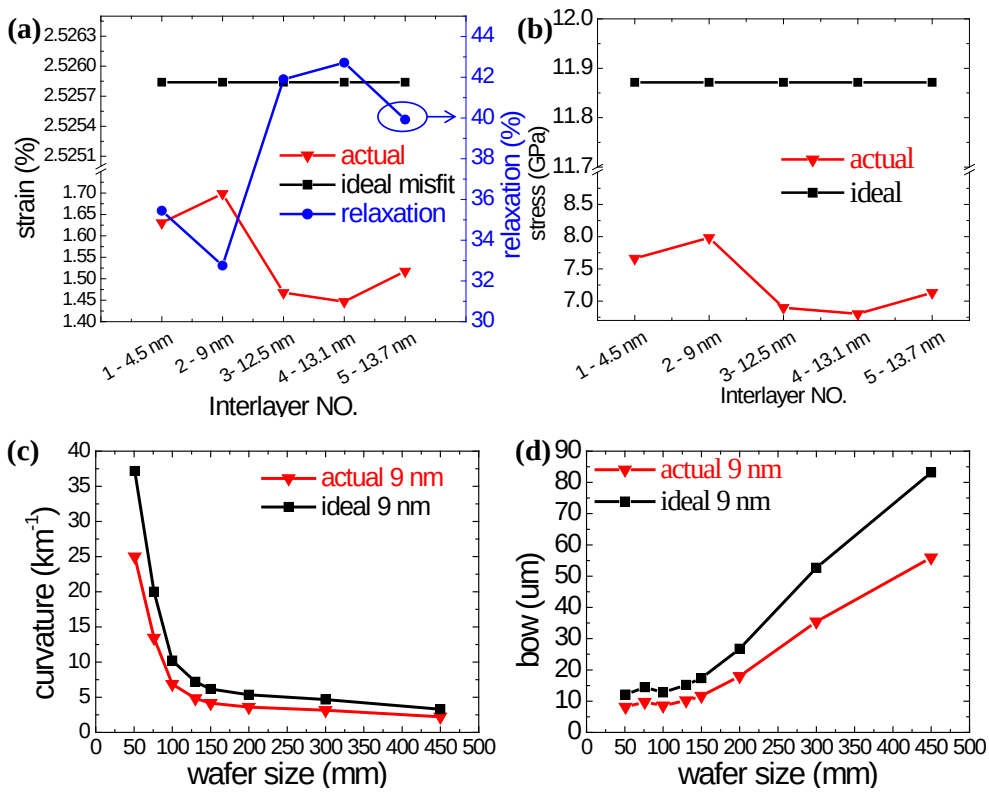


**Fig. 4.17** Ideal and actual strain and relaxation (a), stress (b) of the stage before cracking in **AlN interlayers** for thickness test, and wafer size depending curvature (c) and bow (d) caused by them.

extracted in Fig. 3.18 and Fig. 3.22 respectively. In Fig. 3.18 it was shown that there was cracking point in 22.5-nm and 45-nm thick AlN interlayers, which divided the growth of them into two stages. Before cracking, the slope of it was large and constant and almost the same as that of thin ones. The strain and stress in this stage was plotted in Fig. 4.17. For the 22.5-nm and 45-nm thick AlN ILs, the thicknesses prior to cracking were adopted, which were 13.1 nm and 13.7 nm respectively.

The strain and stress was around 1.5% and 7.3 GPa respectively, and the absolute variation is small. Since the lattice mismatch between GaN and AlN $\epsilon_{m-GaN/AlN}$ is small compared with that between Si and AlN $\epsilon_{m-Si/AlN}$, the former ideal misfit strain is only about one tenth of that of the later. The strain was about 2 times higher than that of AlN on Si. It is more strained by underlying GaN and the growth of AlN on GaN is more pseudomorphic. The relaxation rate ranged from 32% to 40%, which was about one third of that of AlN buffer layer on Si substrate. This means higher quality of AlN ILs than AlN buffer layer, even with small thickness of several nanometers. Within such a small thickness, it can cause tens of km$^{-1}$ and um of curvature increment and wafer bow, respectively.

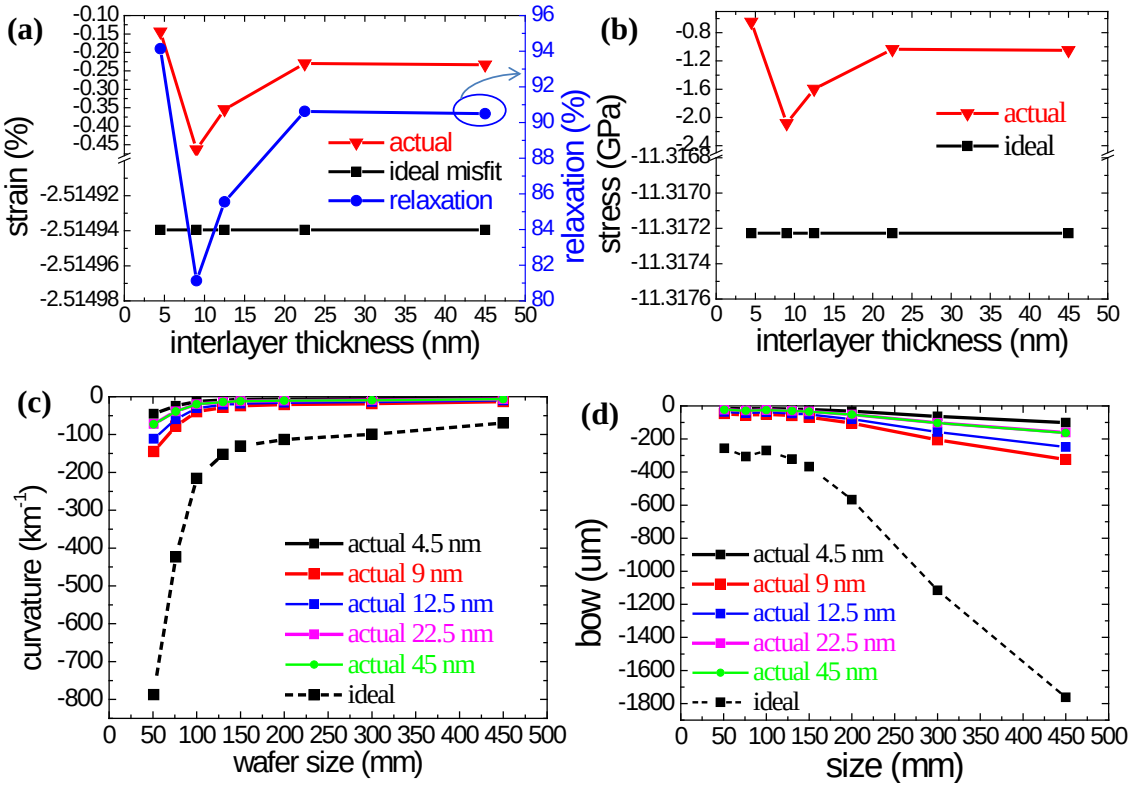


**Fig. 4.18** Ideal and actual strain and relaxation (a), stress (b) in 200-nm-thick **GaN** layers on AlN interlayers for thickness test, and wafer size depending curvature (c) and bow (d) caused by them.

After cracking, there was almost no curvature increase as the thickness rose. According to Stoney formula Eqs. (4-7) and (4-23), curvature increment $\Delta\kappa$ is proportional to the strain and thickness, as shown in Eq. (4-39) as

$$\kappa \propto \epsilon_f \cdot h_f \qquad \text{or} \qquad \Delta\kappa \propto \epsilon_f \cdot \Delta h_f. \tag{4-39}$$

If the curvature $\kappa$ keeps constant, there are two possibilities. One case is that as thickness increased, the strain $\epsilon_f$ decreased reciprocally with the thickness. This is unlikely to occur. Another case is that $\epsilon_f$ decreased to around zero. This is more likely that such strain relaxation can be realized by cracking. It should be noticed that such relaxation doesn't mean that the true lattice constant of AlN has relaxed to its neutral value. As discussed and observed in chapter 3 about the cracked AlN interlayer, the continuous film has cracked into numerous separating small domains. The bonding between the domains is very weak and cannot strain AlN film in the lateral direction effectively. Inside the AlN domains, due to the constraint from underlying GaN, the lattice constant didn't relax to neutral value at that temperature. This can explain that why the strain of thick AlN interlayer has relaxed to around zero but could not induce large compressive stress in overlying GaN.

Strain and stress in overlying 200-nm-thick GaN layers on AlN and incremental component of curvature and wafer bow were calculated in Fig. 4.18. This is a sample of multi-condition AlN interlayers. With the largest strain and smallest relaxation, GaN was mostly compressively strained on 9-nm-thick AlN interlayer. The ideal misfit strain is constant as the growth temperature of GaN has been fixed to be the same. Compared with the relaxation rate, GaN layers were more relaxed than their underlying AlN ILs for that AlN ILs are of only several to tens of nanometers with more pseudomorphic growth. Due to the large relaxation, the caused curvature and wafer bow were only one eighth of the ideal value. In order to induce compressive stress in GaN layer and control the curvature and wafer bow more efficiently, absolute values in Fig. 4.18c and d are expected to be as high as possible.

- **Growth temperature test of AlN interlayers**

Similarly, $\varepsilon$, $\sigma$, $\kappa$ and $\delta$ of AlN interlayers for growth temperature test was also analyzed. There is no cracking or sudden relaxation in AlN interlayers in this test as the thickness of it was designed to be around 7 nm and the true thickness was less than 12 nm. In the ideal case, misfit strain $\epsilon$ and stress $\sigma$ of AlN on GaN are decreasing at high temperature as temperature increases. However, the practical cases were more complicated. Highest strain appeared around AlN-IL growth temperature at around 900 ℃, and then dropped at higher temperature. Theoretically, if AlN IL and underlying GaN both were perfect crystalline film and no relaxation in AlN ILs, the misfit strain should be decreasing, as shown in Fig. 4.19a. But the quality of AlN ILs was far from being perfect, especially at low temperature. With general knowledge in chapter 3, higher growth temperature leads to better quality of AlN; such that also leads to higher strain and stress at higher growth temperature as AlN-IL quality improves, if ILs are pure AlN. From the TEM observation images (shown in Fig. 5.15 in chapter 5), the quality of quality of high-temperature ILs was indeed better than that of low-temperature ones, with sharper interfaces and less newly generated dislocations. Therefore, the real experimental results of strain were contradictory to the theoretical prediction. The real strain behavior can be interpreted only by assuming the composition of ILs was AlGaN but not pure AlN. This is verified by the composition analysis of EDS characterization in Fig. 3.26.

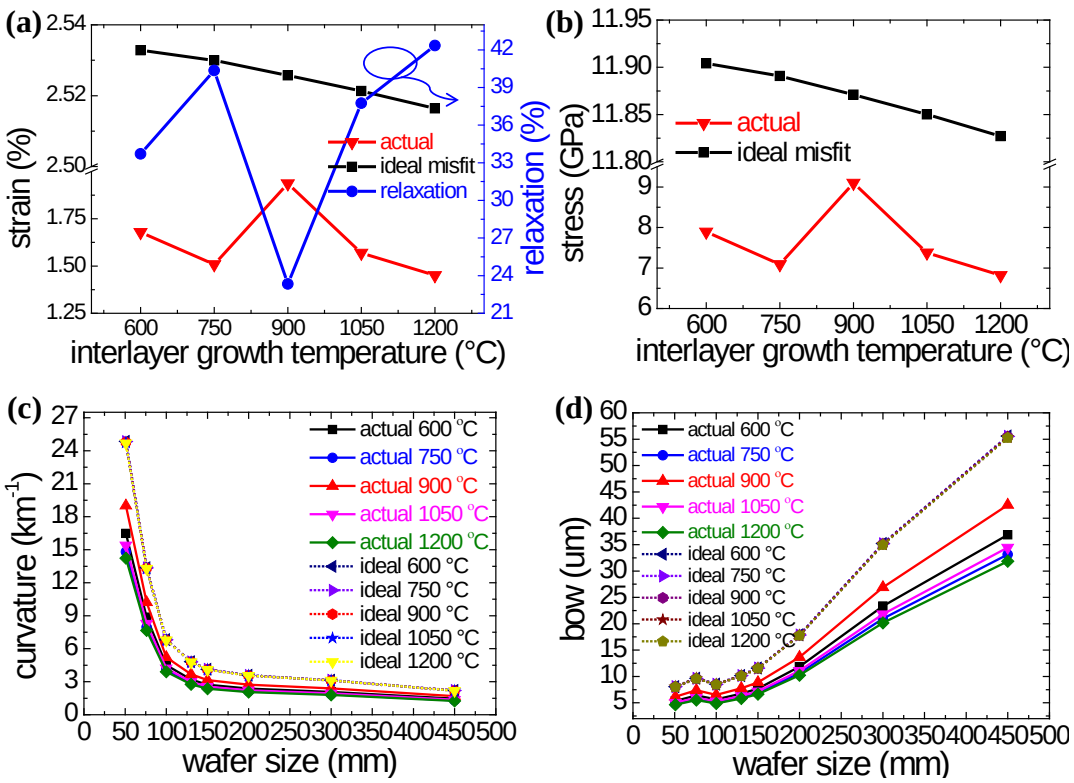


**Fig. 4.19** Ideal and actual strain ϵ and relaxation ς (a), stress σ (b) of **AlN interlayers** for growth temperature test, and wafer size depending curvature κ (c) and bow δ (d) caused by them, supposing that interlayers were pure AlN.

The percentage of Ga content in the ILs were extracted approximately from EDS measurement in Fig. 3.26 and plotted in Figs. 4.19 and 4.20. At low growth temperature (≤ 900 ℃), the content of Ga could be ignored, while at higher temperature of 1050 ℃ and 1200 ℃, Ga content can be as high as 34% and 40% respectively. According to the Vegard's law of Eq. (4-40) [25, 26], the lattice constant of $Al_xGa_{1-x}N$ is available depending on the Al content x, and then ideal misfit strain also can be calculated. The practical strain and ideal misfit strain are quite consistent at high temperature (≥ 1050 ℃). Due to the incorporation of Ga into AlN and closer lattice constant to GaN, even with better quality and smaller

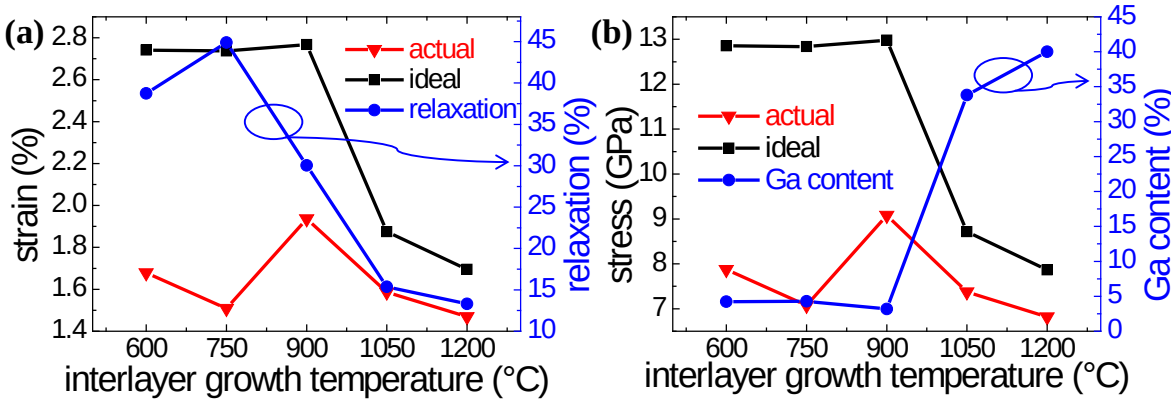


**Fig. 4.20** Ideal and practical strain ϵ and relaxation ς (a), stress σ (b) of **interlayers** for growth temperature test, supposing the composition of ILs is **AlGaN**.

relaxation, the true strain was small at high growth temperature.

$$a_{Al_xGa_{1-x}N}(T) = a_{GaN}(T) - 0.0891x \text{ Å} \tag{4-40}$$

Next, what we care most is the strain and stress in GaN on interlayers. The counted thickness of GaN was also 200 nm, which was a thickness that holds the constant stress before rapid relaxation starts. The curvature increment in GaN layers in the sample for AlN interlayer growth temperature test was extracted in and Fig. 3.25. The calculated strain and stress were plotted in Fig. 4.21. The mechanisms of how the growth conditions of AlN interlayers influence the amount of compressive stress that induced in overlying GaN layers on AlN interlayers has been discussed in chapter 3. GaN on AlN interlayer grown at 900 ℃ was mostly compressively stressed with strain of about -0.4%.

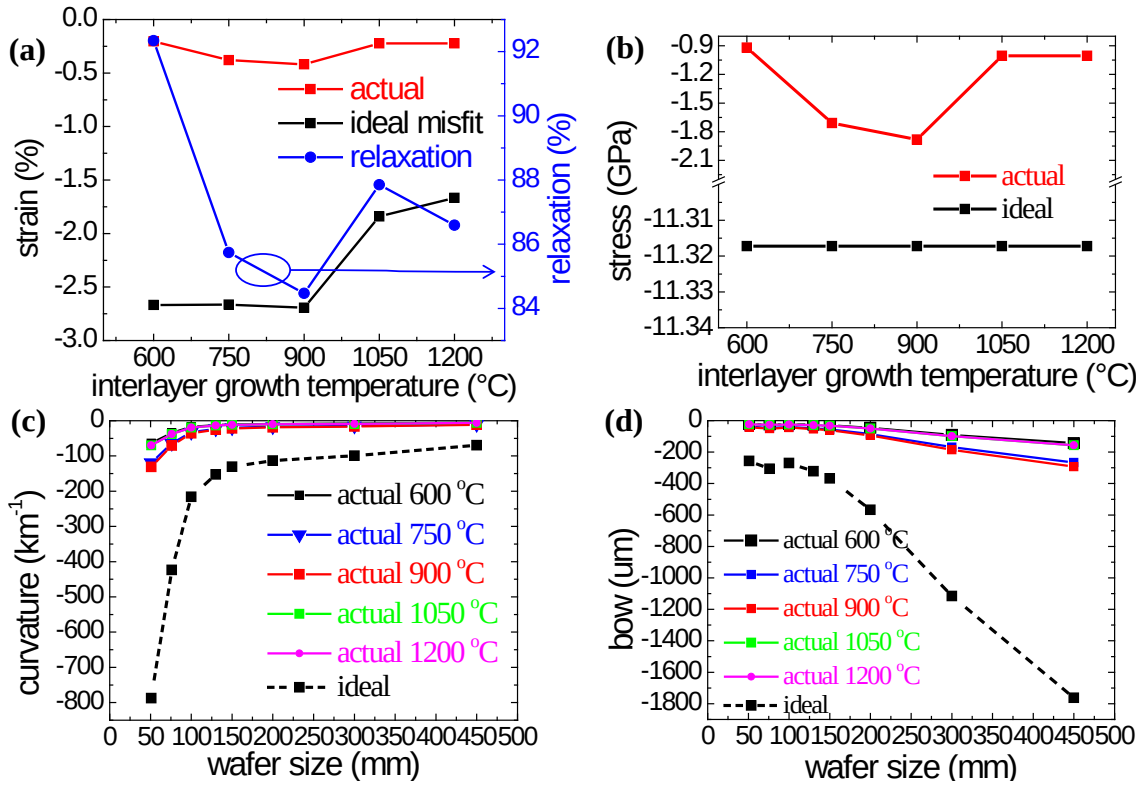


**Fig. 4.21** Ideal and practical strain and relaxation (a), stress (b) in 200-nm-thick **GaN** layers on AlN ILs for growth temperature test, and wafer size depending curvature (c) and bow (d) caused by them.

Here what should to be noted is that AlN interlayers were 5 ~ 10 times more strained than overlying GaN layers. The strain in GaN and underlying AlN interlayers ranged from -0.15% to -0.45% and from 1.5% to 1.9%, respectively. Such difference lies in the quality of lower and upper interfaces of AlN interlayers. Since crystal quality of GaN is much better than that of AlN, the quality of lower AlN(overlying)/GaN(underlying) interface is much better than that of the upper GaN(overlying)/AlN(underlying) interface. AlN interlayers could be grown more pseudomorphically on GaN layers than the opposite. On underlying interlayers with much higher defect density, the overlying GaN can relax rapidly which leads to much smaller compressive strain. This gives us a clue to induce more compressive stress in GaN, which is improving the quality of the upper interface of AlN interlayers.

- **Curvature variation due to thermal strain**

The third part is the curvature transition during temperature ramping from the growth condition of GaN to that of AlN, and vice versa. This is important to predicting the curvature increment caused by thermal strain of GaN/AlN multilayer structure on Si during temperature ramping and then to designing the final curvature and wafer bow at room temperature after cooling which is the ultimate target.

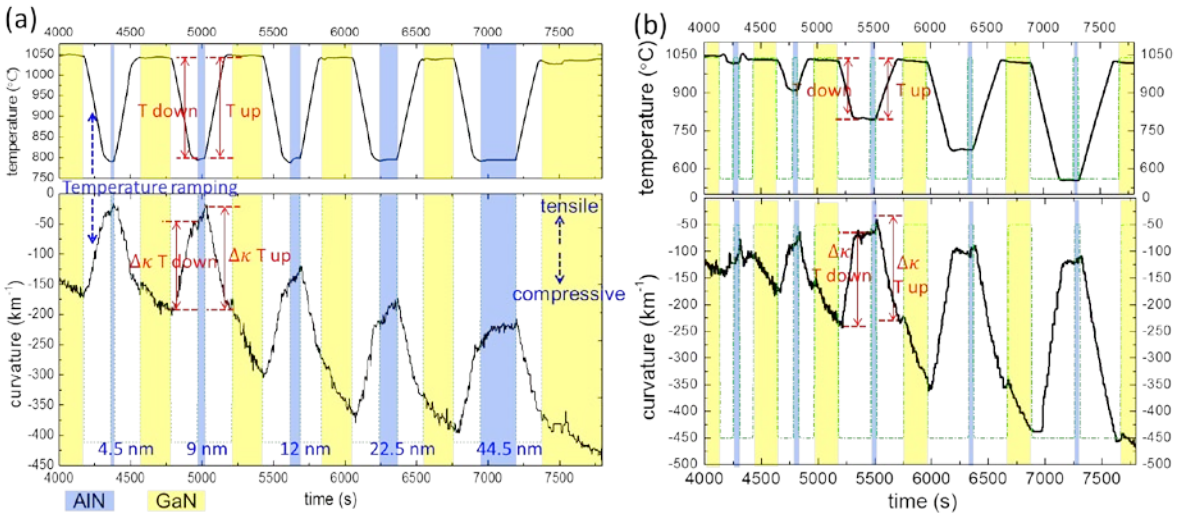


**Fig. 4.22** Temperature ramping and curvature transition during the growth of AlN interlayers and overlying GaN for (a) thickness test and (b) growth temperature test of AlN interlayers.

Temperature ramping and curvature transition in samples for thickness and growth temperature investigation of AlN ILs were plotted in Fig. 4.22a and b respectively. The absolute curvature increment $|\Delta\kappa|$ during temperature ramping down and up before and after the growth of AlN interlayers were extracted and plotted in Fig. 4.23a and b from the two samples in Fig. 4.22 respectively. The predicted theoretical $|\Delta\kappa|$ were calculated using the ideal thermal strain model for perfect multilayer structure, Eqs. (4.18) and (4.26), supposing that the as-grown overlying layer doesn't affect the underlying layer, by summing the

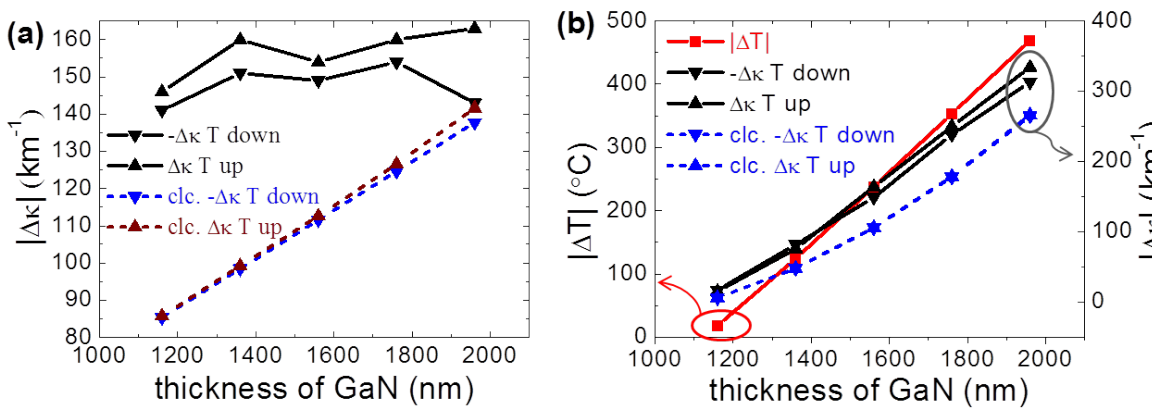


**Fig. 4.23** Measured and calculated curvature increment (absolute value) during temperature ramping down and up before and after the growth of AlN interlayers in samples for (a) thickness test and (b) growth temperature test of AlN interlayers. They were plotted as the function of GaN thickness. Temperature variation $|\Delta T|$ was also recorded because the growth temperature of AlN ILs were varied, to check the $|\Delta T|$ dependence of $|\Delta\kappa|$.

curvature contribution from every individual layer including GaN layers, AlN buffer layer and interlayers. Since the thickness of AlN layers was only about 1/20 of that of the total thickness of GaN layers, over 90% of thermal $|\Delta\kappa|$ came from GaN.

In Fig. 4.23a of the thickness test sample, it is interesting that $|\Delta\kappa|$ fluctuated in the range from 140 $km^{-1}$ to 160 $km^{-1}$, which showed little dependence on GaN total thickness. The temperature variation $|\Delta T|$ between the growth temperature of GaN and AlN interlayers was constant, as shown in Fig. 4.22a. However, theoretically, according to Stoney equation Eq. (4-7), even for the curvature variation $|\Delta\kappa|$ caused by thermal stress, it should be strongly affected by GaN thickness proportionally, as shown by the dashed lines in Fig. 4.23a. The difference between experimental and calculated values is hard to be interpreted properly.

On the other hand, in the sample of growth temperature test of AlN interlayers, both experimental and theoretical result of $|\Delta\kappa|$ showed strong dependence on temperature variation $|\Delta T|$, as shown in Fig. 4.23b. The practical experimental values were still larger than calculated values. Consequently, from the comparison between Fig. 4.23a and b, it can be concluded that $|\Delta\kappa|$ caused by thermal strain is much more strongly dependent on temperature variation than on film thickness, if the thickness variation is relatively small.

## 4.5 Plastic deformation of Si substrate

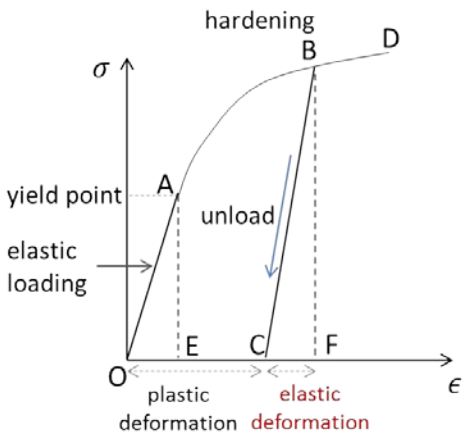


**Fig. 4.24** Process of elastic and plastic deformation.

Plastic deformation of Si substrate is another problem that may bring trouble to the growth of nitrides on it. As Hooke's law describes, solid material extends or expands or contracts if it is suffered from external or internal forces. If the force is small, the material undergoes elastic deformation and it can return to its original state as the load is removed. This is the elastic deformation stage OA shown in Fig. 4.24. If the loading force is too large beyond the yield point, the plastic deformation starts from point A. After reaching point B, the load starts decreasing and the unload stage is BC. As represented in Fig. 4.24, even the load is completed removed to zero, but the deformation (strain) of the material cannot go back to zero. Only the reversible elastic deformation component can be released (|OE|=|CF|) while the plastic deformation (|OC|) remains permanently. Especially with metals, significant

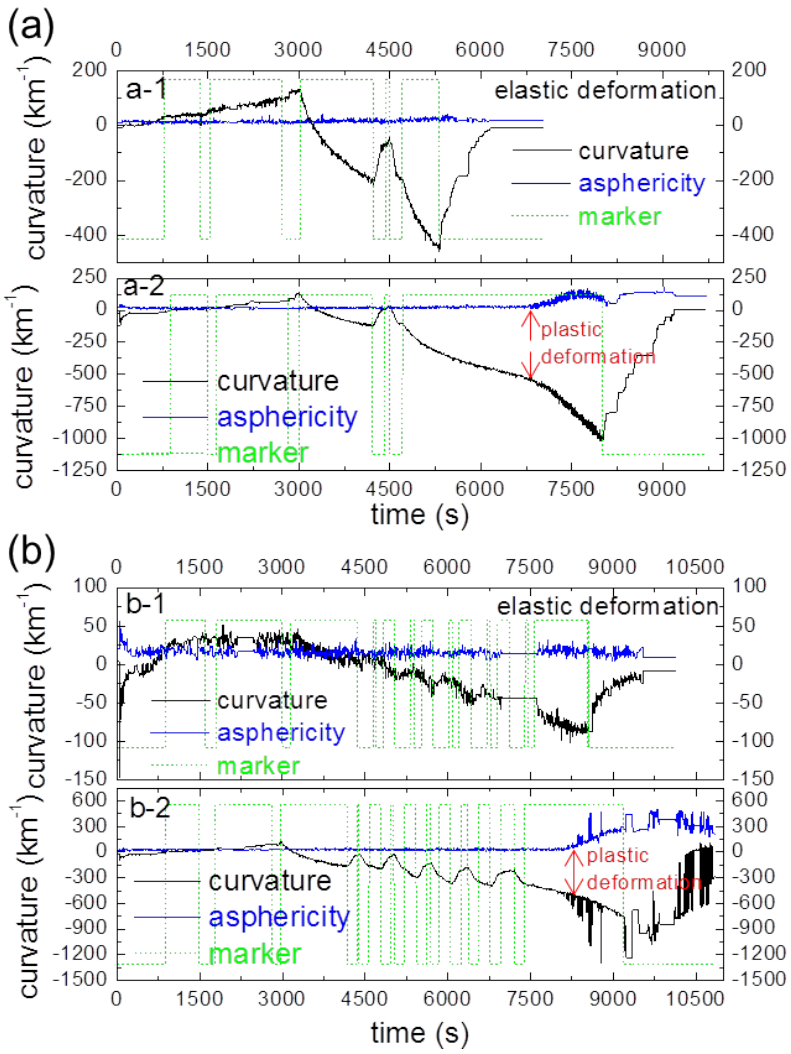


**Fig. 4.25** Examples of plastic deformation of GaN on Si, with single-layer AlN interlayer (a) and 5 layers of AlN interlayers.

permanent plastic deformation can occur easily when the stress reaches some critical value, called the yield stress.

The mechanism of plastic deformation is complicated. It can be produced by the movement of dislocations or slips. It mostly readily occurs on low index plane with largest atomic density, such as {110} and {112} in bulk centered cubic crystal in <111> direction, {111} plane in face centered cubic crystal in <110> direction and (1000) basal plane in hexagonal crystal in <1120> direction. Plastic deformation is also a strain hardening process, in which dislocation density increases dramatically for example from $10^4$ cm$^{-2}$ in annealed condition to $10^{10}$ cm$^{-2}$ in cold-worked condition [27]. In the later unload process the dislocation interaction with each other or with barriers impedes their motion in crystal lattice, which accounts for the permanent remaining deformation or strain in the material. In most cases, plastic deformation is unfavorable since it deteriorates the material performance and cause material or device failure.

It also happens in semiconductor crystals, like during the growth of GaN on Si, in Si substrate, as shown in the curvature curves in Fig. 4.25. There are two evidences to show the

plastic deformation in sample a-2 and b-2. The first direct evidence is the rise of wafer asphericity, which is an indication of asymmetric wafer bending and can be caused by plastic deformation. The other evidence is the final curvature at room temperature. Compared with the properly stress controlled sample a-1 and b-1, the samples (a-2 and b-2) with plastic deformation have thicker GaN and applied the same numbers of AlN interlayer. So they should be ending with large curvature to the tensile side ($\kappa > 0$). This is due to the presence of plastic deformation in Si substrate, which keeps the wafer deforms elastically to have concave bending. Plastic deformation should also be avoided in the system of GaN-on-Si. It leads to very high density of dislocations in Si substrate and makes it brittle and more difficult to be fabricated. Because the plastic deformation of the substrate is not released, in fact this may cause higher stress and more cracks in the film.

The yield stress $\sigma_Y$ in Si wafer is depending on temperature. As marked both in sample a-2 and b-2, the onset curvature of plastic deformation was around -600 km$^{-1}$. Supposing the average stress in Si substrate is $\sigma_s$, according to the Stoney equation of Eq. (4-4), $\sigma_s$ around the onset of plastic deformation can be calculated as $\sigma_{s-c}$

$$\sigma_{s-c} = \frac{f}{h_s} = \frac{\kappa M_s h_s}{6} = 6.27 \text{ Mpa} \tag{4-41}$$

with $h_s$ being 275 um and $M_s$ being 216 GPa. Theoretically, for a Si wafer with diameter of 300 mm and thickness of 750 um, the yield stress $\sigma_Y$ can be predicted by [28]

$$\sigma_Y = 4.27 \times 10^{-3} \exp(0.7eV/k_B T) \text{ Mpa} \tag{4-42}$$

in which $k_B = 8.6173 \times 10^{-5}\, eV/K$ . Using this calculation, the $\sigma_Y$ at GaN growth temperature around 1040 ℃ is about 2.08 MPa. The calculated value from experimental result and theoretical predication were on the same level, although the former is 3 times of the later.

From the experiments for the growth of GaN on Si, the $\sigma_Y$ is too small to grow thick GaN, plastic deformation is very readily to occur in Si wafer. Si should be hardened to elevate its $\sigma_Y$ significantly. One of the solutions is doping of special impurities into Si during growing its ingot. This can be achieved by applying Czochralski process to grow crystal silicon ingot. Impurities which can improve the stiffness of Si such as oxygen can be doped during the process.

## 4.6 Arbitrary bow design and curvature simulation

After analyzing every layer from the bottom AlN buffer to the top GaN layer including AlN interlayers, including the curvature transition caused by temperature ramping, it is possible to know about the strain and stress in each layer, depending on the growth condition of them, especially of the AlN layers. Theoretically, it is possible to recover the curvature curve from the fitted strain of every layer. After knowing the mechanical properties of every layer, it is possible to predict the final curvature (bow) for the samples with any structure. As the experimental results and theoretical analysis had shown that, due to the existence of microstructures and a great amount of defects, the quality of AlN and GaN is far from the

perfect single crystal. This results in that the strain in the layers cannot be predicted theoretically from the ideal misfit strain. Conversely, the route should be that extracting the strain and stress from the experimental results firstly. After knowing the strain of each layer and thermal stress of multilayers, then the final curvature (bow) can be predicted. Bow is an engineering definition to evaluate the bending of a wafer, which is defined to be the derivation of the center point of the median surface of a free, unclamped wafer from a median surface reference plane [29]. The relationship between wafer bow $\delta$ and curvature $\kappa$ had been given by Eq. (4-30). Since bow is proportional with curvature, for a Si wafer with certain size, $\delta \to 0$ can be achieved by pursing $\kappa \to 0$.

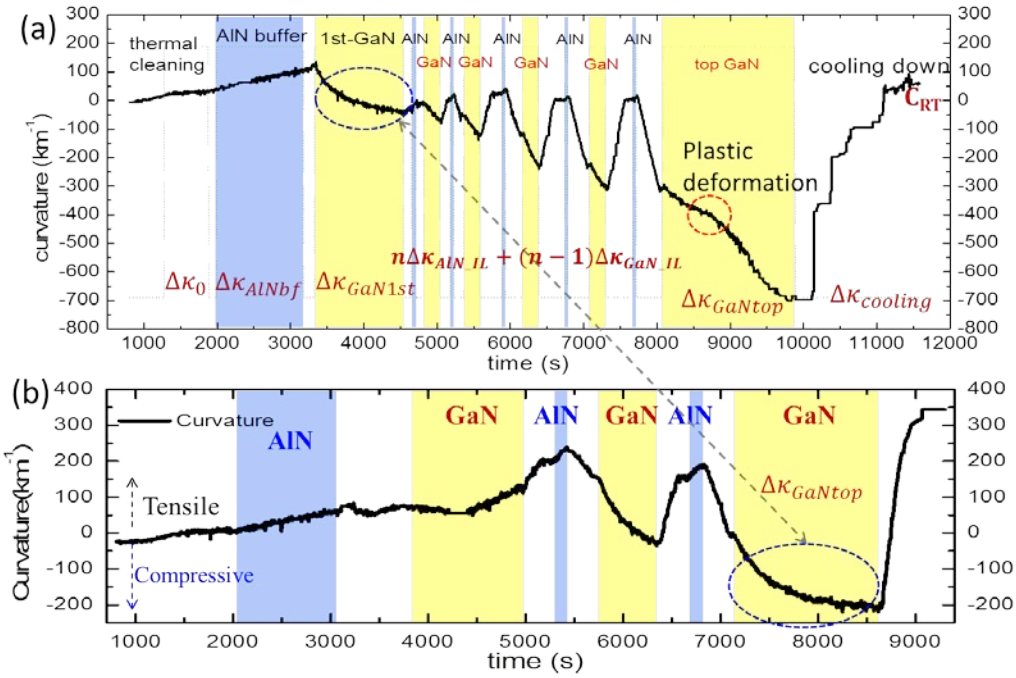


**Fig. 4.26** Curvature origination during every stage of the growth (a) with plastic deformation and (b) without plastic deformation.

As an example, the curvature origination in every stage during a growth was marked in Fig. 4.26a. It should be noted that plastic deformation occurred in sample a. If there is no plastic deformation, the curvature transition pattern in the top GaN should be similar to that of the 1st GaN layer, like the top GaN shown in Fig. 4.26b. Then the strain and curvature behavior of the top GaN can be fitted and predicted. The final curvature at room temperature $C_{RT}$ is the sum of the curvature originated at every stage during the growth and cooling down. Tensile curvature $\Delta\kappa_t$ comes from the bending of Si wafer caused by the temperature difference distributed inside the wafer during heating, AlN layers and thermal stress during cooling, given by

$$\Delta\kappa_t = \Delta\kappa_{AlN\_bf} + n\Delta\kappa_{AlN\_IL} + \Delta\kappa_{cooling} \tag{4-43}$$

with $\Delta\kappa_{AlN\_bf}$ and $\Delta\kappa_{AlN\_IL}$ being the curvature occurred in AlN buffer layer and interlayers, $n$ being the number of AlN interlayer, and $\Delta\kappa_{cooling}$ being the curvature occurred during cooling down.

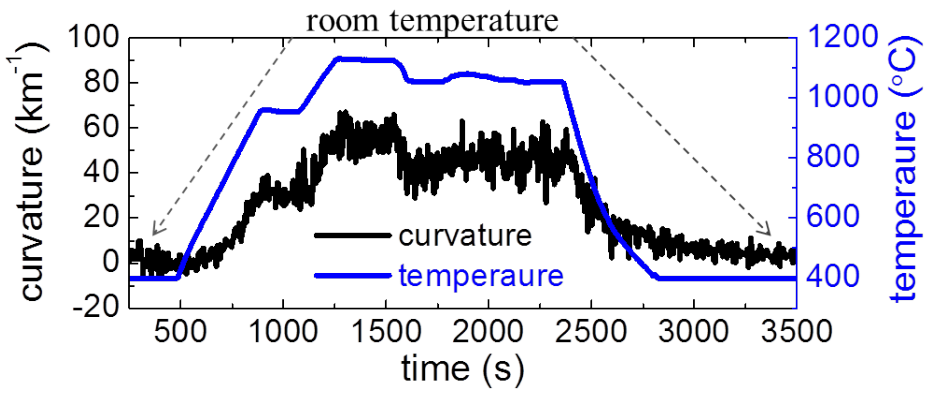


**Fig. 4.27** Thermal curvature of a bare 2-inch Si wafer caused by temperature difference between its bottom and upper surface.

In order to improve the accuracy of curvature during growth, wafer curvature caused by the temperature difference between wafer surface bottom should be counted, such as $\Delta\kappa_0$. Positive curvature or concave bending occurs if the thermal field through the wafer is not uniform. In most MOVPE systems, the substrate is heated from the bottom side and leads to temperature difference in the perpendicular direction through the substrate and the temperature at the bottom is higher than that at the top growth surface. Supposing that the temperature difference between the bottom and top of the substrate is $\Delta T$, curvature $\kappa_0$ caused by the presence of $\Delta T$ is expressed as [21]

$$\kappa_0 = \frac{\alpha_s \cdot \Delta T}{h_s} \tag{4-44}$$

with $\alpha_s$ being the thermal expansion coefficient of the substrate, $h_s$ being the substrate thickness. Generally, during the MOVPE of GaN, there is temperature difference of 80 ℃ between the set point and true temperature, depending on specific conditions. However, it is hard to tell the true $\Delta T$ during growth. $\kappa_0$ of a bare 2-inch 275-um-thick Si wafer during heating was measured in Fig. 4.27. Under the growth conditions of GaN (true temperature of ~ 1040 ℃) $\kappa_0$ was as high as 45 km$^{-1}$, which is not ignorable. After thermal cycling, when the temperature cooled to room temperature, the wafer curvature also went back to its original value around 0. So it can be not considered for the prediction of final curvature after growth at room temperature, $\kappa_{RT}$.

The compressive curvature $\Delta\kappa_c$ comes from all GaN layers as

$$\Delta\kappa_c = \Delta\kappa_{GaN\_1st} + (n-1)\Delta\kappa_{GaN\_IL} + \Delta\kappa_{GaN\_top} \tag{4-45}$$

with $\Delta\kappa_{GaN\_1st}$ being the curvature during the growth of the first layer of GaN, $\Delta\kappa_{GaN\_IL}$ being the curvature occurred in GaN in between the AlN interlayers and $\Delta\kappa_{GaN\_top}$ being the curvature during the growth of the top GaN layer. Then the final curvature $\kappa_{RT}$ is

$$\kappa_{RT} = \Delta\kappa_t + \Delta\kappa_c \ . \tag{4-46}$$

Tensile curvature $\Delta\kappa_t$ is plus and compressive curvature $\Delta\kappa_c$ is minus. One point here should be noticed is that the curvature increments during temperature ramping for the growth of AlN interlayers was not counted here, because the curvature increase during temperature

ramping down $\Delta\kappa_{T-down}$ before the growth of AlN interlayer and $\Delta\kappa_{T-up}$ during temperature ramping up after the growth of AlN interlayer are almost equal and the curvature value can go back to its original value at the end of the growth of the previous GaN layer.

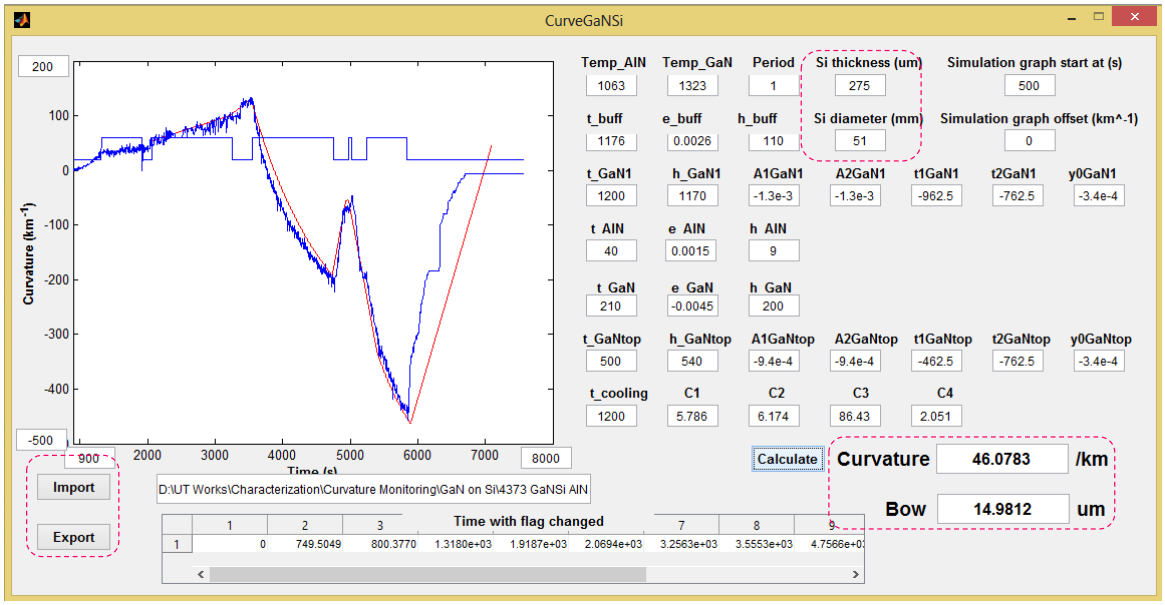


**Fig. 4.28** The interface of the program to design arbitrary bow and simulate curvature curves.

The final curvature at room temperature can be the function of the strain, thickness of individual AlN and GaN layers, number of AlN interlayers and thermal strain during cooling down. Based on this function, a program (appendix A) to design GaN-on-Si wafer with any bow and to simulate the growth curvature curves has been made. There are three features of this program. In the 1st and top GaN, the strain distribution has the form of exponent function due to the exponent relationship between strain, dislocation density and thickness.

(1) As long as the mechanical properties of every individual layer and thermal strain of multilayer systems were known, by setting those values in the interface, final curvature and wafer bow can be predicted and designed.
(2) The raw in-situ curvature data can be imported and simulated by fitting the strain distribution in every individual layer. Through curvature fitting, the strain distribution through the multi-layer system is accessed.
(3) Suitable for Si wafers with all sizes and thickness.

## 4.7 Conclusion

Growth and thermal stress and strain of GaN and AlN in some samples with typical growth conditions has been analyzed theoretically, for example, the samples for AlN buffer layer and interlayer growth condition investigation. The problem of plastic deformation of Si substrate has also been studied. Based on the extracted stress and strain result of GaN and AlN layer grown under individual conditions, an arbitrary wafer bow design model has been built.

Stoney equation of curvature calculation is the basic tool to derive the stress and strain from the measured curvature. It was firstly introduced in section 1. In the second section, the

stress generation mechanisms in heterostructures has been reviewed, including intrinsic and extrinsic stresses, which can be also named as growth and thermal stress respectively, for crystalline and polycrystalline materials. It is complicated. The dominant stress origins in the system of GaN growth on Si can be considered to be lattice constant mismatch stress and thermal expansion stress, for simplicity. The calculation method for the thermal stress of multilayer structure has been deduced. Based on the analysis above, the growth stress and thermal stress had been only considered during layer growth and temperature ramping respectively, supposing that the microstructure of nitride layers didn't change during thermal cycles. The total curvature of the substrate can be decomposed into the curvature contribution from every individual layer. Since the thermal expansion coefficient is temperature dependent, the expressions of temperature dependent thermal expansion coefficient had been derived based on the lattice constant data in the references.

In section 3, stress and strain of samples for AlN buffer layer study has been analyzed. Due to the large lattice constant difference between AlN and Si, the ideal misfit strain can be as large as 23%. While in fact AlN buffer layer is highly relaxed. The practical strain was on the level from 0.25% to 0.50%. The relaxation can be as high as 98.8%. As the growth conditions were improved (higher temperature and optimal V/III ratio), both the ideal and practical strains were decreasing. Strain and stress distribution as a function of GaN thickness at growth and room temperature has been obtained. GaN on AlN buffer undergo a strain transition process from compressive to tensile, in a critical thickness, depending on the quality of AlN buffer layer. If the buffer layer quality was very high, then the strain transition of GaN to tensile side would be very slow and it could be strained compressively in a very large thickness (> 1.75 um).

Two series of multi-condition AlN interlayer samples have been studied, for AlN interlayer thickness and growth temperature tests respectively. Strain in GaN layers ranged from 0.15% to 0.45%, which was on the same level of that of AlN buffer layers, but with lower relaxation of a range from 82% to 90%. AlN interlayers were much more strained than AlN buffer layer and GaN layers, with strain on the level of 1.5%. This was due to that they were grown on better quality GaN layers with small thickness. The quality of lower interface of AlN interlayer is better than that of the upper interface. That's why GaN was much more relaxed than AlN interlayers. This is an important discovery which reminds us that the quality of upper interface of AlN interlayer should be improved to induce more compressive stress in GaN layers.

Next, the problem of Si substrate plastic deformation was discussed. It could easily occur in 2-inch Si wafer when the curvature reached -600 $km^{-1}$. The yield stress of Si wafer was estimated to be several MPa. In the end, the model to design arbitrary wafer bow for the growth of GaN on Si has been proposed. This is the final target of this chapter.

## References

[1] P.A. Laplante and etc. *Wafer (electronics)*. 2014; Available from: http://en.wikipedia.org/wiki/Silicon_wafer.

[2] L.B. Freund and S. Suresh, *Thin film materials*. 2003: Cambridge University Press.
[3] S. Figge, H. Kröncke, D. Hommel, and B.M. Epelbaum,Temperature dependence of the thermal expansion of AlN, Applied Physics Letters ***94***, 101915(2009).
[4] Y. Okada and Y. Tokumaru,Precise determination of lattice parameter and thermal expansion coefficient of silicon between 300 and 1500 K, J. Appl. Phys. ***56***, 314(1984).
[5] C. Roder, S. Einfeldt, S. Figge, and D. Hommel,Temperature dependence of the thermal expansion of GaN, Physical Review B ***72***, 085218(2005).
[6] A.F. Wright,Elastic properties of zinc-blende and wurtzite AlN GaN and InN, J. Appl. Phys. ***82***, 2833(1997).
[7] G.G. Stoney,The Tension of Metallic Films Deposited by Electrolysis, Proceedings of the Royal Society of London. Series A ***82***, 172(1909).
[8] R. Koch,The intrinsic stress of polycrystalline and epitaxial thin metal films, Journal of Physics: Condensed Matter ***6***, 9519(1994).
[9] R. Koch, D. Winau, and K.H. Rieder,Intrinsic stress of epitaxial thin films, Physica Scripta ***T49B***, 539(1993).
[10] J.P. Douglas. *Misfit Dislocation*. 2014; Available from: http://userweb.eng.gla.ac.uk/douglas.paul/SiGe/misfit.html.
[11] J.W. Matthews and A.E. Blakeslee,Defects in epitaxial multilayers. I. Misfit dislocations, Journal of Crystal Growth ***27***, 118(1974).
[12] C. Hollauer, *Modeling of Thermal Oxidation and Stress Effects*. 2009: Lighting Source Incorporated.
[13] C.H. Hsueh,Thermal stress in elastic multilayer systems, Thin Solid Films ***418***, 182(2002).
[14] J.F. Wang, D.Z. Yao, J. Chen, J.J. Zhu, D.G. Zhao, D.S. Jiang, H. Yang, and J.W. Liang,Strain evolution in GaN layers grown on high-temperature AlN interlayers, Appl. Phys. Lett. ***89***, 152105(2006).
[15] J.A. Floro, E. Chason, R.C. Cammarata, and D.J. Srolovitz,Physical origins of intrinsic stresses in Volmer-Weber thin films, MRS Bulletin ***January***, (2002).
[16] S. Raghavan and J. Redwing,Growth stresses and cracking in GaN films on (111) Si grown by metalorganic chemical vapor deposition. II. Graded AlGaN buffer layers, Journal of Applied Physics ***98***, 023515(2005).
[17] S. Raghavan and J.M. Redwing,Intrinsic stresses in AlN layers grown by metal organic chemical vapor deposition on (0001) sapphire and (111) Si substrates, Journal of Applied Physics ***96***, 2995(2004).
[18] S. Raghavan, X. Weng, E. Dickey, and J.M. Redwing,Correlation of growth stress and structural evolution during metalorganic chemical vapor deposition of GaN on (111) Si, Applied Physics Letters ***88***, 041904(2006).
[19] L.B. Freund and S. Suresh, *Thin Film Materials: Stress, Defect Formation and Surface Evolution*. 2008: Cambridge University Press. 506.
[20] S. Hearne, E. Chason, J. Han, J.A. Floro, J. Figiel, J. Hunter, H. Amano, and I.S.T. Tsong,Stress evolution during metalorganic chemical vapor deposition of GaN, Applied Physics Letters ***74***, 356(1999).
[21] 泉. 聡志, *薄膜の応力計算*. 2014.
[22] S. Figge, H. Kröncke, D. Hommel, and B.M. Epelbaum,Temperature dependence of the thermal expansion of AlN, Appl. Phys. Lett. ***94***, 101915(2009).
[23] B.B. He, *Two-Dimensional X-Ray Diffraction*. 2009, Hoboken: John Wiley & Sons. 264.
[24] M.A. Moram and M.E. Vickers,X-ray diffraction of III-nitrides, Reports on Progress in Physics ***72***, 036502(2009).
[25] K. Saarinen, *III-V Nitride Semiconductors: Electrical, Structral and Defects Properties (ed. Manasreh M. O.)*. 2000, Amsterdam: Gordon and Breach.

[26] G.P. Dimitrakopulos, T. Kehagias, P. Komninou, G. Nouet, and T. Karakostas,Disconnections at translation domain doundaries in epitaxial GaN, Journal of Physics: Condensed Matter ***14***, 12709(2002).
[27] T. Udomphol, *Plastic deformation of single crystals*. 2007, Suranaree University of Technology.
[28] 泉. 聡志, *シリコンウェーハの自重応力と熱応力*. 2014.
[29] ZebraOptical. *Definitions*. 2014; Available from: http://zebraoptical.com/Definitions.html.

# 5 Quality of GaN on conventional AlN

High quality of GaN is another goal to pursue while the bowing (curvature, stress and strain) is well controlled. In fact, in crystal growth, especially the epitaxy of thin films, quality and stress (or strain) are not independent and cannot be separated. On the contrary, they are very closely correlated and interact with each other. In this chapter, the importance of GaN quality, the quality of GaN on sapphire and silicon was reviewed first. Then in the following section 2 and 3, the effects of AlN buffer layer and interlayers on the quality of GaN would be investigated. In the final section, effort to improve GaN quality by applying 3D growth mode was studied. The relationship between GaN quality and strain behavior would be addressed while discussing the quality of GaN. Conventional AlN was the same as that in chapter 3, both for the buffer layer and interlayer.

## 5.1 Introduction

By reviewing the history of many fields in science and technology, it can noticed that in general, it was the new discovery or vital progress in material brought the invention or improvement of new devices, like the development of diode and computer, as well as the realization of blue light emission diodes (LEDs) and lasers, which the largest market of III-nitride currently. In the end of 1980s, one of the most difficult problems to fabricate GaN based LEDs was to grow sufficient high-quality crystalline layers for GaN and InGaN [1]. In 1986, Akasaki firstly demonstrated the feasibility of growing relatively high quality GaN layers by MOVPE [2]. After realizing p-type conducting GaN, the first GaN based blue LED had been demonstrated in 1989.

In semiconductor devices, higher crystal quality leads to better device performance as long as sufficient conductivity is satisfied. Defects in GaN such as screw and edge dislocations can trap carriers and act as centers of nonradiative carrier recombination and lead to degradation of LEDs, for example, increase threshold voltage and injection current and decrease the device efficiency [3-5]. In another major GaN based device, high electron mobility transistors (HEMT), as scattering centers, dislocations can cause reduced carrier mobility in the two dimensional electron gas [6-9]. Improved GaN quality was also favorable to enhance the breakdown voltage in HEMTs [10]. Compared to LEDs and HEMTs, nitrides-based solar cells suffer negative effects of defects much more severely. InGaN is very attractive for producing high efficiency solar cells for its band gap which can cover almost the whole solar spectrum from 0.7 eV to 3.4 eV. However, even using GaN with relatively low dislocation density of magnitude of $10^8$ $cm^{-2}$ which is normal to LEDs, the short circuit current of InGaN-based solar cell can only be around 1-3 $mA/cm^2$ and the efficiency was only in the range of 0.7-3% [11, 12]. Along with the difficulty of indium incorporation to obtain proper band gap, very high-density dislocations also act as recombination centers and carrier traps

and reduce the lifetime of photon generated carriers drastically. In a word, very high quality GaN is desirable for the application of any devices based on nitride and it should be improved as high as possible.

Since the beginning of 1990s when III-nitrides were available by MOVPE, in the last two decades, people have put great efforts to improve the quality of GaN. GaN was grown on AlN buffer layer, low temperature GaN buffer layer, in multi-step growth methods, selective area growth, epitaxial lateral overgrowth, with masking layers (AlN or $SiN_x$) and so on. Detailed introduction of these strategies is beyond the theme of this thesis. The interest here is to introduce the quality level of GaN at present. In most cases of practical application, GaN is grown on sapphire. Generally, the FWHM of XRD rocking curves for GaN on sapphire for the production of LEDs is in the range of 200-250 arcsec, 300-350 arcsec and 450-550 arcsec for the plane of (0002), (10-12) and (10-10) respectively. For the growth of GaN on Si, which is the topic of this thesis, in previous studies by other researchers, the best quality evaluated by FWHM of XRD rocking curves can be around the upper limit of that grown on sapphire as listed above or even slightly higher, but required very large thickness which ranged from 8 um to 10+ um. We hope that better and better crystal quality of GaN can be achieved with thickness as small as possible.

## 5.2 Effects of AlN buffer layer on the quality of GaN

For the MOVPE of GaN on sapphire, prior to applying low temperature GaN buffer layer, GaN template was originally grown on AlN buffer layer [2]. Amorphous AlN was grown at low temperature of 600 ℃ and 3D crystalline columns were formed after annealing at high temperature, then GaN was grown upon those columns. People have investigated AlN buffer layer for GaN growth on sapphire very intensively but yet not for it on silicon substrate. Typical strategies include low temperature and high temperature bi-layer AlN buffer layer [13-16], pulsed source supply growth [17], sputtered AlN buffer layer [18], multi-layer low temperature AlN nucleation [19] and so on. By using various technologies, very high quality AlN on sapphire can be acquired with etched pit density of $3\times10^6$ $cm^{-2}$ and the quality of GaN on it is also better than that on low temperature GaN buffer layer. However, this is not the case for GaN and AlN on silicon. Some work have also been done to study the effects of AlN buffer layer on the quality of GaN, but not systematic and without in-situ curvature observation [20-23]. Although some work has been devoted to the investigation of structural properties of AlN on Si [24-28], very few study about the optimization of AlN quality on Si. Due to the crystal structure and chemical polarity difference between silicon and nitrides, the detailed nitride growth mechanism between that on silicon and on sapphire might differs significantly. The strategies and conditions which are successful for AlN growth on sapphire are not suitable for that on silicon any more. For example, as mentioned in chapter 3, GaN cannot grow properly on AlN buffer layer grown at temperature lower than 900 ℃. The growth of AlN buffer layer on Si for GaN must starts with high temperature, otherwise GaN cannot grow epitaxially, even though the starting low-temperature AlN buffer layer is followed by high-temperature ones. In addition, sputtered AlN buffer, which works better

than CVD-grown AlN buffer on sapphire, has not yielded good result on silicon yet [18]. Therefore, to grow high-quality GaN, AlN buffer layer needs to be optimized.

Prior to introducing experimental results, the major problems to grow high quality AlN by MOVPE are reviewed here briefly. The first problem is parasitic reactions between group-III and group-V precursors. This could lower the growth rate, deteriorate the surface morphology and cause particles on the surface significantly [29-34]. Secondly, due to the high Al-N bond energy of 2.88 eV, the migration of Al atoms needs very high activation energy and leads to low mobility of precursor atoms, especially that of Al ad-atoms. This resulted in large surface roughness formed by V-pits or grain boundaries [35]. The third is impurity incorporation of atoms like C, O and so on. This problem is not as complicated and troublesome as the former two and demands very low growth pressure at 25 or 50 mbar [16]. From the experimental studies, parasitic reactions in the gas-phase can be enhanced at high pressure, low total flow rate, and high group-III and/or high group-V precursor flows; then the surface roughness is increased with enhanced parasitic reactions [29-33, 36]. Low total flow rate caused long residence time of precursor atoms on the surface and leaded to larger roughness [29, 33]. After suppressing the parasitic reactions, in order to improve crystal quality and surface morphology, next efforts should be made to increase the mobility or surface diffusion length $\lambda_s$ of ad-atoms. $\lambda_s$ can be greatly increased at higher growth temperature and lower growth rate. AlN surface became rougher at higher V/III or increased $NH_3$ flow rate [36-38]. It is assumed that large amount of $NH_3$ lower the $\lambda_s$ of Al atoms by some mechanism which was not clear [32]. Although parasitic reactions can be enhanced at high temperature, the favorable effects of increased $\lambda_s$ at high temperature overtook the detrimental effects from parasitic reactions. Additionally, it has been found that higher $H_2$ flow rate could also improve the crystal quality and surface morphology by suppressing the parasitic reactions [39]. To summarize, to achieve a single layer of high quality AlN with flat surface, without applying techniques like multilayer nucleation or 3D growth mode, it should be grown at high temperature, low pressure, low growth rate, proper V/III ratio and high hydrogen flow rate. These trends are the same regardless of what substrate it grows on, although the detailed growth mechanism and optimal condition might be different.

In this section, the effects of growth conditions of AlN buffer layer on the quality as well as the relationship between quality and curvature behavior would be described. In this study, it didn't aim to obtain the final optimized AlN buffer layer on silicon, but to investigate the basic effects of AlN buffer layer on GaN quality systematically, including the growth temperature, V/III ratio and thickness. A relatively good condition was proposed based on the study.

### 5.2.1 Effect of growth temperature of AlN buffer layer

The AlN buffer layer was grown at temperatures from 800 ℃ to 1250 ℃, while the thickness and V/III ratio of it were fixed to be 110 nm and 470 respectively. GaN was grown in 2D mode with constant conditions to test the effects of growth conditions of AlN buffer layer.

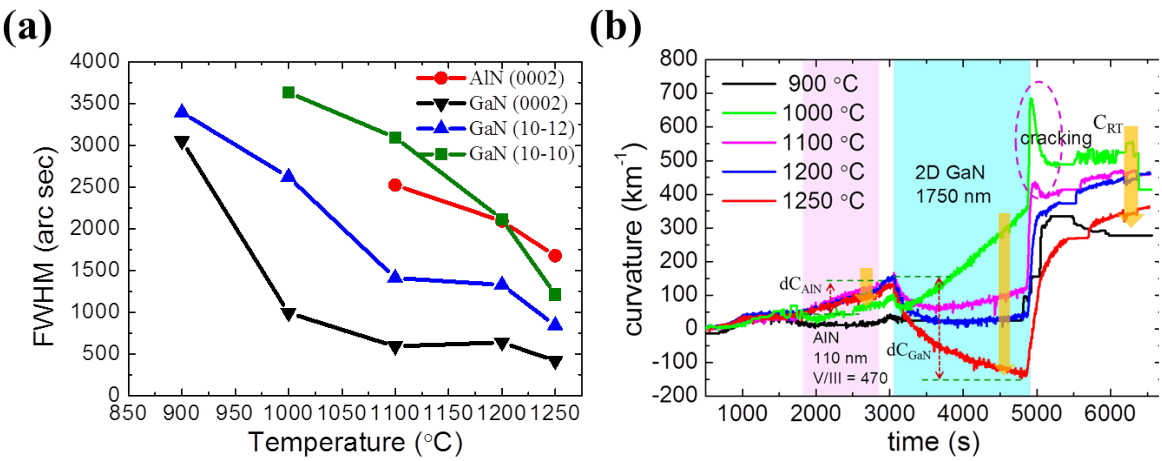


**Fig. 5.1** (a) Dependence of FWHM of XRD rocking curve of GaN and AlN buffer on the growth temperature of AlN buffer layer ($T_{AlN}$); (b) curvature transition dependence on $T_{AlN}$.

From Fig. 5.1a, it is very clear that the quality of GaN was strongly dependent on the growth temperature of AlN buffer layer. In Fig. 5.2 we can see that GaN cannot grow properly on AlN buffer grown at 800 ℃ and 900 ℃. As shown in Fig. 5.2c and d, on 800-℃ grown AlN buffer layer, instead of an epitaxial film, GaN grew on it as crystal grains with various orientations and size ranged from tens of nanometers to several micrometers. On 900-℃ grown AlN buffer, in Fig. 5.2a and b, the quality of GaN improved with uniform orientation to (0002) plane, but still not coalesced completely within the thickness of 1.75 um. FWHM of XRD rocking curve for GaN grown on 800-℃ AlN buffer cannot be measured, it is only available above 900 ℃. As $T_{AlN}$ was elevated from 900 ℃ to 1100 ℃, the quality of GaN was improved significantly. From the knowledge of XRD rocking curve measurement, peak width of rocking curve relates to the out-of-plane and in-plane

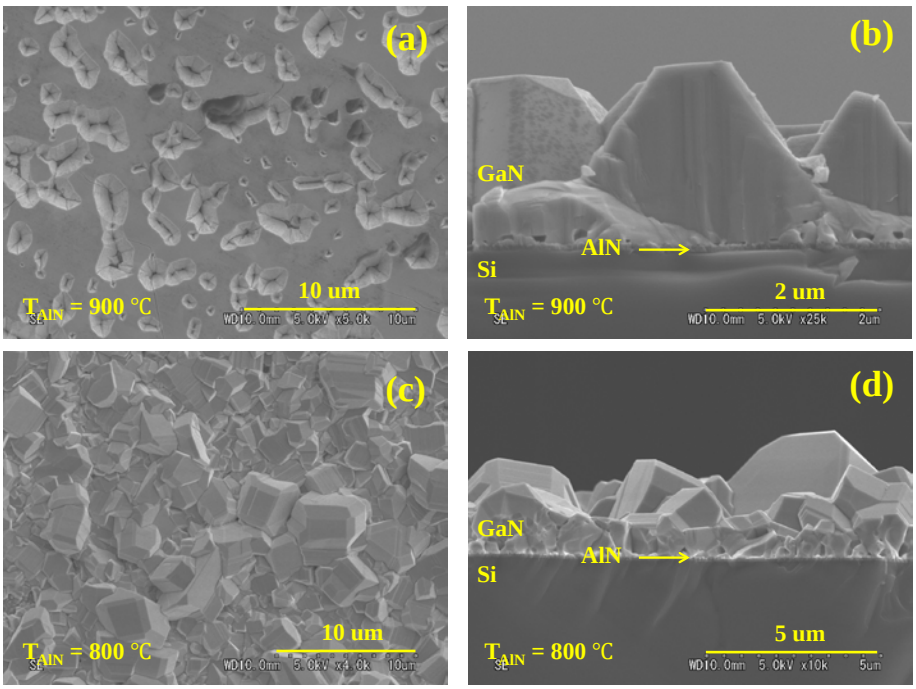


**Fig. 5.2** SEM images of the surface and cross section of GaN on AlN buffer layer grown at 800 ℃ and 900 ℃.

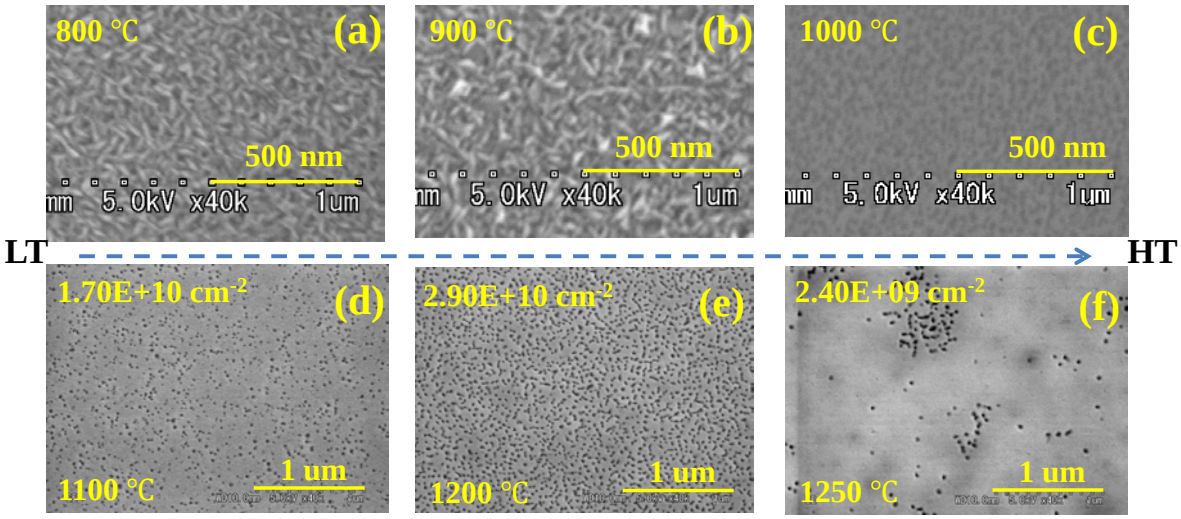


**Fig. 5.3** SEM images of AlN buffer layer surface: grown at temperatures from 800 ℃ to 1250 ℃.

misorientations of crystallites in the epitaxial layers which originates from screw and edge threading dislocations respectively. For c-axis orientated GaN film, FWHM of the plane of (0002) and (10-10) corresponds to the tilt of (0002) plane caused by screw dislocation and twist of (10-10) plane caused by edge dislocations [40]. The densities of screw and edge dislocations in GaN can be calculated from the following equations [41]:

$$\rho_{screw} = \frac{\alpha^2}{2\pi b_{screw}^2 \cdot \ln(2)}, \ \rho_{edge} = \frac{\beta^2}{2\pi b_{edge}^2 \cdot \ln(2)}. \tag{5-1}$$

$\rho$ is the dislocation density, $\alpha$ and $\beta$ correspond to tilt angle and twist distortion angle of the planes of (0002) and (10-10) respectively which are proportional to the values of FWHM, $b$ is the Burgers vector for screw and edge dislocations which are 5.185 Å and 3.189 Å respectively for GaN. Therefore, for GaN on AlN buffer layer grown at temperatures from 900 ℃ to 1100 ℃, both the density of screw and edge dislocations dropped rapidly. While as $T_{AlN}$ increased from 1100 ℃ to 1200 ℃, the density of screw dislocations didn't change much but the density of edge dislocations decreased significantly. As $T_{AlN}$ was elevated further from 1200 ℃ to 1250 ℃, even with only increase of 50 ℃, the quality of GaN on it was enhanced substantially, with great reduction of the density of both screw and edge dislocation.

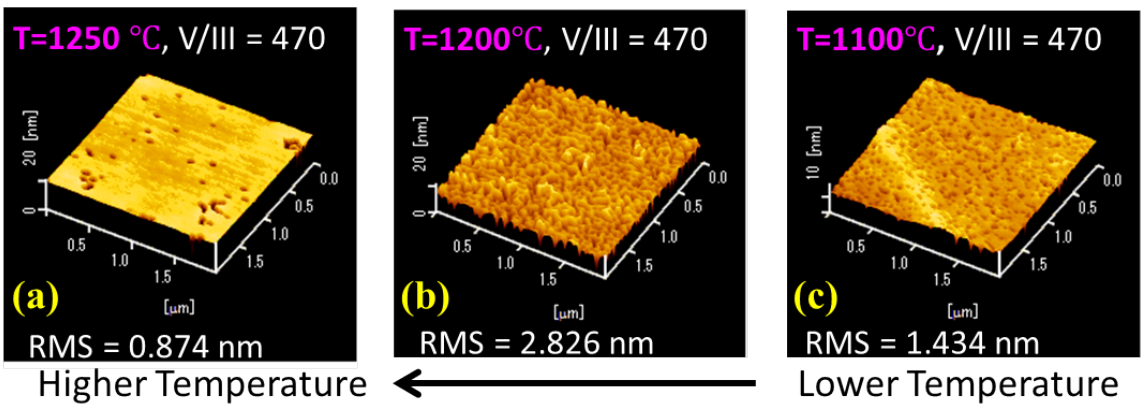


**Fig. 5.4** AFM of AlN buffer layer surface grown at 1100 ℃, 1200 ℃ and 1250 ℃.

To investigate the improvement of GaN quality, it is necessary to discuss the crystal quality enhancement of AlN buffer layer. Since no structural techniques like 3D growth mode or multi-layer buffer was applied, the improvement of GaN quality is brought simply by the quality enhancement of AlN buffer layer by the growth temperature elevation here. In Fig. 5.1a, as indicated by the FWHM of XRD rocking curve of plane (0002) ($\theta_{0002}$) of AlN buffer layer, as $T_{AlN}$ was raised from 1100 ℃ to 1250 ℃, the quality of AlN buffer also improved considerably. Because $\theta_{0002}$ of AlN buffer layer grown under 1100 ℃ cannot be measured, so the surface of them have also been characterized by SEM and AFM. Fig. 5.3 are the surface images of AlN buffer layer grown at temperature from 800 ℃ to 1250 ℃. In it we can clearly see the transition of growth mode and crystal quality improvement of AlN buffer. At 800 ℃, AlN grew on Si as polycrystalline grains with size of about 20×100 $nm^2$. As $T_{AlN}$ increased to 900 ℃, it was still poly-crystallites but with larger size. It might be that because these two AlN buffer layers consisted of crystallites with various orientations, so the GaN grown on them also was of grains with various facets and sizes, and could not coalesce in large thickness of 1.75 um, as shown in Fig. 5.2. There was a crystalline phase transition for the growth of AlN on Si when the growth temperature was elevated from 900 ℃ to 1000 ℃. At $T_{AlN}$ of 1000 ℃, AlN could be grown epitaxially on Si without any grains, while the pit density was very large around $10^{11}$ $cm^{-2}$. As $T_{AlN}$ increased to 1100 ℃, the crystal quality was enhanced with significant reduction of pit density to about $1.7\times10^{10}$ $cm^{-2}$ along with huge quality improvement of GaN on it. From the slope of curvature curves in Fig. 5.1b, it should be noticed that the tensile stress of AlN buffer layer grown at 1100 ℃ was the highest. This was brought by the crystal quality improvement of it. However, as $T_{AlN}$ was elevated higher to 1200 ℃, pit density was almost doubled. The roughness from AFM images in Fig. 5.4 was also doubled. But from the result of XRD rocking curve, the crystal quality of it was actually improved. This may explain why the screw dislocation density didn't change much but the edge dislocation density was reduced very much. From 1200 ℃ to 1250 ℃, with only an increase of 50 ℃, but the pit density was reduced to $2.4\times10^{9}$ $cm^{-2}$, which was one tenth of that at 1200 ℃. The surface morphology also became very smoother, especially the part without pits. Consequently, the quality of GaN on it was also improved substantially. It is not clear that why a small temperature increase of 50 ℃ caused so significant crystal quality improvement both for AlN buffer layer and GaN. It can be supposed that the temperature range of 1200 ℃ ~ 1250 ℃ is a critical temperature window to enhance the quality of AlN. Based on the observation above, it can be concluded that temperature is a decisive factor of the growth mode and quality of AlN. At low temperature, the surface mobility and diffusion length $\lambda_s$ of ad-atoms is very small, especially for Al adsorbed atoms; it is also easy to form clusters and move to the surface. These reasons cause easy atom accumulation on the surface and leads to 3D growth and poly-crystalline grains. At higher temperature above 1000 ℃, $\lambda_s$ can be enhanced and epitaxy with single orientation is available. So, for AlN on Si, roughly, the growth temperature can be divided into several stages. As $T_{AlN}$ increased from low and up to 900 ℃, it is amorphous firstly and then poly-crystalline with larger and larger grains. From 900 ℃ to 1000 ℃, there is a phase transition from poly-crystal to single crystal epitaxy. From 1000 ℃ to 1200 ℃, there is a steady crystal quality improving stage but it is not as sharp as at

higher temperature. Above 1200 ℃, there is a sharp quality enhancement, both for the crystal quality and surface morphology.

The relationship between the dislocation density of buffer layer (AlN) and epilayer (GaN) is evident that high-quality buffer layer leads to high-quality epilayer. A part of defects on the surface of the buffer layer can be the source of dislocations in the epilayer or propagate into the epilayer, such as threading dislocations including screw and edge dislocations. Some of them will be multiplied by mechanisms like Frank-Read source, spiral source and Hagen-Strunk multiplication [42]. Threading dislocations can propagate to the epilayer and they can be annihilated by bending or increasing the epilayer thickness. The dislocation density in the epilayer is proportional to that in the buffer layer. Consequently, for simple epitaxy of GaN on AlN/Si substrate without special techniques like 3D growth or masking, the quality of AlN buffer layer should be as high as possible.

Another point should be discussed is the correspondence of crystal quality and the curvature (stress-strain) behavior. This is a complementary discussion to the part of 3.2.1 in chapter 3. Higher quality of GaN corresponds to more compressively stressed GaN layers. Based on the strain relaxation mechanisms introduced in the part of 3.1.3 in chapter 3, GaN on AlN grown at higher $T_{AlN}$ should undergo less compressive stress due to the thermal expansion of AlN buffer and the reduction of $\Delta a_{GaN-AlN}$. But $\Delta a_{GaN-AlN}$ is only one of the factors for strain relaxation. Another major mechanism is the relaxation by the formation of dislocations. Higher misfit dislocation density causes more rapid relaxation and smaller strain. As indicated by the theoretical analysis in chapter 4, the large dislocation density at the interface of between GaN and AlN grown at 1000 ℃ and 1100 ℃ caused rapid strain relaxation in GaN. The stress in GaN is affected by the AlN buffer and Si substrate. It was directly tensilely strained by AlN buffer firstly. The amount of tensile strain in GaN was determined by the perfection of its lattice. The lattice of GaN with higher quality is more perfect than low-quality one. High-quality GaN goes through compressive strain in larger thickness. After it has completely relaxed, it would be free from the constraint of underlying AlN buffer and strained by Si substrate, and then tensile strain occurs. This is the transition from compressive stress to tensile stress for GaN on AlN buffer grown at 1000 ℃, 1100 ℃ and 1200 ℃. From low to high $T_{AlN}$, the transition became slower and slower and the critical thickness of this transition of strain from compression to tension also increased. GaN on 1250-℃ grown AlN buffer, it was compressively strained through the thickness of 1.75 um. So the enhancement of compressive strain brought by the improvement of GaN and AlN quality overtook the relaxation of it caused by the reduction of $\Delta a_{GaN-AlN}$.

### 5.2.2 Effect of V/III ratio of AlN buffer layer

V/III ratio is another important factor affecting the crystal quality and surface morphology significantly [43, 44]. To testify the effects of V/III ratio of AlN buffer layer on the performance of GaN on it, the buffer layer thickness was fixed to be 110 nm and the highest growth temperature of 1250 ℃ was applied. Due to the low limit of the mass flow controller of $NH_3$ is 100 sccm for our system, to achieve V/III ratio of 115 for the growth of AlN buffer

layer, the flow rate of TMAl was increased to 90 sccm. Due to large supply of TMAl, the growth rate under V/III ratio of 115 was 4 times higher than that under higher V/III ratio, as shown in Fig. 3.10 in chapter 3. From V/III ratio of 470, it was adjusted by changing the flow rate of $NH_3$ while it of TMAl was kept constant at 22 sccm. From 470 to 9156, the growth rate decreases slightly with the increase of V/III ratio.

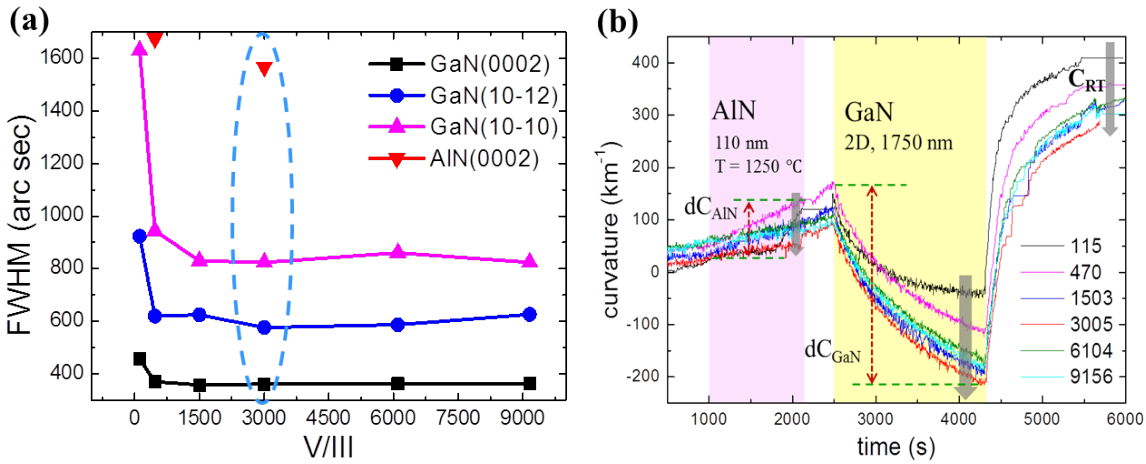


**Fig. 5.5** (a) FWHM of XRD rocking curve for GaN and AlN buffer; (b) Curvature transition of GaN growth on AlN buffer grown under V/III ratio from 115 to 9156.

In Fig. 5.5a, the quality of GaN can be discussed in two ranges of V/III ratio of AlN buffer which can be divided by the V/III ratio value of 1503. In the range below 1503, the quality of GaN gets better as the V/III ratio of AlN buffer increases, especially the quality of (10-10) plane. The twist distortion disorientation from (10-10) plane which caused by edge dislocations was reduced substantially, while the quality of (0002) plane was also improved but not as significant as that of the plane of (10-10). Above 1503, the variation of the quality of GaN on AlN buffer layer was very minimal and the best one emerged under V/III ratio value of 3005. This is very consistent with the plot of AlN growth rate as the function of V/III ratio. In Fig. 5.5a it also can be noticed that the quality of AlN buffer layer was also improved as its V/III increased from 470 to 3005, although the improvement was not as significant as that brought by the elevation of growth temperature. The quality improvement was also verified by AFM and SEM images in Fig. 5.6. Compared with AlN buffer grown under lower V/III ratio of 470, surface of it grown under higher V/III ratio of 3005 was much smoother. Although the pit density was on the same level, but the crystallinity was improved. This can be proved by the result of XRD rocking curve in Fig. 5.5a and SEM images in Fig. 5.6b. In SEM images, under V/III ratio of 470, the pits were of irregular shape; while under V/III ratio of 3005, the pits showed regular hexagonal shape with regular facets which could be observed in etched crystal nitrides and indicate the improvement of crystallinity of AlN. As reviewed in the beginning of this section, under relatively high flow rate $NH_3$ (very high V/III ratio) or high flow rate TMAl (very low V/III), there is a degradation of the quality and surface morphology of AlN as the parasitic reactions is enhanced or the surface diffusion length of Al ad-atoms is reduced. By comparing (a) and (b) in Fig. 5.5, similar to the result in part 5.2.1 of the effects of $T_{AlN}$, as the GaN quality improved, it was also more compressively stressed with larger curvature to the compressive side ($dC_{GaN}$) in the end of the growth of it.

More interestingly, the final tensile curvature which people care mostly was also completely consistent with the result of $dC_{GaN}$ and GaN quality. Higher GaN quality led to larger $dC_{GaN}$ and then lower tensile $C_{RT}$.

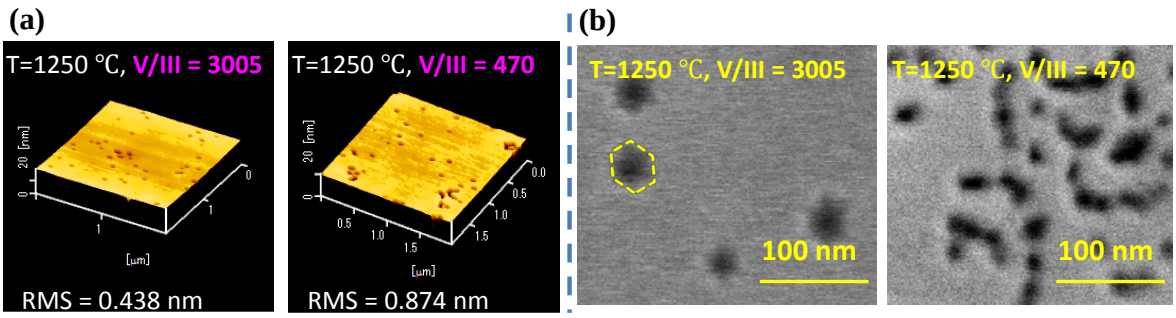


**Fig. 5.6** (a) AFM and (b) SEM images of the surfaces of AlN buffer layer grown under V/III ratio of 470 and 3005 respectively.

### 5.2.3 Effect of AlN buffer layer thickness

To investigate the effects of AlN buffer layer on the properties of GaN on it, AlN was grown at temperature of 1250 ℃ and under V/III ratio of 470. The thickness of it was increased from 55 nm to 220 nm.

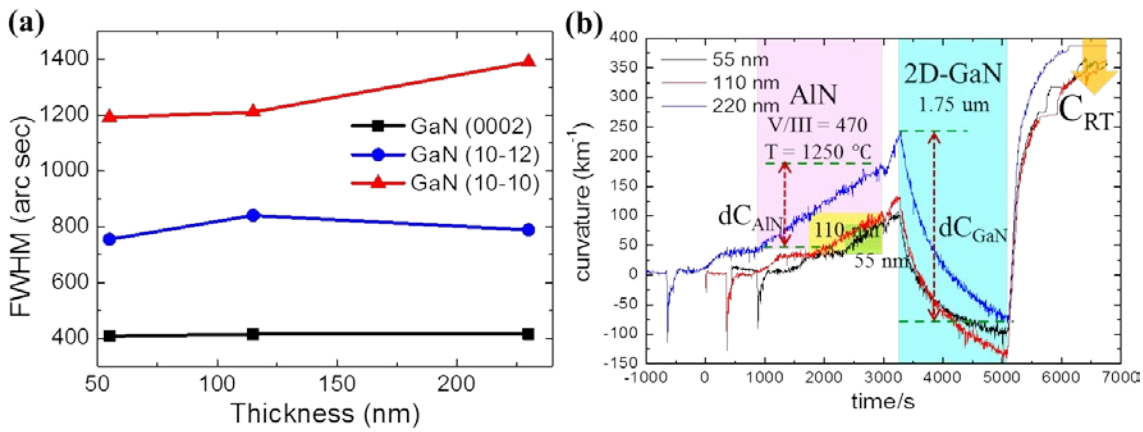


**Fig. 5.7** (a) FWHM of XRD rocking curve of GaN and (b) Curvature transition of GaN growth on AlN buffer layer with thickness of 55nm, 110 nm and 220 nm.

Fig. 5.7 indicated that the influence from AlN buffer thickness on the quality was not as remarkable as that from the growth temperature and V/III ratio. As the buffer thickness increased, the quality of GaN on it didn't change much from 55 nm to 110 nm or even degraded as the thickness of AlN buffer increased to 220 nm, especially the quality of (10-10) plane, which indicated the increase of edge dislocation density in GaN on 220-nm-thick AlN buffer layer. From the general knowledge of crystal growth it is evident that generally the quality is improved with increased film thickness. So the quality of AlN buffer with largest thickness should be the best. But this is only the case when growth conditions are proper. Since the V/III ratio of 470 is not the optimal value, so the quality and surface morphology (pit density and roughness) can be imperfect. It would be worse with the increase of

thickness. In Fig. 5.7b, $dC_{GaN}$ showed small improvement with the increase of AlN buffer thickness. The sample with 110-nm-thick AlN buffer layer yielded the lowest $C_{RT}$. Therefore, based on overall consideration, thickness of 110 nm has been chosen for the growth of AlN buffer layer.

Based on the study of AlN buffer layer growth temperature and V/III ratio on the quality of GaN on it, it can be concluded that for GaN on AlN buffer layer, the compressive curvature increase $dC_{GaN}$ in GaN is an indicator of the quality of it. Higher quality leads to larger $dC_{GaN}$, and for the most cases here (not safe for all cases because besides high quality, factors like lattice constant difference also contributes to large $dC_{GaN}$), larger $dC_{GaN}$ also indicates higher quality. This point would be utilized for the discussion in the next section about the effects from AlN interlayers on GaN quality.

## 5.3 Effect of AlN interlayers on GaN quality

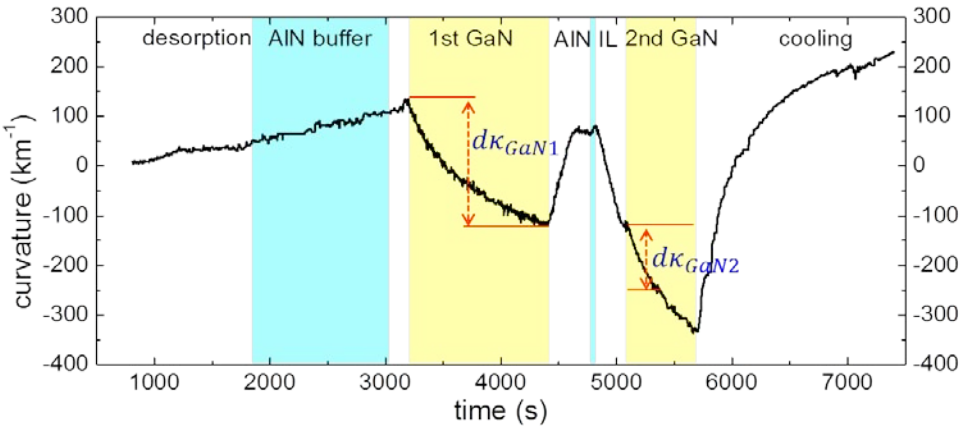


**Fig. 5.8** Structure and curvature curve of single-condition AlN IL sample.

AlN interlayers (ILs) not only affect the compressive stress introduction to overlying GaN, but also affect the quality of GaN on them. AlN interlayer was first applied to reducing the dislocation density in GaN and the control of stress to yield crack free AlGaN on sapphire [45, 46]. Some study reported that AlN IL was favorable to improving the quality of GaN [47], but based on our study it is not true for any AlN IL and dependent on the growth conditions of them. In this section, the effect of AlN ILs on the quality of overlying GaN was studied by XRD rocking curve measurement and detailed TEM observation about the dislocation generation and propagation. The investigated conditions and structures were the same as those for stress study of effects of AlN IL, as sketched in Table 3.2 and Fig. 3.17 in chapter 3, including conditions of thickness, growth temperature and V/III. Multi-condition and single-condition samples had been grown. XRD rocking curve measurement was carried out only for the single-condition-AlN -IL sample, while the TEM observation was executed only for multi-condition-AlN-IL sample. Prior to introducing XRD results, the curvature curves of the single-condition-AlN-IL samples were introduced first for the later discussion. As shown in Fig. 5.8, the curvature increase for the 1$^{st}$ GaN $d\kappa_{GaN1}$ was extracted to evaluate

its quality which may influence the behavior of the following layers. Because based on the results in the previous section, for GaN on AlN buffer layer, large $d\kappa_{GaN1}$ usually indicates high quality of it. Only the first 200 nm of the 2nd GaN layer was sampled to compare the compressive curvature increment brought by AlN interlayers grown under various conditions, as the curvature curves in the first 200 nm were linear, and the sampled thickness was the same with that of the GaN layer in between AlN interlayers in multi-condition samples.

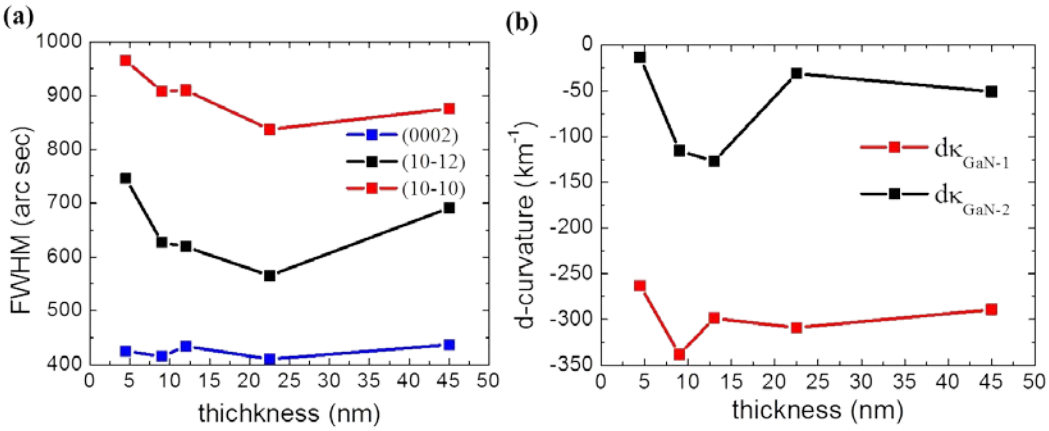


**Fig. 5.9** (a) FWHM of XRD rocking curve of GaN samples with single-layer AlN IL for thickness study; (b) curvature increase to the compressive side in the 1st GaN and the first 200 nm in the 2nd GaN layer.

The first investigated condition is the thickness of AlN ILs, which was varied from 4.5 nm to 45 nm. The results of XRD rocking curve as well as the curvature increase to the compressive side in the first and second GaN were extracted in Fig. 5.9a and b respectively. From Fig. 5.9a, the quality of GaN became higher as the thickness of AlN IL increased from 4.5 nm to 22 nm and after that it degraded. But such description is not reliable without examining the measurement carefully. For confirming the effects of AlN ILs on GaN quality, the quality of only the 2nd GaN layer should be accessed. But in the measurement for the planes of (0002) and (10-12), as sketched by Fig. 5.10a, b and d, because the X-ray incident angel $\theta$ is very large, so the penetration depth of X-ray $t$ would be very large [48]. $t$ can be calculated by the following equation [49]:

$$t = -\frac{\sin\theta \ln(1-G_t)}{2\mu}, \mu = (m_{Ga} \cdot u_{Ga} + m_N \cdot u_N) \cdot N \cdot m/V_{GaN} \quad (5\text{-}2)$$

$\theta$ is the incident angel, $G_t$ is the fraction of , $\mu$ is mass absorption coefficient, $m_{Ga}$ and $m_N$ are the atomic mass of gallium and nitrogen respectively, $u_{Ga}$ and $u_N$ are mass absorption of gallium and nitrogen respectively, $N$ is the number of gallium or nitrogen in a unit cell of GaN crystal, $m$ is a unit of atomic mass (1 amu), $V_{GaN}$ is the volume of a unit cell of GaN crystal. By calculation, the largest penetration depth ($\theta = 90°$) can be 42.59 um. The penetration depth of the measurement of plane (0002) ($\theta \approx 17.3°$) can be 12.665 um. So for the measurements of planes of (0002) and (10-12), the diffraction information came from not only the 2nd GaN, but also from the 1st GaN. Due to larger thickness of the 1st GaN than the 2nd, the information from the 1st GaN layer is dominant in the results of planes of (0002) and (10-12). The information of the results of measuring (10-10) plane comes from only the top

2nd GaN layer since the incident angel of in-plane measurement is very small around the critical angle and the sampled depth can be only tens of nanometers.

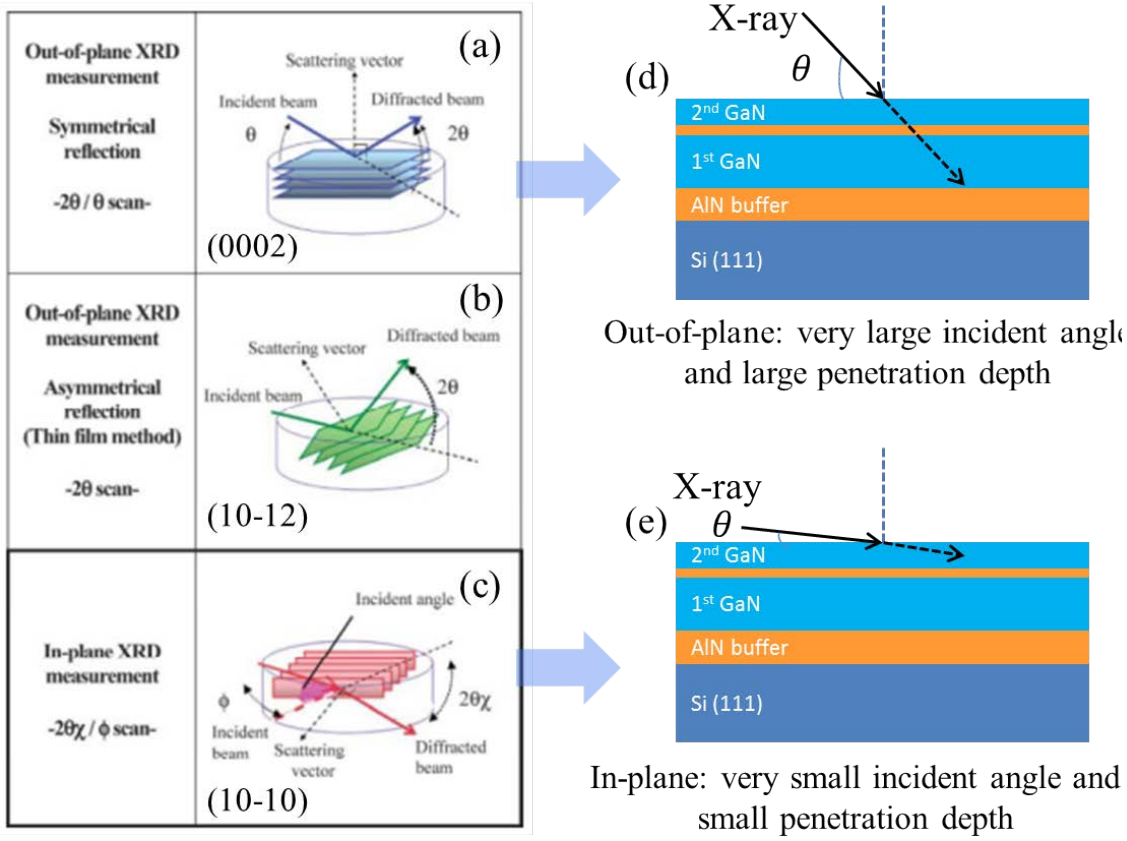


**Fig. 5.10** Schematic diagram of XRD rocking curve measurement for the planes of (a) (0002), (b) (10-12) and (10-10) of GaN.

Another point should be noticed is that the factors of the quality of the 2nd GaN layer, or, the source of dislocations in the 2nd GaN layer. Dislocations in the 2nd GaN can come from the 1st GaN layer, i.e., by propagation of threading dislocations; or originate from the AlN IL. Consequently, the quality of the 2nd GaN is determined by the quality of the 1st GaN and the AlN IL. In order to survey the influence only from the AlN IL, the quality of the 1st GaN should be as identical as possible, which usually is not the case but with some minimal variation from round to round due to the fluctuation of reactor conditions. However, basically, such variation doesn't affect the reliability of studies principally. Based on these preliminaries, the discussion of effects of AlN ILs can be started.

Fig. 5.9a is the results of XRD rocking curve measurements. The tendency of (0002) plane and (10-10) plane showed slight difference. There was minimal variation of the FWHM of (0002) plane which included the information from the 1st GaN dominantly. By comparing Fig. 5.9a and b, it can be found that the tendency of FWHM of (0002) plane and $d\kappa_{GaN-1}$ as functions of AlN IL thickness was the similar. There was some variation of $d\kappa_{GaN-1}$ due to some reactor condition fluctuation or contamination of the wafer surface, although the conditions were designed to be identical. From the discussion in last section, $d\kappa_{GaN-1}$ is an indication of the quality of the 1st GaN layer. Except the sample of 9-nm-thick AlN

interlayer, $d\kappa_{GaN-1}$ and then the quality of the first GaN layer was on the same level. This proved that FWHM of (0002) included the information from the 2nd GaN layer but was dominated by the quality of the 1st GaN layer.

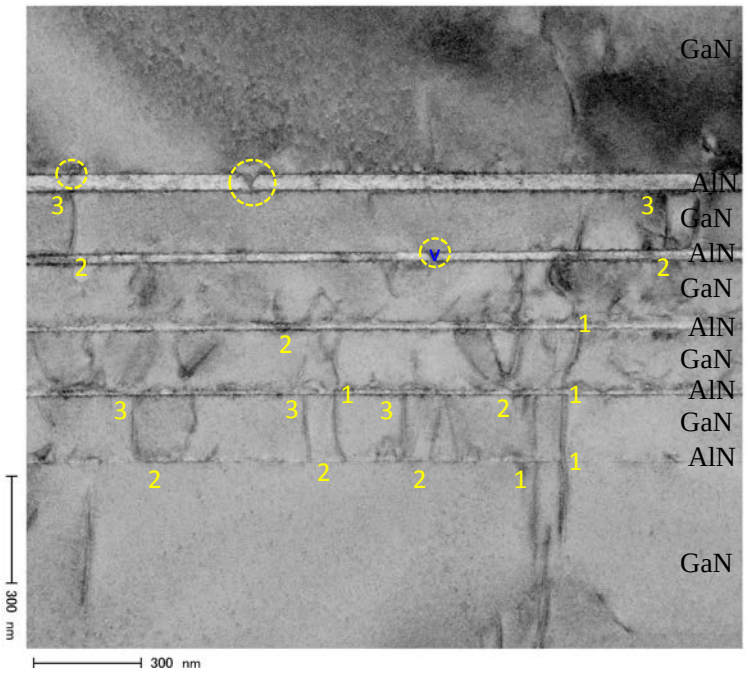


**Fig. 5.11** TEM image of the cross section of multi-condition sample of AlN-IL thickness study.

However, the results of the planes of (10-12) and (10-10) differed. Their tendency was more evident that the quality of the 2nd GaN became higher as the thickness of AlN IL increased from 4.5 nm to 22 nm, and after that the quality degraded. FWHM of (10-10) plane included the quality information from only the 2nd GaN. Nevertheless, it was influenced by the 1st GaN and showed a strong coupling or combination effect of the 1st GaN layer and an AlN IL on the quality of the 2nd GaN. FWHM of (10-10) plane also had the same tendency with that of $d\kappa_{GaN-1}$ partially, for example as a function of AlN IL thickness, the improvement from 4.5 nm to 9 nm, from 13 nm to 22 nm and the degradation from 22 nm to 45 nm. The quality improvement of the plane of (10-10) was determined by the dominant influence of the 1st GaN for the samples with AlN interlayer thickness increased from 4.5 nm to 9 nm. Thin AlN interlayer doesn't contribute to the quality enhancement or even introduce new dislocation, as shown in Fig. 5.11. The difference emerged when the thickness was increased from 9 nm to 13 nm. The quality of the 1st GaN degraded while that of the 2nd GaN was almost constant. Here indicated the quality improvement of the 2nd GaN brought by the favorable effects of 13-nm-thick AlN IL which compensated the degradation caused by the lower quality of the corresponding 1st GaN. AlN IL showed dominant influence on the compressive stress introduction in the 2nd GaN, as shown by the plot of $d\kappa_{GaN-2}$ in Fig. 5.9b which held different tendency with that of XRD results.

The best quality of 2nd GaN turned up when the thickness of AlN IL was raised to 22 nm, in spite of lower $d\kappa_{GaN-1}$ than the sample with 9-nm-thick AlN IL. As AlN IL thickness became larger to 45 nm, quality of the 2nd GaN started degrading. On the contrary, $d\kappa_{GaN-2}$ dropped a lot when the thickness of AlN IL was thickened from 13 nm to 22 nm and 45 nm.

The overall conclusion is that thicker AlN IL leads to higher quality of the top GaN, while there a proper thickness around 22 nm exists. Nonetheless, thicker AlN IL brings better quality but low compressive stress (curvature). In terms of compressive stress in GaN, the optimal AlN IL thickness exists in the range from 9 nm to 13 nm. Thicker AlN IL is of higher quality and then higher quality of overlying GaN. Based on the strain relaxation theory in chapter 3, higher quality is favorable to keep strain in epilayer and sustain larger compressive strain in GaN. There is some other mechanism has counteracted the merit brought by higher crystal quality which can cause more compressive stress in GaN, for example cracking in thick AlN ILs as discussed in chapter 3. Therefore, from the XRD rocking curve measurement of single-AlN-IL samples, in terms of the quality of 2$^{nd}$ GaN, due to the influence from the 1$^{st}$ GaN, it is very hard to conclude that what thickness is the best for AlN interlayer. We can only say that 13 nm was better than 9 nm. The thickness which is favorable to yield higher GaN quality might be not proper to induce larger compressive stress in overlying GaN.

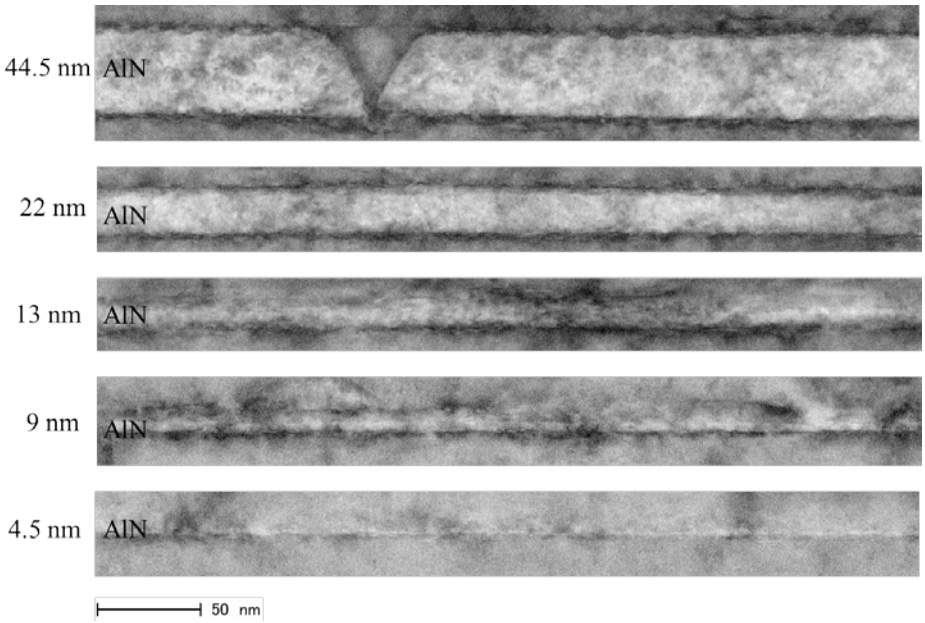


**Fig. 5.12** Interfaces of AlN ILs with varied thickness.

More direct information can be accessed by TEM observations. For convenience, only the multi-condition samples were characterized by TEM to observe the dislocation behavior in GaN on Si with multiple AlN ILs. Fig. 5.11 is the cross section image of the sample for AlN-IL thickness investigation. The dark lines are threading dislocations. From the TEM image, we can see the interaction between dislocations and AlN ILs, which can be classified into 3 types as marked in Fig. 5.11. Interaction type 1 is the threading of dislocations through GaN and AlN ILs from bottom to the up. Type 2 is the origination of new dislocations from AlN ILs at the interfaces of GaN/AlN, which is unfavorable. The first AlN IL with thickness of 4.5 nm generated the most new dislocations and after that as the thickness increased, the newly generated dislocations became less and less. This is consistent with the AFM results in Fig. 3.23 in chapter 3. As the thickness increased, the sizes of AlN grains became larger with higher quality and then the dislocation source density at GaN/AlN interface decreased and

lead to less new dislocations. Interaction type 3 is blocking of the propagation of threading dislocations, which is advantageous to the reduction of dislocation density. The dislocation blocking effect became stronger and stronger as the thickness of AlN ILs increases. Combining interaction type 2 and 3, thicker AlN IL is beneficial to reducing the dislocation density while this is not the case for introducing higher compressive stress in GaN layers. On the other hand, in AlN ILs with thickness of 22 nm and 45 nm, some V-pits and cracks have been observed and circled in Fig. 5.11, which have been observed also in AFM scanning of AlN-IL surfaces in Fig. 3.23. This can prove that the fine crackles in Fig. 3.23 were generated during growth but not cooling after growth. In the discussion of chapter 3, these crackles are responsible for the reduction of compressive stress in their overlying GaN.

More enlarged images at the interfaces can be seen in Fig. 5.12. For thin AlN ILs with thickness less than 13 nm, their interfaces are hazy and not abrupt. In most locations it is hard to tell where the interface is. When the thickness was 4.5 nm, it was too thin to form a continuous AlN film due to 3D growth. It could not separate the GaN layers sufficiently and then GaN could not be strained intensively. As shown by the AFM images in Fig. 3.23, AlN IL with the smallest thickness of 4.5 nm has the smallest grains and highest grain density as well as grain boundary density. Then at the grain boundaries, the most dislocations were generated. As the thickness increased to mediate thickness of about 9 nm, grains grew bigger and started to coalesce and the roughness also increased. After the thickness increased to 22 nm and higher, the coalescence has completed and the interfaces were more smooth and abrupt. There was no grain boundary to act as the source of dislocations. This is why thinnest AlN IL led to highest dislocation density in GaN and it decreased with the thickness of AlN IL. So, larger thickness is good for the improvement of GaN quality. However, it might not favorable for inducing higher compressive stress in GaN. Thin AlN ILs with thickness less than 13 nm are continuous 3D grains and are more relaxed. When the thickness increased to more than 22 nm, cracking occurred, as shown in AFM image of Fig. 3.23 as well as TEM image of Fig. 5. 12. After cracking, the AlN IL is not a whole piece of continuous film anymore and it could not sustain the tensile stress in itself, as indicated in Fig. 3. 18. As the AFM result of Fig. 3.23 showed, the crack density was high. With large amount of crack, although the tensile stress in AlN IL was relaxed, it could not induce much shear stress in

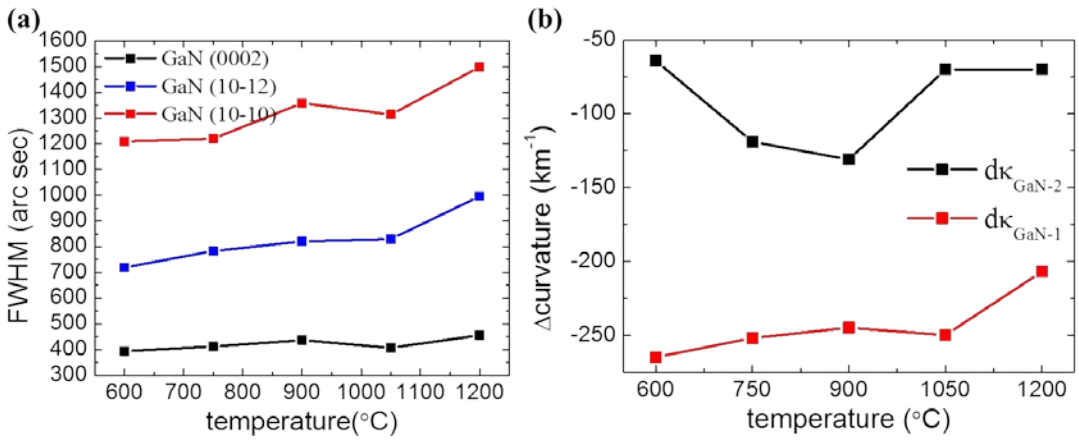


**Fig. 5.13** (a) FWHM of XRD rocking curve of GaN samples with a single-layer AlN IL for temperature study; (b) curvature increase to the compressive side in the 1st GaN and the first 200 nm in the 2nd GaN layer.

lateral direction in GaN as AlN IL consisted of separated domains.

The same study has also been carried out as a series of growth temperature of AlN ILs. The results of FWHM of XRD rocking curve measurement for single-AlN-IL samples in Fig. 5.13a showed the same tendency as that of $d\kappa_{GaN-1}$ for all the measured planes. This indicated that the influence of the 1st GaN was more dominant than that of AlN ILs or the growth temperature of AlN IL was not very influential on the quality of GaN above it. It is hard to interpret properly because the quality and morphology of AlN grown at low and high temperature was substantially different, as shown by the surface morphology in Fig. 3.27. Compared with growth temperature, the influence on overlying GaN of AlN-IL thickness is more effective. As the thickness of AlN ILs was fixed to be around 8 nm which was sufficiently thin, they didn't coalesce completely. The density of grain boundary which can be the source sites of dislocations were on the same level regardless of growth temperature. This accounts for the weak dependence of GaN quality on the growth temperature of AlN ILs.

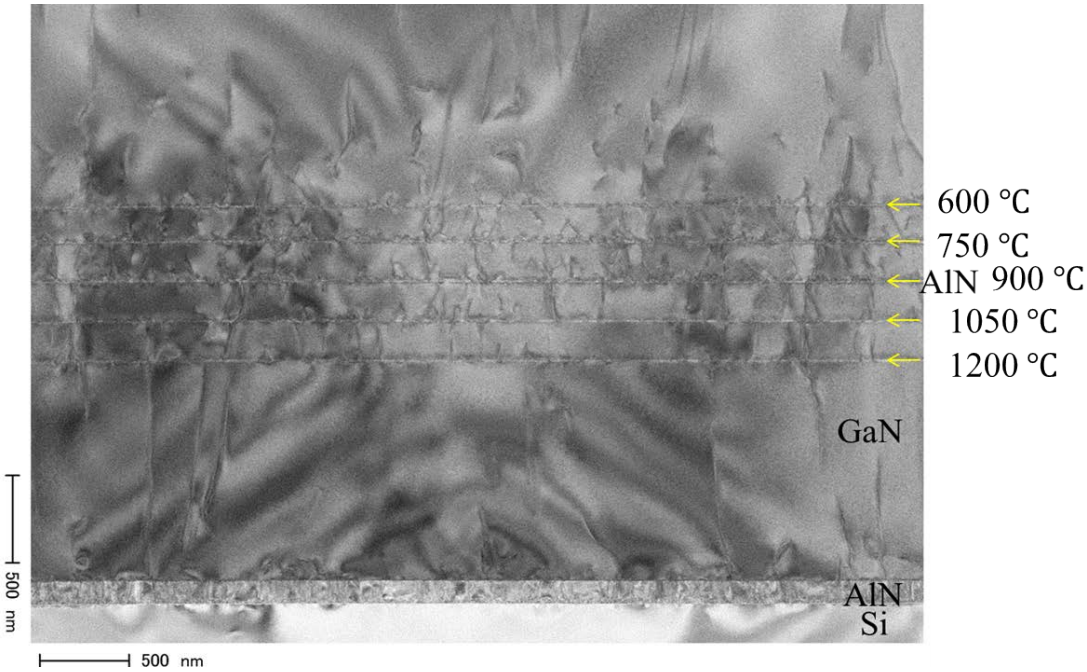


**Fig. 5.14** TEM image of the cross section of multi-condition sample of AlN-IL temperature study. AlN ILs are marked by arrows and their growth temperature (bottom to top) are 1200 ℃, 1050 ℃, 900 ℃, 750 ℃ and 600 ℃ respectively.

On the other hand, $d\kappa_{GaN-2}$ was very sensitive to the growth temperature of AlN IL, which the relative optimal value was around 900 ℃. In the TEM image of the cross section of the multi-condition sample (Fig. 5.14), the density of newly generated dislocation at the upper interface of AlN ILs increased slightly as the growth temperature increased from bottom to up while with no substantial difference. 1200-℃ grown IL caused the least dislocation. Besides the highest growth temperature and better quality, the thickness of it was also larger than others which may be due to the incorporation of gallium at high temperature, as shown in Fig. 5.15, and larger thickness causes less dislocation. Most of the new dislocations were blocked by the following AlN IL. After 5 layers of AlN IL, the dislocation

density in GaN increased. The weak dependence of the density of newly generated dislocation may be due to the small thickness of about 8 nm of them. They did not coalesce well and the grain density may on the same level. The interfaces were more abrupt and clear at higher growth temperature, which is an indication of quality improvement of AlN ILs. However, this also verified that high abruptness or smoothness is not the most impacting factor to introducing high compressive stress in GaN, compared with lattice constant difference.

To summarize this section, because the tendency of FWHM of XRD rocking curve measurement of the 2nd GaN is similar to that of $d\kappa_{GaN-1}$ but different from that of $d\kappa_{GaN-2}$, the effects of AlN ILs on the quality of overlying GaN is not as strong as that on the compressive stress introduction. The quality of upper GaN layers are determined by the underlying GaN layers dominantly if the thickness of AlN IL is small (< 13 nm). Certainly, AlN could introduce huge amount of new dislocations at the upper interface of AlN ILs if the growth conditions of it are not proper. AlN ILs can also block the propagation of threading dislocations.

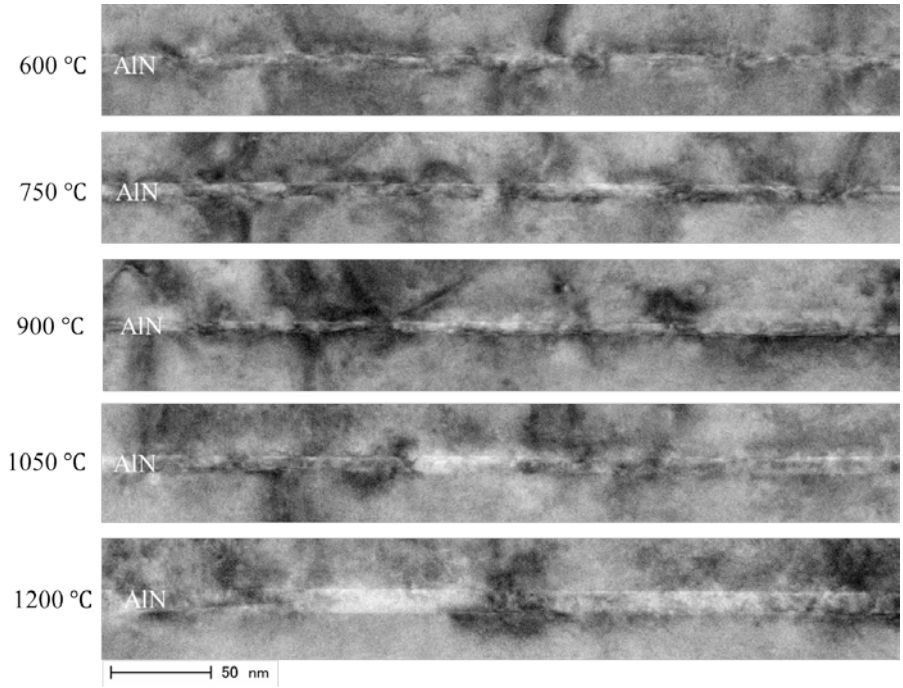


**Fig. 5.15** Interfaces of AlN ILs grown at varied temperature.

## 5.4 High quality brought by 3D growth mode

Basic introduction of modes of crystal growth has been given in section 3.4 in chapter 3, by listing the classification of 3 types of growth modes. Applying Volmer-Weber growth mode or 3D growth mode is the most efficient strategy to improve the crystal quality of epitaxial films without any ex-situ treatment like patterning, just by modifying the growth mode through controlling the growth conditions. Conventionally, 3D growth mode of GaN was realized using low temperature GaN buffer layer [50]. 2D amorphous GaN buffer layer

was grown at 550 ℃ and recrystallized through annealing at high temperature around 1100 ℃. After annealing, it evolved to 3D islands and high-temperature GaN was grown on these islands. In this study, 3D growth was realized also at high temperature by only adjusting the source flow rate and V/III ratio. The growth procedure and conditions of the sample in Fig. 5.16b were summarized in Table 5.1.

**Table 5.1** Growth conditions for 3D-mode grown GaN on high-temperature AlN buffer layer.

| Layer | Temperature (℃) | Time | TMGa (sccm) | TMAl (sccm) | $NH_3$ (sccm) | V/III ratio |
|---|---|---|---|---|---|---|
| **AlN** | 1250 | 17’ | | 22 | 640 | 3005 |
| **GaN nucleation** | 1130 | 6’ | 2 → 15 | | 100 → 600 | 509 → 407 |
| **GaN** | 1130 | 28’ | 35 | | 2500 | 728 |

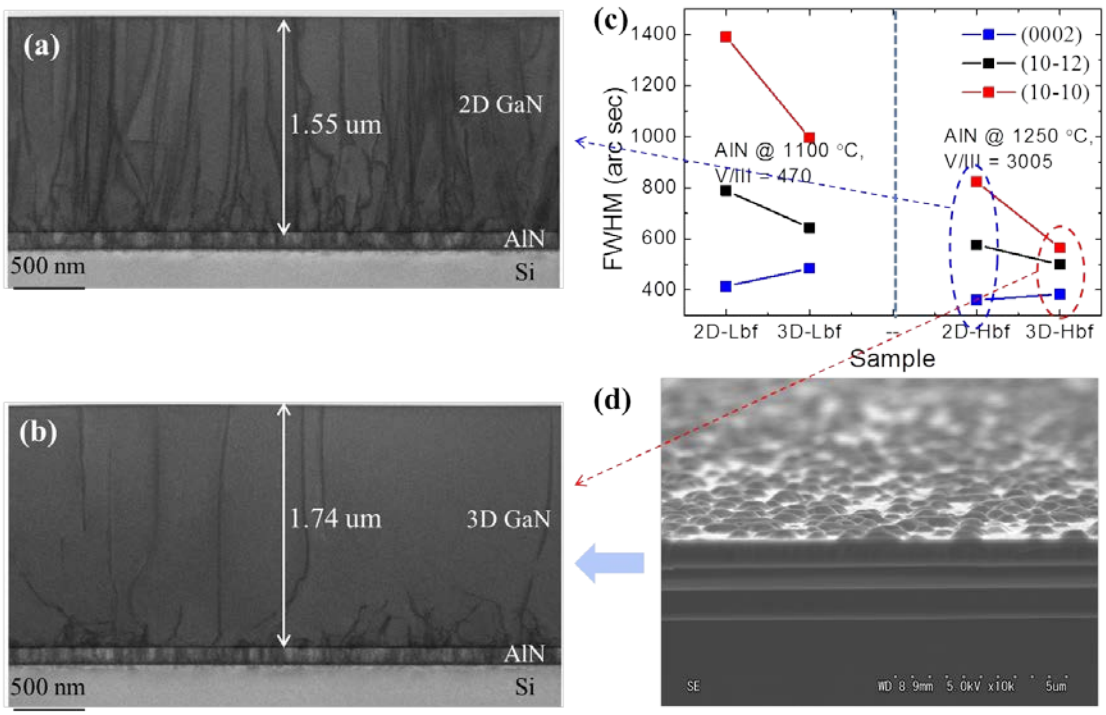


**Fig. 5.16** (a) and (b) TEM images and (c) FWHM of XRD rocking curve measurements of GaN samples grown in 2D mode and 3D mode on low-quality AlN buffer layer (Lbf) and high-quality AlN buffer layer (Hbf) respectively; (d) 3D islands in the initial stage of 3D growth.

By direct observation from TEM images of Fig. 5.16a and b, from 2D mode to 3D mode, the dislocation density in GaN was reduced substantially. As Fig. 5.16c shows that, on both low and high temperature AlN buffer layer, the quality of GaN was improved significantly as the growth mode was shifted from 2D to 3D, especially the quality of (10-10) plane, which corresponds to the twist of (10-10) plane and the density of edge dislocation. On the contrary, the quality of (0002) plane degraded slightly, which indicated the rise of screw dislocation density. So, it can be speculated that most dislocations which could be observed in Fig. 5.16a were edge dislocations. Fig. 5.16d is the 3D GaN nucleation layer. As the summarized conditions in Table 5.1 shows, this layer was formed by small flow rate of TMGa. In a period of 6 min, the flow rate of TMGa was raised from 2 sccm to 15 sccm and that of $NH_3$ was

increased from 100 sccm to 600 sccm. The V/III ratio decreased from 509 to 407. After that both of the flow rates of TMGa and $NH_3$ were raised by several times while the V/III ratio didn't increase a lot. Like the basic mechanism of dislocation annihilation in 3D-mode grown films, most of the dislocations annihilated in the first 300 nm of GaN.

The influence of AlN buffer layer on the quality, curvature transition and growth mode was examined. AlN buffer layer grown at higher temperature (1250 ℃) and proper V/III ratio (3005) lead to better GaN. Fig. 5.17a shows that, both using the same 3D growth mode conditions, for that on the improper AlN buffer, curvature went to the compressive side at the starting stage, but within a small thickness of about 400 nm after coalescence, it relaxed immediately and evolved to tensile strain; while for that on improved buffer layer, it was compressively stressed through a large thickness of 1.74 um. The growth mode also differed very much from them. GaN coalesced much earlier on improper AlN buffer than on improved one. This might be due to higher density of GaN islands with smaller size on improper AlN buffer. Usually, later coalescence leads to better GaN quality.

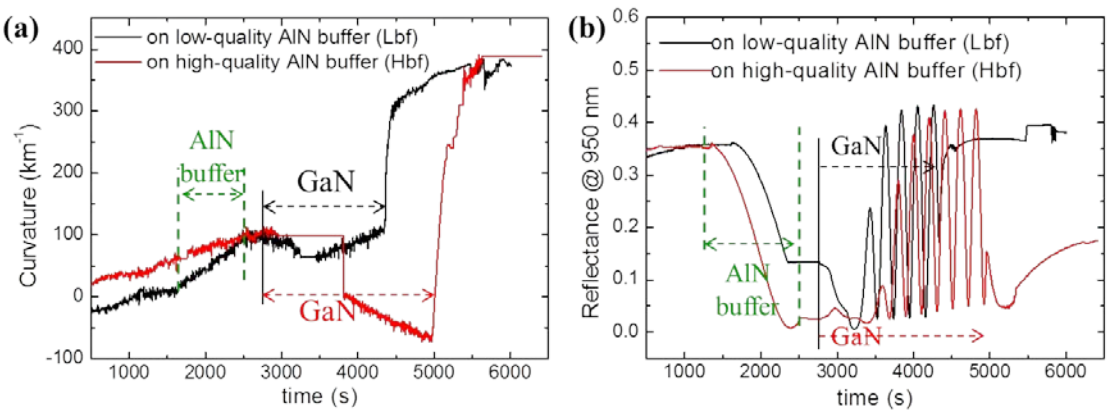


**Fig. 5.17** (a) Curvature transition curve and (b) reflectance of the growth at 950 nm of the growth of GaN on improper and improved AlN buffer layer.

It is noticeable that the best GaN quality here is close to that on sapphire. With thickness of only 1.74 um, the FWHM of (0002) and (10-10) planes are 356 arc sec and 568 arc sec respectively. They are on the same level if with the same thickness on sapphire. In most of other groups of growing GaN on Si, this level could be achieved with thickness beyond 8 um.

## 5.5 LED on GaN-on-Si

Based on all the work in previous chapters, a demonstration of blue LEDs on GaN-on-Si was grown and fabricated. Photoluminescence (PL) of them was characterized, as shown in Fig. 5.18a and c. In the center of the wafer, the peak position was around 438 nm and the intensity was stable. The device performance uniformity in the through whole wafer was checked by picking 6 points from the center to the edge.

As the sampled location moved from center to the edge of point 5 in Fig. 5.18c, the distribution of PL peak position was relatively narrow and varied from 439 nm to 444 nm. Only the peak of the sample on the very edge, point 6, was smaller at 425 nm. The narrow

distribution of PL peak indicated that the distribution of indium content in InGaN/GaN multi-quantum well (MQW) structure through the area of the whole wafer was uniform. However, the PL intensity was not uniform at all. It increased by 7 times from the center to the edge. In the area with radius smaller than 10 mm ($r$ < 10 mm), from point 1 to point 3, the increase was small from 30 a.u. to 46 a.u.. Beyond that, in the outer part of the wafer, PL intensity rose rapidly from 46 a.u. to 227 a.u.. Contrarily, the intensity of yellow luminescence in the wavelength range from 500 nm to 600 nm was decreasing as the sample location moved from center to the edge, which was favorable. PL intensity relates to the crystal quality of the device, especially the active area. High material quality leads to high PL intensity. In fact, for the growth of GaN on Si without upper LED structure, generally the quality in the center is better than it in the outer edge area, which is contrary to the PL intensity here. Another possibility to interpret such contradiction is, in spite of inferior quality of underlying GaN-on-Si substrate in the outer part, due to some unclear factor such as some condition distribution through the wafer, the quality of the active area of the LED, InGaN/GaN MQWs, in the outer part was better than that in the center, which led to higher PL intensity in the edge. Electroluminescence also succeeded as shown in Fig. 5.18b.

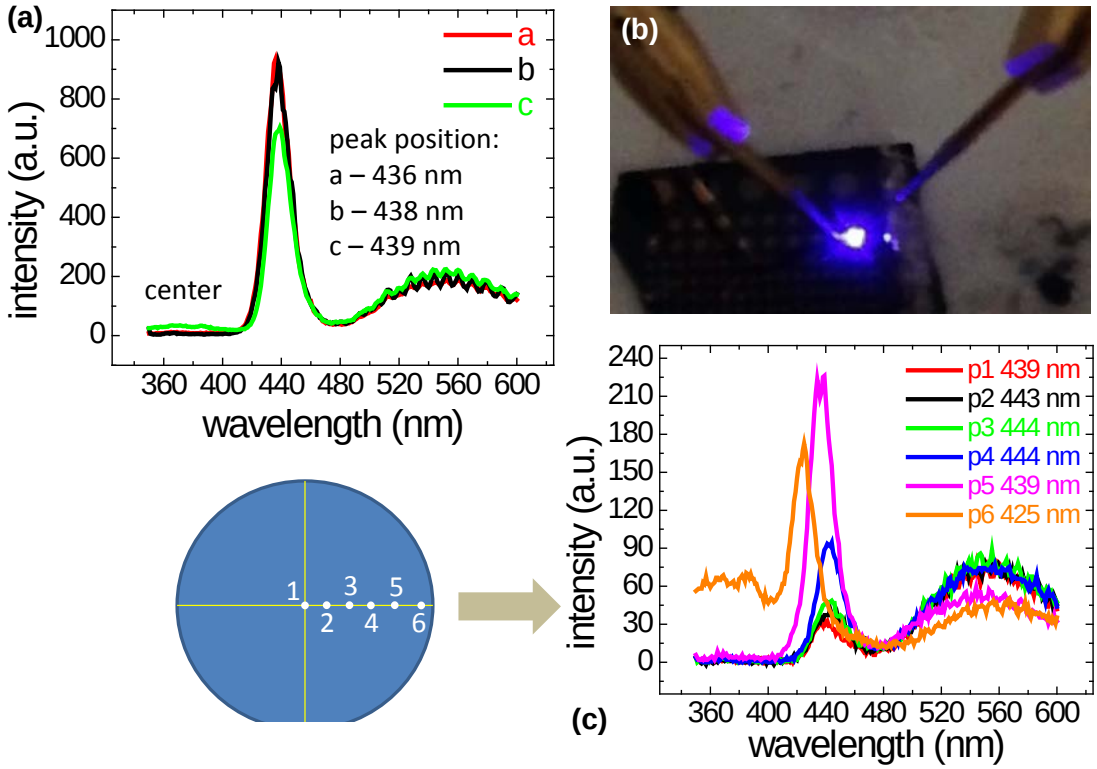


**Fig. 5.18** (a) Photoluminescence of three sampled points in the center area of the wafer, (b) electroluminescence of blue LED and (c) photoluminescence intensity depending on the location.

## 5.6 Conclusion

The other important aspect of GaN on Si other than stress control, crystal quality of GaN, has been examined in this chapter. In the past GaN quality was once a bottleneck of its

application; in the last two decades, quality improvement of GaN was the hottest topic in the field of III-N nitride. After introducing basic strategies which can enhance GaN quality, factors that affect the quality of GaN on Si have been observed. Following the structure of the sample, these factors include AlN buffer layer, AlN interlayer as well as the growth conditions of GaN itself.

In chapter 3, in terms of compressive stress introduction to the 1$^{st}$ GaN layer, it has been concluded that the quality of AlN buffer layer should be as high as possible. It is also valid for the enhancement of GaN quality. As long as the growth mode of GaN was kept to be 2D and the conditions were identical, high-quality AlN buffer layer led to high-quality GaN. Growth temperature of AlN buffer layer is the most influential condition of the quality of both it and GaN. GaN quality can be improved by elevating the growth temperature of AlN buffer layer, as the elevated temperature can enhance the surface mobility of Al ad-atoms. GaN cannot grow properly on AlN buffer which is grown at temperature lower than 1000 ℃. Low-temperature AlN buffer layer turns up to be amorphous or poly-crystalline, and the overlying GaN is also polycrystalline. Dislocations in a substrate or underlying layer can propagate to or be amplified in the overlying epitaxial layer. GaN quality on it was improved as the defect density in AlN buffer decreased. If it is available, the growth temperature can be up to 1400 ℃. In this work, the achievable highest growth temperature is 1250 ℃. Optimizing V/III ratio could also lead to higher quality of AlN buffer layer. The proper range is from 1000 ~ 3000. Thickness of AlN buffer is not influential like growth temperature and V/III ratio. As it was double from 55 nm to 110 nm and quadrupled to 220 nm, GaN quality stayed on the same level.

AlN interlayer is less influential than AlN buffer layer if its thickness is small (< 13 nm). In terms of GaN quality, thicker AlN interlayer is favorable. Thicker AlN interlayer (> 22 nm) blocks the propagation of dislocations from underlying layers more effectively than thinner one. The density of defect source sites like grain boundaries is much lower in thick AlN interlayers than it in thin ones. If the thickness is small, the effect of growth temperature on the quality of GaN is weak.

In this chapter it has been proved that crystal quality and strain state cannot be separated. Higher-quality AlN buffer layer yields better GaN and larger compressive stress in it. But this is not the case for AlN interlayers. Higher-quality AlN interlayer may not lead to large compressive stress in GaN since that there may be some other mechanism to counteract the merits of higher-quality of AlN interlayer, such as cracking. Consequently, optimal growth conditions of AlN interlayers for good GaN may be not favorable to achieving large compressive stress in it.

In the end, based on all the study, blue LEDs were demonstrated with PL peak around 438 nm. The PL uniformity was analyzed. The narrow peak position distribution indicated uniform distribution of indium content in InGaN/GaN MQWs through the wafer. Nevertheless, the PL intensity differed much depending on the location. The intensity in the center was only one seventh of that in the edge. Probably this could be assigned to the better MQW quality in the out part of the wafer, which needs further investigation.

## References


[1] S. Nakamura, s. Pearton, and G. Fasol, *The Blue Laser Diode*. 2nd ed. 2000, Berlin et al.: Springer.

[2] H. Amano, N. Sawaki, I. Akasaki, and Y. Toyoda,Metalorganic vapor phase epitaxial growth of a high quality GaN film using an AlN buffer layer, Applied Physics Letters ***48***, 353(1986).

[3] S. Dassonneville, A. Amokrane, B. Sieber, J.L. Farvacque, B. Beaumont, V. Bousquet, P. Gibart, K. Leifer, and J.D. Ganiere,Cathodoluminescence intensity and dislocation contrast evolutions under electron beam excitation in epitaxial GaN laterally overgrown on (0001) sapphire, Physica B ***273-274***, 148(1999).

[4] S. Tomiya, H. Nakajuma, K. Funato, T. Miyajima, K. Kobayashi, T. Hino, S. Kijima, T. Asano, and M. Ikeda,Dislocations in GaN-Based Laser Diodes on Epitaxial Lateral Overgrown GaN Layers, Phys. Status Solidi (a) ***188***, 69(2001).

[5] S. Dassonneville, A. Amokrane, B. Sieber, J.L. Farvacque, B. Beaumont, and P. Gibart,Luminescence of epitaxial GaN laterally overgrown on (0001) sapphire substrate: Spectroscopic characterization and dislocation contrasts, J. Appl. Phys. ***89***, 3736(2001).

[6] Z. Bougrioua, I. Moerman, L. Nistor, B. Van Daele, E. Monroy, T. Palacios, F. Calle, and M. Leroux,Engineering of an insulating buffer and use of AlN interlayers: two optimisations for AlGaN–GaN HEMT-like structures, Phys. Status Solidi (a) ***195***, 93(2003).

[7] M. Miyoshi, T. Egawa, H. Ishikawa, K.-I. Asai, T. Shibata, M. Tanaka, and O. Oda,Nanostructural characterization and two-dimensional electron-gas properties in high-mobility AlGaN⁄AlN⁄GaN heterostructures grown on epitaxial AlN/sapphire templates, J. Appl. Phys. ***98***, 063713(2005).

[8] M. Miyoshi, A. Imanishi, T. Egawa, H. Ishikawa, K.-i. Asai, T. Shibata, M. Tanaka, and O. Oda,DC Characteristics in High-Quality AlGaN/AlN/GaN High-Electron-Mobility Transistors Grown on AlN/Sapphire Templates, Jpn. J. Appl. Phys. ***44***, 6490(2005).

[9] D. Zanato, S. Gokden, N. Balkan, B.K. Ridley, and W.J. Schaff,The effect of interface-roughness and dislocation scattering on low temperature mobility of 2D electron gas in GaN/AlGaN, Semiconductor Science and Technology ***19***, 427(2004).

[10] S.L. Selvaraj, T. Suzue, and T. Egawa,Breakdown Enhancement of AlGaN/GaN HEMTs on 4-inch silicon by improving the GaN quality on thick buffer layers, IEEE Electron Device Letters ***30***, 587(2009).

[11] W.C. Lai, Y.Y. Yang, and R.-H. Horng,Efficiency Improvement of Short-Period InGaN/GaN Multiple-Quantum Well Solar Cell With H2 in the GaN Cap Layer, Journal of Display Technology ***9***, 953(2013).

[12] N.C. Das, M.L. Reed, A.V. Sampath, H. Shen, M. Wraback, R.M. Farrell, M. Iza, S.C. Cruz, J.R. Lang, N.G. Young, Y. Terao, C.J. Neufeld, S. Keller, S. Nakamura, S.P. DenBaars, U.K. Mishra, and J.S. Speck,Optimization of Annealing Process for Improved InGaN Solar Cell Performance, J. Electronic Mater. ***42***, 3467(2013).

[13] Z.-Y. Lin, J.-C. Zhang, H. Zhou, X.-G. Li, F.-N. Meng, L.-X. Zhang, S. Ai, S.-R. Xu, Y. Zhao, and Y. Hao,Influence of double AlN buffer layers on the qualities of GaN films prepared by metal—organic chemical vapour deposition, Chinese Physics B ***21***, 126804(2012).

[14] M.L. Nakarmi, B. Cai, J.Y. Lin, and H.X. Jiang,Three-step growth method for high quality AlN epilayers, physica status solidi (a) ***209***, 126(2012).

[15] Y.A. Xi, K.X. Chen, F. Mont, J.K. Kim, E.F. Schubert, C. Wetzel, W. Liu, X. Li, and J.A. Smart,Optimization of High-Quality AlN Epitaxially Grown on (0001) Sapphire by Metal-Organic Vapor-Phase Epitaxy, Journal of Electronic Materials ***36***, 533(2007).

[16] Y.A. Xi, K.X. Chen, F. Mont, J.K. Kim, C. Wetzel, E.F. Schubert, W. Liu, X. Li, and J.A. Smart,Very high quality AlN grown on (0001) sapphire by metal-organic vapor phase epitaxy, Applied Physics Letters ***89***, 103106(2006).

[17] H. Kröncke, S. Figge, T. Aschenbrenner, and D. Hommel,Growth of AlN by pulsed and conventional MOVPE, Journal of Crystal Growth ***381***, 100(2013).

[18] C.H. Yen, W.C. Lai, Y.Y. Yang, C.K. Wang, T.K. Ko, S.J. Hon, and S.-J. Chang,GaN-Based Light-Emitting Diode With Sputtered AlN Nucleation Layer, IEEE Photonics Technology Letters ***24***, 294(2012).
[19] M. Iwaya, T. Takeuchi, S. Yamaguchi, C. Wetzel, and H. Amano,Reduction of etch pit density in organometallic vapor phase epitaxy-grown GaN on sapphire by insertion of a low-temperature-deposited buffer layer between, Jpn. J. Appl. Phys. ***37***, L316(1998).
[20] E. Arslan, M.K. Ozturk, A. Teke, S. Ozcelik, and E. Ozbay,Buffer optimization for crack-free GaN epitaxial layers grown on Si(1 1 1) substrate by MOCVD, Journal of Physics D: Applied Physics ***41***, 155317(2008).
[21] Y. Lu, X. Liu, X. Wang, D.-C. Lu, D. Li, X. Han, G. Cong, and Z. Wang,Influence of the growth temperature of the high-temperature AlN buffer on the properties of GaN grown on Si(111) substrate, Journal of Crystal Growth ***263***, 4(2004).
[22] M. Wei, X. Wang, X. Pan, H. Xiao, C. Wang, Q. Hou, and Z. Wang,Effect of AlN buffer thickness on GaN epilayer grown on Si(111), Materials Science in Semiconductor Processing ***14***, 97(2011).
[23] J.H. Yang, S.M. Kang, D.V. Dinh, and D.H. Yoon,Influence of AlN buffer layer thickness and deposition methods on GaN epitaxial growth, Thin Solid Films ***517***, 5057(2009).
[24] O.E. Contreras, F. Ruiz-Zepeda, A. Dadgar, A. Krost, and F.A. Ponce,Atomic Arrangement at the AlN/Si(110) Interface, Applied Physics Express ***1***, 061104(2008).
[25] Z. Liliental-Weber, R.L. Maltez, J. Xie, and H. Morkoç,Propagation of misfit dislocations from AlN/Si interface into Si, Journal of Crystal Growth ***310***, 3917(2008).
[26] D. Litvinov, D. Gerthsen, R. Vöhringer, D.Z. Hu, and D.M. Schaadt,Transmission electron microscopy investigation of AlN growth on Si(111), J. Cryst. Growth ***338***, 283(2012).
[27] R. Liu, F.A. Ponce, A. Dadgar, and A. Krost,Atomic arrangement at the AlN/Si (111) interface, Appl. Phys. Lett. ***83***, 860(2003).
[28] G. Radtke, M. Couillard, G.A. Botton, D. Zhu, and C.J. Humphreys,Structure and chemistry of the Si(111)/AlN interface, Appl. Phys. Lett. ***100***, 011910(2012).
[29] A.A. Allerman, M.H. Crawford, A.J. Fischer, K.H.A. Bogart, S.R. Lee, D.M. Follstaedt, P.P. Provencio, and D.D. Koleske,Growth and design of deep-UV (240–290nm) light emitting diodes using AlGaN alloys, J. Cryst. Growth ***272***, 227(2004).
[30] A. Hanlon, P.M. Pattison, J.F. Kaeding, R. Sharma, P. Fini, and S. Nakamura,292 nm AlGaN Single-Quantum Well Light Emitting Diodes Grown on Transparent AlN Base, Japanese Journal of Applied Physics ***42***, L628(2003).
[31] M. Imura, N. Fujimoto, N. Okada, K. Balakrishnan, M. Iwaya, S. Kamiyama, H. Amano, I. Akasaki, T. Noro, T. Takagi, and A. Bandoh,Annihilation mechanism of threading dislocations in AlN grown by growth form modification method using V/III ratio, Journal of Crystal Growth ***300***, 136(2007).
[32] A.V. Lobanova, E.V. Yakovlev, R.A. Talalaev, S.B. Thapa, and F. Scholz,Growth conditions and surface morphology of AlN MOVPE, Journal of Crystal Growth ***310***, 4935(2008).
[33] Z. Sofer, N. Kaluza, H. Hardtdegen, R. Steins, Y. Suk Cho, J. Stejskal, and D. Sedmidubský,Investigation of AlN growth on sapphire substrates in a horizontal MOVPE reactor, Journal of Physics and Chemistry of Solids ***68***, 1131(2007).
[34] K. Uehara, Y. Aota, S. Kameda, H. Nakase, Y. Isota, and K. Tsubouchi,Growth of Atomically Flat-Surface Aluminum Nitride Epitaxial Film by Metalorganic Chemical Vapor Deposition, Japanese Journal of Applied Physics ***44***, 2987(2005).
[35] M. Imura, H. Sugimura, N. Okada, M. Iwaya, S. Kamiyama, H. Amano, I. Akasaki, and A. Bandoh,Impact of high-temperature growth by metal-organic vapor phase epitaxy on microstructure of AlN on 6H-SiC substrates, Journal of Crystal Growth ***310***, 2308(2008).
[36] J. Bai, T. Wang, P.J. Parbrook, I.M. Ross, and A.G. Cullis,V-shaped pits formed at the GaN/AlN interface, Journal of Crystal Growth ***289***, 63(2006).

[37] S. Keller, G. Parish, P.T. Fini, S. Heikman, C.H. Chen, N. Zhang, S.P. DenBaars, U.K. Mishra, and Y.F. Wu,Metalorganic chemical vapor deposition of high mobility AlGaN/GaN heterostructures, Journal of Applied Physics ***86***, 5850(1999).
[38] S. Çörekçi, M.K. Öztürk, M. Çakmak, S. Özçelik, and E. Özbay,The influence of thickness and ammonia flow rate on the properties of AlN layers, Materials Science in Semiconductor Processing ***15***, 32(2012).
[39] M.-J. Lai, L.-B. Chang, T.-T. Yuan, and R.-M. Lin,Improvement of crystal quality of AlN grown on sapphire substrate by MOCVD, Crystal Research and Technology ***45***, 703(2010).
[40] M.A. Moram and M.E. Vickers,X-ray diffraction of III-nitrides, Reports on Progress in Physics ***72***, 036502(2009).
[41] V. Ivantsov and A. Volkova,A Comparative Study of Dislocations in HVPE GaN Layers by High-Resolution X-Ray Diffraction and Selective Wet Etching, ISRN Condensed Matter Physics ***2012***, 1(2012).
[42] J.E. Ayers, *Heteroepitaxy of Semiconductors: Theory, Growth and Characterization*. 2007, New York: CRC Press, Taylor & Francis Group. 161-241.
[43] A.V. Lobanova, K.M. Mazaev, R.A. Talalaev, M. Leys, S. Boeykens, K. Cheng, and S. Degroote,Effect of V/III ratio in AlN and AlGaN MOVPE, Journal of Crystal Growth ***287***, 601(2006).
[44] R. Luo, P. Xiang, M. Liu, T. Chen, Z. He, B. Fan, Y. Zhao, Y. Xian, S. Huang, Z. Zheng, Z. Wu, H. Jiang, G. Wang, Y. Liu, and B. Zhang,Influence of V/III Ratio of Low Temperature Grown AlN Interlayer on the Growth of GaN on Si(111) Substrate, Jpn. J. Appl. Phys. ***50***, 105501(2011).
[45] M. Iwaya, S. Terao, N. Hayashi, T. Kashima, H. Amano, and I. Akasaki,Realization of crack-free and high-quality thick AlGaN for UV optoelectronics using low-temperature interlayer, Appl. Surf. Sci. ***159-160***, 405(2000).
[46] H. Amano, M. Iwaya, T. Kashima, M. Katsuragawa, I. Akasaki, J. Han, S. Hearne, J.A. Floro, E. Chason, and J. Figiel,Stress and Defect Control in GaN Using Low Temperature Interlayers, Jpn. J. Appl. Phys. ***37***, 1540(1998).
[47] S. Fritze, P. Drechsel, P. Stauss, P. Rode, T. Markurt, T. Schulz, M. Albrecht, J. Bläsing, A. Dadgar, and A. Krost,Role of low-temperature AlGaN interlayers in thick GaN on silicon by metalorganic vapor phase epitaxy, J. Appl. Phys. ***111***, 124505(2012).
[48] S. Kobayashi,X-ray thin-film measurement techniques: In-plane XRD measurement, The Rigaku Journal ***26***, 3(2010).
[49] B.B. He, *Two-Dimensional X-Ray Diffraction*. 2009, Hoboken: John Wiley & Sons. 264.
[50] S. Nakamura,GaN Growth Using GaN Buffer Layer, Jpn. J. Appl. Phys. ***30***, L1705(1991).

# 6 Innovative AlN interlayers

Based on the experimental study and theoretical analysis, the ideal AlN interlayer with completely relaxed lower interface and completely coherent upper interface has been proposed in chapter 3. The method to achieve arbitrary wafer bowing for GaN growth on Si has been proposed in chapter 4. From the previous work, the knowledge that high quality upper interface of AlN interlayer is favorable to induce more compressive stress in overlying GaN has been discovered. In this chapter, three types of AlN interlayers would be proposed and tried to achieve more ideal AlN interlayer. They are pulse-injection AlN interlayer, low-temperature/pulse-injection two-step AlN interlayer and low-temperature/high-temperature two-step AlN interlayer, respectively.

## 6.1 Why innovative AlN interlayer?

There are several reasons for searching after higher performance Al(Ga)N interlayers to induce compressive stress in GaN layers more efficiently. Usually interlayers are more readily deteriorate the quality of GaN layer by introducing more dislocations. More efficient interlayer can reduce the needed number of it to control the overall stress properly and then improve the GaN quality within smaller thickness. On the other hand, applying more efficient interlayers which cause higher compressive stress can achieve the same required curvature increment amount to the compressive side within less GaN thickness.

Ideal interlayers are supposed to be of completely relaxed incoherent lower interface which make the interlayer maintains the neutral lattice constant of AlN itself, and fully strained coherent upper interface which stress the overlying GaN mostly. The most important property of it can also be expressed alternatively as being of smallest lattice constant of neutral AlN and perfect coherent upper interface. Following the experimental observation and theoretical analysis in the previous chapters, it is hardly being possible to realize such ideal AlN interlayer in a one-step conventional single layer. Maybe realizing such ideal AlN interlayer is out of the question. However, it can be approached by using special growth technology or applying new structure.

There are some routines to produce more efficient AlN interlayer to induce compressive stress in GaN layers. The first strategy is growing high-quality AlN interlayer at low temperature, which holds small lattice constant and coherent upper interface of GaN/AlN. Another strategy is applying two-step structure which consists of low-temperature AlN as the lower part (the first step) and the pulse-injection or high-temperature AlN as the upper part (the second part). The following parts are the experimental results and some of them indeed exceeded the performance of conventional single-step AlN interlayers.

## 6.2 Pulse-injection AlN interlayer

Pulse-injection (PI) growth method is a technology invented to produce high-quality AlN at low temperature, which can eliminate the drawbacks of growing conventional high-quality AlN. As reviewed in chapter 3 and 5, in order to grow high-quality AlN using conventional MOVPE method, it should be grown at high temperature (> 1200 ℃) to enhance the surface mobility of Al ad-atoms, under proper V/III ratio (500 ~ 3000) and low pressure (50 mbar). There are some disadvantages of conventional MOVPE method for growing AlN. Gas-phase pre-reactions between TMAl and $NH_3$ occur easily, which can form adducts on the surface and degrades AlN quality[1, 2]. Growth at high temperature leads to GaN decomposition and Ga diffusion especially in AlN/GaN multi-quantum well structures as well as in AlN interlayers. Then non-uniform and non-abrupt GaN/AlN interface which can lower the performance of devices or AlN interlayers may be formed [3]. PI method is a good technology to suppress the pre-reactions effectively. It can also control the abrupt GaN/AlN interface precisely. Moreover, the concentration of impurities like hydrogen, carbon and oxygen is several time lower than conventional AlN grown at the same temperature and with the same level of it of conventional AlN grown at 1240 ℃ [4, 5].

The PI technology has been developed in our lab several years ago [4, 5]. Growth procedures and conditions for AlN interlayers here were the optimized ones adopted in previous studies. It was grown at temperature of 800 ℃, under TMAl and $NH_3$ partial pressure of $3.9\times10^{-4}$ mbar and 0.86 mbar respectively. The optimal flow time of TMAl and $NH_3$ was 3.5 s and 5 s. The hydrogen purge time also influence AlN quality significantly and the optimal purge time $\tau_{H1} = \tau_{H2} = 1\ s$.

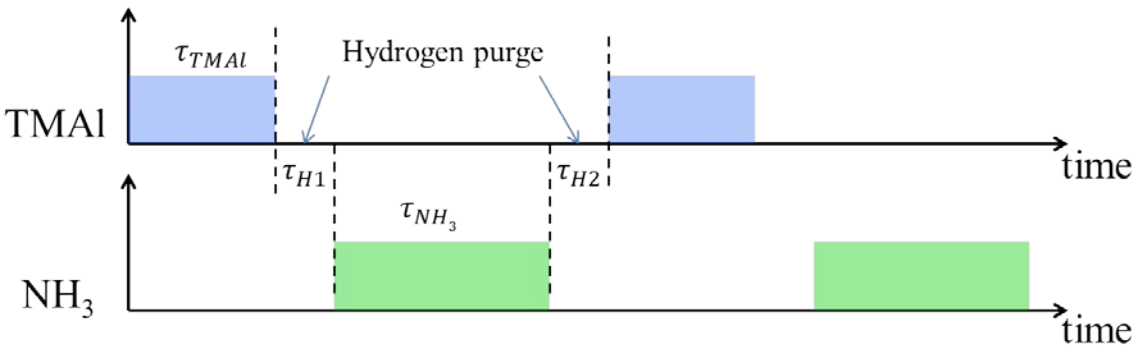


**Fig. 6.1** Procedure of pulse-injection growth method of AlN.

The sample for the trial of PI-AlN interlayer was of seven layers of AlN interlayers, with varied thickness. From the bottom to the up, the first six layers were PI-AlN, with thickness of 3/6/9/12/25/37 nm respectively, keeping other growth conditions constant. The top 7$^{th}$ AlN interlayer was a conventional AlN (c-AlN) reference grown under the best conditions in previous study which yielded largest compressive stress in GaN, with growth temperature at 900 ℃, thickness of 9 nm, V/III ratio of 1503. The best performance of conventional AlN interlayer in multi-condition sample was causing curvature increment of -124 km$^{-1}$ in overlying GaN (the sign of minus means compressive stress). This value is chose to be a standard to evaluate the innovative AlN IL. If it could induce curvature increment more than

that, then it is better than c-AlN IL. The curvature increments, strains and stresses of AlN interlayers and GaN layers were extracted in Fig. 6.2 from the raw data of curvature curve.

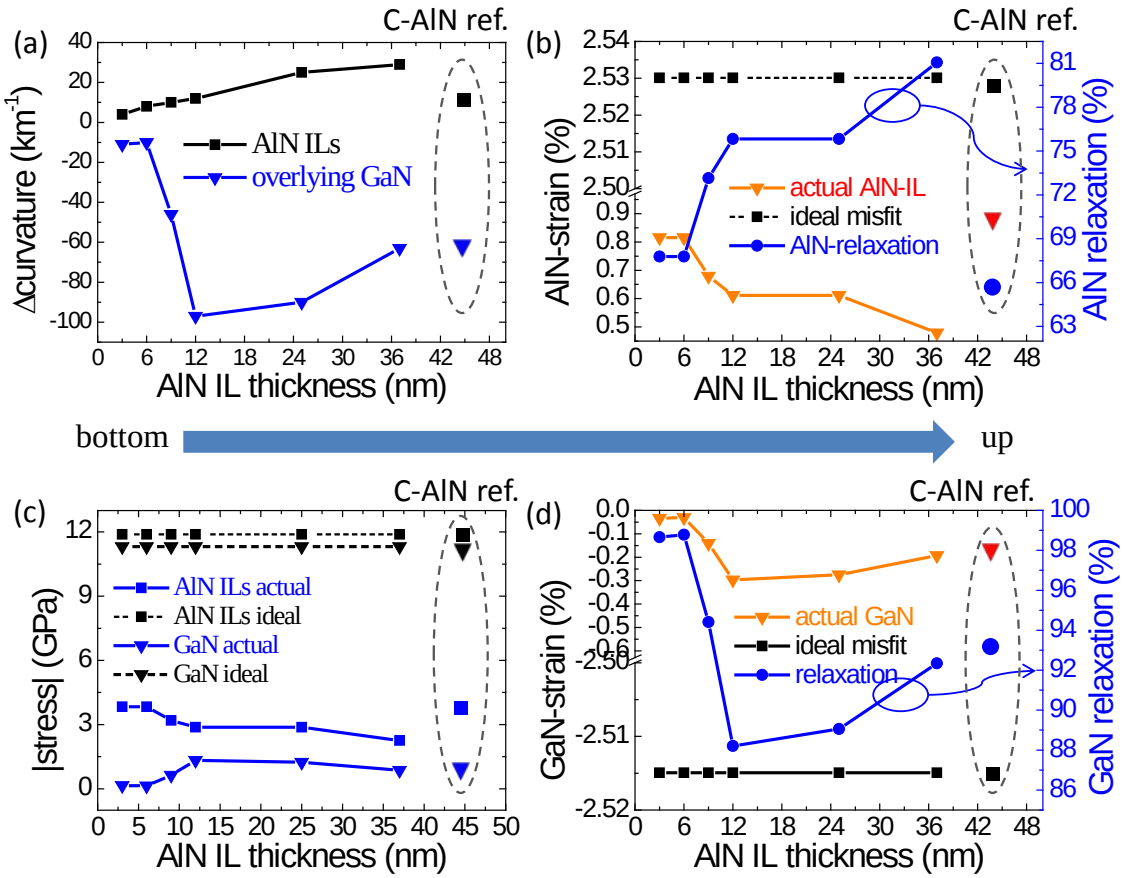


**Fig. 6.2** Experimental results of PI-AlN interlayer test, (a) the curvature increment of AlN and GaN, (b) strain and relaxation of AlN interlayers, (c) stress in AlN and GaN and (d) strain and relaxation of overlying 200-nm-thick GaN.

From the curvature increment results in Fig. 6.2a, largest compressive strain (~ 0.297%) and stress (~ 1.334 GPa) in GaN was brought by 12-nm-thick PI-AlN interlayer. This optimal PI-AlN interlayer thickness is in the same range of that of optimal conventional AlN interlayer from 9 to 12 nm. By observing the strain in AlN interlayers, it could be found that thinner PI-AlN ILs were more strained. Within small thickness (< 6 nm), it was grown more pseudomorphically. Higher strain means larger lattice constant, which is not favorable to induce compressive stress in overlying GaN. It relaxed more as thickness increased. In the thickest 36-nm PI-AlN, sudden relaxation occurred around the thickness of 26 nm (not shown). As shown in Fig. 3.18 and discussed in chapter 3, the same thing also happened in conventional AlN interlayers with thickness exceeding 13 nm. In previous discussion, such sudden relaxation was assigned to cracking. Such interpretation is also reasonable for the relaxation here. That's why the overall strain in 36-nm-thick PI-AlN decreased. Analogous to the case of thick c-AlN ILs, the cost of sudden relaxation was introducing high-density dislocations. In spite of smaller AlN lattice constant due to higher relaxation, the newly introduced high-density defects also caused rapid relaxation and then smaller compressive stress in overlying GaN.

The reference c-AlN interlayer was more strained than PI-AlN ILs. Compared with the c-AlN reference IL in this sample, although the 12-nm-thick PI-AlN worked better, for two reasons, it is hard to say that PI-AlN IL is more efficient than c-AlN IL in terms of stressing overlying GaN compressively. Firstly, 12-nm-thick PI-AlN was better in this particular sample, but it was inferior to the best performance which ever achieved by c-AlN IL. Secondly, the best PI-AlN IL was in the lower part of the sample while the c-AlN reference was in the upper. Empirically, under the same growth conditions, the lower ILs induce more compressive stress in GaN layer than the upper ILs, due to the disadvantageous influence from the underlying layers. However, such influence is ignorable if the number of interlayer is less than 5, since it doesn't change the conclusion. Strictly, for safety and solidity, the result from multi-condition structure should be double-checked by reversing the growth sequence of AlN ILs, or by growing single-condition samples, as that in chapter 3.

What should be noticed is that the performance of reference c-AlN interlayer has been deteriorated in spite of using the same conditions.

The single PI-AlN IL may be not enough to stress the overlying GaN more compressively. If the PI-AlN IL growth conditions were optimized and PI-AlN IL is perfect with high quality, it would grow pseudomorphically on GaN and be highly strained. Highly strained AlN ILs are of larger lattice constant and cause less compressive strain in GaN. As described by the ideal AlN IL model, the lower interface or lower part of it should be relaxed and incoherent to maintain the neutral AlN lattice constant. Therefore, some more relaxed layer should be grown prior to PI-AlN layer. This leads to the combination of low-temperature AlN and PI-AlN in the next section.

## 6.3 Pulse-injection/Low-temperature two-step AlN interlayer

As shown by SEM images in Fig. 3.27 and Fig. 5.3, low-temperature (LT) (≤ 800 ℃) AlN turns to be amorphous or polycrystalline, which is more relaxed than crystalline high-temperature AlN. It is a most promising candidate to produce relaxed lower interface of AlN interlayer. This section is about a test of a new type two-step AlN interlayer, which consists of lower LT-AlN and upper PI-AlN, as represented schematically in Fig. 6.3a. The lower first step of LT-AlN was grown at 600 ℃, with thickness of 6 nm and under V/III ratio of 1503. Growth conditions of the second step PI-AlN were the same as that in last section. In this testing sample, all conditions were kept to be constant while only the thickness of upper PI-AlN was varied from bottom to up, of 12/18/24/36 $nm$ respectively. Curvature increment, strain and stress states in AlN and GaN layers were summarized in Fig. 6.3.

From Fig. 6.3b and d it is clear that highest compressive strain occurred in GaN on 12-nm-thick upper PI-AlN. Similar to the single-layer PI-AlN interlayer, the strain in the upper PI-AlN part also decreased as thickness rose. Interlayer with 12-nm upper PI-AlN was mostly strained. This again confirmed that in thick PI-AlN, the detrimental effect brought by high-density defect introduction during relaxation overtook the advantageous effect of lattice

constant decreasing brought by relaxation. Limited by the number of interlayers, the smaller thickness (< 12 nm) of upper PI-AlN was not tested in this two-step AlN interlayer structure. It is possible that thinner PI-AlN part may has better performance.

Compared with the strain of single-step PI-AlN interlayer in Fig. 6.2b it could be found that the upper part PI-AlN here was more strained. It is not clear that why the PI-AlN part was more strained here, although it was grown on LT-AlN which should make the upper part PI-AlN more relaxed. Even with larger strain, the interlayer with 12-nm-thick upper part of PI-AlN introduced slightly higher compressive than the single-step 12-nm-thick PI-AlN interlayer.

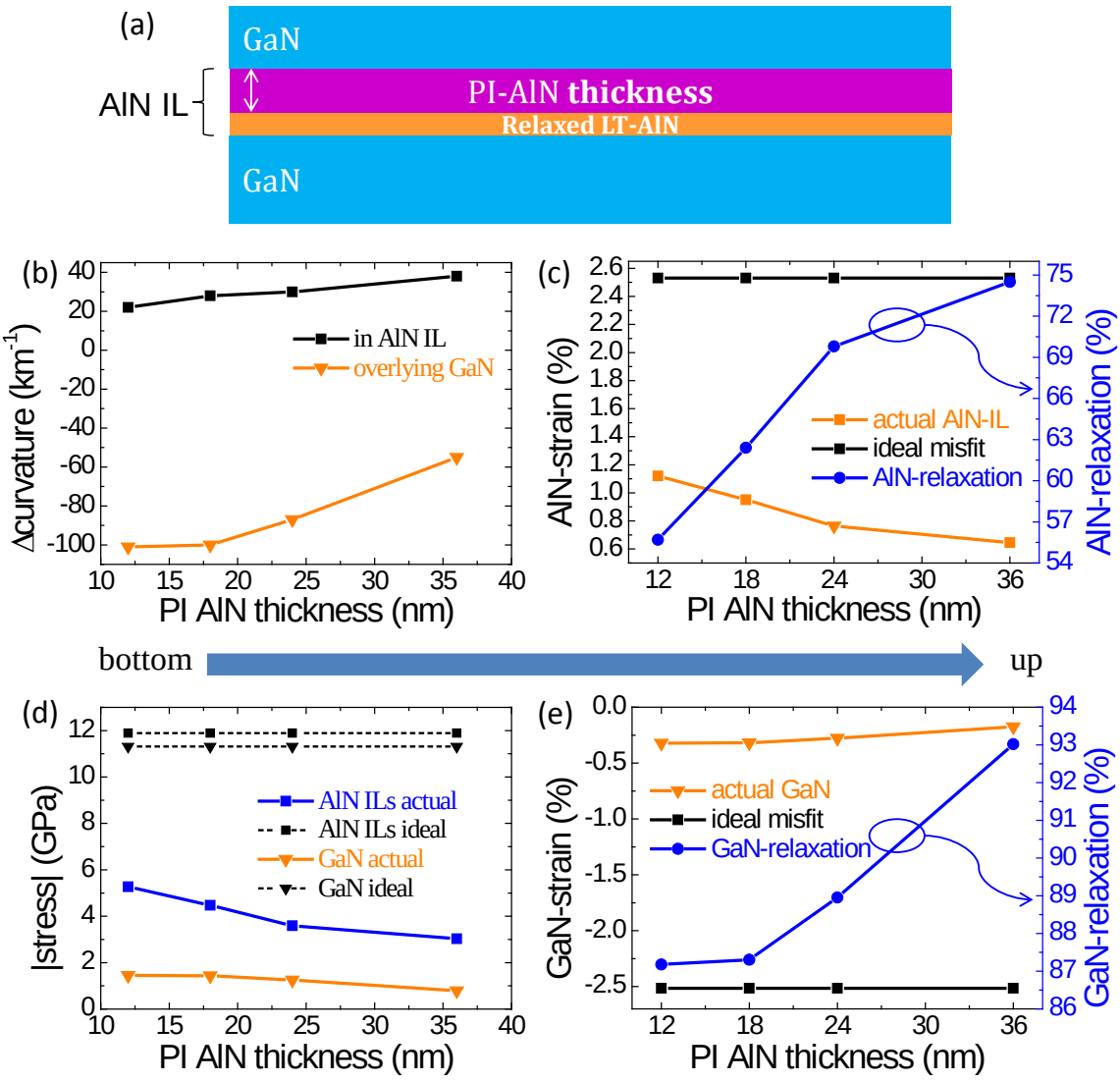


**Fig. 6.3** Experimental results of PI/LT-AlN interlayer test, (a) interlayer structure, (b) the curvature increment of AlN and GaN, (c) strain and relaxation of AlN interlayers, (d) stress in AlN and GaN and (e) strain and relaxation of overlying 200-nm-thick GaN..

## 6.4 High-temperature/Low-temperature two-step AlN interlayer

The combination of lower low-temperature AlN and upper high-temperature (HT) AlN is another routine to approach relaxed lower interface and coherent upper interface of AlN interlayer, as shown in Fig. 6.4 schematically. In this section, this HT/LT-AlN two-step structure was investigated more intensively.


**Fig. 6.4** Structure of HT/LT-AlN two-step interlayer.

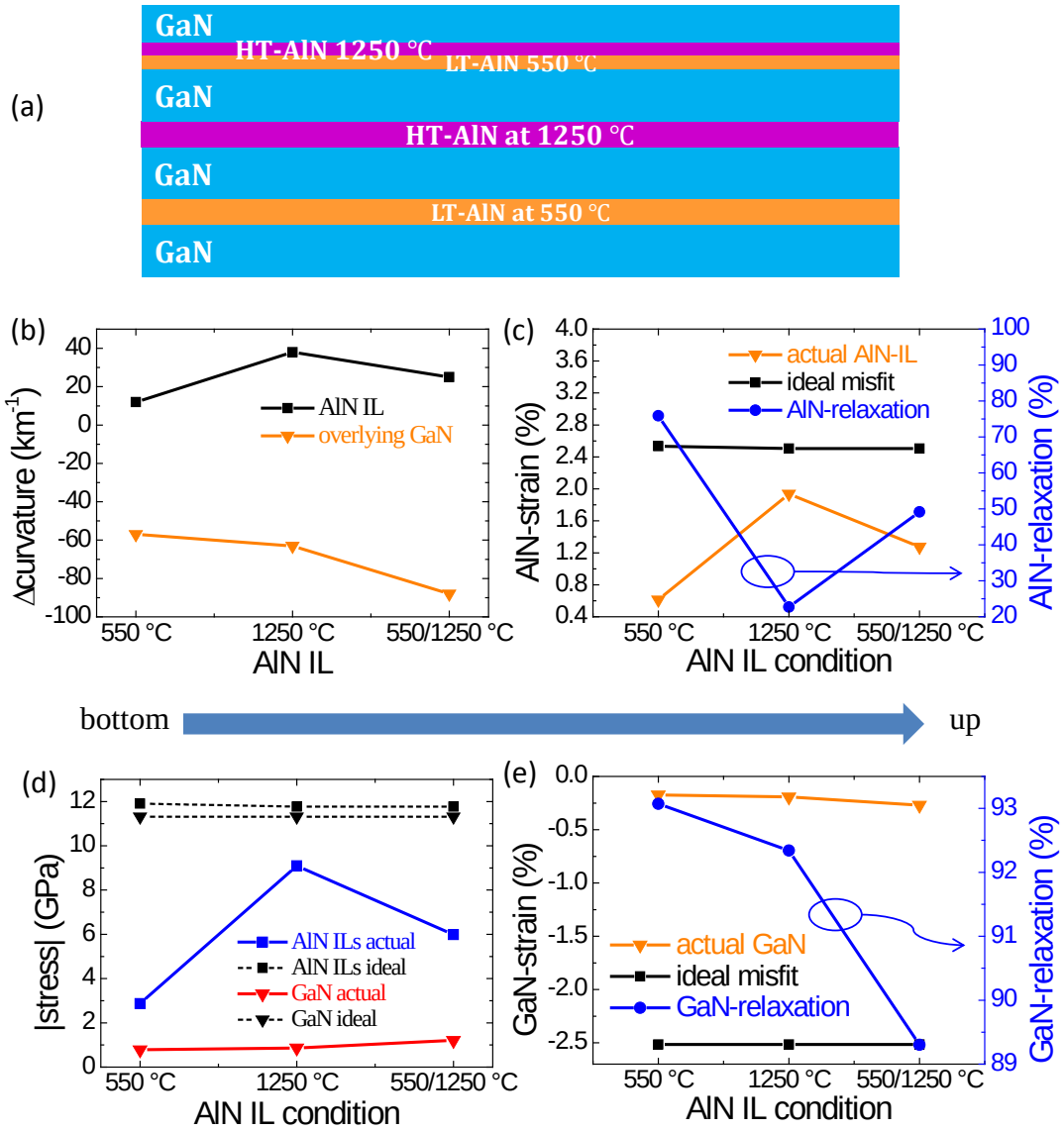


**Fig. 6.5** Experimental results of comparison of one-step and two-step interlayer tests, (a) sample structure, (b) the curvature increment of AlN and GaN, (c) strain and relaxation of AlN interlayers, (d) stress in AlN and GaN and (e) strain and relaxation of overlying 200-nm-thick GaN.

As mentioned above, due to amorphous morphology or crystal domains, LT-AlN should be more relaxed than HT-AlN in spite of its higher theoretical ideal strain at low temperature. With large relaxation, the lattice constant of LT-AlN is more close to its neutral value. It is expected that the upper HT-AlN part can be grown coherently with high-quality (low-density defects) on LT-AlN which would maintain the small lattice constant of the lower part while yielding abrupt coherent upper interface to stress the overlying GaN as much as possible. This is the ideal case.

The first experiment was designed to test the above assumption. There were three AlN interlayers in this sample, with the first two were one-step ILs and the third top one was two-step IL. From bottom to up, the sequence of AlN interlayers was 12-nm-thick one-step LT-AlN grown at 550 ℃, 12-nm-thick one-step HT-AlN grown at 1250 ℃, and 12-nm-thick top two-step IL which consists of lower LT-AlN at 550 ℃ and upper HT-AlN at 1250 ℃, as represented by Fig. 6.5a.

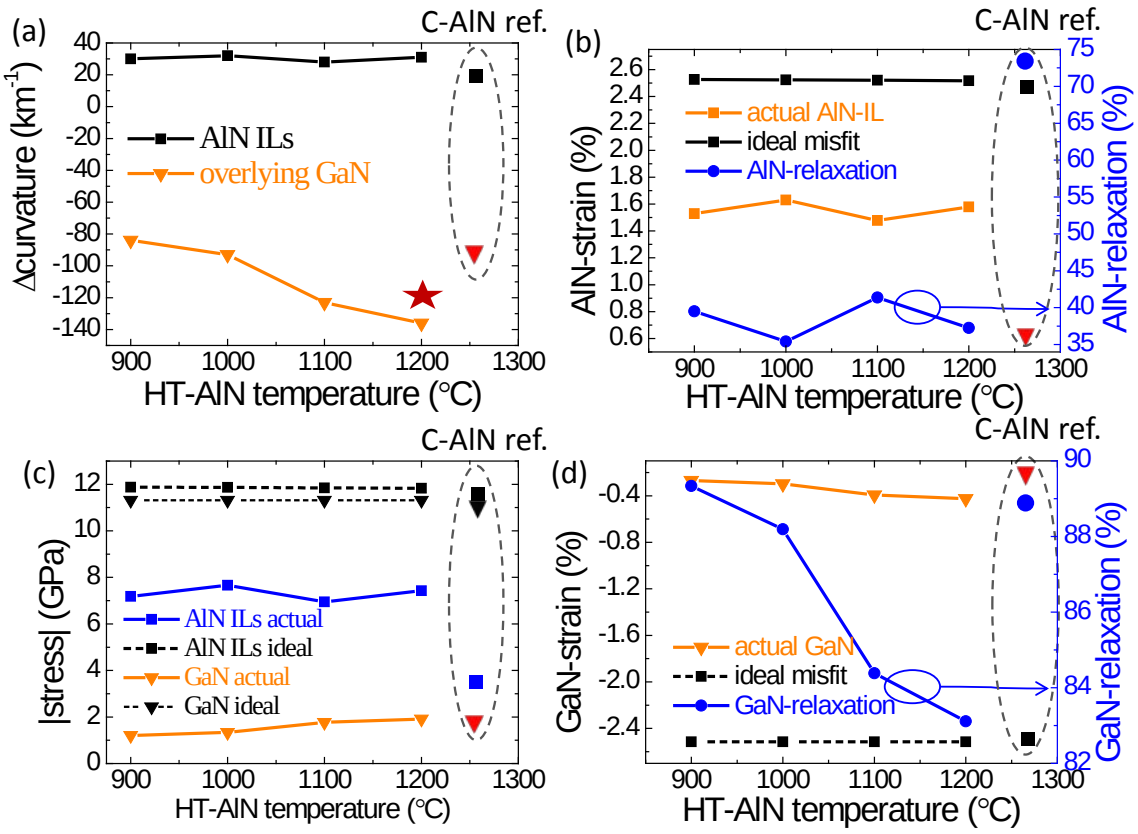


**Fig. 6.6** Experimental results of the effect of growth temperature of the upper HT-AlN part, (a) the curvature increment of AlN and GaN, (b) strain and relaxation of AlN interlayers, (c) stress in AlN and GaN and (d) strain and relaxation of overlying 200-nm-thick GaN.

Although the two-step AlN IL which combined LT and HT AlN was on the top, it still induced the more compressive strain in GaN than the one-step ones either grown at low temperature or high temperature. This directly verified that the ideal AlN model of relaxed lower interface and coherent upper interface was reasonable. HT-AlN may contain Ga diffusion. The LT-AlN was indeed more relaxed than HT-AlN. Another reason that might

enhance the performance of two-step AlN IL was that Ga diffusion from the underlying GaN might had been stopped by the isolation of LT-AlN. As it was pure AlN, it was of smaller lattice constant than AlGaN.

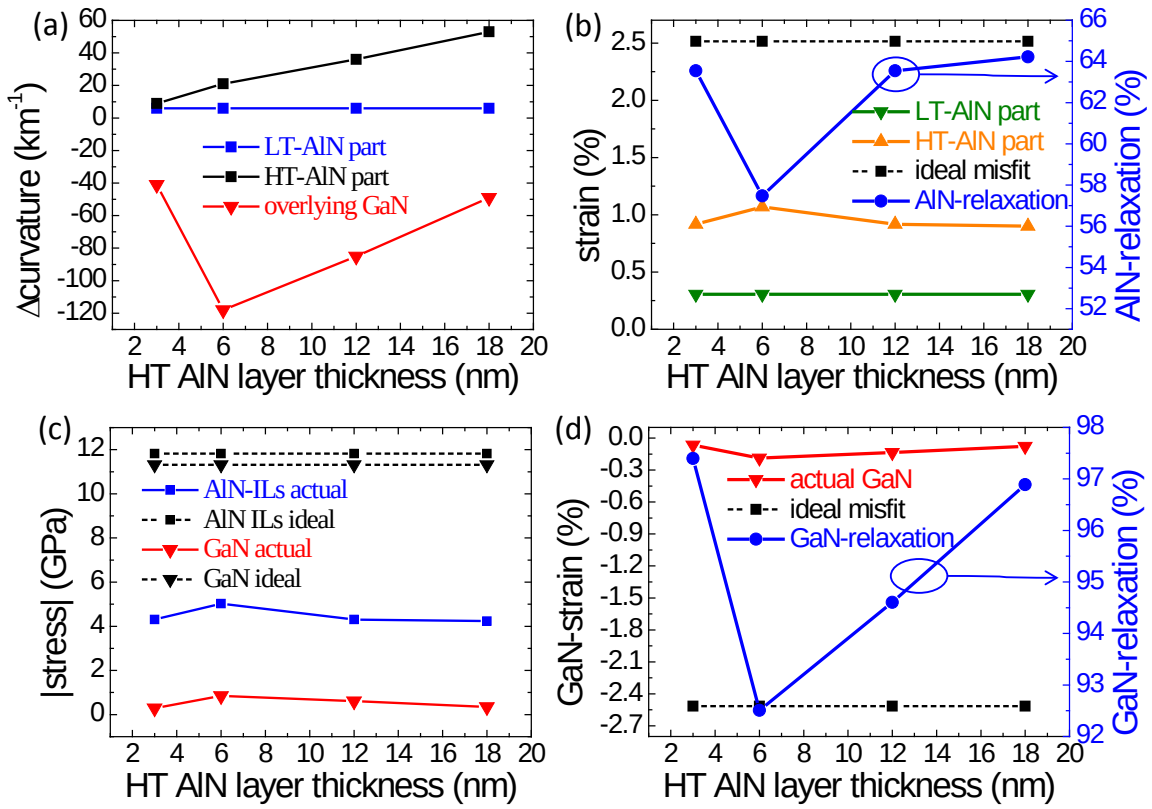


**Fig. 6.7** Experimental results of the effect of thickness of the upper HT-AlN part, (a) the curvature increment of AlN and GaN, (b) strain and relaxation of AlN interlayers, (c) stress in AlN and GaN and (d) strain and relaxation of overlying 200-nm-thick GaN.

The second experiment was assigned to investigate the effect of growth temperature of the upper HT-AlN part. All the ILs were grown using the LT/HT two-step method with constant total thickness of 12 nm. The thickness of LT-AlN and HT-AlN were both kept to be 6 nm. The growth temperature of LT-AlN was fixed to be at 600 ℃ while that of HT-AlN was varied from 1200 ℃ to 900 ℃, with step of 100 ℃.

As shown in Fig. 6.6, the curvature increment, strain and stress in GaN showed strong dependence on the growth temperature of the upper HT-AlN part. The overlying GaN layer was more and more compressively stressed as the growth temperature of HT-AlN increased from 900 ℃ to 1200 ℃. Higher growth temperature of the upper HT-AlN might lead to larger lattice constant of it, but it improved the quality of the upper interface between AlN IL and GaN. This also confirmed that ideal AlN interlayer should have high-quality coherent upper interface. On the contrary, the strain in AlN ILs showed very little dependence on their growth condition, like the ideal misfit strain of AlN on GaN. The two-step IL which had the 1200-℃ upper HT-AlN part induced larger compressive stress in GaN than the best conventional one-step 900-℃ AlN IL in multi-condition sample in Fig. 3.22, but little less than the one-step 900-℃ AlN IL in single-condition sample. This result shows that the two-

step structure of LT- and HT-AlN combination is promising to produce more compressive stress in GaN than conventional one-step AlN IL, as if the growth conditions of it can be optimized further.

The third experiment was designed for searching the optimal thickness of the upper HT-AlN part. The LT-AlN and HT-AlN was grown at 550 ℃ and 1250 ℃ respectively. The thickness of LT-AlN was 6 nm, while the upper HT-AlN thickness was varied from 3 nm to 18 nm.

The summarized results in Fig. 6.7 showed that the optimal thickness of HT-AlN part turned to be around 6 nm. When it was too thin, like 3 nm, AlN IL still held the morphology of LT-AlN, which could not stress the overlying GaN effectively. As it was thickened more, like to 6 nm, it was more strained. But after some critical thickness it started more relaxation accompanied by dislocation generation which is unfavorable to stressing the overlying GaN. This critical thickness was in the range from 6 to 12 nm. The strain of lower LT-AlN was almost constant of 0.31%, which was about one third of that of HT-AlN part.

## 6.5 Conclusion

In this chapter, some prototypes of innovative AlN interlayer were proposed and tested primarily, in order to approach the ideal AlN interlayer model in chapter 3 and 4. The most important points of ideal AlN interlayer model demand smallest lattice constant and high-quality upper interface. There are some strategies might be possible to approach the ideal AlN interlayer.

The first was one-step AlN interlayer grown by the special pulse-injection method. By supplying TMAl and $NH_3$ alternatively, this method was able to grow high-quality AlN at relatively low temperature of 800 ℃. In this growth, effect of the thickness of PI-AlN interlayer was investigated and the optimal thickness was shown to be around 12 nm. Thinner ones were more strained and of larger AlN lattice constant. Thicker ones were more relaxed but high-density dislocations might be generated and that was detrimental to inducing compressive strain in GaN.

The second type was two-step AlN interlayer which consisted of underlying LT-AlN and overlying PI-AlN. LT-AlN was introduced to produce relaxed lower interface of the interlayer to yield smaller lattice constant of it. The influence of the thickness of PI-AlN part has also been studied and the one with PI-AlN thickness of 12 nm caused highest compressive strain in GaN.

The third type was also two-step AlN interlayer but the upper PI-AlN in the second type was replaced by high-temperature AlN to produce high-quality upper interface of the interlayer. The two-step HT/LT-AlN interlayer induced larger compressive strain in GaN than the single individual HT- or LT-AlN interlayer. Moreover, if the growth temperature of the upper HT-AlN was higher, it performed better since higher growth temperature led to higher quality of it and then more coherent upper interface. These two experiments strongly supported the concept of ideal AlN interlayer model. Like the conventional one-step AlN

interlayer or PI-AlN interlayer, there also existed an optimal thickness of the upper HT-AlN, which was around 6 nm.

Here what should be noted is that the novel interlayers in this chapter may be more advantageous to GaN quality improvement than conventional AlN interlayer in chapter 3. It was learned that conventional AlN interlayer which was good for inducing compressive stress in GaN might not be favorable for GaN quality since its small thickness and high density of non-coalesced grain boundary which acts as the source of dislocations. The latest result (not shown) demonstrated that the upper surface of HT/LT-AlN IL was of better morphology (smoother and coalesced) than conventional single-step interlayer. As the quality of the upper part of the novel interlayer was elevated, the density of newly generated dislocations may decrease.

## References


[1] A. Thon and T.F. Kuech,Applied Physics Letters ***69***, 55(1996).

[2] I. Waki, C. Kumtornkittikul, Y. Shimogaki, and Y. Nakano,applied Physics Letters ***82***, (2003).

[3] N. Iizuka, K. Kaneko, and N. Suzuki,Applied Physics Letters ***81***, (2002).

[4] J.-S. Yang, H. Sodabanlu, I. Waki, M. Sugiyama, Y. Nakano, and Y. Shimogaki,Low Temperature Metal Organic Vapor Phase Epitaxial Growth of AlN by Pulse Injection Method at 800 °C, Japanese Journal of Applied Physics ***46***, L927(2007).

[5] J.-S. Yang, H. Sodabanlu, I. Waki, M. Sugiyama, Y. Nakano, and Y. Shimogaki,Process design of the pulse injection method for low-temperature metal organic vapor phase epitaxial growth of AlN at 800°C, Journal of Crystal Growth ***311***, 383(2009).

# 7 Conclusions

This work has been devoted to the clarification of basic growth mechanism of GaN on Si employing AlN buffer layer and AlN interlayers, including the stress behavior of both GaN and AlN layers as well as the influence of AlN buffer and interlayers on the quality of GaN, based on the in-situ curvature monitoring and other characterizations. The originalities of this work which are distinguishing from the studies in previous reports and publications are summarized as follows.

(1) A model of ideal AlN interlayer to induce compressive stress in GaN layers has been proposed, based on systematic in-situ curvature monitoring and morphology observations. This model has pointed out the key features that ideal AlN interlayer should possess, which are small lattice constant close to neutral AlN and high-quality coherent upper interface of it. In most of the cases small lattice constant of the interlayer demands relaxed lower interface of it. This model has never been proposed in previous publications. Before this, people didn't know what kind of AlN interlayer they should grow.

(2) A routine of arbitrary wafer bow design has been discovered and a program to realize it has been produced. Prior to applying this routine, the strain and stress states in every individual AlN and GaN layer under certain growth conditions should have been known. After setting the mechanical properties of AlN and GaN layers, arbitrary wafer bow design is available. This routine was put forward for the first time.

(3) Prototypes of innovative AlN interlayers have been invented and tested, following the model of ideal AlN interlayer. They are one-step pulse-injection method AlN IL, two-step low-temperature/pulse-injection AlN IL and two-step low-temperature/high-temperature AlN IL. All the interlayers employed in previous studies were one-step conventional AlN. These new AlN ILs grown by special methods or with special structure have proved the reliability of the ideal AlN IL model and are induced larger compressive strain in GaN than normal conventional AlN ILs.

The work flow started with demonstration of successful GaN growth on Si (111) substrate by clearing all obstacles. Following the sample structure, conventional AlN buffer layer and AlN interlayer were investigated successively, including their growth conditions, stress introduction in overlying GaN and influence on GaN quality. Then based on the in-situ curvature monitoring data, strain states in every layer were analyzed and model of ideal AlN interlayer and a routine of arbitrary bow design were proposed. In the end, three prototypes of innovative AlN interlayer were designed and tested.

In chapter 1, the benefits of GaN-on-Si has been given, which were cost reduction by using Si substrate and the advantages of combining nitrides and silicon. The basic difficulties of the growth of GaN on Si lie in the large lattice constant mismatch (~ 17%) and thermal expansion coefficient mismatch (~ 54%) between them. Previous research in this field has been reviewed. The targets, new study objects and strategies of this work have been

introduced. This work aimed at understanding and clarifying the stress control mechanism and the roles of AlN buffer layer and AlN interlayers in the growth of GaN on Si.

In chapter 2, the obstacles to successful GaN growth on Si were introduced and cleared. Growth method of MOVPE and characterization methods like in-situ curvature monitoring, SEM and XRD were reviewed briefly. The most serious difficulties included Si melt-back, Si surface nitridation and the stability of growth environment inside the reactor. There were many factors to facilitate Si melt-back, such as the adsorption of H atoms and cleanliness of Si surface, Ga contamination on Si surface from the parts in the reactor prior to the growth of AlN buffer layer, and most importantly the quality of AlN buffer layer. The first factor can be cleared away by improving the wet and thermal cleaning procedure outside and inside the reactor respectively. Ga contamination can be eliminated by using clean liner tube and susceptor parts, or AlN coating of the inner of reactor. Nothing was working to stop Si melt-back if the AlN buffer quality was poor. Finally, after changing for new gas purifiers, AlN buffer quality was improved significantly and Si melt-back was eliminated. Nitridation of Si surface was avoided by pre-flowing TMAl source, 10 s under flow rate of 22 sccm. Proper TMAl pre-flow also improved the GaN quality substantially. The chemical environment inside the reactor should be kept to be constant to yield controllable growth. The most important point was deposited GaN or Ga should be covered since they may cause Ga contamination on Si surface. Therefore, AlN coating or AlN dummy growth should be performed prior to every growth of GaN on Si. Based on the efforts above, a procedure of growing GaN on Si was outlined in the end.

In chapter 3, it was experimental observation of how to adjust curvature or wafer bow. Curvature can be adjusted by tuning the quality of AlN buffer layer which determines the stress in the 1$^{st}$ GaN, changing the growth conditions and the number of AlN interlayers, and tuning the growth mode and thickness of the 1$^{st}$ GaN. Before experimental results, theories of strain relaxation had been reviewed briefly, to interpret the strain behaviors of the layers. AlN buffer layer is important for both of the strain and quality of the 1$^{st}$ GaN. The AlN buffer with higher quality caused more compressive strain in the overlying GaN. There was a strain relaxation process during the growth of the 1$^{st}$ GaN through its thickness. It was initially compressively strained. The strain transited from being compressive to tensile as the thickness increased. However, the relaxation speed was depending on the growth conditions and quality of AlN buffer layer. The relaxation was very rapid and the critical thickness from being compressive strain to tensile was only several hundreds of nanometers, if the AlN buffer quality was low, such as grown at 1000 ℃. This was because of high-density defects in AlN buffer propagated into or caused more dislocations in overlying GaN and led to more rapid relaxation in GaN. The best AlN buffer layer which induced most compressive strain was grown at 1250 ℃, under V/III ratio of 3005 and with thickness of 110 nm. Growth conditions of conventional one-step AlN interlayers were studied intensively, including thickness from 4.5 nm to 45 nm, growth temperature from 600 ℃ to 1200 ℃ and V/III ratio from 115 to 9015. The investigated growth condition ranges were very large compared with other studies. Optimized AlN interlayer which induced the most compressive strain in GaN was grown at 900 ℃, under V/III ratio of 1503 and with thickness of 9 nm. If it was too thin, it consisted of neighboring separated grain domains. In too thick AlN IL, cracking occurred.

Both lost the capability of inducing compressive strain in GaN. If the growth temperature was too low like 600 ℃, although with smaller lattice constant, since it was amorphous and not coalesced, the GaN on it relaxed rapidly. In high-temperature (> 1000 ℃) ones, Ga diffusion into the interlayer happened, formed AlGaN with lattice constant more close to GaN and then small compressive strain in GaN. V/III has minimal influence on the performance of AlN IL if it was in the range from 500 to 1500. A model of ideal AlN IL was proposed based on the observations above, with relaxed incoherent lower interface and high-quality coherent upper interface.

In chapter 4, the strain and stress states in every stage including growth and temperature ramping was analyzed theoretically employing the basic Stoney equation. Based on the review of stress generation mechanisms in heterostructure, methodology of analysis was built. Only growth stress and thermal mismatch stress was considered during growth and temperature ramping respectively. The tensile strain of AlN buffer layer ranged from 0.25% to 0.5% while the ideal misfit strain of AlN on Si is about 23.2%, which indicates that AlN buffer on Si is almost completely relaxed. The tensile strain decreases as the growth temperature is elevated. Such relaxation is favorable to stressing overlying GaN more compressively. Depending on the growth conditions of AlN buffer layer, the relaxation speed from compressive (~ -0.45%) to tensile strain (~ 0.05%) differs in the 1$^{st}$ GaN. The thickness of neutral point is only about 600 nm if the quality of AlN buffer is poor such as grown at

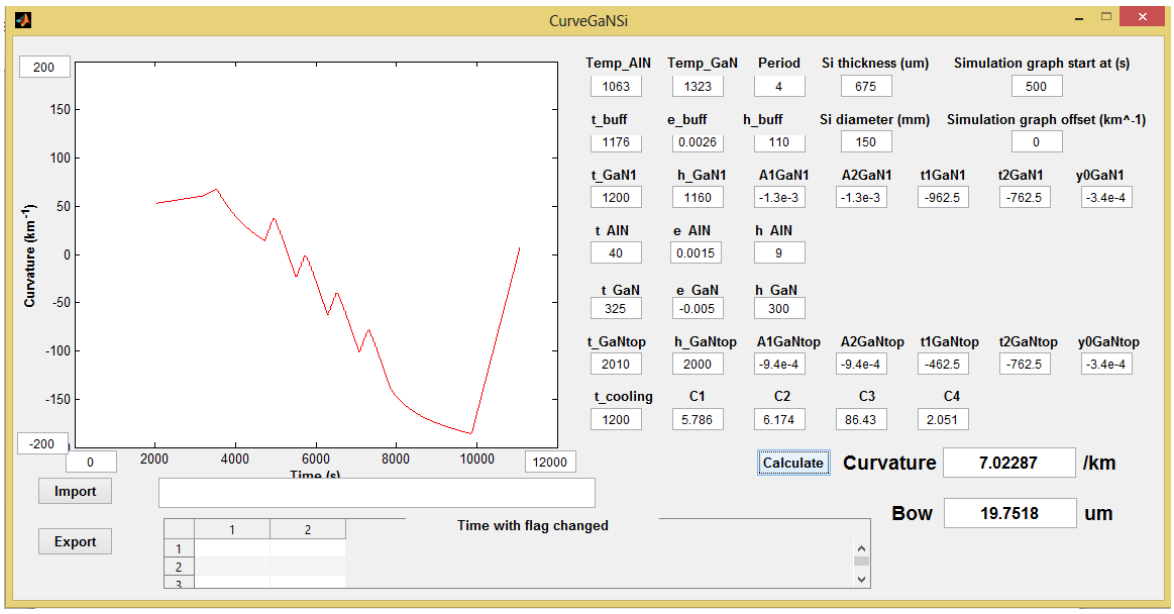


**Fig. 7.1** An example of 6-inch crack-free structure design for GaN-on-Si.

**Table 7.1** Structure design of 6-inch crack-free GaN-on-Si.

| Layer | AlN buffer | 1$^{st}$ GaN | AlN IL | GaN on ILs | Top GaN |
|---|---|---|---|---|---|
| **Strain (%)** | 0.26 | -0.13*(exp(-h*10$^{-9}$/962.5)+exp(-h*10$^{-9}$/762.5))-3.4*10$^{-2}$ | 0.15 | -0.50 | -9.4*10$^{-2}$*(exp(-h*10$^{-9}$/452.5)+exp(-h*10$^{-9}$/762.5))-3.4*10$^{-2}$ |
| **Stress (GPa)** | 1.220 | Strain*450 | 0.705 | -2.25 | Strain*450 |
| **Thickness (nm)** | 110 | 1160 | 9 | 300 | 2000 |

h: thickness of that layer of GaN.

1100 ℃. On the best AlN buffer, compressive strain through the large thickness of 1.75 um can be maintained. In spite of smaller lattice constant between AlN and GaN, tensile strain in AlN interlayers is much higher than that in AlN buffer, which ranges from 1.45% to 1.9%. The relaxation was in the range from 22% to 42%, which is about only one third of that in AlN buffer. These results show that the crystal quality of AlN interlayers is better than that of AlN buffer layer. The largest compressive strain in GaN layers is about 0.45% on AlN interlayer grown at 900 ℃ and with thickness of 9 nm, which is the same of the initial value of the 1$^{st}$ GaN. This leads to compressive stress of about 2 GPa in GaN and is 2~3 times of that in previous publications. Curvature due to thermal stress was also calculated. Based on the strain and stress states in every individual stage, the curvature curve can be recovered and the final curvature and wafer bow can be predicted, using the arbitrary bow design program. The size of Si wafer which the curvature and wafer bow is easiest to be controlled is 6 inch, 150 mm. An example of bow design for 6-inch GaN-on-Si wafer was given in Fig. 7.1 and Table 7.1, as long as the strain distribution in every layer can be the set values in the table.

In chapter 5, factors which influence the GaN quality were studied. Quality elevation of AlN buffer layer and 3D growth mode are the most effective methods to improve the quality of GaN. The same with compressive stress introduction in the 1$^{st}$ GaN, it also demands high-quality AlN buffer layer to produce high-quality GaN, since the defects in the buffer can propagate into overlying GaN and they can also act as defect sources to generate new dislocations in GaN. Using conventional AlN, higher quality is achieved at higher temperature, 1250 ℃ in this work, under mediate V/III ratio of 3005. By alternating growth mode from 2D to 3D, the FWHM of XRD rocking curves of the plane (10-10) reduced from 820 arcsec to 570 arcsec while that of (0002) plane keeps almost constant. Thick AlN interlayer (≥ 22 nm) is favorable to the reduction of dislocations in GaN, but not for stress inducing. Since it doesn't coalesce completely, thin AlN IL (< 13 nm) increase the dislocation density in GaN by introducing new defects at the grain domain boundaries. With small thickness from 6 to 9 nm, growth temperature has slight influence on dislocation density in GaN. Blue LEDs has been demonstrated.

In chapter 6, following the key features of ideal AlN interlayer, concepts of innovative prototypes of AlN interlayers were designed and tested, including one-step pulse-injection method AlN IL and two-step IL consists of lower low-temperature AlN and upper pulse-injection AlN or high-temperature AlN. Optimal thickness of PI AlN is around 12 nm in one-step sample. In two-step sample, the lower LT-AlN was grown at 550 ℃ or 600 ℃. In the structure of LT/PI-AlN, in the range of thickness > 12 nm, the thickness of upper PI-AlN shows the smallest the best. In the structure of LT/HT-AlN, the growth temperature of HT-AlN higher is better such as 1200 ℃, with optimal thickness around 6 nm. They confirmed the solidity of ideal AlN model and showed the same performance of the best conventional AlN. For that the growth conditions of them were not optimized, more compressive strain in overlying GaN on them can be expected.

This work has achieved the targets of understanding the role of AlN layers, especially the key features of AlN interlayers and producing a program to design arbitrary wafer bow. Crack-free up to 3-um-thick GaN was realized on 2-inch Si wafer. Promising innovative AlN

interlayers were proposed and tested. The quantitative comparison between the performance of AlN buffer layer, AlN interlayer and GaN in this work and previous publications is shown in the tables. The performances of them are competitive. Quantitative results of this work compared with previous studies were summarized in Fig. 7.2. The compressive stress in GaN layers achieved 2.1 GPa (> 1.6 GPa). FWHM of XRD rocking curve of (0002) plane of this work is higher than that on sapphire, while the result of (10-10) plane (~ 550 arcsec with thickness of 1.7 um without interlayers) was on the same level of that on sapphire (~ 500 arcsec).

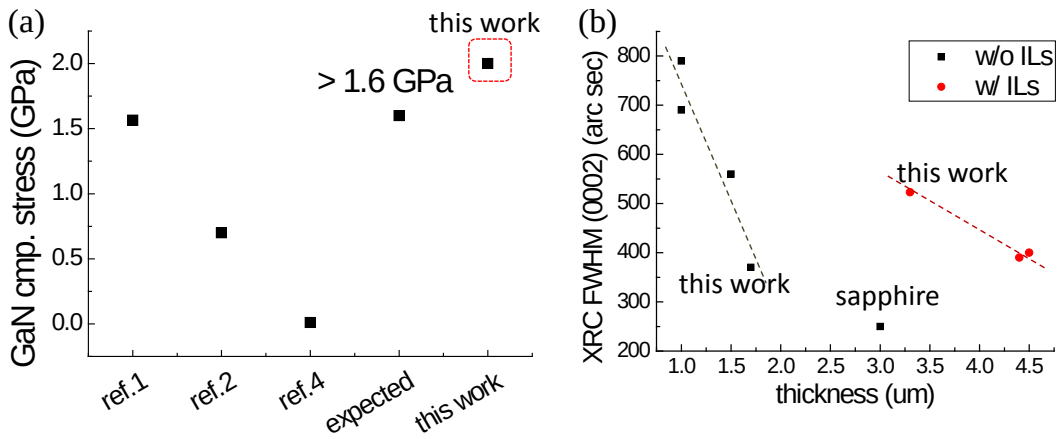


**Fig. 7.2** Comparison of (a) compressive stress in GaN layers and (b) GaN quality between this work and previous studies. References are the same as those in Fig. 1.7 in chapter 1.

In the end by the way, in Appendix B, voids formation due to hydrogen etching of GaN has been observed. Voids are formed after the growth of AlN interlayers and prior to the growth of overlying GaN. It is unfavorable to stress control of GaN-on-Si and has minimal influence on GaN quality. The light scattering effect of them has potential application to devices like solar cells and LEDs. It can be avoided by protecting GaN by supplying high flow rate of $NH_3$ above 1000 sccm. Careful attention should be paid to GaN decomposition during the growth, especially at high temperature > 1000 ℃ and under low flow rate of $NH_3$ < 500 sccm.

# Appendix A Program for predicting curvature and wafer bow

```
function Calculate_Callback(hObject, eventdata, handles)
% hObject    handle to Calculate (see GCBO)
% eventdata  reserved - to be defined in a future version of MATLAB
% handles    structure with handles and user data (see GUIDATA)

rawfile = get(handles.rawfile,'Data');

hSi = str2double(get(handles.Si_thick,'String'))*1e-6;    %m
MGaN = 450;
MAlN = 470;
MSi = 228;


alpha_AlN = @(T) (6090930425698157*T)/184467440737095516160000000 -
(1913*exp(412932347673824389/562949953421312000 - (71*T)/16000))/312500000
+ 1913/312500000;

alpha_GaN =@(T) (945810685519273*T)/4611686018427387904000000 -
(57859*exp(432959582156388961706758391636 81/811296384146066816957890051440 6
4 - (7118713830194977*T)/1152921504606846976))/10000000000 +
57859/10000000000;

alpha_Si =@(T) (511712680604703*T)/922337203685477580800000 -
(149*exp(4557/6250 - (147*T)/25000))/40000000 + 149/40000000;


Temp_AlN = str2double(get(handles.Temp_AlN,'String'));    %K
Temp_GaN = str2double(get(handles.Temp_GaN,'String'));    %K
period = str2double(get(handles.period,'String'));


e_buff = str2double(get(handles.e_buff,'String'));
h_buff = 1e-9*str2double(get(handles.h_buff,'String'));    %m
t_buff = str2double(get(handles.t_buff,'String'));      %s

t_GaN1 = str2double(get(handles.t_GaN1,'String'));      %s
h_GaN1 = 1e-9*str2double(get(handles.h_GaN1,'String'));   %m
A1GaN1 = str2double(get(handles.A1GaN1,'String'));    %s
A2GaN1 = str2double(get(handles.A2GaN1,'String'));    %s
t1GaN1 = str2double(get(handles.t1GaN1,'String'));    %s
t2GaN1 = str2double(get(handles.t2GaN1,'String'));    %s
y0GaN1 = str2double(get(handles.y0GaN1,'String'));    %s


t_AlN = str2double(get(handles.t_AlN,'String'));         %s
h_AlN = 1e-9*str2double(get(handles.h_AlN,'String'));       %m
e_AlN = str2double(get(handles.e_AlN,'String'));
t_GaN = str2double(get(handles.t_GaN,'String'));        %s
h_GaN = 1e-9*str2double(get(handles.h_GaN,'String'));     %m
e_GaN = str2double(get(handles.e_GaN,'String'));

t_GaNtop = str2double(get(handles.t_GaNtop,'String'));    %s
```

```
h_GaNtop = 1e-9*str2double(get(handles.h_GaNtop,'String')); %m
A1GaNtop = str2double(get(handles.A1GaNtop,'String'));    %s
A2GaNtop = str2double(get(handles.A2GaNtop,'String'));    %s
t1GaNtop = str2double(get(handles.t1GaNtop,'String'));    %s
t2GaNtop = str2double(get(handles.t2GaNtop,'String'));    %s
y0GaNtop = str2double(get(handles.y0GaNtop,'String'));    %s

t_cooling = str2double(get(handles.t_cooling,'String'));    %s
C1 = str2double(get(handles.C1,'String'));    %s
C2 = str2double(get(handles.C2,'String'));    %s
C3 = str2double(get(handles.C3,'String'));    %s
C4 = str2double(get(handles.C4,'String'));    %s

startcurve = str2double(get(handles.startcurve,'String'));
offset = str2double(get(handles.offset,'String'));
x_min = str2double(get(handles.x_min,'String'));
x_max = str2double(get(handles.x_max,'String'));
y_min = str2double(get(handles.y_min,'String'));
y_max = str2double(get(handles.y_max,'String'));

% Cintergrate = @(M, A1, A2, t1, t2, y0, x)
6*M*(A1*exp(x/t1)+A2*exp(x/t2)+y0)/MSi/hSi^2*1000; %km^-1
Cconstant = @(M,e,h) 6*M*e*h/MSi/hSi^2*1000;   %km^-1
Ccooling = @(M, h, c1, c2, c3, c4, T) 6*M*h*((3.725*(1-exp(-5.88e-3*(T-
124.0)))+5.548e-4*T)*1e-6-(c1*(1-exp(-c2*1e-3*(T-c3)))+c4*1e-4*T)*1e-
6)/MSi/hSi^2*1000; %km^-1
%--------- Initial values ----------
Time = 1539;
Curve = 53;
%---------- First AlN buffer ----------
A = Time(length(Time)):(Time(length(Time))+t_buff);
B = linspace(Curve(length(Curve)),Curve(length(Curve))+Cconstant(MAlN,
e_buff, h_buff),length(A));
Time = [Time A];
Curve = [Curve B];

A = Time(length(Time)):(Time(length(Time))+320);    %4 min interval to next
growth
B = linspace(Curve(length(Curve)),Curve(length(Curve))+30,length(A));
Time = [Time A];
Curve = [Curve B];

%---------- First GaN  ----------
A = Time(length(Time)):(Time(length(Time))+t_GaN1);
B = zeros(1,length(A));
accumulate_thickness = h_GaN1/t_GaN1;
B(1) = Curve(length(Curve));
for j = 1:length(B)-1
    strainGaN_1 =
A1GaN1*exp(accumulate_thickness*1e9/t1GaN1)+A2GaN1*exp(accumulate_thickness
*1e9/t2GaN1)+y0GaN1;
    curve_increment_GaN_1 =
6*MGaN*strainGaN_1*h_GaN1/t_GaN1/hSi/hSi/MSi*1000;
    B(j+1) = B(j)+curve_increment_GaN_1;
    accumulate_thickness = accumulate_thickness + h_GaN1/t_GaN1;
end
Time = [Time A];
Curve = [Curve B];

A = Time(length(Time)):(Time(length(Time))+200);
```

```
C_GaN_AlN = -
2000*6/MSi/hSi^2*((MGaN*h_GaN1+MAlN*h_buff)*quad(@(T)alpha_Si(T),Temp_AlN,T
emp_GaN)+(MGaN*h_GaN1-
MAlN*h_buff)*quad(@(T)alpha_AlN(T),Temp_AlN,Temp_GaN)-
2*MGaN*h_GaN1*quad(@(T)alpha_GaN(T),Temp_AlN,Temp_GaN));
B = linspace(Curve(length(Curve)),Curve(length(Curve))+C_GaN_AlN,length(A));
Time = [Time A];
Curve = [Curve B];

%-------------- Loop for AlN and GaN  ------------
for i = 1:period
    A = Time(length(Time)):(Time(length(Time))+t_AlN);
    B =
linspace(Curve(length(Curve)),Curve(length(Curve))+Cconstant(MAlN,e_AlN,
h_AlN),length(A));
    Time = [Time A];
    Curve = [Curve B];

    A = Time(length(Time)):(Time(length(Time))+210);    %3 min interval
    B = linspace(Curve(length(Curve)),Curve(length(Curve))-
C_GaN_AlN,length(A));
    Time = [Time A];
    Curve = [Curve B];

    A = Time(length(Time)):(Time(length(Time))+t_GaN);
    B =
linspace(Curve(length(Curve)),Curve(length(Curve))+Cconstant(MGaN,e_GaN,
h_GaN),length(A));
    Time = [Time A];
    Curve = [Curve B];

    A = Time(length(Time)):(Time(length(Time))+210);    %3 min interval
    B =
linspace(Curve(length(Curve)),Curve(length(Curve))+C_GaN_AlN,length(A));
    Time = [Time A];
    Curve = [Curve B];
end

Time = Time(1:(length(Time)-length(A)));        %delete last interval
Curve = Curve(1:(length(Curve)-length(B)));

A = Time(length(Time)):(Time(length(Time))+t_GaNtop);
B = zeros(1,length(A));
accumulate_thickness = h_GaNtop/t_GaNtop;
B(1) = Curve(length(Curve));
for j = 1:length(B)-1
    strainGaN_top =
A1GaNtop*exp(accumulate_thickness*1e9/t1GaNtop)+A2GaNtop*exp(accumulate_thi
ckness*1e9/t2GaNtop)+y0GaNtop;
    curve_increment_GaN_top =
6*MGaN*strainGaN_top*h_GaNtop/t_GaNtop/hSi/hSi/MSi*1000;
    B(j+1) = B(j)+curve_increment_GaN_top;
    accumulate_thickness = accumulate_thickness + h_GaNtop/t_GaNtop;
end
Time = [Time A];
Curve = [Curve B];

A = Time(length(Time)):(Time(length(Time))+t_cooling);
```

```
B = linspace(Curve(length(Curve)),Curve(length(Curve))+0.95*quad(@(T)
Ccooling(MGaN, h_GaN1+h_GaN*i+h_GaNtop, C1, C2, C3, C4, T), Temp_GaN,
300),length(A));
Time = [Time A];
Curve = [Curve B];

%-------------- ploting ------------
cla(handles.Graph);

plot(handles.Graph,Time+startcurve,Curve+offset,'Color','r');

hold (handles.Graph,'on');
testraw = size(rawfile);
if testraw(2) == 3
    plot(handles.Graph,rawfile(:,1), rawfile(:,2));
    plot(handles.Graph,rawfile(:,1),20*rawfile(:,3));
end


set(handles.Graph,'Xlim',[x_min x_max],'Ylim',[y_min y_max]);
set(get(handles.Graph,'XLabel'),'String','Time
(s)','fontsize',10,'fontweight','b');
set(get(handles.Graph,'YLabel'),'String','Curvature (km^-
^1)','fontsize',10,'fontweight','b');

Si_dia = str2double(get(handles.Si_dia,'String'))*1e-3;    %m
bowing = (Si_dia)^2*Curve(length(Curve))/8*1e3;            %um
set(handles.Curve,'String',Curve(length(Curve)));
set(handles.Bow,'String',bowing);
set(handles.XC,'Data',[Time; Curve]);
```

# Appendix B Void formation and its effects

During the growth of GaN on Si (111), voids were found in GaN layers in between AlN interlayers. Void formation mechanism is the decomposition of GaN in $H_2$ and this was introduced in section B.1. Void formation process was carefully studied in section B.2. It was clarified that voids were formed during the period between the growths of two neighbouring GaN layers, after the growth of AlN interlayer between them. There are some openings in AlN interlayers and they act as the pass for $H_2$ to react with GaN. Conditions such as $NH_3$ partial pressure, temperature, etching time, and the thickness of AlN interlayers could be utilized to tune the volume, size and shape of the voids. The effects of voids on curvature and properties of GaN were studied in section B.3. Voids can scatter the lights and act as anti-reflectance structure in solar cells. The potential application is why it is described here.

## B.1 Introduction

Although 8-inch GaN on Si (111) is available at present, people generally have to grow more than 10 um thick GaN to obtain acceptable device level quality [1]. Long growth time and thick film pushes up the cost substantially. On the other hand, for LEDs on GaN-on-Si, which is the dominating product of this industry, a part of emitted light is absorbed by Si substrate. It was found that some voids can be formed in GaN layers which are in between AlN interlayers (ILs). AlN ILs were applied to introduce compressive stress in GaN layers to compensate tensile stress during cooling for GaN on Si. In this study, it was tried to investigate whether these voids are beneficial to relieve the two problems above or not.

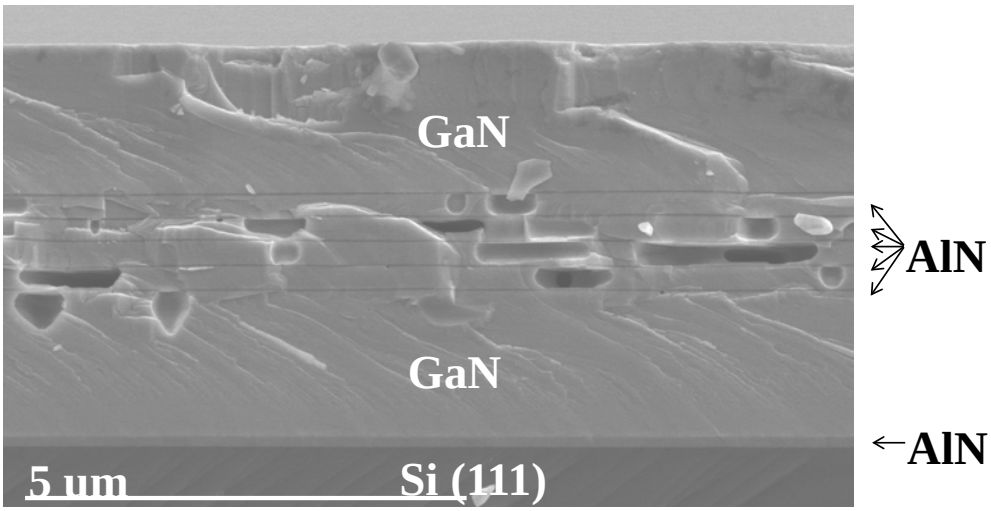


**Fig. B.1** Voids in GaN layers.

The voids were formed by etching effect of hydrogen on GaN. Detailed mechanisms of this phenomenon had been studied, based on the decomposition of GaN in hydrogen atmosphere, including factors of temperature, pressure, ammonia partial pressure, time and

so on [2-4]. Using this effect, one can tune the nucleation layer to improve the quality of GaN [5], control layer composition [6], growth anisotropies and surface quality [7, 8], and pattern GaN to improve its quality and produce free-standing GaN template. In the growth of GaN/InGaN multi-quantum wells, this effect should be suppressed to protect GaN barriers. Otherwise they can be etched and abrupt interface between the barriers and wells cannot be formed then the performances of LEDs or solar cells based on it would deteriorate seriously. In all these previous studies, GaN was grown on sapphire and exposed directly in hydrogen ambiance. In this work, GaN was grown on Si with AlN buffer layer and covered by a 15-nm-thick AlN layer. So the existence of a piece of thin covering AlN layer made the case here more complicated and introduced more additional factors in the formation of voids.

In this study, the void formation processes during the growth of GaN on Si (111) was clarified, applying AlN as buffer layer and interlayers. Factors in void formation were also investigated to obtain proper void size, density and shape.

## B.2 Void formation by hydrogen etching

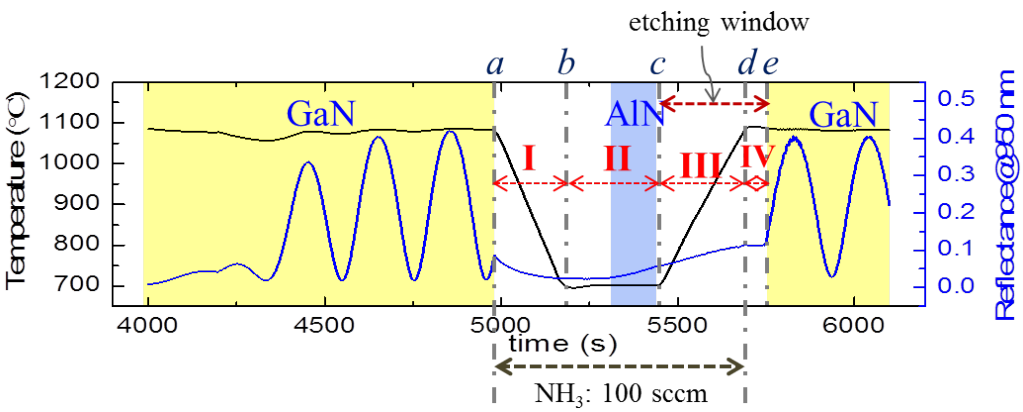


**Fig. B.2** Curves of growth temperature and reflectance at 950 nm for two neighboring GaN layers and AlN IL between them.

In initial observations, as shown in Fig. B.1, voids were found beneath AlN ILs. AlN ILs survived very well but some volume of GaN had gone and formed some voids. Lateral length of voids distributed from 50 nm to 2 um. Therefore special attention was paid to the period between the growths of two neighboring GaN layers, including the growth of AlN IL between them also. As represented in Fig. B.2, the period between the growth of two layers of GaN is divided into four stages, marked by points of *a*, *b*, *c*, *d* and *e*. In stage I, conditions ramped from the growth of GaN to that of AlN. AlN was grown in stage II. Growth conditions ramped again in stage III to grow GaN. Stage IV was condition stabilization for the growth of GaN.

Growth was stopped at points of *b*, *c*, *d* and *e* respectively. Then the cross section image was observed by scanning electron microscope (SEM), as shown in Fig. B.3. No voids could be found at points of *a* and *b*, which means no void was formed just after the growth conditions ramping to that of AlN IL growth and the growth of AlN IL respectively. In the

end of stage III at point *a*, after growth conditions ramping to that for GaN, some voids could be seen. At point *d*, after growth conditions stabilization and just before the growth of the next layer of GaN, voids were found to be larger.

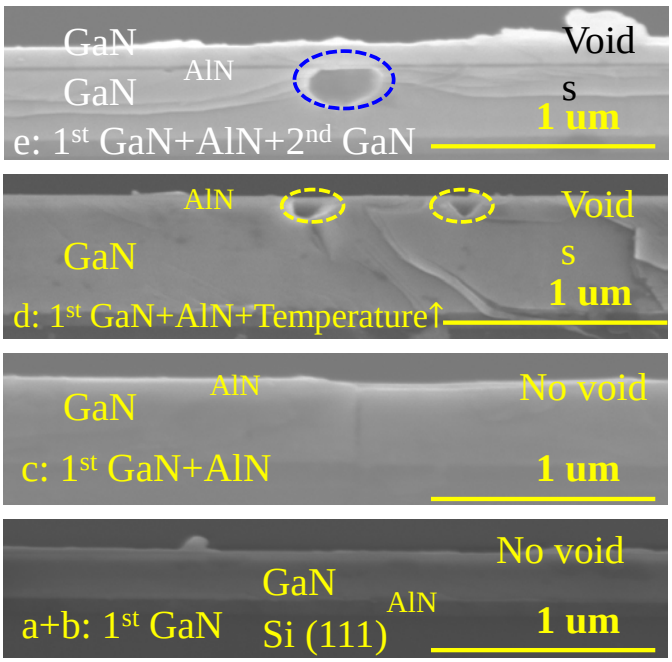


**Fig. B.3** SEM images at points of *a*: after the growth of 1st GaN layer and condition ramping (a); *b*: after the growth of AlN IL (b); *c*: after condition ramping for the growth of GaN (c); *d*: after condition stabilization for GaN growth (d).

What happened during stage III and IV? $H_2$ was carrier gas. AlN was grown under the conditions that with temperature at 750 ℃, pressure of 50 mbar and $NH_3$ flow rate of 100 sccm. In stage III, temperature rose from 750 ℃ to 1130 ℃, pressure increases from 50 mbar to 200 mbar. In this process, the $NH_3$ flow rate was kept constant, resulting in $NH_3$ partial pressure increases from 0.588 mbar to 2.353 mbar. There was a reversible reaction to describe the decomposition of GaN in $H_2$, written as Eq. (B-1) [4]. In stage III, the partial pressure of $NH_3$ was too low to make the reaction to the left direction to be dominant. GaN was safe at low temperature, for example, below 800 ℃ [9]. As temperature ramped up, GaN decomposition started if the temperature was high enough. In stage IV, etching continued and became more efficient at high temperature, even though $NH_3$ partial pressure ramped up to 58.8 mbar during this stage. As a result, voids become larger in stage IV.

$$2GaN(s) + (ads) + 3H_2 \rightleftarrows 2Ga(ads) + 2NH_3 \tag{B-1}$$

So period from point *b* to *d* can be called as etching window. In this case, there was a covering AlN layer on GaN, this kept the GaN layer from being attacked by hydrogen atoms directly, lowered the GaN decomposition rate and made etching effect milder. How $H_2$ could react with GaN? Actually, there were some openings in AlN IL, as shown in Fig. B.4a. These openings were formed by cracking and grain boundaries. As long as the thickness of AlN IL exceeds its critical value, cracking occurs to release elastic strain energy in AlN IL. Based on the observations above, a scheme of GaN decomposition under AlN layer was proposed in

Fig. B. 4b. $H_2$ went through the openings in AlN IL and reacted with GaN, and the reaction products escaped through the same pass.

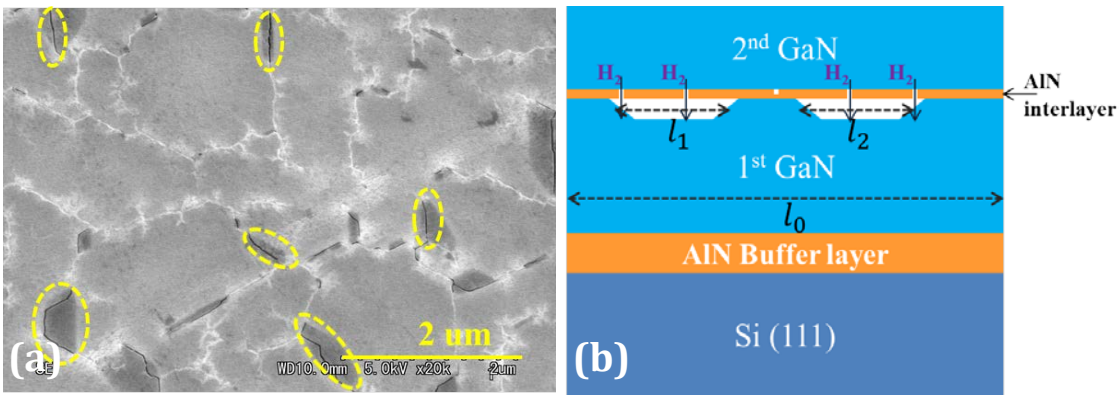


**Fig. B.4** (a) Plane view of AlN IL with openings, some of them were circled. (b) Animation of GaN etching process by $H_2$.

## B.3 Factors in the formation of voids

Based on the careful analysis in stage III and IV, as well as the observation of AlN IL, factors in the formation of voids could be divided into two parts. The first part can be called as general factors, including $NH_3$ partial pressure, temperature, etching time and so on. The second part related to AlN IL, for example, its thickness and quality (growth conditions), which can affect the size and number of openings in AlN ILs. Consequently, strategies to tune the size, volume and shape of voids also lied in these factors. One can adjust the conditions in stage III and IV, e.g. $NH_3$ partial pressure, etching temperature and etching time. Growth conditions for AlN ILs could also be changed to tune its protecting effect on GaN. Longer etching in pure $H_2$ makes more openings in AlN ILs. "proper voids" was defined to be voids with proper size, proper volume and density, which didn't worsen the quality of GaN. A simple way was adopted to estimate the volume of voids in GaN layers

**Table B.1** Tested conditions for void formation.

| Sample | Layer 1 | Layer 2 | Layer 3 | Layer 4 | Layer 5 |
|---|---|---|---|---|---|
| **A** | 11.76 mbar | 2.353 mbar | 0.335 mbar | | |
| **B** | 3 min | 4 min | 6 min | 8 min | **10 min** |
| **C** | 30 nm | 20 nm | 15 nm | 10 nm | **5 nm** |
| **D** | 10 s | 20 s | 30 s | 40 s | **50 s** |
| **E** | 5s | 10 s | 15 s | 20 s | **30 s** |
| **F** | **5s** | **10 s** | **15 s** | **20 s** | **30 s** |

* A: $NH_3$ partial pressure; B: condition ramping time in stage III; C: AlN IL thickness; D: etching time at 1130 ℃ with $NH_3$ partial pressure of 2.353 mbar; E: etching time at 1130 ℃ in pure $H_2$, $NH_3$ flow rate = 100 sccm in stage II; F: etching time at 1130 ℃ in pure $H_2$, GaN surface protected by $NH_3$ flow rate of 1000 sccm in stage II. Layer 1 to 5 means void formation from bottom to up, in 5 layers of GaN.

roughly, as shown in Fig. B.4b and Eq. (B-2), by counting the sum of the length of voids and dividing it by the total length of that layer.

$$void\ rate = \frac{l_1+l_2+\cdots+l_n}{l_0} \times 100\% \tag{B-2}$$

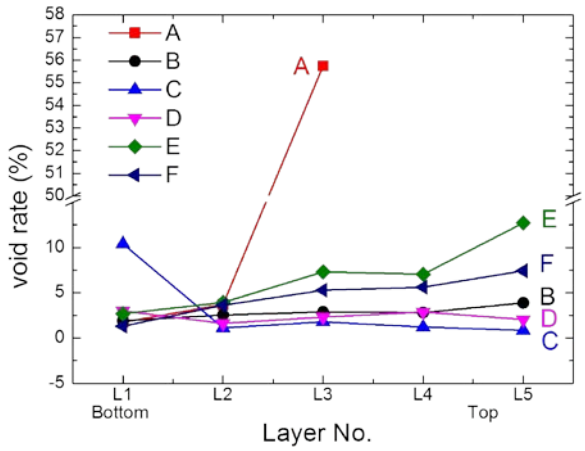


**Fig. B.5** Void rate under various testing conditions.

Some conditions discussed above were tested to get proper voids, as shown in Table B.1. Void rate was summarized in Fig. B.5. In sample A, there were data only about three layers. Because as long as the partial pressure decreased to lower than 2.353 mbar, etching rate rose rapidly and resulted in voids with too large individual length and the failure of the growth of next GaN layer. Although AlN was robust in $H_2$ atmosphere, too high volume of voids can destroy the surface of it and lead to improper growth of the succeeding GaN with uneven surface. For sample B, C and D, void rate seemed not sensitive to the condition ramping time in stage III, AlN IL thickness and etching time at 1130 ℃ with $NH_3$ partial pressure of 2.353 mbar. It should be noticed that for AlN with very large thickness around 30 nm, void rate can be more than 10%. The lateral lengths of them were larger than 1 um. Shape of them was also very regular, and they may be the desired voids. For sample F, etching time in pure $H_2$ in stage IV at temperature of 1130 ℃ and pressure of 200 mbar was tested while during other stages GaN was protected by high $NH_3$ partial pressure. With shorter etching time in sample F but much higher void rate than that in sample D, this showed that etching rate in pure $H_2$ was much higher than that with $NH_3$ partial pressure of 2.353 mbar at 1130 ℃. The difference between sample E and F was that GaN was protected in sample F during stage II by high $NH_3$ partial pressure. This verified that in stage II, GaN decomposition also occurred. By tuning such conditions, proper voids can be formed, as shown in Fig. B.1.

## B.4 Effects of voids on the property of GaN

Presence of voids in GaN/AlN multilayer system on Si affects the mechanical, crystallographic, and optical properties of the material structure. Specifically, the stress control, crystal quality, and optical performance of GaN on Si are influenced by voids.

To investigate the influence from voids on stress control efficiency in GaN growth on Si, two samples had been grown. The only difference between them was voids existed in one and not in the other. The growth conditions of AlN buffer layer, GaN layers and AlN interlayers were controlled to be the same with each other. In GaN on Si, in order to balance the tensile stress occurs during cooling, it is well known that the compressive stress in GaN layers should be well maintained.

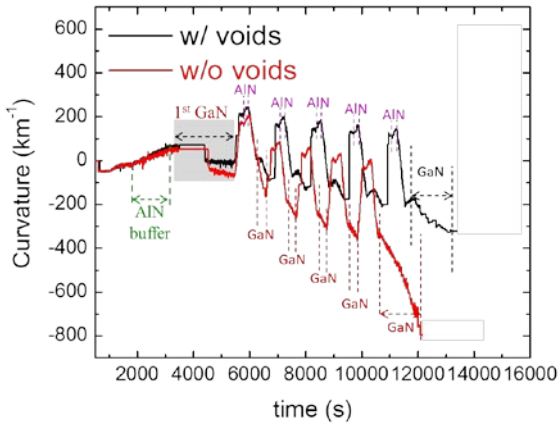


**Fig. B.6** Curvature transition curves during the growth of the samples with and without voids.

It was clear that compressive stress was introduced much more efficiently in the sample without voids than the one with voids. The compressive stress was released rapidly in the sample with voids. Under the influence from voids, there were two sources of stress releasing effect. The first came from GaN itself. As shown in Fig. B.1, due to the presence of voids, GaN layers became loose in lateral direction. GaN layer was separated into domains by the spacing of voids. The contact area of between GaN and underlying AlN interlayer was also reduced by voids and then GaN would be less stressed. Consequently, the shear stress in lateral direction of GaN layer dropped. On the other hand, as shown in Fig. B.4a, many openings in AlN interlayers were generated by the formation of voids in underlying GaN. These openings broke AlN IL and the capability of inducing shear stress in overlying GaN was degraded. Openings also acted as the sources of defects generated in overlying GaN. Introduction of defects made GaN relax more rapidly.

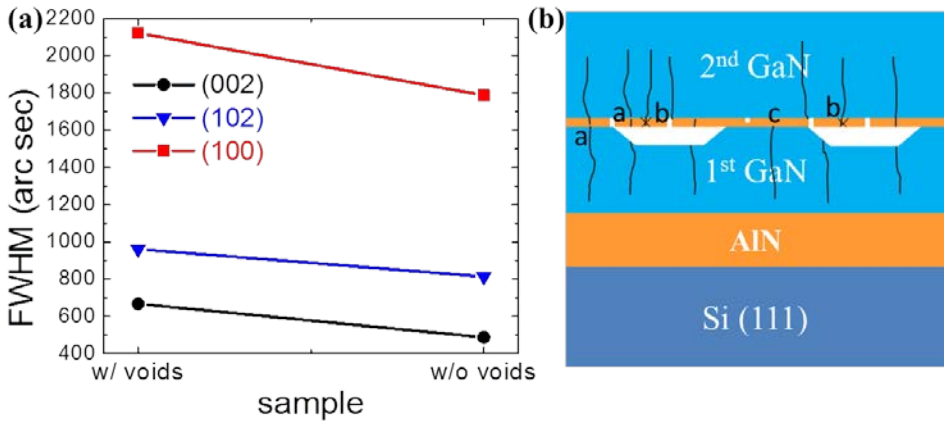


**Fig. B.7** (a) FWHM of XRD rocking curve of samples with and without voids; (b) types of the interaction between AlN interlayer and dislocations.

Voids also deteriorate the crystal quality of GaN. The crystal quality of GaN without voids was better than that with voids. This was assigned to the more dislocation introduction by the openings in AlN interlayer due to the formation of voids. As represented in Fig. B.7b, there are three types of behavior of the interaction between the dislocations and AlN interlayer. Type *a* is the propagation of dislocation through the interlayer. This doesn't affect the dislocation density. Type *b* is new dislocation introduction generated on the upper interface of AlN interlayer. In interlayer, the dislocation, grain boundaries and the openings caused by the voids in underlying GaN can be the sources of new dislocations. This behavior increases the dislocation density in overlying GaN. Type *c* is blocking. Some propagating dislocations are blocked by AlN interlayer and this is favorable to the reduction of dislocation density. However, voids are barely capable of blocking dislocations, because if there are dislocations in the area of voids, they have already propagated into AlN interlayer. After the formation of voids, the dislocation which had propagated into the interlayer could not be

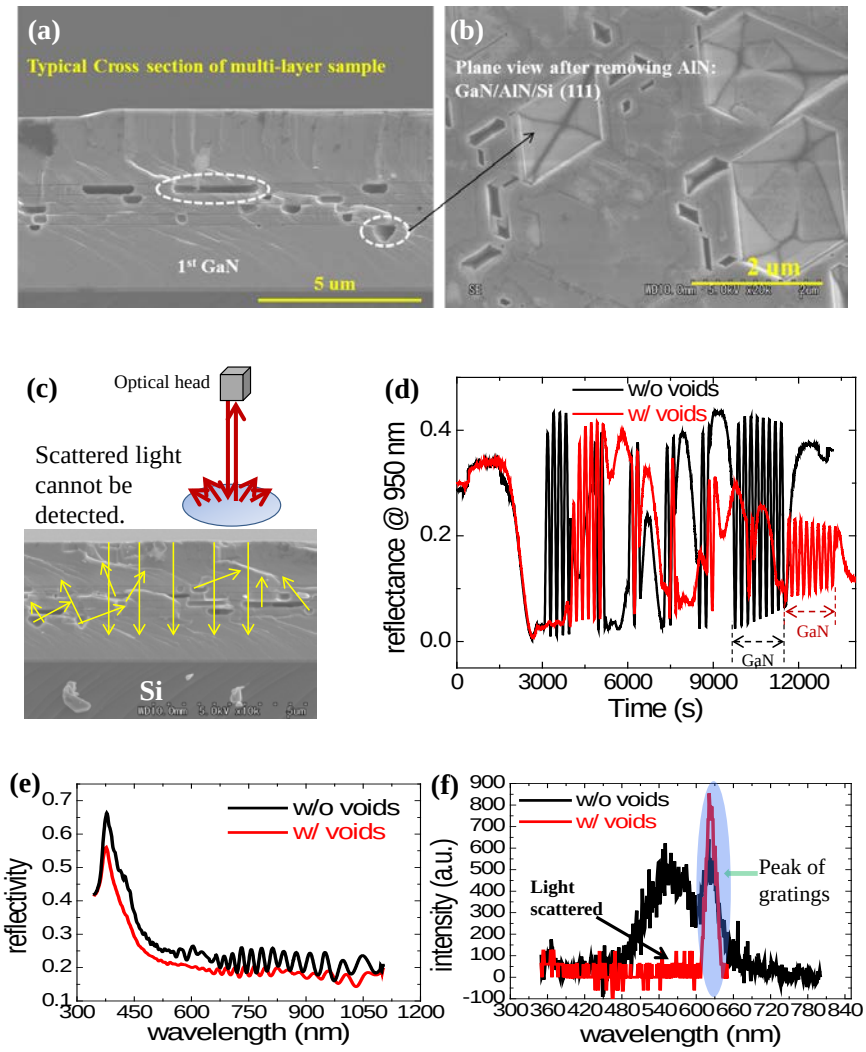


**Fig. B.8** Effects of voids on the optical properties of GaN on Si, (a) cross section of voids in GaN/AlN structure; (b) plane view of etched voids in GaN after removing overlying AlN interlayer; (c) illustration of scattering by the facets of voids; (d) reflectance pattern at 950 nm, (e) reflectivity and (f) photoluminescence characterization of samples with and without voids respectively.

removed while the etching of GaN. Therefore, compared with the sample without voids, openings above the voids in AlN interlayer may introduce additional dislocations into overlying GaN which leads to quality degradation.

Moreover, voids brought more significant effect to the optical properties of GaN/AlN multilayer structure on Si than to crystal quality. The cross-section view and plane view of voids in GaN layers were shown in Fig. B.8a and b. From the plane view it was found that etching of GaN occurred along the regular facets of GaN. Such voids with crystal facets are good light scattering structure. When light comes to the facets, it would be reflected or scattered to various directions which it not normal to the plane of (0001) of GaN anymore. Only a part of the light goes back to the direction which it comes along, as represented in Fig. B.8c. As a result, as plotted in Fig. B.8d, as the GaN thickness increased and the density of voids accumulated, the intensity of reflected incident light with wavelength of 950 nm from the curvature and temperature monitor head was decreasing. The same thing happened with the reflectivity measurement of these two samples. Depending on the wavelength, the reflectivity of GaN with voids was about 0.05 lower than that without voids. More significantly, in the photoluminescence (PL) measurement, no PL light could be collected from the sample with voids. The normal peak around 550 nm from GaN was obtained. These experimental results proved that the assumption of scattering by the voids was reasonable.

There are some potential applications of the light scattering effect of void structure in devices. Such light scattering structure is favorable in solar cells to trap lights and increase the optical path length in the device to enhance its light-electricity conversion efficiency. Another application is in LEDs. Due to scattering of the voids, the intensity of emitted light from LED would be less angle-dependent. Especially, it may be helpful to improve the external quantum efficiency of LESs on GaN-on-Si wafer if the influence of voids on the stress control and GaN quality is ignorable. Because on GaN-on-Si wafer, a portion of the light emitted from the LED active area may be absorbed by Si substrate. The presence of void structure reduces the intensity of the light goes to the Si substrate side.

## B.5 Conclusion

Voids in GaN layers grown on Si (111) applying AlN interlayers were formed by the reaction between hydrogen and GaN. Hydrogen goes through the openings in AlN interlayers and reacts with GaN. $NH_3$ partial pressure, temperature, etching time, and conditions such as thickness of AlN interlayers can be utilized to tune the volume, size and shape of the voids. Relatively proper voids were formed using two-step etching, among which the first step was at 800 ℃ under pure hydrogen atmosphere for 1 min and the second step was at 1130 ℃ under $NH_3$ partial pressure of 2.353 mbar for 3 min. Conditions should be optimized further to get more proper voids.

Effects of voids on the performance of GaN-on-Si also were investigated. The presence of voids in GaN layers made the compressive stress introduction by AlN interlayers less effective. It is also unfavorable in terms of GaN quality. In the regards of these two points, voids should be eliminated completely. However, as long as the influence of the above two

points is ignorable, the light scattering effect of the voids has potential application in some devices like solar cells and LEDs.

## References


[1] S. Arulkumaran, G.I. Ng, S. Vicknesh, H. Wang, K.S. Ang, J.P.Y. Tan, V.K. Lin, S. Todd, G.Q. Lo, and S. Tripathy,Direct Current and Microwave Characteristics of Sub-micron AlGaN/GaN High-Electron-Mobility Transistors on 8-Inch Si(111) Substrate, Jpn. J. Appl. Phys. ***51***, (2012).

[2] D.D. Koleske, A.E. Wickenden, R.L. Henry, J.C. Culbertson, and M.E. Twigg,GaN decomposition in H2 and N2 at MOVPE temperatures and pressures, J. Cryst. Growth ***223***, 466(2001).

[3] M.A. Mastro, O.M. Kryliouk, M.D. Reed, T.J. Anderson, A. Davydov, and A. Shapiro,Thermal Stability of MOCVD and HVPE GaN Layers in H2_HCl_NH3 and N2, Phys. Status Solidi (a) ***188***, 467(2001).

[4] E.E. Zavarin, D.S. Sizov, W.V. Lundin, A.F. Tsatsulnikov, R.A. Talalaev, A.V. Kondratyev, and O.V. Bord,In-situ investigatioins of GaN chemical unstability during MOCVD, Proceedings of the Fifteenth International European Conference on Chemical Vapor Deposition (EUROCVD-15) ***2005-09***, 299(2005).

[5] D.D. Koleske, M.E. Coltrin, A.A. Allerman, K.C. Cross, C.C. Mitchell, and J.J. Figiel,In situ measurements of GaN nucleation layer decompostion, Appl. Phys. Lett. ***82***, 1170(2003).

[6] E.V. Yakovlev, R.A. Talalaev, A.S. Segal, A.V. Lobanova, W.V. Lundin, E.E. Zavarin, M.A. Sinitsyn, A.F. Tsatsulnikov, and A.E. Nikolaev,Hydrogen effects in III-nitride MOVPE, J. Cryst. Growth ***310***, 4862(2008).

[7] Y.-H. Yeh, K.-M. Chen, Y.-H. Wu, Y.-C. Hsu, and W.-I. Lee,Hydrogen etching on the surface of GaN for producing patterned structures, J. Cryst. Growth ***314***, 9(2011).

[8] Y.-H. Yeh, K.-M. Chen, Y.-H. Wu, Y.-C. Hsu, T.-Y. Yu, and W.-I. Lee,Hydrogen etching of GaN and its application to produce free-standing GaN thick films, J. Cryst. Growth ***333***, 16(2011).

[9] D.D. Koleske, A.E. Wickenden, R.L. Henry, J.C. Culbertson, and M.E. Twigg,<GaN decomposition in H2 and N2 at MOVPE temperatures and pressures.pdf>, J. Cryst. Growth ***223***, 466(2001).

# Appendix C Suggestions on further research

This section is for the people who want to do further research in the field of GaN-on-Si. Although this field has been studied more than a decade, there are still some public problems which should be solved or improved further. The key topic is how to control the stress and improve the crystal quality more efficiently in smaller thickness. The flow of this part is the same as the growth sequence of the sample structure.

(1) First of all is the buffer layer. Buffer layer plays a critical role in the system of GaN-on-Si, it influence both of the stress and quality of the 1$^{st}$ GaN layer as well as the whole system. As discussed in previous chapters, the quality of AlN buffer layer should be as high as possible. So far, the growth of AlN on Si is far from being optimized. The quality of AlN on Si substrate is much lower than that on sapphire even employing the same growth conditions. The microstructural growth mechanism of AlN on Si is different from that on sapphire which is yet to be clarified. The growth technologies of AlN on sapphire like 3D growth mode and pulse-injection method can be transplanted to it on Si.

(2) The quality improvement of the 1$^{st}$ GaN. Since the interlayers may be not helpful to improve the GaN quality, it should be enhanced in the 1$^{st}$ GaN as much as possible. There are some other strategies to improve the quality of the 1$^{st}$ GaN besides optimizing the growth of AlN buffer and applying 3D growth of itself. Masking and patterning on GaN are promising methods for it, by $SiN_x$ or $MgN_x$ for example.

(3) Most importantly, the capability of AlN interlayers of inducing compressive stress in overlying GaN layers can be elevated further. Employing more effective interlayers, the number of interlayers and total GaN thickness can be reduced. The growth conditions of new prototypes of interlayers in chapter 6 can be optimized and better performance of them is highly expectable. The micro-structures of them are highly worth investigating. Moreover, another type of two-step interlayer which consists of lower AlGaN and upper AlN is also attractive since it is capable of producing high-quality upper interface of it with small AlN lattice constant.

(4) More attention should be paid to the device on the template of GaN-on-Si, such as LED. In the end of chapter 5, there is an interesting phenomena that the peak position of blue LEDs through the wafer was uniform but not for the case of PL intensity. Surprisingly, PL intensity in the edge was seven times of that in the center in spite of generally better template quality in the center. Topics including the uniformity of wafer bow, temperature and stress distribution, InGaN composition, thickness and morpholgy of InGaN/GaN layers in the MQW are quite critical to the performance of LEDs on GaN-on-Si. The influence of wafer bow which can affect the stress state and bandgap profile in the MQW on the LED performance is also very important and interesting. There are little reports about the topics listed above.

Moreover, there is some comment on the production efficiency of MOVPE of GaN-on-Si. Up to date, almost all buffer layers were grown by MOVPE for GaN-on-Si. This requires

cleaning of Si wafer and reactor dry cleaning or AlN coating every time prior to the growth of GaN-on-Si. This is not time efficient. If the AlN buffer layer is grown by physical vapor deposition (PVD), such cleaning processes can be simplified to save time. MOVPE of GaN-on-Si can start directly from the growth of the 1$^{st}$ GaN layer. More importantly is, according to the work of Hongbo Wang, quality of GaN on PVD-AlN buffer is much better than that on MOVPE-AlN buffer, which would lead to more efficient stress control in GaN-on-Si and better crystal quality. In conclusion, PVD-AlN buffer layer on Si is a promising routine to improve the growth of GaN on Si.

# List of Publications

## Presentations

1. Cai Liu, Hassanet Sodabanlu, Masakazu Sugiyama, Yoshiaki Nakano. *GaN thickness optimization by in-situ observation of GaN growth on Si (111)*. JSAP (Japan Society of Applied Physics), Kanagawa, 2013, spring.
2. Cai Liu, Hassanet Sodabanlu, Masakazu Sugiyama, Yoshiaki Nakano. Factors of *Compressive Stress Introduction in GaN Layers in MOVPE of GaN on Si (111)*. ISCS (International Symposium on Compound Semiconductors), Kobe, 2013.
3. Cai Liu, Hongbo Wang, Hassanet Sodabanlu, Masakazu Sugiyama, Yoshiaki Nakano. *Voids Formation during MOVPE of GaN on Si (111) Employing Low Temperature AlN Interlayers*. E-MRS (European Material Research Society), Strasburg, 2013, spring.
4. Cai Liu, Hassanet Sodabanlu, Masakazu Sugiyama, Yoshiaki Nakano. *In-situ Growth Condition Analysis of AlN Interlayers for Wafer Curvature Control in GaN MOVPE on Si (111)*. ICNS-10 (International conference on nitride semiconductors), Washington D.C., 2013.

## Papers

1. Cai Liu, Hassanet Sodabanlu, Masakazu Sugiyama, Yoshiaki Nakano. *Thickness Optimization of GaN Layers by In-situ Observation of GaN MOVPE on Si (111)*. **physica status solidi C 10, No. 11, 1541–1544 (2013)/DOI 10.1002/pssc.201300266**.
2. Cai Liu, Hongbo Wang, Hassanet Sodabanlu, Masakazu Sugiyama, Yoshiaki Nakano. *Voids Formation during MOVPE of GaN on Si (111) Employing Low Temperature AlN Interlayers*. **physica status solidi C 11, No.02, 293-296 (2013)**.
3. Cai Liu, Hassanet Sodabanlu, Masakazu Sugiyama, Yoshiaki Nakano. *In-situ Growth Condition Analysis of AlN Interlayers for Wafer Curvature Control in GaN MOVPE on Si (111)*. **physica status solidi C 11, No. 03-04, 598-603 (2014)**.
4. Preospective : Cai Liu, Hongbo Wang, Hassanet Sodabanlu, Masakazu Sugiyama, Yoshiaki Nakano. $H_2$ etching during MOVPE of GaN on Si (111) and its effects on GaN, submitted to Journal of Crystal Growth.
5. Prospective: Detailed characterization and analysis about AlN interlayers, to JAP etc..